1-1-2017

# Ligand Binding Studies Of A Peptide Targeting Helix 69 Of 23s Rrna In Bacterial Ribosomes

Hyosuk Seo
*Wayne State University,*

# LIGAND BINDING STUDIES OF A PEPTIDE TARGETING HELIX 69 OF 23S rRNA IN BACTERIAL RIBOSOMES

by

**HYOSUK SEO**

Submitted to the Graduate School

of Wayne State University,

Detroit, Michigan

in partial fulfillment of the requirements

for the degree of

**DOCTOR OF PHILOSOPHY**

2017

MAJOR: CHEMISTRY (BIOCHEMISTRY)

Approved By:

_____

Advisor Date

_____

_____

_____

## DEDICATION

To my parents

**ACKNOWLEDGEMENTS**

I would first like to thank my advisor, Dr. Christine S. Chow. She has been a wonderful advisor throughout the years, and has helped me with everything I could imagine. I struggled a lot during the whole program, and she helped me out so I could survive. I could never thank her enough for all the support. Even at the hard times, I know she has always helped me to grow and appreciate more of what I have. I admire her work ethics and self-motivation, how she always seeks to do something productive, and how she balances life. Also, I thank her for exposing me to food culture, art, films, gardening, and cats. She is a great role model and I will always be grateful for letting me join her lab and learn under her supervision.

I would also like to thank my committee members, Dr. Andrew L. Feig, Dr. Mary T. Rodgers, and Dr. Olivia Merkel. I would like to thank Dr. Feig, with immense knowledge, who gave me a lot of help and guidance in phage display and binding studies. I would also like to thank him and Christine for the ReBUILD and BEST program, and I am grateful for the opportunity I had. I would like to thank Dr. Rodgers, who has let me use her instruments, and also gave me lots of suggestions on my studies. I would also like to thank Dr. Merkel, who was always so kind, and for letting me use the plate reader and giving me suggestions with the fluorescence assays. I consider myself to be lucky to have committee members who would take their precious time to read my documents and give me insightful suggestions.

I would like to thank all the professors whom I had a chance to interact with. I would like to thank Dr. Cha, I was able to join the program because of him and learned a lot from him the first year I joined the program. I would also like to thank Dr. Guo, Dr. Kodanko, and Dr. Andreana, for their classes, which helped me understand organic chemistry better. I would like to thank Dr. Crich for letting me observe some synthesis in his lab and for suggestions. I would like to thank Dr. Brock and for letting me learn how

to make gold nanoparticles, and also for the chance to participate in the Go-Girls program. I would like to thank Dr. Allen for his inorganic chemistry class, and how he taught us chemistry could be fun as well. I would like to thank Dr. Hendrickson for her drug design class and the ethics class, wherein she taught me to be very cautious of what I cite and present. I would like to thank Dr. Pflum, for going through step by step in my cume and suggesting how I could improve. I would like to thank Dr. Bhagwat for letting me use his lab French press and his molecular biology class, wherein I could get familiarized with molecular biology, which I never thought I would learn. I would like to thank Dr. Ahn, Dr. Cunningham, Dr. Schrader, Dr. Romano, and Dr. Stemmer for letting me use their lab instruments and giving suggestions. I would also like to thank Dr. Hashemi, her class in analytical chemistry was something new to me. She has always been so kind and warm, especially at one of my darkest moments during this program. I will always thank her for that. I would also like to thank Dr. Li and Dr. Suk-kyung Lee, especially Dr. Lee for giving me valuable suggestions and encouraging me to get through this program. I would also like to thank Dr. SantaLucia, Dr. Barber, Dr. Zibuck, Dr. Campanalli, and Dr. Maguire, those I had a chance to teach for, and especially Dr. Barber for their support. I would like to thank Dr. Udugamasooriya, for the suggestions on branched peptide synthesis. I would like to thank Dr. Abigail Fusaro from Marygrove college, whom I had a chance to teach for and learn her teaching style. I was really amazed how she could teach with such passion. I would also like to thank Dr. Andreoli and Dr. Knight, whom I had interaction with during the ReBUILDetroit program. I would like to thank the BEST program, Dr. Kenaga and Carmen Gamlin, for the support and help for ReBUILDetroit program. I would like to thank Dr. Judith Moldenhauer for the design class I had a chance to participate in. It has helped me learn how to draw better figures. I would like to thank Dr. Yoon-Sik Lee, my previous advisor, for giving me the opportunity to come study in the U.S.

Wayne State has great facilities, and I would also like to thank Dr. Westrick and the LIC Instrument Center, Dr. Ksebati, Dr. Yuriy Danylyuk, and Dr. Olena Danylyuk for the help on NMR, ESI-MS, and MALDI-TOF. I would like to thank Dr. Stemmer and the proteomics core, Dr. Caruso, Dr. Duncan, and Namhee Shin for the help and guidance with the instrument and facilities. They were extremely skilled and patient, and I would not have been able to obtain ESI-MS data without their help.

I would also like to thank the department staff for the help I received. I would like to thank Melissa Barton, who helped me in so many ways to get through this program. I would also like to thank Mary Wood, Debbie, Bernie, Diane, Kellie, Tenecia, and Jackie in the office support, and Liz, Greg, Bonnie, Jason, and Lorraine in the science store, for all the help on ordering and receiving samples, and Larry at the electronic store, for the help with our lab PCR. I would like to thank Dr. Lozanov, for teaching me how to use the GC and IR in the undergraduate labs. I would also like to thank Nestor Ocampo for the help and friendship during the program, and also for the help with all the funky computer problems.

I would like to thank my labmates and their families, whom I learned from and laughed with during the program. Moninder, for teaching me phage display when I first joined the lab. Holly, for letting me adjust in the lab with warmth and for the moral support. Yogo, for the help and suggestions throughout the years, and for being a great friend. Jun, for teaching me how to use CD and the help with NMR. Sakina, for always being positive, I learned a lot from her attitude. Daya, for teaching me how to use HPLC, UV-melting, and being an awesome friend, whom I miss always. Xun, for helping me with HPLC, ribosome preparation, and giving good suggestions, and being strong and positive friend. Gayani, for teaching me how to do ribosome preparation. Danielle, for teaching me how to use HPLC and do ESI-MS data analysis. Nisansala, for the help with ribosome preparation and the friendship throughout the years. Supuni, for being a great friend, I

will always miss our lunch dates. Bett, for being a great “macho” friend and support. Prabuddha, for being a great friend and for all the food Kumudu cooked for lab functions. Evan, for the help with NMR and friendship, introducing me to the Game of Thrones, and also for Bonu’s concerts he took me to. Mariem, for always asking about how I am doing anytime we would run into each other. Rabiul, the witty new student. Mina, for being my favorite alum and giving moral support. Sanjaya, for taking his time to come visit for the PfLAGS workshop and giving suggestions. Dinuka, for teaching me how to use BLItz. I would like to thank Amer whom I had the pleasure to work with. I also had the pleasure to work with Anna, Kareem, Rogelio, Rafael, Patrick, Eleni, Nate, and Mackenzie and I would like to thank them for the time we spent together. Also, Alain, Laura, Harjot, Ahmad, Rafael, Diana, Sue, Marwa, Andrew, Laimar, Brigid, Klea, Sherrell, and Shapnil, especially Shapnil for being a great friend.

I would also like to thank graduate students and postdocs I interacted with. Das and Parida from the Cha lab, for teaching me many experiments in organic labs and the friendship, Yuran from the Merkel lab, for letting me in to the pharmacy department and helping me with the instruments, Wes from the Cunningham lab, for the help with the ultracentrifuge, Indika and Jessica from the Brock lab for teaching me how to make gold nanoparticles and use the DLS, Dandan, Martha, Nilshad, Sanofar, Rebecca, Adam, and Amit from the Feig lab for teaching me how to use the sequencer and centrifuge, Ashley from the Romano lab for teaching me how to use SPR, Shirin, Gayathri, Dilani, Liangjun, Nilesh, and Travis from the Hendrickson lab for the help with the lyophilizer and PCR, Thisari, Shanqiao and Vimukthi from the Bhagwat lab for teaching me how to use the French Press, Todd from the Pflum lab for the help with the MS analysis program, Dilini, Fidelis, Garrett, Kusal, Nalin, Shima, and Sewvandi from the Ahn lab for the help with the plate reader, lyophilizer, Schlenk line, Eric, Gayan, Chandani, Imali, Hansini, May, Rawan, Pramodha, Sara, and Amanda from the Rueda lab for the help with the

fluorimeter, Chenchen, Yanlong, Lucas, and Sam from the Rodgers lab for the help with mass spectrometry. Whitney and Kyle for chairing the graduate symposium that I enjoyed organizing. Yuanyuan, Lauren, Hasina, Nour, Renata, Krista, Habib, Tomasz, Raj, Casey, Amr, Appi, Girish, Roshini, Kasun, Youngmin, Beixi, Shameemah, Bishnu, Yi-jung, Alex, Khanh, Monika, Nirmeen, Japnam, Aivy, David, Cong, Alfonso, Sanghyun, Seohee, Yumin, Jaeseung, Tolu, Seon-Yeong, Goldung, Jun Dong, Youjin, Shannon, Sojin, Doyoung, Jun Soo, Yoonjee, Yongsok, Byungchan, Sunhyung, Heeyoung, Song, Hongjun, SengYun, Young-Eun, Hyeonjeong, Jayoung, Hame, Kyeong Eun, Donghun, Saehan, Jin Young, Suk Joon Kim, and Yoojin for the friendship. Also, my late friend, Soojin Lee, whom I still miss dearly. I would especially like to thank Sai, Taeho, and Ranran for being there for me throughout these years.

Finally, I thank my family for the love and support throughout my life. My father, Dr. Jae-Myeong Seo, and my mother, Eun-kyung Lee, for their endless love and dedication. I would not have started Ph.D. or would have thought of continuing my studies without them. They have been role models throughout my life and set standards for me that would make me push through. They would believe in me even when I would doubt myself. Also, my sister, Yesuk, for the love and support, and for being a fantastic artist who inspires me all the time. I would also like to thank my grandparents, especially my late grandfather Dr. Kwangyoon Seo for the memories and inspiration.

## TABLE OF CONTENTS

## LIST OF TABLES

## LIST OF FIGURES

## LIST OF SCHEMES

# CHAPTER 1 – INTRODUCTION

## 1.1. Antibacterial resistance

Since the discovery of penicillin over 70 years ago,[1-2] many antibiotics have been developed. Antibiotics have improved public health and human well-being, which has also led to widespread overuse.[3] Some commonly used antibiotics and their class designations are listed in **Table 1.1**. There are antibiotics that target cell wall synthesis (*e.g.*, penicillins),[1-2] folate synthesis (*e.g.*, sulfonamides),[4] DNA topoisomerases or DNA gyrases (*e.g.*, fluoroquinolones),[5] and protein synthesis (*e.g.*, tetracyclines,[6-7] macrolides,[8] and aminoglycosides[9-12]). Structures of some antibiotics from each class are shown in **Figure 1.1**. Many drugs that target protein synthesis inhibit the elongation step,[3] but numerous modes of action exist. Some mechanisms involving the bacterial ribosome include binding to the 30S subunit[10-11, 13-14] and inhibiting tRNA binding,[6] or disrupting translocation[8, 15] and tRNA recognition by interacting with the peptidyl transferase center (PTC) or the decoding region (A site).[15] Macrolides, lincosamides, and streptogramin A (MLS) are known to target the PTC region of the 50S subunit and block the peptide exit tunnel.[8, 15-16] Aminoglycosides are known to interact with the decoding region of the 30S subunit and interfere with tRNA selection.[10-11, 14, 17]

**Table 1.1.** Major antibiotic classes, examples, and their targets

| classes | examples | target |
|---|---|---|
| penicillins[1-2] | penicillin, amoxicillin | peptidoglycan cell wall synthesis |
| tetracyclines[6-7] | tetracycline, doxycycline | A site of 30S subunit |
| macrolides[8] | azithromycin, erythromycin | peptide exit tunnel |
| aminoglycosides[9-12] | neomycin, kanamycin, paromomomycin | A site of 30S subunit |
| sulfonamides[4] | prontosil, sulfafurazole | dihydroopteroate synthetase |
| fluoroquinolones[5] | ciprofloxacin, levofloxacin | DNA topoisomerase, DNA gyrase |

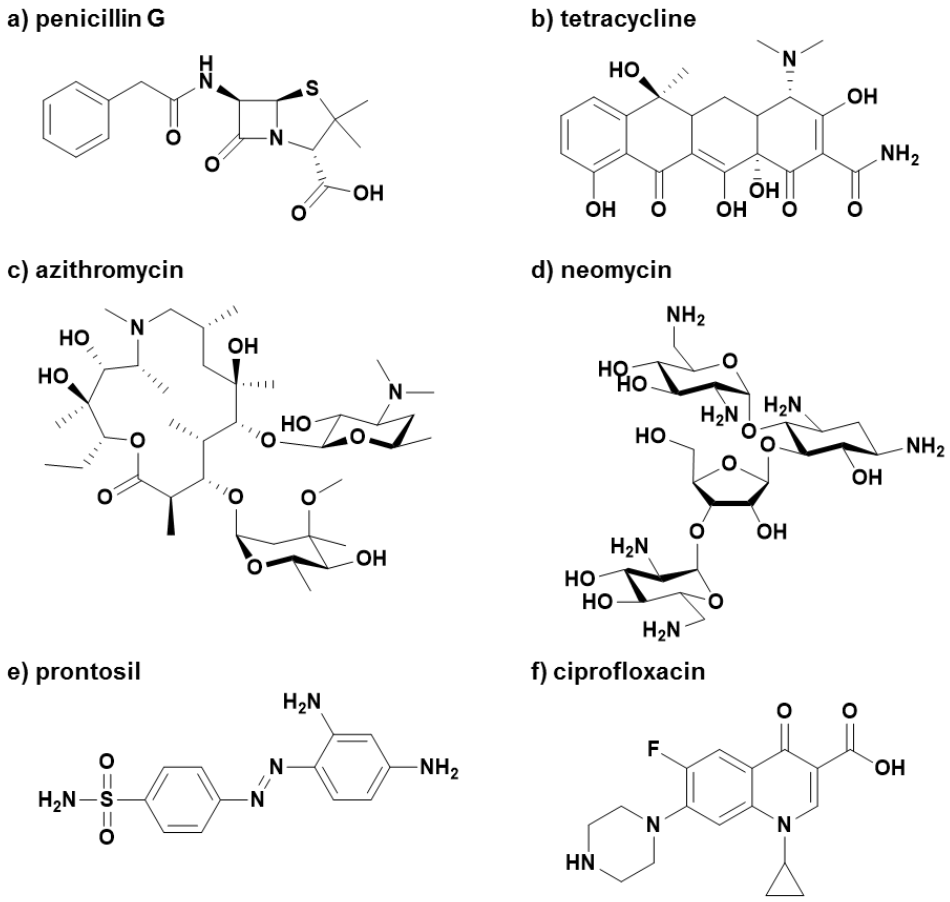


**Figure 1.1.** Structures of antibiotics from each class are shown.

Although antibiotics have helped decrease the number of deaths in the world, antibacterial resistance has emerged due to overuse. According to the U.S. Center for Disease Control & Prevention (CDC), antibacterial resistance causes 23,000 deaths per year in the U.S. Along with *C. difficile* and *N. gonorrhoeae*, ESKAPE (*E. faecium*, *S. aureus*, *K. psneumoniae*, *A. baumannii*, *P. aueruginosa*, and *E. coli*) defines the list of antibacterial resistance threats.[18-19] The antibiotic targets and resistance mechanisms are summarized in **Figure 1.2**.[7-8, 14] The mechanism of action for antibiotics generally relies on interacting with a given target and altering its structure and/or function. The locations are indicated in **Figure 1.2**. Organisms have found ways to avoid these mechanisms, leading to drug resistance. The resistance mechanisms fall into four

general categories: efflux, target modification, drug modification by enzymes, and target enzyme inactivation.[20-22] It can be noted that the mode of action is usually through one type of mechanism, while the resistance happens in more than one type of mechanism (**Figure 1.2**). Understanding these resistance mechanisms is critical for the development of new classes of drugs.

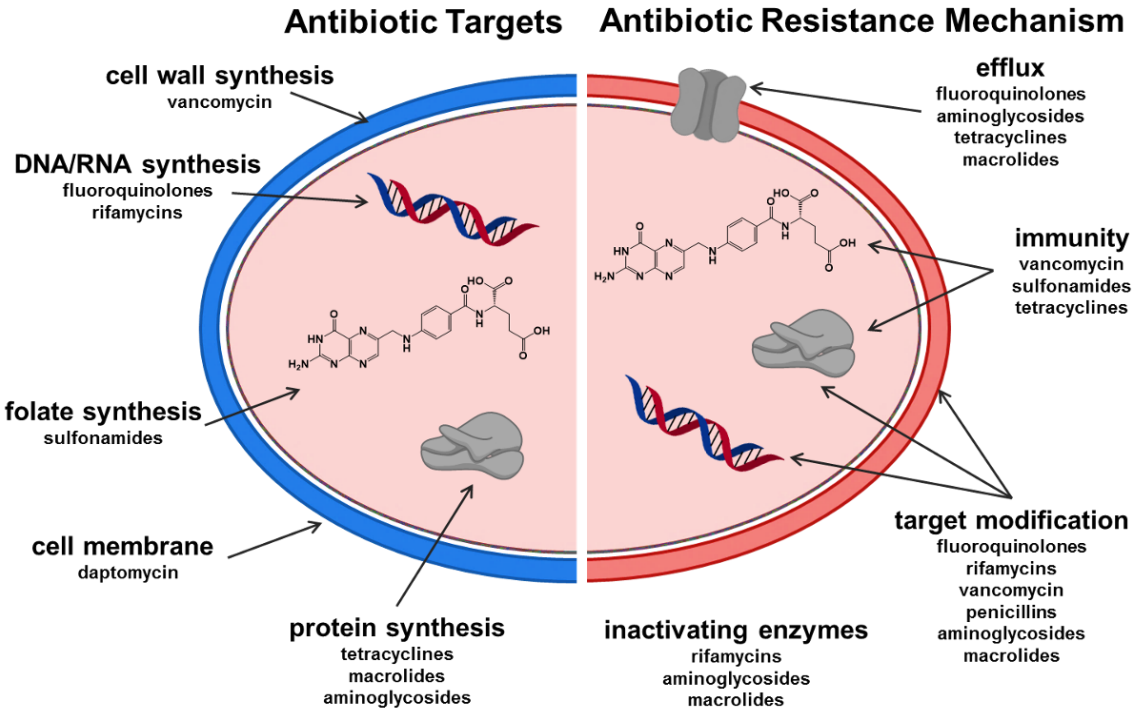


**Figure 1.2.** The locations of antibiotic targets and the resistance mechanisms are summarized, along with examples of drugs in each category.[7-8, 14-15] Modes of action are labeled on the left side of the figure. Most of the known antibiotics have developed resistance through four main mechanisms, which are listed on the right.

Aminoglycosides are widely used drugs that have been subject to multiple routes of resistance.[13-14, 17] Aminoglycosides contain 2-deoxystreptamine (2-DOS) moieties that are highly charged (**Figure 1.3**), and bind to many RNAs through electrostatic interactions.[9, 14] The 2-DOS moiety is proposed to stabilize a specific conformational state of A1492 and A1493 in the 30S subunit that results in miscoding.[23] The amino

groups are positively charged under physiological conditions, which make the aminoglycosides overall highly charged. Aminoglycosides face resistance mainly due to modification on their amino or hydroxyl groups.[10, 17, 24] For that reason, they have been modified by addition of different moieties, simplification of their structures, or the formation of hybrid structures, in helping protect them from further modification by resistance enzymes and/or to improve their binding to the RNA target.[25-26]

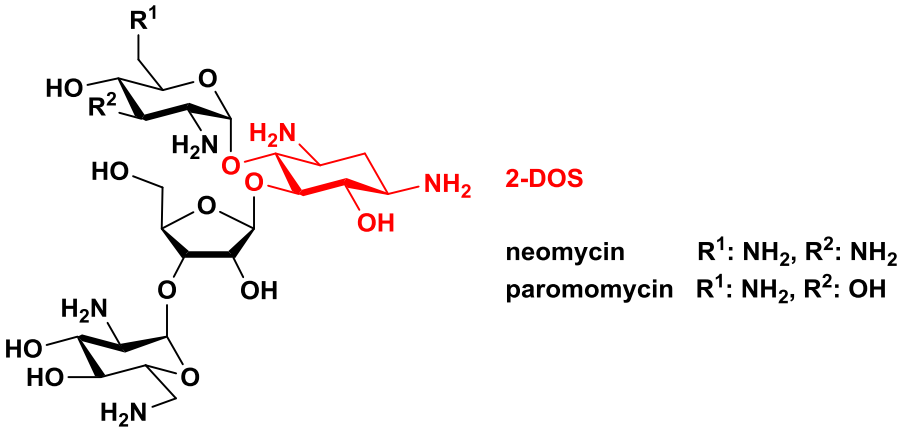


**Figure 1.3.** Structures of two representative aminoglycosides that contain the 2-DOS moiety are shown. The 2-DOS moiety highlighted in red, which is an important scaffold for RNA binding, is highly conserved among this class of antibiotics.

Although drug resistance is increasing, approval and discovery of new compounds is decreasing.[27-28] The reason for this decline in drug discovery is due to high costs and low profitability because of inherent resistance of naturally derived compounds.[29] To overcome this problem, new approaches are needed such as discovery of new targets or development of new classes of compounds to target bacteria.[3] In this thesis work, my goal was to catch two birds with one stone by studying a new target, helix 69 (H69) of 23S rRNA of the bacterial ribosome that is known to play important functional roles,[30-33] and by using phage display to identify a new class of peptide molecules to target H69.

### 1.2. Helix 69 of the 50S ribosome subunit

#### 1.2.1. Structure of helix 69

Helix 69 (H69) is a 19-nucleotide (nt) motif residing in 23S ribosomal RNA (rRNA) of the 50S subunit in bacterial ribosomes.[33] The sequence of H69 is 5′-GGCCGΨAACm$^3$ΨAΨAACGGUC-3′, in which A, G, C, U, Ψ, and m$^3$Ψ are adenosine, guanosine, cytidine, uridine, pseudouridine, and 3-methylpseudouridine, respectively (**Figure 1.4**).[34-35] Pseudouridinylation is the most commonly occurring modification of the nucleoside, in which the uracil base is detached from the ribose by an enzyme called RluD, rotated by 120°, then reattached to the sugar.[36-39] The glycosidic linkage becomes a C-C bond, and through the isomerization reaction, an extra imino group becomes available for hydrogen bonding.[40] Three Ψs are observed in H69, with methylation at Ψ1915.[33-34, 41]

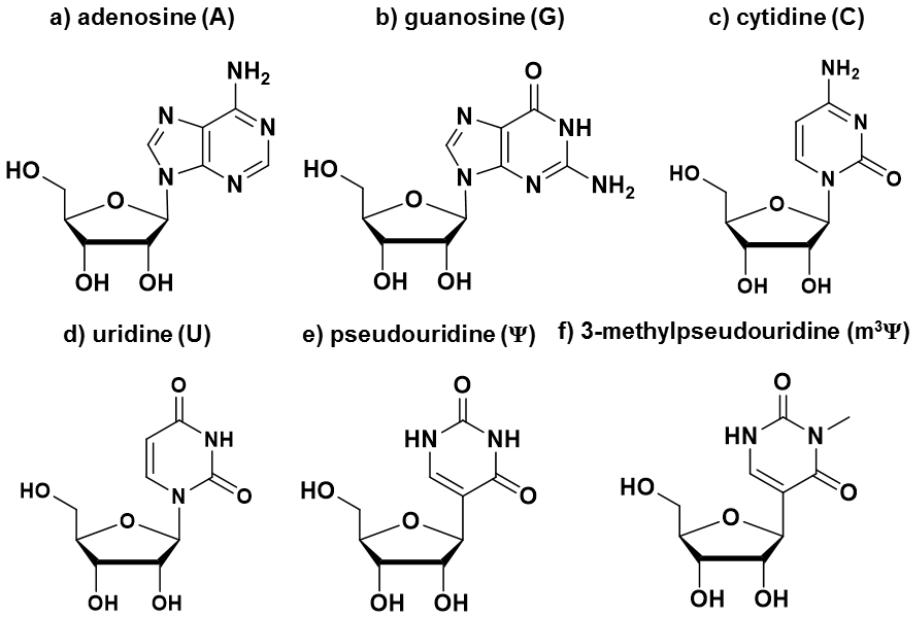


**Figure 1.4.** The structures of the nucleosides found in H69 are shown.

The sequence and structure of H69 are conserved throughout phylogeny, and the H69 motif is also observed in humans (**Figure 1.5**).[34, 41-42] In human H69, five Ψs are observed, and unlike *E. coli*, methylation does not occur at Ψ3731.[34] Previous NMR studies showed that the Ψs stabilize RNA due to increased base stacking,[43-44] while the individual nucleoside modification destabilizes the overall H69 structure.[45] The secondary structure of H69 is reported to be a hairpin loop, in which residues G1906-Ψ1911 form hydrogen bonds to residues A1919-C1924 to stabilize the hairpin structure, and A1912-A1918 form the loop.[46] In human H69, there is a G at position 3734, whereas *E. coli* H69 contains an A at the corresponding 1918 position.[47] There is a G1907-U1923 wobble base pair in the stem.[46] There is also a reverse-Hoogsteen base pair at A1912-Ψ1917 in the wild-type (WT) and ΨΨΨ variants, which was suggested to stabilize H69 structure.[48-49]

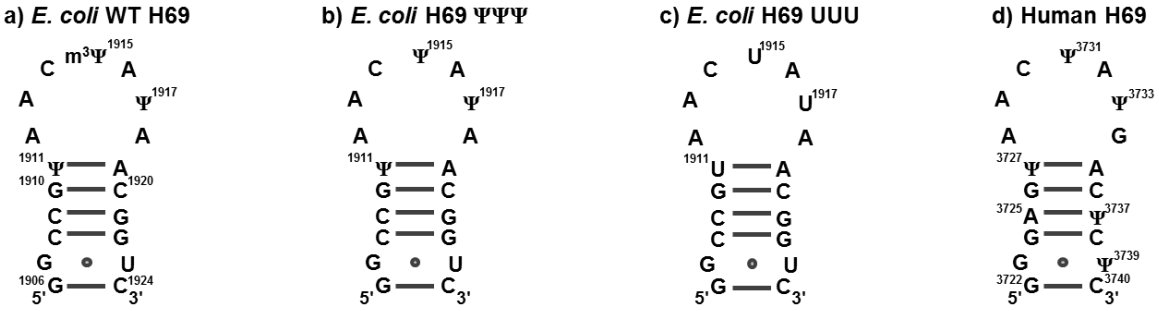


**Figure 1.5.** The sequences and secondary structures of H69 synthetic variants are shown. Variations include: a) *E. coli* WT H69, b) *E. coli* modified H69 ΨΨΨ, c) *E. coli* unmodified H69 UUU, and d) human H69.

### 1.2.2. Post-transcriptional modifications in the ribosome

Post-transcriptional modifications, such as Ψ, observed in rRNA, are proposed to play roles in regulation of the functions of rRNA by altering binding interactions or ligand recognition.[48, 50-51] Modifications can occur by breaking the glycosidic bond or altering the bases in either a simple or complex manner (**Figure 1.6**). More specifically, there are

four major types of modifications: isomerizations, methylations of the base, methylations of the sugar (2'-OH), and multiple modifications.[48, 52]

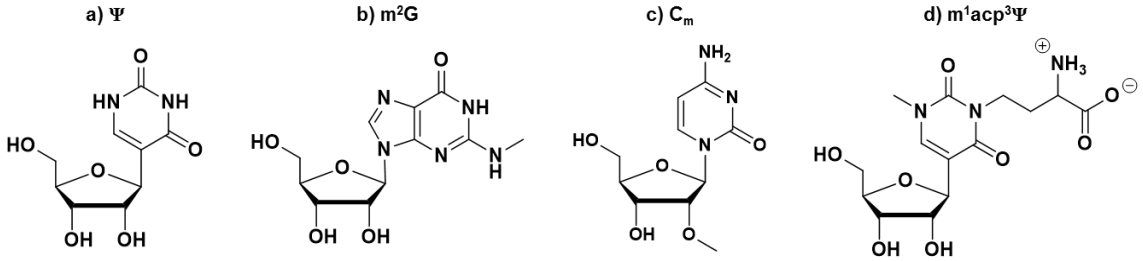


**Figure 1.6.** Nucleoside structures and examples of the four major types of modifications: isomerization, methylation of the base, methylation of the sugar, and multiple modifications are shown in pars a-d, respectively.

To date, 36 modified nucleosides have been reported to occur in *E. coli* ribosomes in the PTC and A site, regions essential for translation.[50, 52-53] This correlation implies a functional significance of the modified nucleosides for translation. Modifications of the rRNA can result in altered interactions with other RNAs, proteins, or cofactors, likely fine-tuning the ribosome structure and function during translation.[32, 54] Modifications of the rRNA will affect direct contacts, stacking, or base-pairing interactions, thus stabilizing or sometimes destabilizing the complex.[48, 50] Therefore, rRNA modifications are factors that cannot be overlooked in antibiotic development studies.

### 1.2.3. Function of helix 69

Helix 69 comprises the intersubunit bridge B2a, where the 50S and 30S subunits interact to form the complete 70S ribosome (**Figure 1.7**).[46, 55-56] The interaction is mainly between those two subunits with helix 44 (h44) of the 30S subunit, in which A1913 of H69 moves into a pocket formed by h44 and contacts the ribose of the A-site tRNA.[57-58] Residue A1912 also interacts with C1407 and G1494 of h44, and A1919 interacts with U1495.[46, 49, 59] The loop region of H69 interacts with tRNA, which is important for tRNA selection and can lead to miscoding when mutations take place.[59-60] Crystal structures

have also shown that residues in the stem region, namely G1921 and G1922, interact with the D stem of the P-site tRNA.[46, 58] It was also reported that H69 interacts with release factors (RF1 and RF2) at C1914 and the ribosome recycling factor (RRF) at Ψ1915 and A1916, which indicates the multiple roles of H69 in translation.[61-63] Ribosomes lacking Ψ have been reported to cause slower growth rates of *E. coli* and have reduced subunit association *in vitro*, with a corresponding loss in fidelity and translation termination.[30, 64]

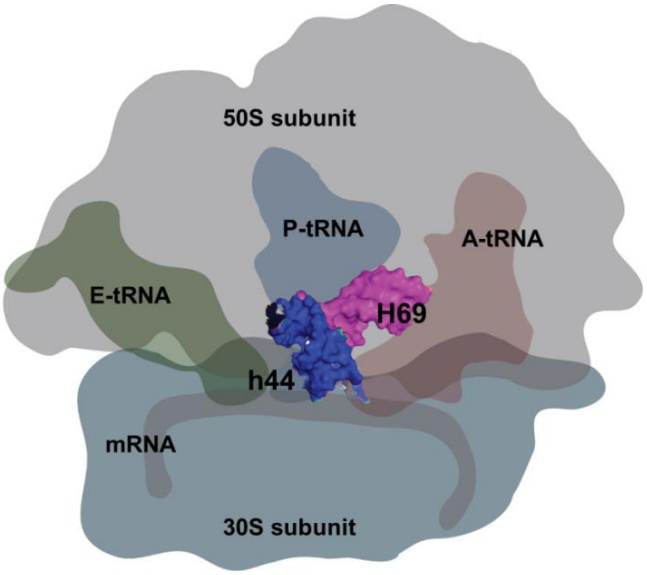


**Figure 1.7.** The location of H69 in the ribosome is shown. The figure is a cartoon representation of the PDB structure 4V50 with h44 and H69 of bridge B2a in space-filling mode.[65]

### 1.2.4. The conformational change of helix 69

As mentioned in the previous section, H69 is located in the B2a intersubunit bridge.[46, 55-56, 63] Helix 69 undergoes a conformational change involving A1913 in the loop as it makes direct contacts with A1493 in h44 during ribosome assembly.[32] Residue A1493 of h44 plays important roles in decoding; thus, certain modifications or mutations in the interacting H69 loop region will affect translation. H69 can be induced to undergo conformational changes with differing solution conditions, such as altered pH or $Mg^{2+}$

concentrations.[66-67] At low pH values (~5.5) and low $Mg^{2+}$ concentrations (0 to 5 mM), residue A1913 of H69 displays a stacked-in conformation. In contrast at higher pH values (~7.5) and increased $Mg^{2+}$ concentrations (6 to 10 mM), the same nucleotide flips out and becomes more exposed to solvent.[67] These conformations are referred to as "closed" and "open", respectively (**Figure 1.8**). Higher $Mg^{2+}$ concentrations induce more changes with modified H69 (ΨΨΨ), when compared to the corresponding unmodified H69 (UUU).[67] These changes were observed in solution and in X-ray structures with full ribosomes as well as the model systems.[66-68] Based on these structural changes, which were observed in crystal structures of 50S (closed)[55] and 70S (open)[69] ribosomes, pH- or salt-dependent studies were performed on H69 in this study.

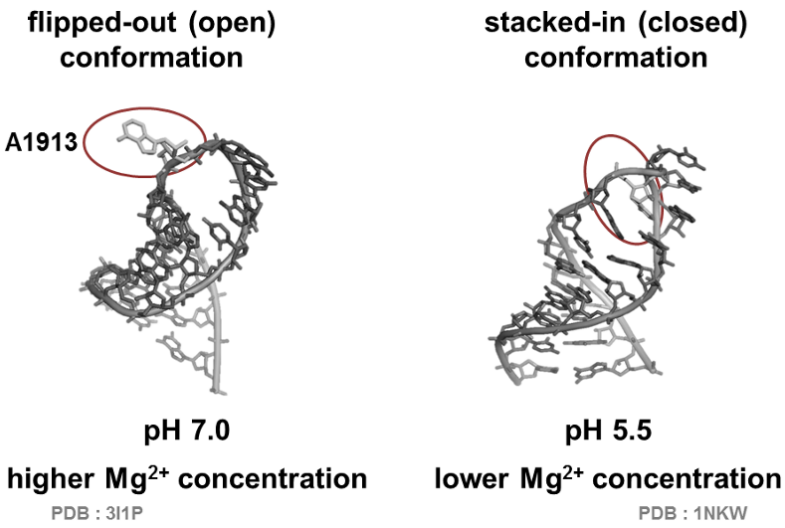


**Figure 1.8.** Two different conformational states of H69 are shown. The H69 domain from X-ray crystal structure of either 70S (open)[69] or 50S (closed)[55] ribosomes is shown.

### 1.3. Peptides as drugs

#### 1.3.1. General information on peptide drugs

Peptides have been used as drugs for more than 70 years,[70] and have been promoted in the field since Merrifield developed solid-phase peptide synthesis.[71] Traditional

peptides such as oxytocin, insulin, and cyclosporine are still commonly used. There are also newer peptide drugs developed commercially in use.[70, 72] Lantus developed by Sanofi-Aventis, also known as insulin glargine (an insulin analogue that helps control sugar level of diabetic patients), was one of the top ten biological drugs sold in 2013.[73] Its structure is very similar to insulin, except that the asparagine residue at position 21 was replaced with glycine, and two arginines were added to the *C*-terminus. The arginines raise the pI of the peptide, causing it to aggregate under physiological conditions such that release into the bloodstream is slowed down.[73-74]

Peptides are desirable drug candidates because of low toxicity, high diversity of sequences, lower immunogenicity, and high specificity for their targets.[70, 75] If the shortcomings of peptides, such as poor membrane permeability or poor metabolic stability could be overcome, peptides would be ideal drug candidates.[70, 75] There are many ongoing studies to improve peptide-based ligands as potential drugs (**Figure 1.9**).[75-76]

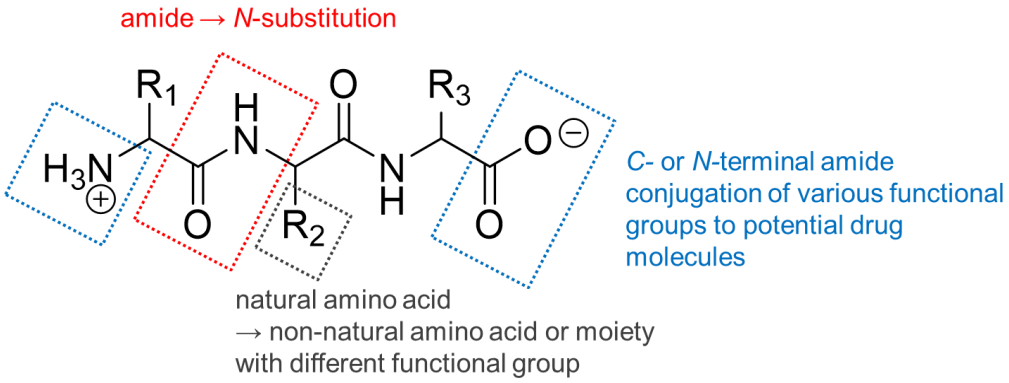


**Figure 1.9.** A generic peptide structure along with some possible modifications is depicted.

One of the methods for improving peptide function is conjugating them to a moiety that has desired activity, such as increasing cell permeability or potency.[77-79] In general, peptides tend to have poor cellular delivery, which can be improved by attaching a

hydrophobic chain, lipids, or sugar moieties. Similarly, conjugating a peptide to a potent drug molecule can lead to synergistic effects.[80]

A weakness of peptides as drugs is their short half-life due to degradation by peptidases.[81-83] However, several methods utilize D-amino acids, non-natural amino acids, peptoids, or cyclization to decrease recognition and breakdown by peptidases, thus improving drug stability.[81, 84-85] Synthetic peptides have other advantages as drug leads because they can be improved in relatively easy fashion, through methods such as peptide scanning of alanine, proline, or D-amino acids.[83, 86-87] Through amino acid scans, important residues for the configuration and activity of a peptide can also be determined.[83] Peptoids employ *N*-substituted glycine to alter the peptide backbone and make it resistant to peptidases.[88] Furthermore, various functional groups can be attached to the amino group, allowing development of large combinatorial libraries.[89]

Combinatorial libraries have been widely used, not only to screen for new drugs against known targets, but also for known drugs against new targets.[90] In addition, structure-activity relationship (SAR) studies that employ molecular dynamics simulations to predict or optimize new drugs have been increasing in the medicinal chemistry field, particularly due to advances in computational chemistry.[76-77, 91] For such applications, peptides are typically easier to synthesize than complex natural products. Nowadays, development of native chemical ligation or click chemistry has also allowed for larger peptides to be generated and tested for activity.[92-93]

### 1.3.2. Antimicrobial peptides

In nature, antimicrobial peptides (AMPs) are produced in plants, fungi, and animals, so that the organisms can protect themselves from microorganisms. The first AMP, defensin, was discovered through extraction from soil by Dubos in the 1930s.[94] Some examples of antimicrobial peptides are listed in **Table 1.2**. Most AMPs target the cell

membrane, strongly relying on their highly charged structures.[95-96] Some of the commonly used AMPs target the ribosome as well.[84]

**Table 1.2.** Antimicrobial peptides and their targets

| name | description | mode of action |
|---|---|---|
| defensin[94] | Cys-rich cationic antimicrobial peptide (AMP) forming β sheets | forms pores in membranes, inducing ion loss |
| vancomycin[97] | tricyclic branched glycopeptide | inhibition of cell wall synthesis |
| capreomycin[98] | cationic cyclic peptide | inhibition of translocation by interacting with h44 and H69 of 70S ribosomes |
| edeine[6] | pentapeptide with non-natural amino acids and a polyamine | translation-initiation inhibition by targeting the 30S subunit |
| thiostrepton[99-100] | macrocyclic thiopeptide with multiple post-translational modifications | translation inhibition by blocking IF2 and EF-G |
| daptomycin[101] | 13-mer cyclic peptide with a decanoyl group attached | disrupts cell membranes by forming aggregation that makes pores, leading to ion loss |

In **Figure 1.10**, the structures of several AMPs are shown. Vancomycin (**Figure 1.10a**) is a glycosylated cyclic peptide that disrupts cell wall synthesis. Unlike the well-known penicillin that forms a peptidoglycan intermediate with a β-lactam, vancomycin blocks transpeptidation and transglycosylation by forming five hydrogen bonds with the peptidoglycan, a property that is enhanced by the concave structure of the drug.[102]

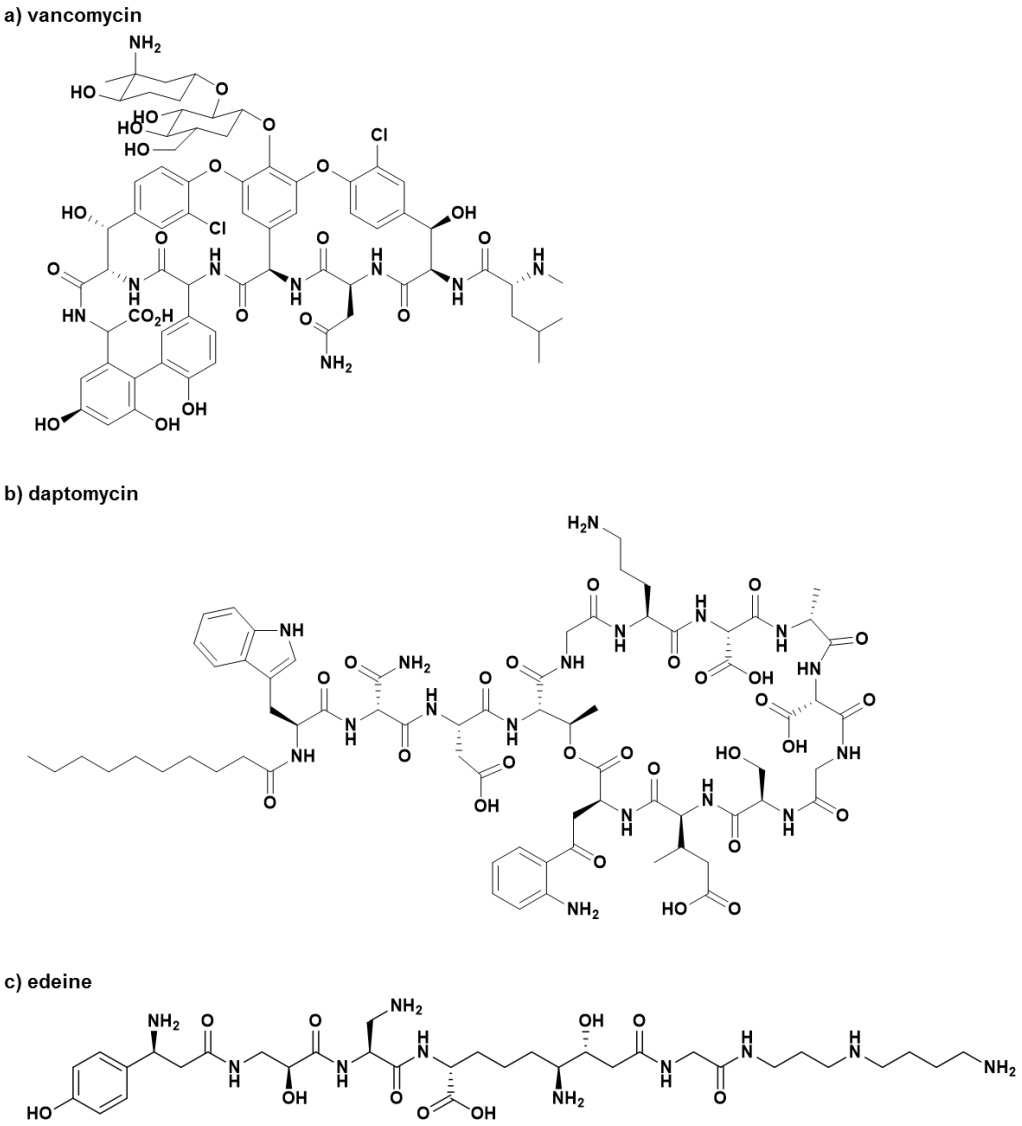


**Figure 1.10.** The chemical structures of several antimicrobial peptides

Daptomycin is a membrane-active lipopeptide that was originally extracted from *S. roseosporus* and is now produced synthetically.[96] Daptomycin has a cyclic peptide structure with D-amino acids and a hydrophobic decaonyl chain.[103] The decanoyl chain attaches the peptide to the membrane. As can be seen in **Figure 1.10b**, the peptide structure contains multiple carboxylic acid groups, making it negatively charged.[103] The anionic peptide attracts $Ca^{2+}$ ions, and after the decanoyl chain attaches itself to the

membrane, a micelle-like structure of daptomycin forms a pore and disrupts the membrane.[96]

Edeine (**Figure 1.10c**) targets the 30S subunit and inhibits translation initiation by blocking fMet-tRNA binding at the P site (peptidyl site).[6, 104] Edeine possesses non-natural amino acids such as β-serine, 2,3-diaminopropanoic acid (DAPA), 2,6-diamino-7-hydroxyazelaic acid (DAHAA), β-tyrosine, and spermidine, which make this molecule highly positive. The cationic nature of the peptide facilitates its interactions with negatively charged rRNA.

The ribosome is a common target for AMPs. Capreomycin (**Figure 1.11**) and viomycin inhibit translocation by interacting with h44 and H69 of the 70S ribosome.[98, 105] Capreomycin is a cyclic peptide containing a decanoyl chain and amino groups that provide cationic properties. The constrained ring structure allows capreomycin to position itself in the binding pocket that includes A1493 of h44 and A1913 and C1914 of H69.[106] Another peptide drug oncocin targets the 70S ribosome by blocking access to the A and P sites, PTC, and the peptide exit tunnel of the 50S subunit.[107] The AMPs are typically rich in cationic residues and interact with the ribosome through H-bonding, charge-charge, or π-interactions, which can be weakened by modification.[105, 107]

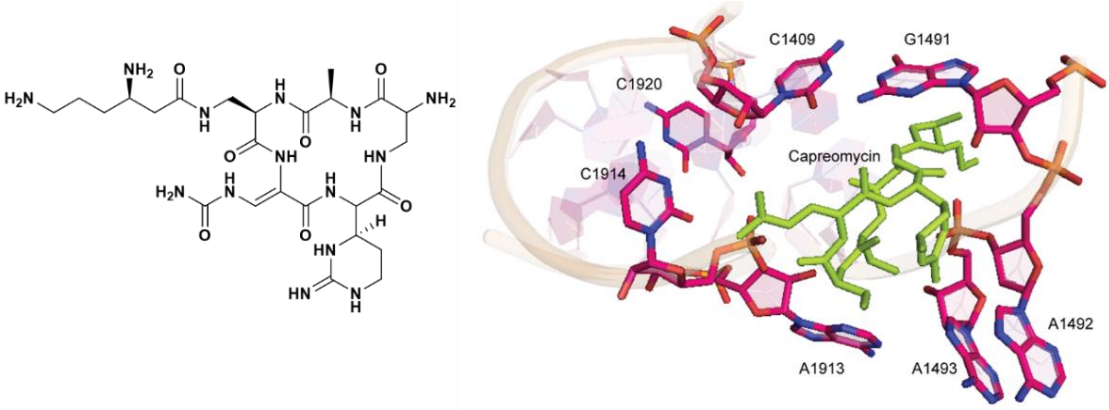


**Figure 1.11.** Antibacterial peptide capreomycin IB, a drug that targets the ribosome, interacts with A1492, A1493, and G1491 of h44, and A1913 and C1914 of H69 and acts by disrupting the interface between h44 and H69 (PDB ID 3KNO).[106]

## 1.4. Background on techniques used in this study

### 1.4.1. Phage display

Phage display was developed by George P. Smith in the early 90s.[108-109] Phage display is a biological tool that uses phage particles to express peptides on their surfaces, which can be used to select peptides that have binding affinity to a target of interest.[109] In this study, the Ph.D.-7 library from New England Biolabs was used. This is a linear heptapeptide library of $20^7$ size complexity (diversity). By integrating DNA sequences encoding the peptide that will be expressed on the pIII coat protein into the M13KE vector, a randomized phage library is obtained. The pIII coat protein is a minor protein among those proteins that comprise the phage particle, which allows it to attach and infect the host. The pIII coat protein is composed of five copies of proteins, to which the randomized peptides are attached through their *N*-termini (**Figure 1.12**). Therefore, five copies of the peptides are expressed on the phage surface. The diversity in peptide sequences is $20^n$ (where n is the number of amino acids in the peptide), and therefore a pool of peptide ligands can be expressed and selected for affinity to a given target.[109-110] The foreign peptide or protein can also be engineered to be attached to other coat proteins or antibodies or manipulating the number of peptides displayed.[111-114]

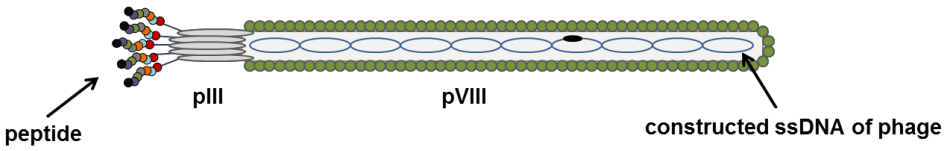


**Figure 1.12.** A generalized structure of M13 phage used for phage display

The DNA of the phage encode a *lac* operon to allow for blue/white screening. Therefore, after each round of selection, the phage can be titered and quantified. Phage titering is an important technique for molecular biology, and in this case, for the phage display method. Following a selection experiment, it is of interest to determine the phage population. In order to quantify this process, the number of phage plaques were counted

after each step of biopanning. Ideally the number of plaques should be about 50 to 500 on each agar plate. Because the phage are viruses, they can use a host such as *E. coli* to reproduce. For the commercial Ph.D.-7 libraries, randomized peptide sequences are inserted into the vector M13KE to be expressed on the *N*-terminus of the pIII coat protein.[115-117] The peptide sequences are inserted in between restriction enzyme sites *EagI* and *KpnI*, with Gly-Gly-Gly-Ser in between the peptide sequence and the pIII surface. A yield can be obtained for the phage selection by comparing the number of input and output phage. Following this step, the phage are amplified using *E. coli* as a host. This step provides enough phage to carry out the biopanning step again. In the case of the Ph.D.-7 library, the initial selection step starts with $20^7$ clones, which contain 1.3 million different sequences with 70 copies each. Thus, carrying out 3 to 4 rounds of selection and getting hundreds of sequences are necessary to identify consensus motifs.

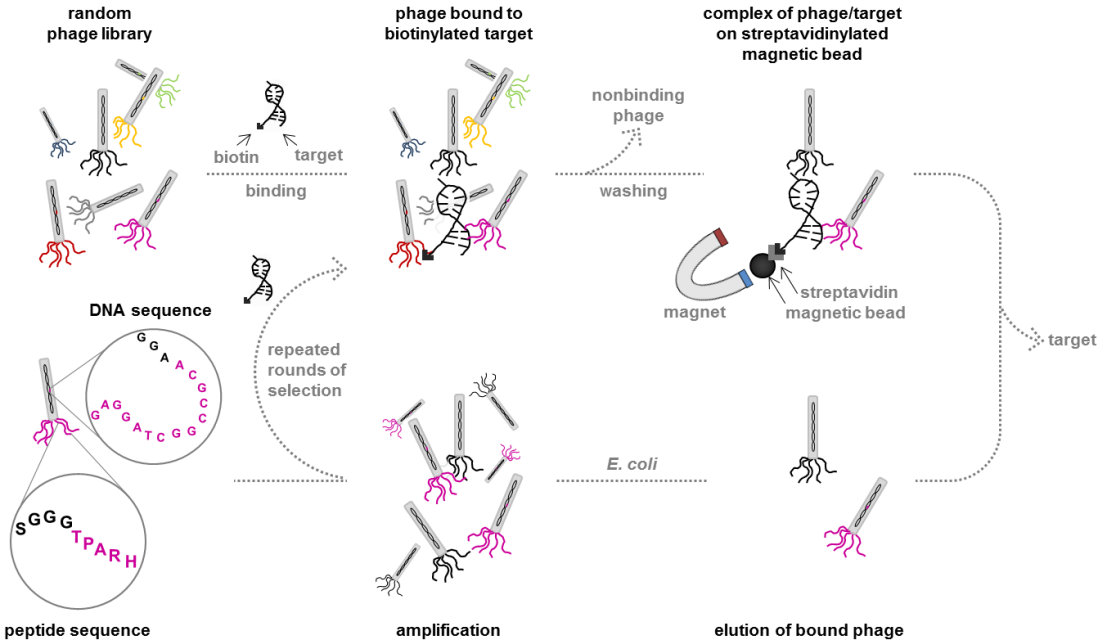


**Figure 1.13.** A general scheme of phage display (biopanning procedure) is shown. To a random phage library, biotinylated target is added. Following incubation, streptavidinlyated magnetic beads are added, and after several washing steps, the bound phage is isolated. Specific/nonspecific elution allows disruption of the complex of phage/target on streptavidinlyated magnetic beads and bound phage are obtained. The bound phage are amplified using *E. coli* as the host. After several repeated rounds of biopanning, the DNA encoding the peptides binding to the target can be identified.

The general protocol (referred to as biopanning) for the phage display experiment is summarized in **Figure 1.13**. The library is incubated with a target that is attached to a surface such as a magnetic bead using streptavidin-biotin chemistry. The phage having affinity to the target can be isolated after the washing steps. In nonspecific elution, noncovalent interactions of the target and phage are disrupted by adding an acidic buffer and the bound phage are released from the target. Specific elution involves incubation with a non-biotinylated target that competes for binding to the selected phage with the immobilized target. Addition of either the target or a variant of the target for counter selection allows for selective elution of phage with affinity for a given molecule, rather than eluting all bound phage that may include some nonspecific binders.

In previous studies in our lab, phage display has been performed under physiological buffer systems against h31, h44, or H69.[118-120] In this thesis work, phage display against H69 was done under several different buffer conditions, and mainly focused on phage display at low pH (pH 5.5). A previous study employed phage display at low pH to select peptides targeting amylases.[121] The low pH was shown to increase binding of phage to the target; however, overall phage survival was lower and more polar sequences were selected.[121] In this study, selection was carried out with nonspecific elution to ensure higher yields of bound phage. To our knowledge, there have not been phage display studies done at low pH against RNA.

One challenge in this study, which will be discussed in a later chapter, is that our RNA target is an essential component of the bacterial ribosome. Because we use *E. coli* as the host for amplification, any peptides that display antibiotic activity through rRNA (H69) targeting will be lethal, and therefore will not be amplified. Therefore, the possibility of selecting a peptide that is fatal for the host is low. Also, some phage are known to be fast growers over other phage, which can decrease the chance of slow-growing phage to be potent. However, considering that the small peptides selected through phage display

are likely to have only moderate binding affinities, the selected peptides will be considered only as starting peptides (*i.e.*, "parents") that can further be modified through amino acid scanning or structure-activity relationship (SAR) studies.

### 1.4.2. Solid-phase peptide synthesis

Solid-phase peptide synthesis was first developed by Bruce Merrifield in 1963, proceeding through anchoring the *C*-terminus of an amino acid onto a solid support.[71] The solid supports are polymer-based resins, and the functional groups vary so that the C-terminus of the cleaved peptide can be a carboxylic acid or an amide.[122] Depending on the size or use of the desired peptide, one can choose resins with different loading levels or swelling properties.

Usually amino acids with a fluorenylmethyloxycarbonyl (Fmoc) on the *N*-terminus are employed (**Figure 1.14**), wherein Fmoc is a base-labile protecting group.[123-124] The side chains are typically protected with acid-labile protecting groups. Having orthogonal protecting groups is essential for the sequential addition of selected amino acids.[125]

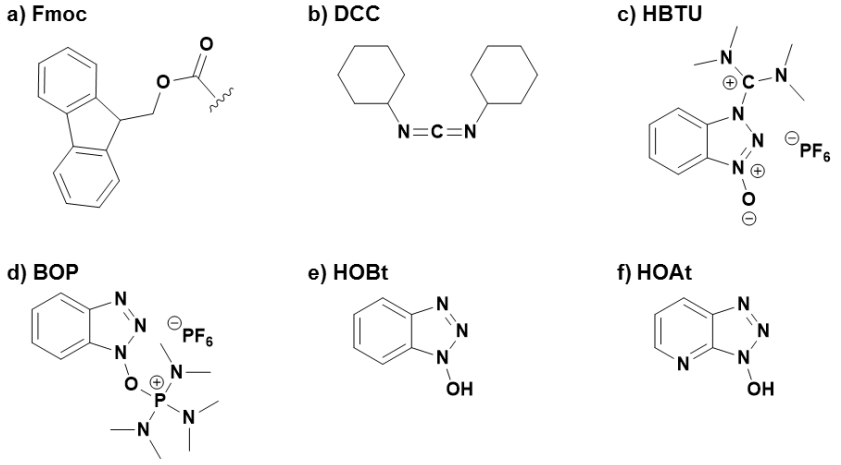


**Figure 1.14.** Structures of reagents commonly used in solid-phase peptide synthesis are shown.

Addition of Fmoc-protected amino acids is done with carboxylate-activating coupling reagents, such as *N,N'*-dicyclohexylcarbodiimide (DCC).[71] Hydroxy groups are poor

leaving groups, so addition of a carbodiimide activates them to increase the electrophilicity of the carbonyl group. To the reaction, the coupling agent is added at a concentration of 2 equivalents (2 *eq.*) relative to the amount of resin (*i.e.,* if there is 1 g of 0.68 mmol/g, 1 *eq.* is 0.68 mmol), along with 2 *eq.* of Fmoc-protected amino acids, to facilitate the reaction. However, the byproduct of the reaction is urea-based, and in the case of DCC coupling, racemization can occur.[126] To reduce this problem, phosphonium salts such as Castro's reagent (benzotriazol-1-yloxytrisphosphonium hexafluorophosphate, BOP) or *O*-(benzotriazol-1-yl)-*N,N,N',N'*-tetramethyluronium hexafluorophosphate (HBTU) were developed as alternative coupling agents.[127] Additives such as 1-hydroxybenzotriazole (HOBt) or 1-hydroxy-7-azabenzotriazole (HOAt) may also be added to increase the rate and yield of the reaction.[126] In addition, 4 *eq.* of diisopropylethylamine (DIPEA) are added to deprotonate the carboxylic acid as well as the amino groups of the Fmoc-protected amino acids. Coupling with these reagents allows a one-pot synthesis of the peptides to be done.

**Scheme 1.1.** Structures of the resins used in this study with a general scheme of solid-phase peptide synthesis

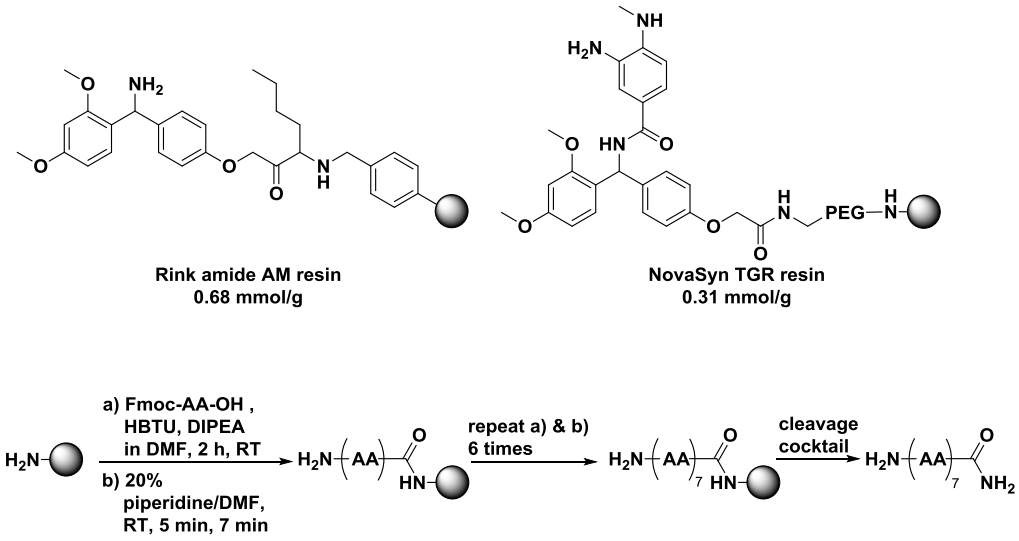

As shown in **Scheme 1.1**, Fmoc-protected amino acids and coupling reagents are added to the resin, followed by deprotection of the Fmoc group using 20% piperidine/DMF. This step is generally performed by adding the basic solution once for 5 min, the solution is then removed, followed by addition of the basic solution for an additional 7 min.

When the peptide coupling steps are completed, the final Fmoc protective group is removed, the peptide is cleaved from the solid support, and removal of the acid-labile protecting groups are removed by using a "cleavage cocktail".[128] The cleavage cocktail typically contains trifluoroacetic acid (TFA) with various scavengers, such as triisopropylsilane (TIPS), thioanisole, phenol, and water. When the protecting groups are cleaved by TFA, radicals can be formed, which can react with the peptide products. Therefore, scavengers are added to increase the purity of the products by capturing the protecting groups. The concentration of each component varies depending on the protecting group or resin in use.

Following incubation with the cleavage cocktail, the slurry is filtered into cold diethyl ether to precipitate the peptide, and after several washes, a crude peptide is obtained. For short peptides, or those with high solubility in ether, precipitation may be inefficient, wherein extraction with organic solvents may be needed. For further purification, high performance liquid chromatography (HPLC) is typically used. In cases in which the peptide is insoluble in water due to high hydrophobicity, HPLC cannot be used for purification. In such cases, extraction in organic solvents followed by column chromatography or prep-TLC (thin layer chromatography) can be used.[129]

Solid-phase peptide synthesis has been widely used because of its advantages compared to conventional solution-phase organic synthesis.[124-125] In general, the procedures are relatively simple and the products can be obtained with high yields and

purity because of the washing and filtering steps, which can also be automated. Unlike natural products that require multi-step syntheses in controlled systems, peptides are easier to synthesize and modify. Therefore, with starting parent sequences or motifs, the development of a potent therapeutic by rational design has been emerging.[130-131] Development of peptoids, cyclic peptides, and multimeric peptides has expanded the range of peptide-related drugs.[89, 130, 132,133] Pharmaceutical research can now leverage these tools in discovery of peptide-related drugs.

### 1.4.3. Fluorescent intercalator displacement (FID) assay

Fluorophores (or dyes) absorb specific wavelengths of light (excitation), followed by emission as they relax.[134] Due to the fact that one can selectively monitor a molecule with fluorescence spectroscopy, many binding studies rely on fluorescence by attaching a dye to the molecule of interest (*i.e.*, the target).[67, 135-136] However, because the dye tag can alter binding affinities of the target, label-free methods are preferred if possible. Most fluorophores used in fluorescence studies have planar structures with multiple aromatic rings conjugated with high resonance, which not only delocalizes the electrons, but allow for favorable interactions with DNA or RNA. A fluorescent intercalator displacement (FID) method is a label-free experiment involving a dye that fluoresces only when it is intercalated or surface bound to the target.[137-141] The fluorescence then generally decreases if a ligand binds and removes the dye through direct or indirect displacement, such as changing the conformation of the target.[140-141] The FID assay has several advantages as a screening assay. First, utilization of a sensitive dye requires only a low amount of material (for both the dye and target). Second, this assay is simple, both in terms of sample preparation and data collection, compared to methods such as surface plasmon resonance (SPR) or electrospray ionization mass spectrometry (ESI-MS) (see **Sections 1.4.4** and **1.4.5**). Third, physiological buffers are typically suitable for use in these experiments, which is not possible with ESI-MS or nuclear magnetic resonance

(NMR). However, there are some weaknesses with the method. One weakness is that only a change in signal is detected, indicating a binding event, but not the binding site. Another shortcoming is that because the dye is displaced by a ligand under equilibrium conditions, there is competition between the ligand and dye for the target, which makes the FID assay a qualitative rather than a quantitative method. In addition, a lack of fluorescence change does not necessarily mean that a binding event did not occur. Despite the shortcomings noted, this method is still relatively fast and can be used in a 96- or 386-well plate format, making it a good tool for high throughput screening (HTS).[138]

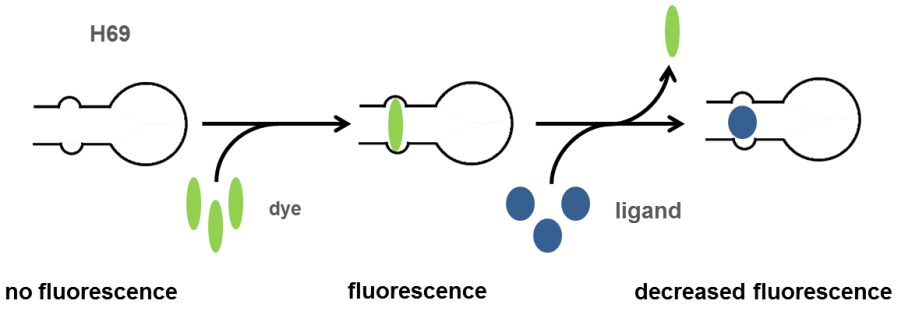


**Figure 1.15.** The general scheme for the FID assay is shown. To the target (non-fluorescent), a dye is added that fluoresces when bound. Addition of a molecule (non-fluorescent ligand) that can remove the dye by direct displacement or by a change in target conformation leads to decreased fluorescence.

### 1.4.4. Electrospray ionization mass spectrometry (ESI-MS)

Electrospray ionization mass spectrometry (ESI-MS) is a soft ionization technique that can be used to determine the mass of a molecule or a target-ligand complex.[142] The method has many strengths. ESI-MS is very sensitive, therefore only requires a small amount of sample (pmol to low nmol range), which does not need to be labeled or tagged. In addition, the apparent dissociation constant, or $K_d$, and stoichiometry of the complex can be obtained. The components of a mass spectrometer typically include an ionizer, analyzer, and detector (**Figure 1.16**). The electrospray process nebulizes the liquid to form highly charged droplets, then a heated nitrogen gas helps to evaporate the

solvent and reduce the droplet size.[143-144] The charges move to the surface to minimize Coulombic repulsion and form ions, and as the solvent evaporates the droplet sizes get smaller. When the Coulombic repulsion exceeds the surface tension (Rayleigh limit), the droplets explode to make smaller droplets.[142] This step leads to fragmentation of the droplet. Compared to laser-assisted methods such as MALDI-TOF, ESI-MS is a soft ionization method. The droplets travel through the analyzer, which filters the ions according to their mass-to-charge ratio (m/z). Those that reach the detector are recorded. The soft ionization of ESI-MS allows noncovalent interactions of complexes to be monitored.[142, 145] Therefore, this method is a powerful tool for examining binding of various ligands to biomolecules such as RNA.[146-147] ESI-MS also provides the stoichiometry of the complexes, which is an advantage when trying to understand ligand binding modes.

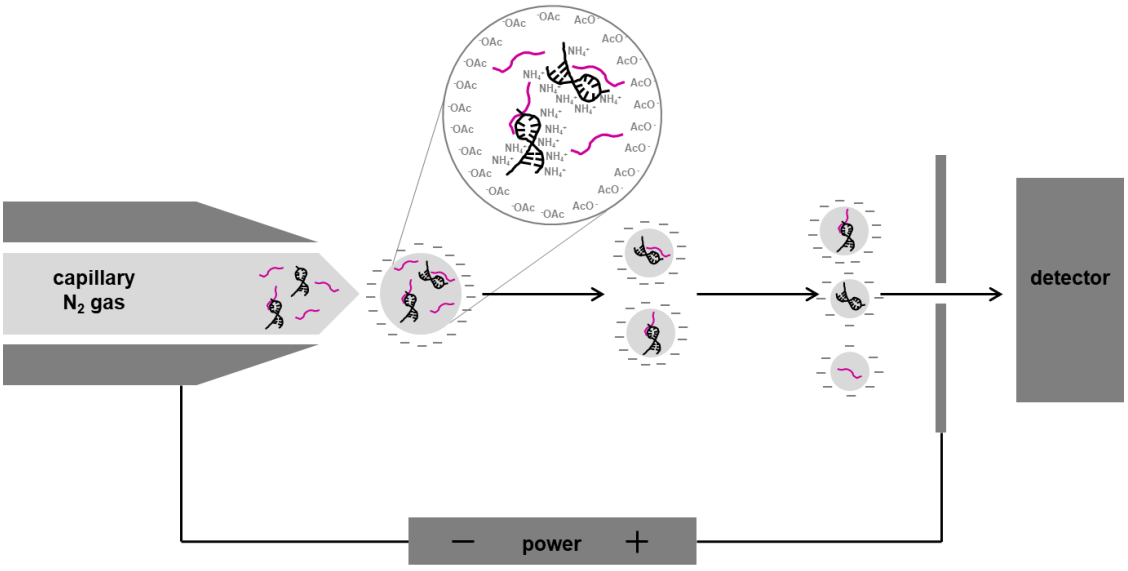


**Figure 1.16.** A general depiction of ESI-MS is given. In RNA-peptide binding studies, the negative ion mode is used. The negative charges on the RNA are neutralized by $NH_4^+$, and $AcO^-$ ions are located on the surface of the droplets, which does not change the overall charge of the molecule. As the negatively charged droplets travel through the source region or mass analyzer, they break into smaller droplets due to Coulombic repulsion, and reach the detector as single ions.

As with the other methods mentioned, there are limitations to the ESI-MS method. The ideal salt concentration of the buffer used in ESI-MS experiments is usually 10-20 mM, which is much lower than physiological conditions.[148] Furthermore, $Na^+$ or $K^+$ typically need to be eliminated, because adducts with these salts can give poor fragmentation and high noise levels. Studies have shown that an increase in the salt concentration also alters the charge state distribution, and can disrupt hydrophobic interactions between molecules.[149-150] Volatile solvents such as acetonitrile or isopropanol are typically employed in ESI-MS. Although these solvents are not physiological buffers, they can help the droplet formation by decreasing the surface tension.[145] The ionization efficiencies of the free target and complex can be different.[146] Therefore, it is necessary to use complementary methods to verify the binding constants obtained from ESI-MS.

### 1.4.5. Surface plasmon resonance (SPR)

#### 1.4.5.1. The principle of SPR on Biacore

As mentioned in previous sections, binding affinities or dissociation constants can be measured using a variety of methods, each with advantages and limitations. Surface plasmon resonance (SPR) (*e.g.*, Biacore) is another powerful method to study biomolecular interactions.[151] A surface plasmon is an electromagnetic wave that occurs when a beam of incident light is shone onto a prism with a thin gold surface. The light generates an evanescent wave with refraction occurring along with reflection (**Figure 1.17a**). At the angle where there is total reflection and no refraction, the angle is called the total internal reflection (TIR). At an angle that is larger than TIR, surface plasmon resonance (SPR) takes place, and the energy of the photon converted into a plasmon creates a dark band in the reflected light (**Figure 1.17b**). The dark band shifts when there is a change in the refractive index (*i.e.*, change on the surface mass). The TIR angle is related to the mass of the surface, and a mass change results in a shift of the

TIR angle. Therefore, by monitoring the change of mass on a surface with an immobilized target, binding of a ligand can be quantified (**Figure 1.17c** and **1.17d**).[152-153]

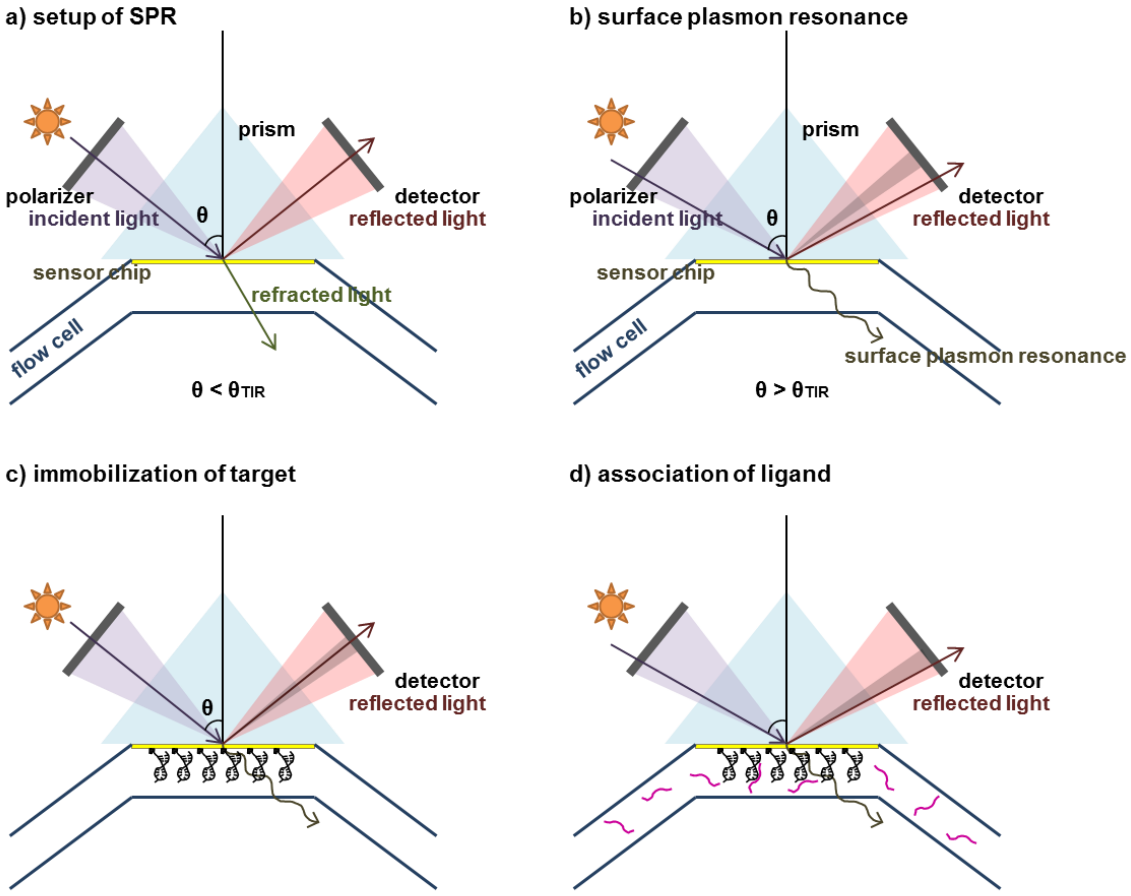


**Figure 1.17.** A description of surface plasmon resonance is given. a) The light shone generates an evanescent wave, with refraction occurring along with reflection. The angle where there is total reflection and no refraction is called the total internal reflection (TIR). b) At an angle that is larger than TIR, surface plasmon resonance (SPR) takes place, and the energy of the photon converted into a plasmon creates a dark band in the reflected light. c) The TIR angle is related to the mass of the surface, and a mass change results in a shift of the TIR angle. d) By monitoring the change of the TIR angle, and thus the mass, on a surface with an immobilized target, binding of a ligand can be quantified.

The SPR method also has several strengths and weaknesses. SPR requires only small amounts of material (pmol to nmol) compared to NMR spectroscopy. By flowing through ligands (called “analytes” in SPR)[152] that have affinity to the immobilized target

(often called “ligand” in SPR), real-time binding can be monitored. This method provides information of kinetics of the interaction along with the apparent dissociation constant. In this case, a wide range of buffers can be used, which allows studies to be carried out under differing conditions including physiological salt concentrations and pH values. Thus, the ability to obtain kinetic information under high salt conditions makes this method advantageous compared to ESI-MS or NMR spectroscopy.

Despite the advantages of SPR, the Biacore system requires use of an expensive sensor chip. In order to immobilize a molecule onto the sensor chip, a tag such as biotin needs to be attached to the target. Also, the signal detected is correlated with the change in mass of the surface; therefore, when a lighter molecule is immobilized as a target, the change of signal when a larger ligand binds is detected more clearly.[154] For studies of RNA-peptide interactions, the RNA is usually immobilized to the surface due to its high cost. To increase the response to smaller ligands, RNA is typically immobilized in high density.[155] As a result, mass transport can also be a problem, which is caused when the binding rate of the ligand to the target is faster than diffusion.[156] Smaller amounts of the target need to be immobilized in order to minimize mass transport effects. In RNA-peptide binding studies, this can cause a conflict with the need for higher loading levels of RNA. Therefore, optimization is required to find the maximal amount of target to immobilize in order to reduce mass transport problems.

**1.4.5.2. Bio-Layer Interferometry (BLItz)**

SPR is an ideal method for monitoring biomolecule interactions; however, the Biacore system is not cost or time efficient compared to methods such as FID. Recently, companies have been developing more cost-effective instruments that operate with similar methods.[157-158] For example, bio-layer interferometry (BLItz) is one of those techniques.[157, 159-161] Though the actual mechanism of the technology is proprietary, the method is based on SPR using white incident light. The light is shone onto the biosensor

with a target immobilized, and when there is a change on the surface, the signal obtained from the biosensor changes. However, a detailed mechanism of the instrument is not provided.

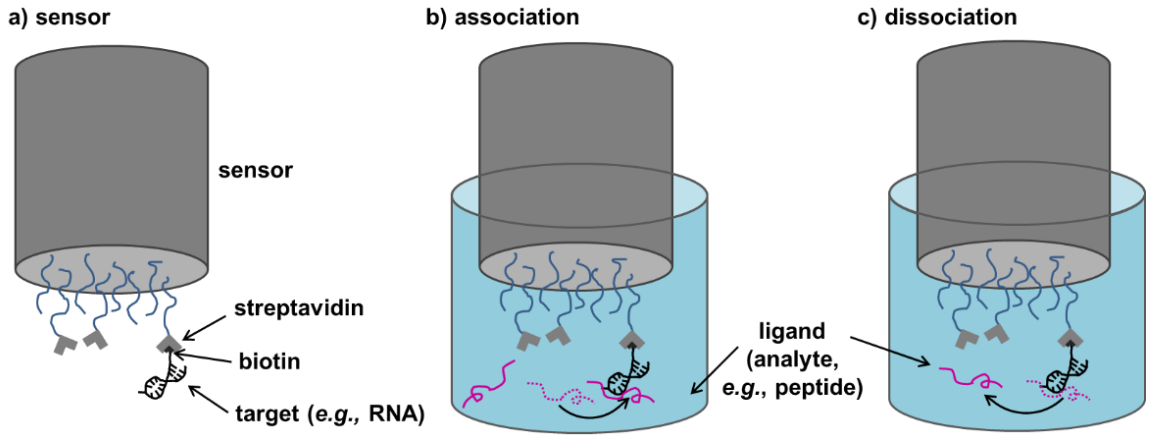


**Figure 1.18.** A schematic diagram of BLItz is shown. a) The sensor components are given. To an optical sensor with streptavidin, a biotinylated target can be immobilized. b) For association, the sensor with the target immobilized is dipped into a buffer containing the ligand, and the association is observed. c) The sensor from b) is dipped into buffer, and the dissociation is measured.[162]

There are two differences between this method and Biacore SPR. One is that the sensor is on a tip that can be easily removed and immobilized with target. The other difference is the association/dissociation method.[157, 162] In Biacore, there is a flow of the buffer containing ligand to allow for association and dissociation.[162] In BLItz, the tip sensor is place into a solution containing the ligand for the association step (with agitation of the sample), and then the tip sensor is placed into another buffer for the dissociation step (**Figure 1.18**).[161] In SPR, the concentration of the ligand solution or buffer stays constant but is flowing over the target. In BLItz the concentration of the ligand solution or buffer may decrease or increase during the association or dissociation step, which may affect the true binding. Therefore, to minimize concentration effects, fresh samples are required, and the sample is agitated takes place while monitoring association and dissociation.

### 1.4.6. Nuclear magnetic resonance (NMR) spectroscopy

NMR spectroscopy is a useful technique for observing RNA structure in solution. Each nucleus of a molecule has an electric charge and spin, which gives a unique chemical shift when an external magnetic field applied. Depending on the chemical environment of the atom, which can vary with neighboring functional groups or interactions, the chemical shifts or coupling patterns are affected. In this study, 2D proton homonuclear correlation spectroscopy (ge-2D COSY) was used to monitor the resonance from the crosspeaks between the H5 and H6 of pyrimidines.[163] This method detects proton coupling; therfore, a change in the chemical environment upon ligand binding can be monitored. Compared to other 2D NMR experiments, COSY experiments require less sample (3 OD, 15 nmol). Therefore, for binding experiments with expensive targets such as the RNA, COSY was selected as the best NMR method.

There are strengths and limitations to NMR spectroscopy. When there is a change in the chemical shift, this typically indicates a change in the local chemical environment such as an altered conformational state of the molecule or interaction with a ligand. In this thesis work, NMR spectroscopy was used for RNA-peptide binding studies. This method can give information about the binding site (*i.e.*, which nucleotides interact with the ligand), which is not obtained directly from SPR or fluorescence studies. However, NMR requires large amounts of highly pure sample. Synthetic RNA, which is typically necessary for modified samples, is expensive; therefore, this method is not as cost-efficient as ESI-MS or fluorescence studies. Because of the various limitations, it is best to have more than one method to obtain the apparent dissociation constant ($K_d$) for a target-ligand complex. In **Table 1.3**, the strengths and limitations of the approaches used for binding studies in this thesis work are summarized.

**Table 1.3.** A comparison of various biophysical methods for determining RNA-ligand interactions.

| Method | Advantages | Disadvantages |
|---|---|---|
| FID assay | ▪ pmoles of sample required (both dye and target)<br>▪ simple to perform<br>▪ label-free<br>▪ physiological buffer can be used | ▪ cannot obtain apparent $K_d$ directly<br>▪ cannot determine stoichiometry<br>▪ changes in fluorescence are difficult to predict or interpret |
| ESI-MS | ▪ pmoles of sample required<br>▪ apparent $K_d$ values obtained<br>▪ stoichiometry obtained<br>▪ label-free | ▪ cannot use physiological buffers<br>▪ extensive sample purification required |
| SPR | ▪ pmoles of sample required<br>▪ physiological buffer can be used<br>▪ apparent $K_d$ values obtained<br>▪ kinetic information obtained | ▪ need to label the target<br>▪ typically the ligand needs to be larger than the immobilized target<br>▪ expensive instrumentation and consumables |
| BLItz | ▪ more cost and time effective compared to SPR<br>▪ pmoles of sample required<br>▪ physiological buffers can be used<br>▪ apparent $K_d$ values can be obtained | ▪ need to label the target<br>▪ typically the ligand needs to be larger than the immobilized target<br>▪ expensive consumables |
| NMR | ▪ label-free<br>▪ binding site of a ligand can be determined | ▪ large amount of sample required<br>▪ limitations on buffers<br>▪ challenging to obtain apparent $K_d$ values<br>▪ challenging to determine stoichiometry |

### 1.5. Overall project objective

Due to the rise of antibiotic resistance, there is a need for discovery of new targets and development of novel drugs. In our laboratory, we are interested in helix 69 (H69), an rRNA motif located in the B2a intersubunit bridge of the bacterial ribosome.[164] Helix 69 interacts with helix 44 (h44), A-tRNA, P-tRNA, RF, and RRF, and forms an intersubunit bridge B2a with h44, which makes it an interesting target.[30-32, 48, 165] Helix 69

also has post-transcriptionally modified nucleosides, pseudouridine (Ψ) and methylated pseudouridine ($m^3\Psi$).[48] Pseudouridine increases the stability of the helix by increasing base stacking, and is conserved across phylogeny.[47-48, 166] Helix 69 shows different conformations in 50S subunits and 70S ribosomes, which can be altered by changing buffer conditions or temperature of the system.[66-67] The goal of this project was to select a peptide ligand for binding to modified H69 in the stacked-in conformation. If we are able to find a peptide ligand that can bind to H69, this ligand may be able to disrupt H69 interacting with other factors or rRNAs, which will inhibit translation. Phage display was used to screen a peptide library under low pH conditions (pH 5.5) with $tRNA^{Phe}$ as a competitor to eliminate nonspecific binding peptides.

The binding studies were performed on model systems. The various methods used were *in vitro* experiments, which give information on the binding interactions in a controlled environment outside of the cell. Although the binding may differ *in vivo*, the *in vitro* experiments allow observations of the binding interactions at the molecular level. In this work, *in vitro* studies are useful because we can observe binding events at both pH 5.5 and pH 7.0 conditions for both ΨΨΨ and UUU H69, which is not possible for *in vivo* studies. By utilization of multiple methods, we were able to obtain information on the relative affinities and modes of binding, stoichiometries, and interaction sites for the peptide ligands. We hope these studies provide information for future studies on peptide-based antibacterial drugs.

## CHAPTER 2 – METHODS AND EXPERIMENTAL DESIGN

### 2.1. Preparation of the RNA

Modified H69 ΨΨΨ (5′-GGCCGΨAACΨAΨAACGGUC-3′) was purchased from Thermo Fisher Scientific (Waltham, MA) on a 1 μmol scale and unmodified H69 UUU was obtained by T7 RNA transcription as described below. Adenosine triphosphate (ATP), cytidine triphosphate (CTP), guanosine triphosphate (GTP), uridine triphosphate (UTP), acrylamide, bisacrylamide, urea, sodium acetate (NaOAc), triethylammonium acetate (TEAA), acetic acid ($CH_3COOH$ or AcOH), hydrochloric acid (HCl), ammonium persulfate (APS), acetonitrile (MeCN), sodium hydroxide, zinc chloride ($ZnCl_2$), ethanol, Microcon 3 (centrifugal filter unit YM-3 membrane), and alkaline phosphatase were purchased from Sigma-Aldrich (St. Louis, MO). Tris, boric acid, ethylenediaminetetraacetic acid (EDTA), dithiothreitol (DTT), spermidine, Triton X-100, ammonium acetate ($NH_4OAc$), and tetramethylethyldenediamine (TEMED) were purchased from Fisher Scientific (Hampton, NH). XTerra C18 column (10 x 50 mm, 2.5 μm) and Sep-pak SPE columns were purchased from Waters (Milford, MA) for a Waters 600 LC with a 717 autosampler (Waters, Milford, MA, USA) and UV-detector.

The H69 UUU was synthesized using T7 *in vitro* transcription.[166-167] To HPLC-purified DNA template (5′-GACCGTTATAGTTACGGCCTATAGTGAGTCGTATTA-3′) (10 μg, 0.9 nmol) and T7 promoter (5′-TAATACGACTCCTATAGG-3′) (4.9 μg, 0.9 nmol) in 1 mL of 1× transcription buffer (40 mM Tris-HCl, 2 mM spermidine, 0.01% Triton X-100), was added 7 mM NTPs, 10 mM DTT, and 100 U of T7 RNA polymerase (Epicenter, Madison, WI), followed by incubation at 37 °C for 4 h. The transcribed RNAs were purified on 20% denaturing polyacrylamide gels with 19:1 acrylamide/bisacrylamide, 1× TBE buffer (90 mM Tris, 90 mM boric acid, 1 mM EDTA, pH 8.2) and 7 M urea. The RNA band was visualized using UV shadowing, followed by excision and extraction through the crush-and-soak method. After eluting the RNA, ethanol precipitation using $1/10^{th}$ volume of 3 M

NaOAc was performed to desalt. Desalted RNA was then characterized by using MALDI-TOF MS as described below. Negative mode on Ultraflex Extreme TOF/TOF from Bruker (Billerica, MA) was used for detection. Three-Hydroxypicolinic acid (HPA) was used as the matrix.

Modified H69 ΨΨΨ was purified by HPLC (XTerra C18) in 25 mM triethylammonium acetate (TEAA), pH 6.5, by increasing the MeCN concentration from 6 to 12% over 30 min at a flow rate of 4 mL/min. The collected sample was dried *in vacuo*, followed by ethanol precipitation. The RNA was characterized by MALDI-TOF MS and 20% PAGE. For MALDI-TOF MS, 10 pmol of H69 ΨΨΨ in 1 µL of $ddH_2O$, 1 µL of supersaturated matrix and 0.05 µL of 10 mM $NH_4OAc$ were mixed and allowed to dry on a 384-well metal plate before measurement. Negative ion mode on Ultraflex Extreme TOF/TOF from Bruker (Billerica, MA) was used for detection, and 3-hydroxypicolinic acid (HPA, **Figure 2.1a**) was used as the matrix. After HPLC, the RNA purity was also checked by running denaturing 20% polyacrylamide gel electrophoresis (PAGE).

**a) 3-hydroxypicolinic acid (HPA)**

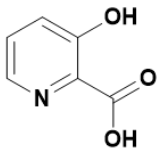


**b) 4-hydroxy-α-cyanocinnamic acid**

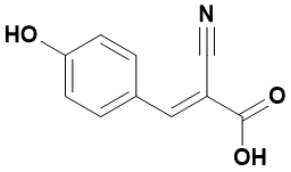


**Figure 2.1.** Structures of matrices used for MALDI-TOF studies are shown.

Digestion with P1 nuclease followed by HPLC analysis was used to confirm the presence of pseudouridine in the H69 ΨΨΨ sample. To 0.1 OD of H69 ΨΨΨ in 86.25 µL of $ddH_2O$ was added 10 U of P1 nuclease, 2.5 µL of 10 mM $ZnCl_2$, and 1.25 µL of 3 M NaOAc. The mixture was incubated at 37 °C for 18 h, followed by centrifugation at 5000

rpm for 30 min through a Microcon 3 filter. Then, to 60 µL of the flow-through was added 5 µL of alkaline phosphatase and 3.6 µL of 1 M Tris-HCl (pH 8), and the mixture was incubated at 37 °C for 4 h, followed by centrifugation at 5000 rpm for 30 min through a Microcon 3. The flow-through was diluted to 100 µL, followed by separation by HPLC. A Discovery C18 column (Supelco C18 4.6 × 250 mm, 5 µm, Sigma-Aldrich, St Louis, MO, USA) on a Waters 600 LC with a 717 autosampler (Waters, Milford, MA, USA) and UV-detector was used for separation of the mixture, with 40 mM $NH_4OAc$ and 40% MeCN used as the buffer. The column was equilibrated with 40 mM $NH_4OAc$, and the eluents were separated with increasing concentration of MeCN from 0 to 12% over 30 min.

For studies such as ESI-MS and NMR studies that are sensitive to impurities and buffer conditions, extensive desalting of the RNA is required. In addition to ethanol precipitation, Sep-pak SPE columns were used for desalting. Each desalting process was done on 50 nmol or less of RNA. The column was first activated by using 10 mL of MeCN, followed by washing the column with 10 mL of $ddH_2O$. After the column was washed, the RNA was loaded to the column, followed by washing the RNA with 20 mL of $ddH_2O$. After desalting, the RNA was eluted with 30% MeCN in $ddH_2O$. The eluted RNA was quantified with UV spectroscopy, and lyophilized before use. The extinction coefficients for ΨΨΨ and UUU H69 were 187,000 $Lmol^{-1}cm^{-1}$ and 189,400 $Lmol^{-1}cm^{-1}$, respectively.[45]

**2.2. Phage display performed against H69**

**2.2.1. Biopanning**

In this study, buffers with differing pHs were used for RNA binding. For higher pH conditions, 20 mM HEPES-KOH, pH 7.0, 100 mM KCl, 5 mM $MgCl_2$, 5% glycerol, 0.1 mg/mL BSA with 0.1% (v/v) Tween-20 (buffer A) was used, and for the lower pH buffer, 20 mM PBS, pH 5.5, 100 mM KCl, 5% glycerol, 0.1 mg/mL BSA with 0.1% (v/v) Tween-20 (buffer B) was used. To 200 µL of buffer A or B in 1 mL microcentrifuge tube was

added the phage library pre-incubated with M-280 streptavidin-magnetic beads ($2 \times 10^{11}$ pfu) and 30 pmol of target (biotinylated UUU, 10 μM, **Figure 2.2**).

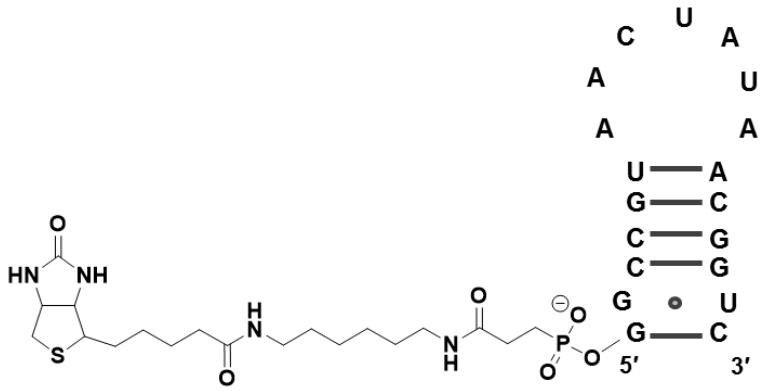


**Figure 2.2.** Structure of biotinylated H69 UUU is shown.

The mixture was then incubated at room temperature (RT) for 30 min. After incubation with RNA, the beads were washed with 200 μL of the buffer five times. After mixing, the beads were held against the sample with a magnet, spun down using a microcentrifuge, then the supernatant was carefully decanted into another microcentrifuge tube. Next, 200 μL of buffer was added, and mixing, centrifugation, and removal of the supernatant was repeated five times. For elution of the phage, the beads were placed in 100 μL of buffer C (0.2 M glycine-HCl, pH 2.2, 1 mg/mL BSA) for 9 min, followed by neutralization with 15 μL of buffer D (1 M Tris-HCl, pH 9.1). Then, 10 μL of the eluate was removed and placed in a separate 500 μL microcentrifuge tube for titering, and 100 μL of the eluate was kept for the next step.

**Table 2.1.** Dilutions prepared for phage libraries

| dilution factor | dilutions |
|---|---|
| $10^1$ | 10 µL of library + 90 µL of LB |
| $10^2$ | 10 µL of $10^1$ solution + 90 µL of LB |
| $10^3$ | 10 µL of $10^2$ solution + 90 µL of LB |
| $10^4$ | 10 µL of $10^3$ solution + 90 µL of LB |
| $10^5$ | 10 µL of $10^4$ solution + 90 µL of LB |
| $10^6$ | 10 µL of $10^5$ solution + 90 µL of LB |
| $10^7$ | 10 µL of $10^6$ solution + 90 µL of LB |
| $10^8$ | 10 µL of $10^7$ solution + 90 µL of LB |
| $10^9$ | 10 µL of $10^8$ solution + 90 µL of LB |
| $10^{10}$ | 10 µL of $10^9$ solution + 90 µL of LB |
| $10^{11}$ | 10 µL of $10^{10}$ solution + 90 µL of LB |

To 5–10 mL of LB, a single colony from *E. coli* strain ER2738 (New England Biolabs, Ipswich, MA) from a plate was inoculated and incubated at 37 °C with shaking to mid-log phase (OD600~0.5, 4–8 h). Then, to a pre-warmed LB/IPTG plate per expected dilution was spread at 37 °C until ready for use. The serial dilutions were prepared in the following manner (**Table 2.1**).

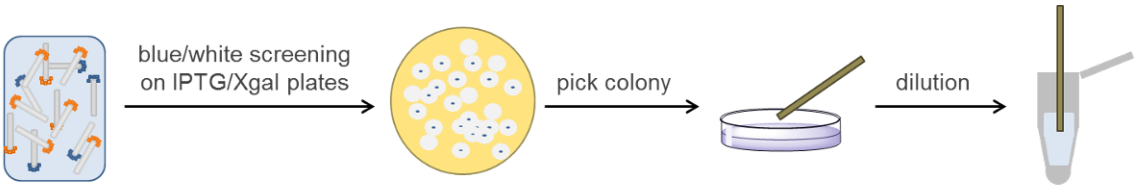


**Figure 2.3.** Schematic figure of the steps performed after biopanning is shown.

When the culture reached mid-log phase, 200 µL of the culture was dispensed into microfuge tubes, which held phage dilutions. Then, to carry out infection, 10 µL of each phage dilution was added to a tube, vortexed quickly, and incubated at room temperature for 1–5 min. The infected cells were vortexed briefly, and the culture was

immediately poured onto a pre-warmed LB/IPTG plate. The plates were allowed to cool and dry for 5 min, inverted, and incubated overnight at 37 °C. Plaques on plates were counted that have approximately 100. To each number, the dilution factor was multiplied for that plate to get the phage titer in plaque forming units (pfu) per 10 µL, and the % yield of the output/input phage was calculated using **Equation 2.1**.

**Equation 2.1.**

$$\% \text{ yield} = 100 \times (\#\text{ of output phage} \times \text{dilution factor}) / \#\text{ of input phage}$$

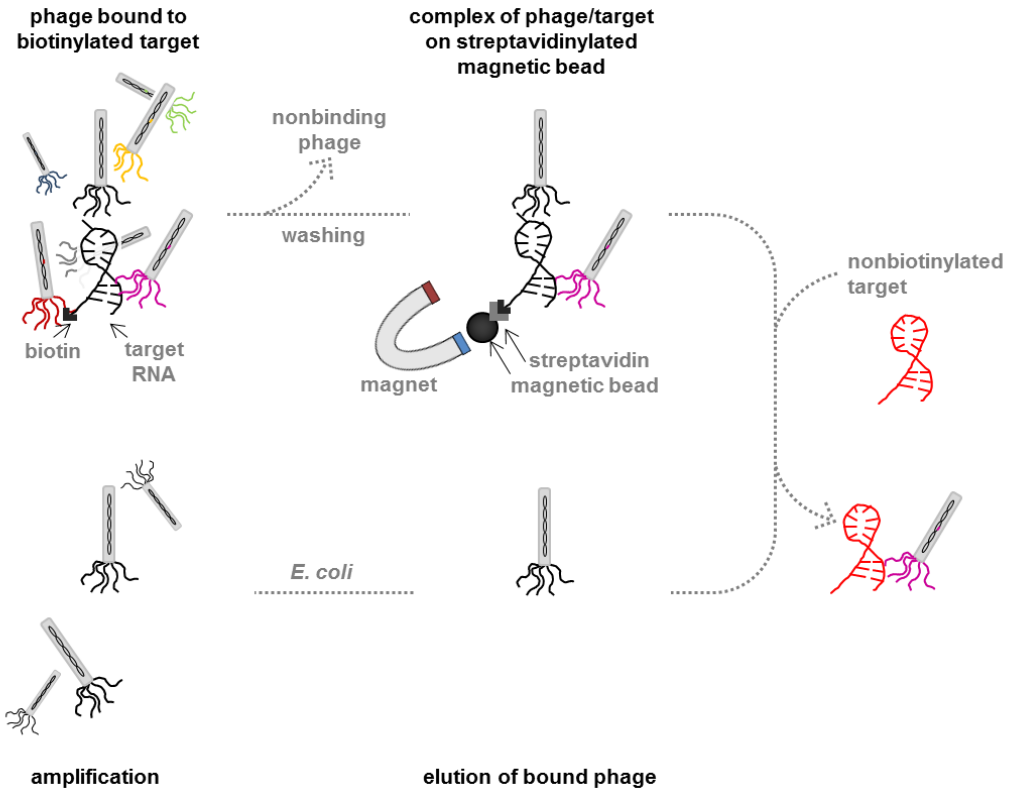


**Figure 2.4.** A schematic representation of specific elution is given. A nonbiotinylated target is added to the complex of phage/target on streptavidinylated magnetic bead to wash off the phage that bind selectively to the biotinylated target.

Phage display was performed under various conditions, including pH 5.5 to favor the closed conformation, and at higher $Mg^{2+}$ concentrations to favor the open conformation.

Elution was done with differing competing RNAs, such as the H69 stem region, human H69, and $tRNA^{Phe}$ to improve peptide selectivity. The elution was performed non-specifically and specifically. Non-specific elution was performed with an acidic glycine buffer, whereas specific elution was performed by eluting the phage with free target (**Figure 2.4**).

The conditions for washing and elution are displayed in **Table 2.2**. The selections were separately performed from round 3, and biopanning using M-280 streptavidin-coated magnetic beads and H69 with various competitors is shown. The washing buffer is the same as the binding buffer (buffer A minus Tween-20) with addition of different concentrations of Triton X-100. For the first two rounds, only tRNA was used as a competitor and only non-specific elution was performed. For specific elution, after two rounds, 3 *eq.* of free (nonbiotinylated) H69 UUU (90 pmol) were added to the solution with biotinylated H69 ΨΨΨ and phage that were washed before addition of the H69 UUU.

**Table 2.2.** Biopanning conditions for rounds 1-4 (pH 7.0)

| round | washing | H69 (pmol) | competitor RNA (pmol) | binding time (h) | elution |
|---|---|---|---|---|---|
| 1 | 3 times, 0.1% Triton-X | 30 | 90 (tRNA) | 2 | non-specific |
| 2 | 3 times, 0.3% Triton-X | 30 | 90 (tRNA) | 2 | non-specific |
| 3 | 10 times, 0.5% Triton-X | 30 | 90 (human H69, H69 UUU, H69 stem, tRNA) | 1 | non-specific and specific |
| 4 | 10 times, 0.5% Triton-X | 30 | 90 (human H69, H69 UUU, H69 stem, tRNA) | 0.5 | non-specific and specific |

Biopanning using M-280 streptavidin-coated magnetic beads and H69 at pH 5.5 is shown in **Table 2.3**. The washing buffer is the same as the binding buffer (buffer B minus Tween-20) with addition of different concentrations of Triton X-100.

**Table 2.3.** Biopanning conditions for rounds 1-4 (pH 5.5)

| round | washing | H69 (pmol) | competitor RNA (pmol) | binding time (h) | elution |
|---|---|---|---|---|---|
| 1 | 3 times, 0.1% Triton-X | 30 | 90 (tRNA) | 2 | non-specific |
| 2 | 3 times, 0.3% Triton-X | 30 | 90 (tRNA) | 2 | non-specific |
| 3 | 10 times, 0.5% Triton-X | 30 | 90 (tRNA) | 1 | non-specific |
| 4 | 10 times, 0.5% Triton-X | 30 | 90 (tRNA) | 0.5 | non-specific |

### 2.2.2. Sequencing

For sequencing, DNA templates were prepared by colony PCR. Using an autoclaved tip, random colonies were picked from a plate with ~100 colonies. The tip was then used to streak a part of the plate, and dipped in 500 µL of $ddH_2O$. The solution was used as the DNA template solution for the colony PCR. In a 200 µL PCR tube, 1× master mix along with the primers were added with the PCR reaction components. The Green Go Taq master mix (2×, Promega, *Taq* DNA polymerase, pH 8.5, 400 µM dNTPs, 3 mM $MgCl_2$) contains DNA polymerase, dNTPs, and buffers needed for the polymerase reaction.

| reagent | amount |
|---|---|
| DNA template | 2 µL |
| forward primer | 4 µL (5'-GCAAGCTGATAAACCGATACAAT-3') |
| reverse primer | 4 µL (5'-CCCTCATAGTTAGCGTAACG-3') |
| Green Go Taq master mix | 10 µL |

The colony PCR reaction was performed using the following program. The PCR protocol included a cycle for 1 min at 98 °C, 34 cycles for 10 sec at 98 °C (denaturing), 30 sec at 55 °C (annealing), 30 sec at 72 °C (extending), and 1 cycle for 5 min at 72 °C, followed by holding at 4 °C. After the PCR cycles are done, the concentrations of the

PCR products were measured using UV-vis spectroscopy (Nanodrop) at 260 nm. Then, to confirm whether the PCR was successful with no contamination, the PCR samples were run on a 2% agarose gel in 1 × TBE buffer. Finally, the samples were diluted to a concentration of 5 µg/µL, and sequenced.

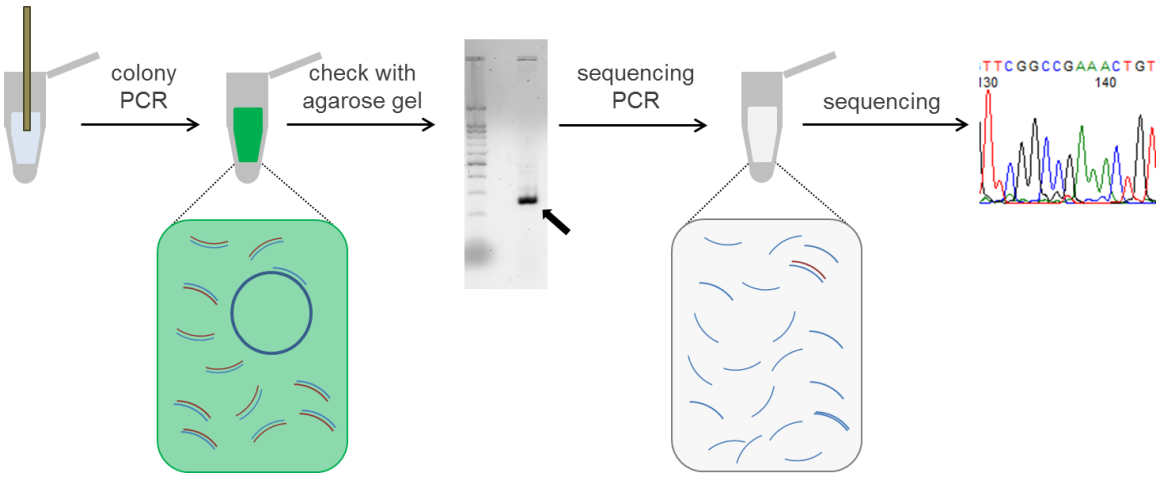


**Figure 2.5.** A schematic representation of steps before sequencing is shown.

The sequences were found with colony PCR, followed by sequencing on the CEQ8000 (Beckman Coulter Inc., Pasadena, CA) in the RNA Instrument Room, Wayne State University, and Illumina (San Diego, CA) in the DNA sequencing core, Wayne State University. Except for the selections carried out at pH 5.5, from each of the selections under varying conditions, 20 of the randomly picked colonies were sequenced and aligned with ClustalW2 (EMBL-EBI, Cambridge, United Kingdom). For the selections done at pH 5.5, 105 randomly picked colonies were sequenced and aligned.

### 2.3. Preparation of the peptides

Peptides were prepared by solid-phase synthesis.[71] Rink amide AM resin, NovaSyn TGR resin, Fmoc (fluorenylmethyloxycarbonyl)-protected amino acids and *O*-benzotriazole-*N, N, N', N'*-tetramethyluronium hexafluorophosphate (HBTU) were purchased from Novabiochem (Darmstadt, Germany). Diisopropylethylamine (DIPEA),

dichloromethane (DCM), dimethylformamide (DMF), piperidine, trifluoroacetic acid (TFA), thioanisole, triisopropylsilane (TIPS), ninhydrin, diethyl ether and acetonitrile (MeCN) were purchased from Sigma-Aldrich (St. Louis, MO).

To Rink amide AM resin with a loading level of 0.68 mmol/g in DMF was added 20% piperidine in DMF for deprotection, and mixed for 30 min. After confirmation of coupling by a ninhydrin test, the mixture was washed with DMF and DCM (five times each). To the Fmoc deprotected resin were added 2 *eq.* of Fmoc amino acid, 2 *eq.* of HBTU and 4 *eq.* of DIPEA, and the solution was mixed for 4 h. Again, the mixture was checked with ninhydrin, and the resin was washed with DMF and DCM (five times each). These steps were repeated for each Fmoc amino acid in the sequence. When the peptide of interest was completed, the resin was dried and the peptide was cleaved with a cocktail of TFA: thioanisole: TIPS: dd$H_2O$=94: 2: 2: 2 with 2 h incubation (**Scheme 1.1**). The cleaved solution was precipitated and washed with cold ether, centrifuged at 5000 rpm for 30 min, and after decanting, the white precipitate was dried *in vacuo*. The crude peptide was then dissolved in dd$H_2O$ and purified by HPLC (Luna C18 reverse phase column 250 × 10.0 mm, 5 µm, Waters, Milford, MA) on a Waters 600 LC with a 717 autosampler (Waters, Milford, MA, USA) and UV-detector by increasing the concentration of MeCN from 0 to 40%. The fractions containing product peptide were lyophilized to give a white powder. The peptide was then characterized by MALDI-TOF MS (Ultraflex, Bruker, Billerica, MA). Positive mode on Ultraflex Extreme TOF/TOF from Bruker (Billerica, MA) was used for detection, and 4-hydroxy-α-cyanocinnamic acid (**Figure 2.1b**) was used as a matrix.

Branched peptides were prepared by solid-phase synthesis as described in the previous section. However, the loading of Rink Amide AM resin is 0.68 mmol/g, which is too high to synthesize branched peptides.[132] Therefore, NovaSyn TGR resin with a loading level of 0.31 mmol/g was used, which was purchased from Novabiochem

(Darmstadt, Germany). Fmoc-Lys(Fmoc)-OH, Boc-Thr(Trt)-OH, and Fmoc-β-Ala-OH (B) were purchased from Novabiochem (Darmstadt, Germany). Fmoc-propargylglycine-OH and Fmoc-Lys(ivDde)-OH were purchased from Anaspec (Fremont, CA).

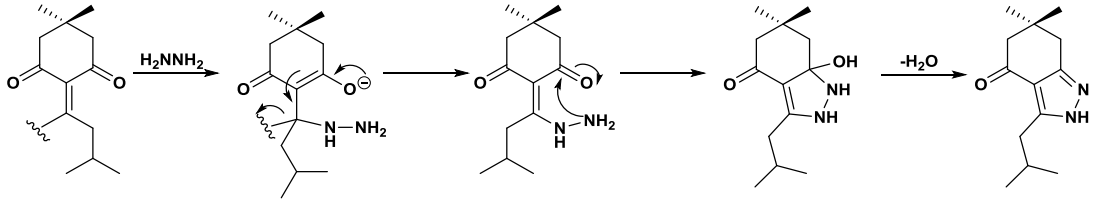


**Figure 2.6.** Structure of ivDde and the deprotection mechanism is shown. Hydrazine removes the protecting group by forming a stable conjugated ring system *via* Michael addition followed by cyclization, which cannot be performed with piperidine, and this enables the branched peptide synthesis with different side chains.

Branches were formed using lysine, because both the backbone and side chain have amino groups. For branched peptides with the same functional groups on each branch, Fmoc-Lys(Fmoc)-OH was used for the synthesis. For branched peptides with different peptides growing on each branch, Fmoc-Lys(ivDde)-OH was used.[168] Both protecting groups Fmoc and ivDde (**Figure 2.6**) are base-labile, but can be orthogonally deprotected. Therefore, they are useful for asymmetric branched peptide synthesis. For the synthesis of mixed peptides with different branch sequences, (TARHIYBBB)(AAAAAABBB)-Lys-OH, TARHIYBBB was first added to the backbone using Fmoc-protected amino acids except for threonine, where Boc-Thr(Trt)-OH was added. Then, 5% hydrazine/DMF was added to remove the ivDde (1-(4,4-dimethyl-2,6-dioxocyclohex-1-ylidene)isovaleryl) protecting group from the peptide, and the resulting slurry was mixed for 30 min, followed by washing. Then, AAAAAABBB was added using Fmoc-protected amino acids. The remaining steps, such as cleavage from the resin, purification, and characterization were done the same way as described for the monomer peptide.

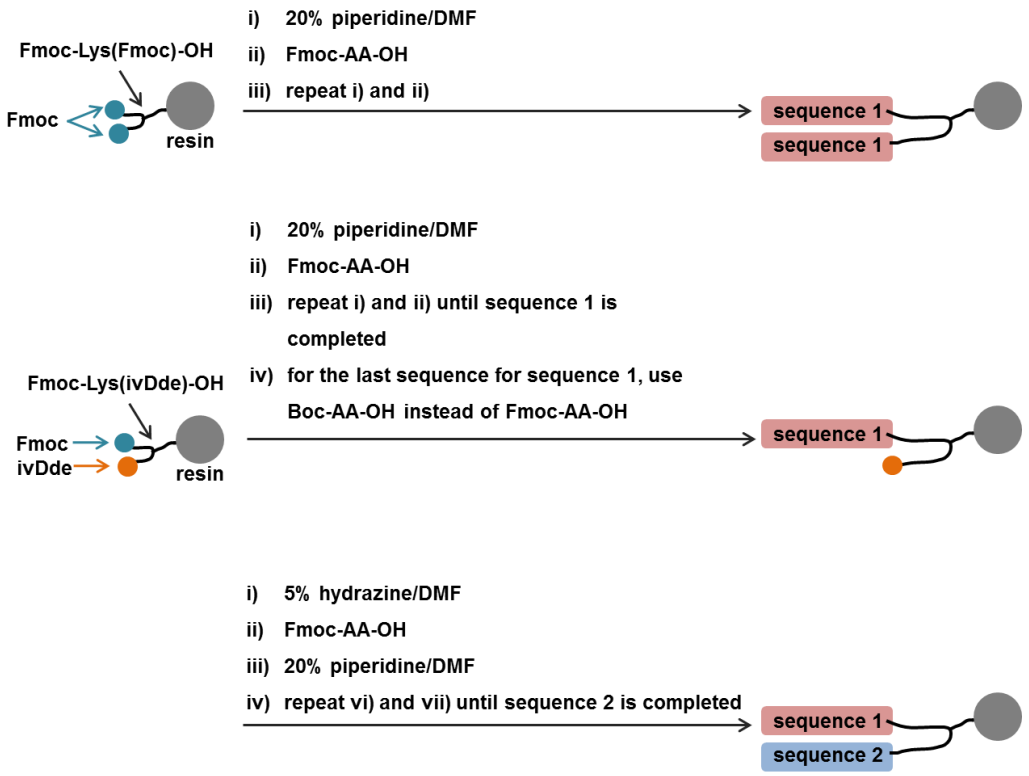


**Figure 2.7.** A general scheme for branched peptide synthesis is shown.

### 2.4. Fluorescent intercalator displacement (FID) assay

TO-PRO®-1 iodide solution (TOPRO, 3-methyl-2-((1-(3-trimethylammonio)propyl)-4-quinolinylidene)methyl)benzothiazolium) was purchased from Thermo Fisher Scientific (Waltham, MA). Potassium hydroxide (KOH) and HEPES were purchased from Fisher Scientific (Hampton, NH). Magnesium chloride ($MgCl_2$), sodium cacodylate, neomycin, and paromomycin were purchased from Sigma-Aldrich (St. Louis, MO). For the FID experiments, a Cary Eclipse Fluorescence Spectrophotometer (Varian, Inc., Walnut Creek, CA) and Synergy H1 Hybrid reader (BioTek, Winooski, VT) were used to measure fluorescence, with excitation at 500 nm and emission from 510 to 560 nm. To the H69 RNA (1 μM) in buffer was added 1 *eq.* of TOPRO solution, and then the solution was titrated with a ligand solution. TOPRO does not exhibit fluorescence in buffer, but exhibits strong emission when bound to RNA.[138] Each ligand was dissolved in 20 mM

HEPES-KOH, 100 mM KCl, 5 mM $MgCl_2$ (pH 7.0) buffer or 20 mM cacodylate, 100 mM KCl (pH 5.5) buffer. The ligand samples were prepared at 0, 1, 10, 50, and 100 μM concentrations. Each sample was mixed and incubated for 2 min before the fluorescence measurement was done. For each experiment, negative controls were done with buffer only, samples without H69, samples without TOPRO, and samples without peptide. Each measurement was taken and the background spectrum was subtracted. Each experiment was performed in triplicate. To calculate the relative fluorescence, the fluorescence of the H69 and TOPRO in buffer before ligand addition was determined ($F_0$). Then, fluorescence from each sample was measured ($F_1$ to $F_n$) and the relative fluorescence was calculated by setting $F_0$ to 1. The relative fluorescence value for each sample was $F/F_0$.

**2.5. Electrospray ionization mass spectrometry (ESI-MS)**

ESI-MS is a method used to obtain an apparent $K_d$ value. This method has been used previously for binding studies with RNA and various ligands.[118, 120, 169] For most of my studies, TriVersa nanospray with LTQ-XL from Advion (Ithaca, NY) was used in the Proteomics Core under the direction of Paul Stemmer (Wayne State University). The data were processed using Xcalibur (Thermo Fisher Scientific, Waltham, MA), and analysis was done on GraphPad Prism (La Jolla, CA). Ammonium acetate (7.5 M, $NH_4OAc$) was purchased from Sigma-Aldrich (St. Louis, MO). In this study, the binding was done at 10 mM $NH_4OAc$ in 50% isopropanol for both pH 5.5 and pH 7.0 conditions, 1 μM of H69 ΨΨΨ or H69 UUU, and the concentration of peptide varied from 0 to 100 μM. The salt concentration was lowered due to the limits of the instrumentation. The samples were mixed and incubated for 10 min before ESI-MS analysis. Each titration experiment was performed in triplicate.

Since RNA and peptides typically have different ionization efficiencies,[147, 170] the binding ratios were determined at different charge states and compared. To then

determine relative $K_d$ values, a single charge state was chosen for calculating binding ratios for a single RNA species (*e.g.*, UUU or ΨΨΨ) with closely related peptide ligands. In this study of H69 and peptides, the binding ratios were determined from the peak intensities at given m/z values for the (6-) charge state for free RNA and the complex.[118, 169, 171] In other reports, the (5-) charge state was used because of stronger peak intensities;[118, 169] however, in this study we were not able to use the (5-) charge state because the m/z of the RNA (1514) overlapped with the dimer peak of the peptide (1514). Therefore, the (6-) charge state of the RNA and the peptide complex was used for our studies. To compare the peptide binding to H69 ΨΨΨ and H69 UUU, the ratios of the peak areas of free RNA, 1:1, and 1:2 complexes were determined.[146, 170]

The apparent dissociation constant of the RNA-peptide binding was obtained by plotting the binding ratio to the peptide concentration. The data were plotted on GraphPad, using nonlinear curve fitting with the quadratic equation (**Equation 2.2**). The equation correlates the peak area for free RNA (R) and the RNA-peptide complex (RP), with the titrated peptide concentration (P).

**Equation 2.2.**

$$\frac{\Sigma RP^{n-}}{\Sigma R^{n-}+\Sigma RP^{n-}} = \frac{([R]_0 + [P]_0 + K_d)-(([R]_0 + [P]_0 + K_d)^2 - 4[R]_0[P]_0)^{1/2}}{2[R]_0}$$

## 2.6. Surface plasmon resonance (SPR) on BLItz

SPR is a method used to obtain an apparent $K_d$ value along with kinetic data of binding interactions. For these studies, the BLItz system and biosensors from ForteBio (Pall ForteBio, Fremont, CA) were used. For the BLItz method, the biosensor was installed onto the instrument and was soaked in the buffer for at least 10 min. The samples were

prepared by serial dilution, and since the BLItz method is light dependent, the samples were placed in black tubes to reduce background light. To the soaked biosensor was loaded the target (*i.e.*, biotinylated H69 ΨΨΨ or biotinylated H69 UUU) from a 5 μM RNA solution onto the biosensor. The sample (ligand) solutions were prepared by serial dilutions from 0, 0.7, 1.5, 3.1, 6.3, 13, 25, 50, to 100 μM in 20 mM HEPES-KOH, 100 mM KCl, 5 mM $MgCl_2$ (pH 7.0) buffer or 20 mM cacodylate, 100 mM KCl (pH 5.5) buffer. The cycles for ligand (peptide) binding included a baseline measurement in buffer for 30 s, association in ligand solution for 300 s, and dissociation in buffer for 300 s. For biomolecular interactions, the response of the optical interference, $k_{on}$, $k_{off}$, and $K_d$ values were obtained. The experiments were performed in triplicate.

The apparent dissociation constant of the RNA-peptide binding was obtained by plotting the binding ratio to the peptide concentration. The data were plotted on the BLItz, using nonlinear curve fitting derived from Langmuir binding (**Equation 2.3**).

**Equation 2.3.**

$$\text{RNA + peptide} \underset{k_d}{\overset{k_a}{\rightleftharpoons}} \text{complex}$$

$$K_d = \frac{[\text{RNA}]\,[\text{peptide}]}{[\text{complex}]} = \frac{k_d}{k_a}$$

$$R = R_{max}\,\frac{[A]}{K_d + [A]}$$

## 2.7. Growth assay

To determine whether the phage selected have actual effects on *E. coli* survival, a growth assay was performed.[172-173] Custom-made phage were prepared by Antibody Design Labs (San Diego, CA). As a negative control, SILPYPY, a known artifact

sequence that was found in this study, as well as previous studies,[119, 174] was also prepared. The custom phage grows kanamycin in LB with 60 mg/L. ER2267, a strain that is *Kan*$^R$, was obtained from New England Biolabs (Ipswich, MA) and used for the growth assay.

To 100 mL of LB with 60 mg/L of kanamycin was added a single colony of ER2267, which was allowed to grow at 37 °C overnight. The overnight culture was diluted 1:1000 times, then the phage of ~$10^{10}$ virions/mL was added. After the phage was added, 2 mL of the culture was withdrawn at 1, 3, 5, 7, 9, 11, and 24 h, then the $OD_{600}$ was measured on a Synergy H1 Hybrid reader (BioTek, Winooski, VT).

**2.8. Nuclear magnetic resonance spectroscopy (NMR)**

In this study, a 2D $^1$H homonuclear NMR experiment (2D COSY) was employed to observe conformational changes of H69 upon binding. Potassium phosphate ($KH_2PO_4$) and potassium chloride (KCl) were purchased from Sigma-Aldrich (St. Louis, MO), 99.96% deuterium oxide ($D_2O$) was purchased from Cambridge isotope laboratories (Tewksbury, MA), and ethylenediaminetetraacetic acid (EDTA) was purchased from Fisher Scientific (Hampton, NH).

Solutions of H69 ΨΨΨ and H69 UUU (50 μM) in NMR buffer (20 mM $KH_2PO_4$, 100 mM KCl, 1 mM EDTA, pH 5.5 or pH 7.0) were prepared, as well as solutions of H69 ΨΨΨ and H69 UUU (50 μM) in the same buffer with peptide 10 times the apparent $K_d$, 500 μM). RNAs were renatured by heating the sample to 80 °C for 2 min then slowly cooling to RT over 2 h. After renaturing, the respective peptides were added and allowed to interact with the RNA for several hours at RT. NMR spectra were recorded using a Bruker ADVANCE 700 MHz NMR (Billerica, MA) equipped with a TXI cryoprobe at 298K. To determine structural effects of binding, ge-2D COSY was used to analyze $J_{H5\text{-}H6}$ of the pyrimidines. Peaks were assigned based off of previously reported values.[47, 166]

## CHAPTER 3 – SELECTION OF PEPTIDES BINDING TO H69 AT pH 5.5 USING PHAGE DISPLAY AND BINDING STUDIES

### 3.1. Biopanning yield and diversity

Peptides targeting H69 ΨΨΨ at different conditions were selected after four rounds of biopanning. In **Table 3.1**, the yield of each condition is shown. For tRNA, human H69, H69 stem, and H69 UUU, the libraries were split after round 3. For rounds 1 and 2, the library was incubated in 20 mM HEPES-KOH, pH 7.0, 100 mM KCl, 5 mM $MgCl_2$, 5% glycerol, 0.1 mg/mL BSA with 0.1% (v/v) Tween-20 with 30 pmol of H69, and to that was added 90 pmol of $tRNA^{Phe}$ as a competitor, which was removed after the incubation time of 2 h. Starting with round 3, different competitors were used (**Table 3.1**), such as human H69, H69 stem, and H69 UUU. For pH 5.5 (**Table 3.1**), the library was incubated in 20 mM PBS, pH 5.5, 100 mM KCl, 5% glycerol, 0.1 mg/mL BSA with 0.1% (v/v) Tween-20.

**Table 3.1.** Yield of each round of phage display with varying competitors.

| round | competitor RNA | | | | | |
|---|---|---|---|---|---|---|
| | tRNA (%) | human H69 (%) | H69 stem (%) | H69 UUU (%) | H69 UUU‡ (%) | pH 5.5 (%) |
| 1 | 0.078 | 0.078 | 0.078 | 0.078 | 0.078 | 0.001 |
| 2 | 0.035 | 0.035 | 0.035 | 0.035 | 0.035 | 0.025 |
| 3 | 0.003 | 0.050 | 0.35 | 0.35 | 0.5 | 0.80 |
| 4 | 8.0 | 10 | 15 | 9.0 | 5.0 | 0.0005 |

‡ specific elution

The competitors in round 3 were chosen with the hope of finding a peptide that prefers H69 ΨΨΨ over human H69, the H69 stem, or H69 UUU. Specific elution was performed with H69 UUU. This experiment was designed to find a peptide that has binding towards H69 in general, but preferred binding to H69 UUU. To increase the stringency, buffer and wash conditions were changed for each step as described in **Table 2.1**.[118, 120] The concentration of detergent Triton-X increased from 0.1 to 0.5%, and the number of

washes increased from three to ten times, and the incubation time decreased from 2 to 0.5 h.

**Table 3.2.** Diversity of each round of phage display

| round | competitor RNA | | | | | |
|---|---|---|---|---|---|---|
| | tRNA | human H69 | H69 stem | H69 UUU | H69 UUU‡ | pH 5.5 |
| 1 | $1.6 \times 10^8$ | $1.6 \times 10^8$ | $1.6 \times 10^8$ | $1.6 \times 10^8$ | $1.6 \times 10^8$ | $2.2 \times 10^6$ |
| 2 | $5.5 \times 10^4$ | $5.5 \times 10^4$ | $5.5 \times 10^4$ | $5.5 \times 10^4$ | $5.5 \times 10^4$ | $5.5 \times 10^2$ |
| 3 | 2 | 27 | 191 | 191 | 273 | 4 |
| 4 | 0 | 3 | 29 | 17 | 14 | 0 |

‡ specific elution

As described in **Table 3.1**, the yields from rounds 1 and 2 were 0.078 and 0.035%, respectively. At round 3, for tRNA, the yield dropped to 0.003%. For tRNA, the increase of number of washes and detergent with the decrease of incubation time led to a 10-fold decrease in yield for non-specific elution. At round 4, an increase in yield was observed, which is commonly seen in phage selection. The yield decrease followed by an increase in biopanning can be explained with the fact that by round 3, the diversity of the library decreased from $>10^9$ to $<10^2$ (**Table 3.2**). In this study, each round started with a plaque forming unit (pfu) of $2 \times 10^{11}$, which has a diversity of about $1.3 \times 10^9$. After the phage were eluted, there was a step to amplify the phage so that the total number for the next round was $2 \times 10^{11}$ pfu. At the first round, there were about 100 copies of each phage in the library, and as more rounds are performed, the diversity decreased while the number of each copy increased. Therefore, by the time the selection reached the 3rd or 4th round, we estimated that there were less than 100 diverse sequences. The sequences surviving all rounds succeed for various reasons. Some contain strong binding sequences for the target, while others are fast growing phage, which amplify faster in the *E.coli* host. The so-called fast growers were also reported in literature. [110, 175] Some sequences are selected due to their ability to bind to plastic or streptavidinylated magnetic beads, and these are called artifact sequences.[176]

An increase in yield was observed when different competitors were added in round 3, such as human H69, H69 stem, and H69 UUU. The yield for human H69 was 0.050%, similar to rounds 1 and 2, and the yields for H69 stem and H69 UUU increased to 0.35%. By round 4, the yields for biopanning done at pH 7.0 increased to 8-15%. This result could be related to the diversity of the library (**Table 3.2**). The diversity dropped to less than 30, and for pH 5.5 conditions or tRNA competitor, the diversity decreased to a theoretical number of 0. Therefore, for the pH 5.5 selection, sequencing was performed on the phage library from round 3. The low yield for the pH 5.5 selection could also be due to the use of more acidic buffers, which have been reported to decrease the survival of phage.[121] As reported by Derda *et al*.,[110] convergence to a few clones is shown in more than 90% of phage display studies, although the drop of diversity leaves many questions as to the validity of the phage selected. In biopanning, the target-phage library incubation starts with $>10^9$ different phage, and after each round, the nonbinding phage are washed out. After each round of selection, the phage are amplified so that incubation of the library with the target is done with the same number of phage in each round. However, this step may be the reason behind the convergence of sequences. Not all phage have the same growth rate, and therefore, fast-growing phage that do not necessarily bind to the target may be amplified during this step. There is a possibility of selecting fast-growing peptides over strong binders. This leads to the conclusion that the relative abundance of sequences may not necessarily correlate to the binding affinity, which has been shown in previous studies by Abdeen *et al*.[177] To overcome the loss of diversity, use of an unamplified library could be considered, but then the ratio of phage to target would be needed to be considered.

### 3.2. Peptide sequence analysis

In the first set of conditions used, to check the effect of differing competitors, several RNAs such as the stem region of H69, human H69, and $tRNA^{Phe}$ were added. The

phage library was incubated in pH 7.0 binding buffer (20 mM HEPES, 100 mM KCl, 5 mM $MgCl_2$, 5% glycerol, 0.1 mg/mL BSA) and competitors, followed by washing and non-specific elution with acidic glycine buffer. After four rounds of selection, 20 randomly picked colonies of each condition were sequenced. The selection conditions are displayed in **Table 2.1**.

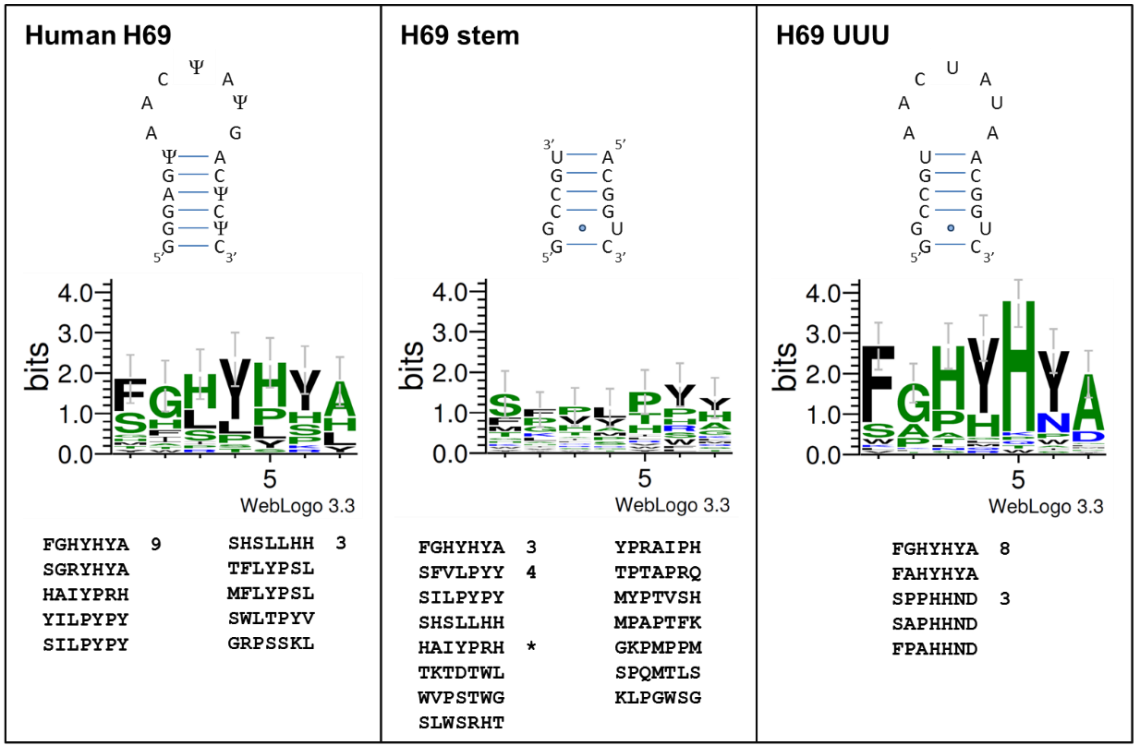


**Figure 3.1.** Sequences from randomly picked colonies from the selection with competitors human H69, H69 stem, and H69 UUU at pH 7.0 are shown. The upper part of the panel displays the sequence of the RNA competitors. The middle part with WebLogo 3.3 shows the consensus of the peptide sequences selected, in which the size of the sequence shows the frequency of the sequence appearing. The sequences of the peptides are aligned on the lower part of the panel.

For all selections, we were able to observe a sequence that shows up more frequently than others, FGHYHYA. However, this sequence also appeared frequently in the negative control experiment, in which $tRNA^{Phe}$ was used as a competitor with H69 ΨΨΨ as a target. From round 3, different competitors were used (**Table 3.1**), such as human H69, the H69 stem, and H69 UUU. These competitors were selected to find a peptide

that prefers H69 ΨΨΨ over human H69, H69 stem, or H69 UUU. Peptide SHSLLHH appeared three times when human H69 was used as the competitor. The sequence SFVLPYY appeared four times when the stem region was used as a competitor. The sequence SPPHHND appeared three times when H69 UUU was used as a competitor (**Figure 3.1**). However, the selectivity of the peptides obtained was questionable. If the sequence prefers to bind to H69 UUU over H69 ΨΨΨ, the sequence would be expected to appear with the specific elution with UUU, not when H69 UUU was used as a competitor. These results imply that the sequences may bind to the loop region of the target H69.

For specific elution with UUU, six different sequences were obtained. Sequence FGHYHYA appeared 12 times, while FAPYNHA, WATQHWA, WPTLQWA, LASHTAP, and KILGWSG were each observed once. In this case, the main peptide was FGHYHYA, which was also found in the selections at pH 7.0 with differing competitors as described above. Unfortunately, this sequence may be a fast grower and lacking selectivity for H69. Therefore, the sequences screened in this study were most likely fast-growing phage, which could also explain the presence SILPYPY, another sequence reported in the literature as a fast-grower.[110, 119] For these reasons, we did not pursue further studies with these sequences.

In the 4th round, the yield was >5% for the non-specific elution conditions at pH 7.0. For the selection at pH 5.5, the yield was still very low (0.0005%) after the 4$^{th}$ round, but a consensus was still obtained from the sequence alignment (**Figure 3.2**). The poor yield may be a result of amplification of sequences that are harmful to the host bacteria. While performing biopanning, there is a possibility of target-unrelated sequences being selected. Among the phage, some of them are prone to propagate faster than others, which would lead to their selection. Therefore, the peptide sequences were checked with the literature and SAROTUP, a program that searches for target-unrelated peptides

developed by Huang *et al*.[176] Among the sequences shown, none of them are known for binding to streptavidin or to be target-unrelated peptides.[176] However, three sequences, SAPHHND, SPPHHND, and SRAHHIA, turned out to be fast-growing peptides. Also, sequences SILPYPY and HAIYPRH were reported previously to be artifact sequences.[110, 119]

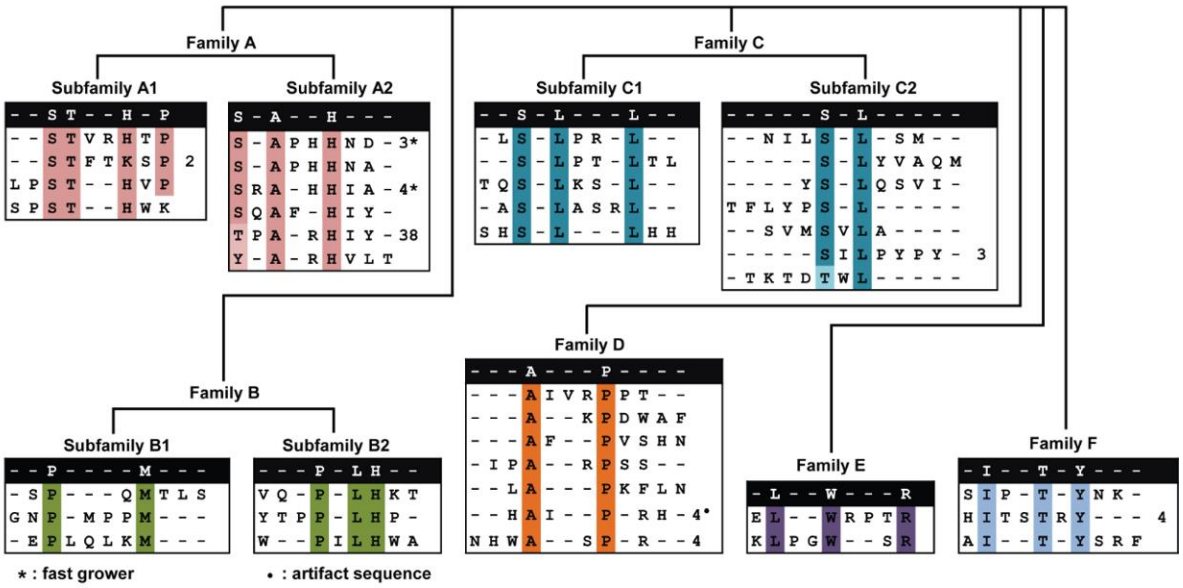


**Figure 3.2.** Sequences selected at pH 5.5 were aligned. Compared to sequences screened under pH 7.0 conditions, these sequences contained more polar residues.

In the third set of conditions, when the buffer conditions were altered, we observed some differences in the selected peptides. Previous work showed that the H69 conformation changes with the $Mg^{2+}$ concentration.[66-67, 178] To determine whether there are different sequences screened under differing $Mg^{2+}$ concentrations or pH conditions, phage display was conducted at pH 5.5 in PBS. After four rounds, 105 randomly picked colonies from each condition were sequenced. The conditions are displayed in **Table 2.3**. The sequences from the pH 5.5 selection showed a consensus. The sequences were sorted, as shown in **Figure 3.2**. Peptides SILPYPY, SAPHHND, and SHSLLHH that

were observed in higher pH buffer selections appeared three, three, and one time(s), respectively. The sequence FGHYHYA that appeared in pH 7.0 buffer conditions was not found in this selection. TPARHIY appeared 38 times out of 105 sequences.

**Table 3.3.** Sequences selected for further studies[176]

| sequence | pH 5.5/ competitor | # appeared | pH 7.0/ competitor | # appeared | reported in literature[180] |
|---|---|---|---|---|---|
| STFTKSP | $tRNA^{Phe}$ | 2 | | | |
| TPARHIY | $tRNA^{Phe}$ | 38 | | | |
| SAPHHND | $tRNA^{Phe}$ | 3 | H69 UUU | 1 | fast grower |
| SRAHHIA | $tRNA^{Phe}$ | 4 | | | fast grower |
| SHSLLHH | $tRNA^{Phe}$ | 1 | human H69 | 3 | |
| SLPTLTL | $tRNA^{Phe}$ | 1 | | | |
| SILPYPY | $tRNA^{Phe}$ | 3 | human H69<br>and H69 stem | 1<br>1 | artifact sequence |
| HAIYPRH | $tRNA^{Phe}$ | 4 | human H69<br>and H69 stem | 1<br>1 | artifact sequence |
| NHWASPR | $tRNA^{Phe}$ | 4 | | | |
| HITSTRY | $tRNA^{Phe}$ | 4 | | | |
| FGHYHYA | | | human H69,<br>H69 stem,<br>and H69 UUU | 9<br>3<br>8 | |
| SFVLPYY | | | H69 stem | 4 | |
| SPPHHND | | | H69 UUU | 3 | fast grower |

Overall, from the sequence analysis we cannot determine whether the goal to find phage that selectively bind to H69 in a closed conformation was achieved or not. However, the sequence TPARHIY that appeared 38 times was only observed from pH 5.5 selections (**Figure 3.2**). For further studies, peptides in **Table 3.3** were chosen based on the selections done at pH 5.5 buffer conditions, and the alignments in **Figure 3.2**, with at least one sequence from each family. Also, if the selected peptides were also found under pH 7.0 buffer conditions, they are listed in **Table 3.3**. These peptides are unlikely to have selectivity for H69 ΨΨΨ over H69 UUU, but may have potential binding to either form of H69.

### 3.3. Preparation of RNA

The RNAs H69 ΨΨΨ and H69 UUU were prepared as mentioned in **Section 2.1**. In **Figure 3.3a**, the 20% polyacrylamide gel is shown after purification and desalting of the RNAs, which was also verified by MALDI-TOF (**Figure 3.3b**).

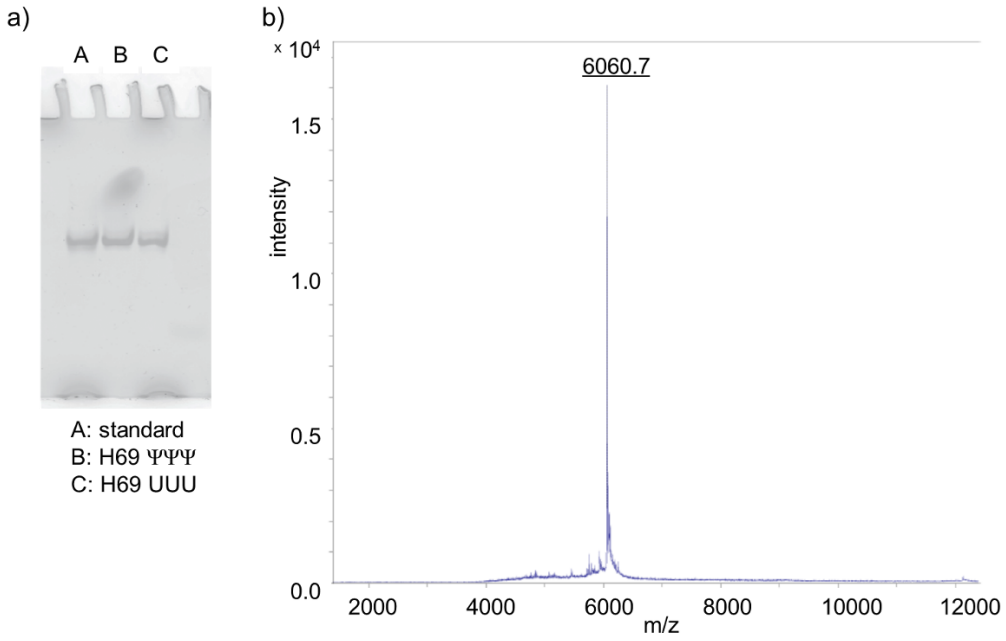


**Figure 3.3**. Representative data of purified H69 ΨΨΨ and H69 UUU are shown. a) Isolated H69 on a 20% polyacrylamide gel is shown. b) The MALDI-TOF spectrum of a purified H69 ΨΨΨ is given. The predicted mass of H69 $(M+H)^+$ is 6060.7 Da.

### 3.4. Preparation of peptides

Selected peptides were synthesized using solid phase peptide synthesis as described in **Section 2.5**. The structures of the peptides are shown in **Figure 3.4**.

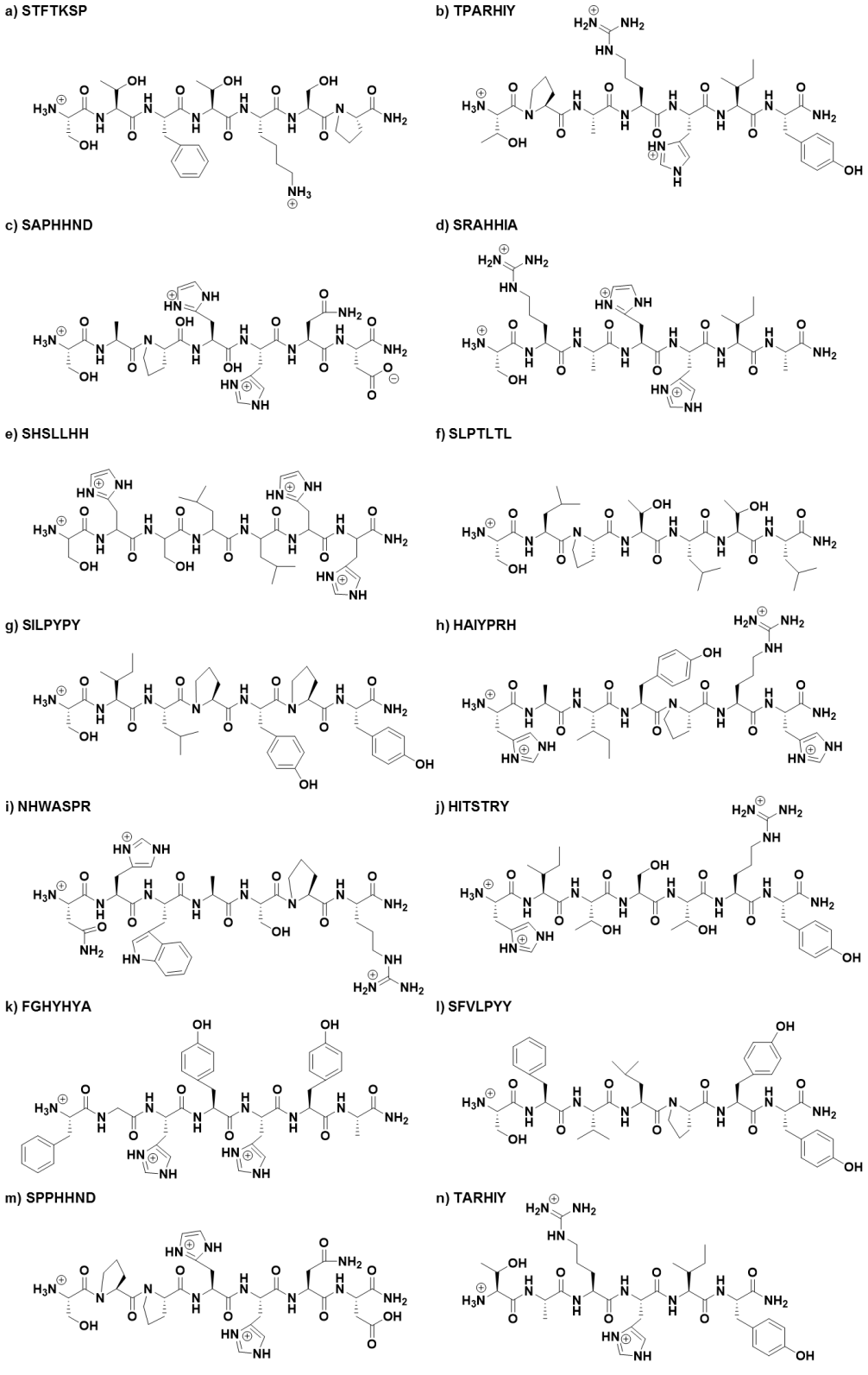


**Figure 3.4.** Structures of the amidated peptides used in this thesis work are shown (with protonation states at pH 7.0). The peptides are all positively charged.

The sequences display positive charges at both pH 5.5 and pH 7.0 conditions. In comparison to previous selections that found neutral and positively charged peptides,[118-120] these peptide sequences contain amino acids with more charges or greater hydrophilicity. Out of 14 peptides in **Figure 3.4**, 10 of them contain one or more histidines, which is neutral at pH 7.0 and positively charged at pH 5.5. This may have resulted from the selection being carried out at lower pH and the target being a negatively charged RNA, which attracts the positively charged peptides.

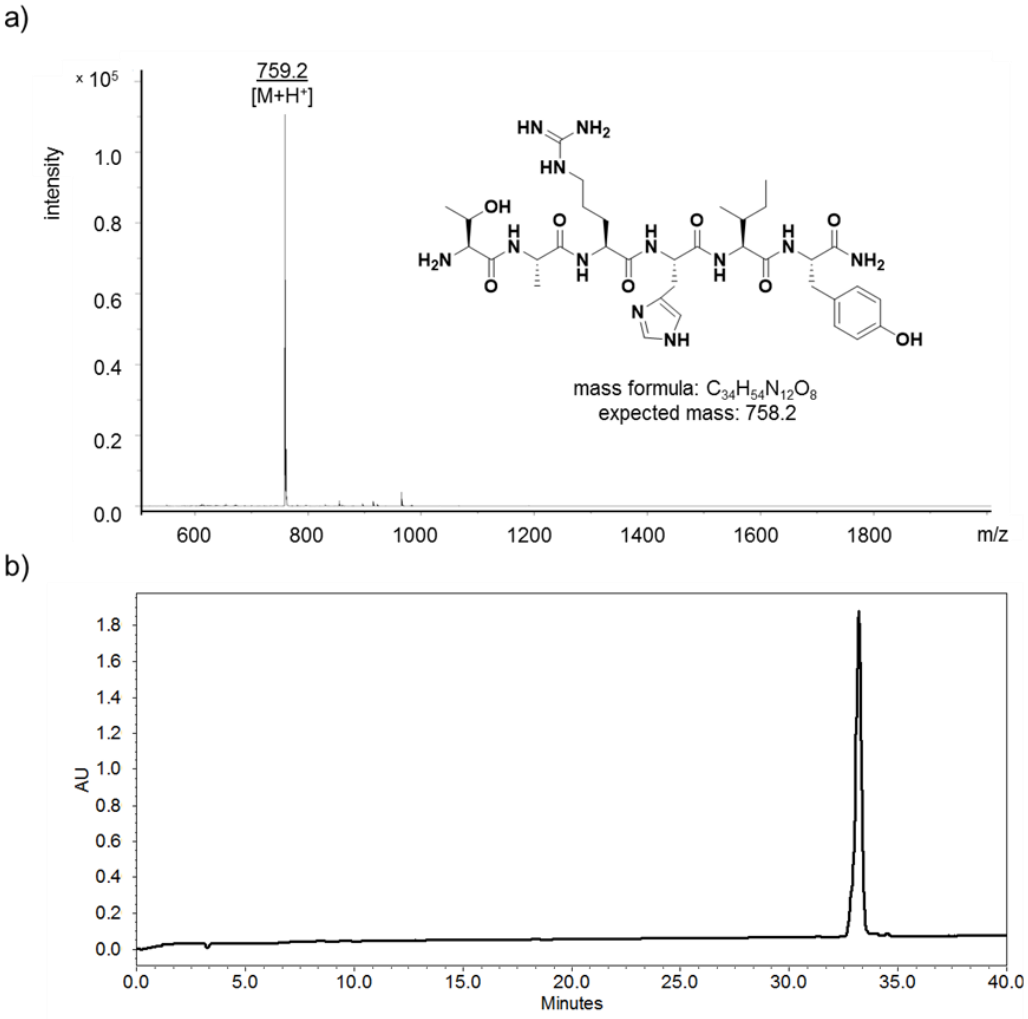


**Figure 3.5.** The MALDI-TOF spectrum (a) and HPLC trace (b) of purified TARHIY are shown. The other peptides are displayed in **Appendix A**.

During the synthesis, peptide TARHIY (**Figure 3.5**) was also obtained in addition to TPARHIY (**Figure 3.4b**). Since proline has a secondary amino group, it is difficult to tell from a Kaiser test[179] if it has been incorporated into the peptide (**Figure 3.6**). The major peptide product was shorter than the heptamer peptide screened from phage display, which happens to make it more druggable according to literature precedence with small peptide drugs.[180] Therefore, the TARHIY peptide was used for subsequent binding and biological experiments. The peptides were HPLC purified and characterized by MALDI-TOF.

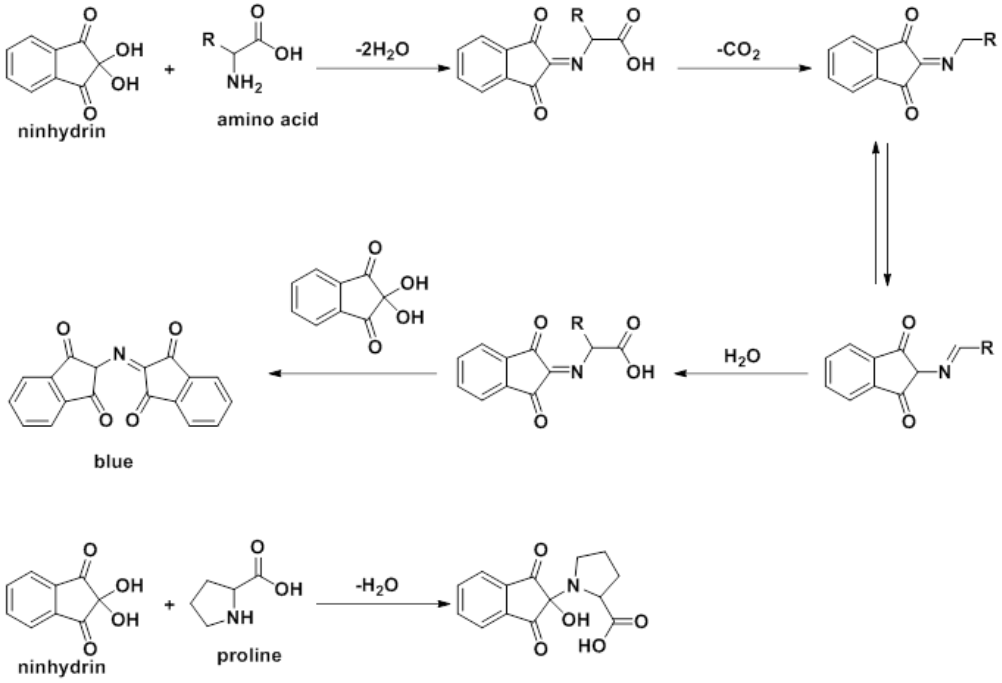


**Figure 3.6** Kaiser test with primary and secondary amino acids is shown.[179]

### 3.5. Screening peptides with the FID assay

The FID assay was performed under buffer conditions that were used previously.[138] The dye, TOPRO, bound to H69 and demonstrated increased fluorescence upon interaction with the RNA. If a ligand displaces the dye, the fluorescence is then expected

to decrease. The change in fluorescence can be therefore used to estimate relative binding affinities of ligands to RNA. The concentration of the ligands varied from 0 to 100 μM. In this study, displacement of fluorescence was determined by the addition of neomycin as a control, and then the selected peptides with H69 UUU or H69 ΨΨΨ were tested. There was little dye displacement by most of the peptides (less than 5%). The low change in fluorescence upon addition of peptide to the TOPRO-RNA complex was noticeably different from the response with neomycin, a known H69 binder. The fluorescence decrease observed with neomycin titration was consistent with results from previous studies employing 2-aminopurine-incorporated H69.[67] The lack of fluorescence change can be interpreted as a lack of peptide binding, or another mechanism such as peptide binding to the complex without dye release, or peptide binding to the dye alone. Some of the peptides, such as TARHIY, TPARHIY, SHSLLHH, and RQVANHQ exhibited some displacement at higher concentrations (>50 μM) (**Figure 3.7**). The displacement was most apparent when the ratio of [RNA]:[TOPRO] was 1:1. Interestingly, however, the shortened peptide TARHIY, showed greater displacement of TOPRO than the phage-selected peptide TPARHIY. TARHIY showed displacement of TOPRO up to 28% at 100 μM.

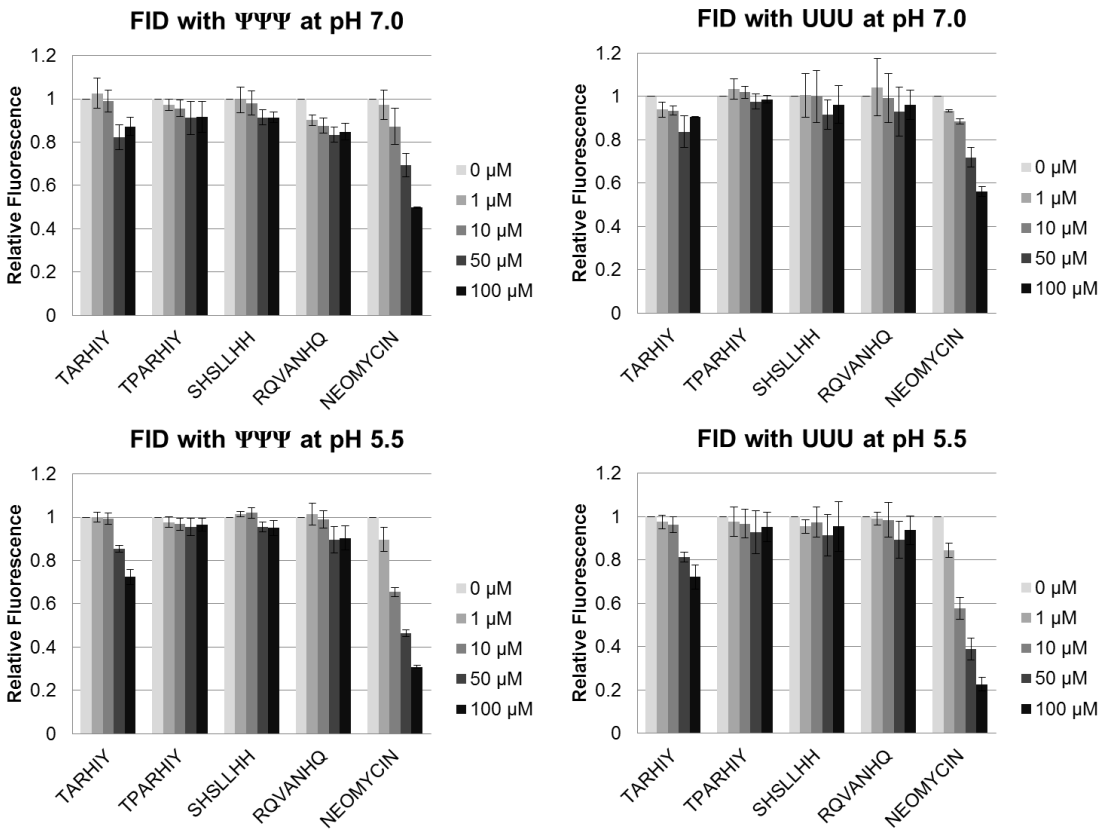


**Figure 3.7.** FID assay of peptides against H69 ΨΨΨ and H69 UUU at pH 5.5 and pH 7.0. For pH 7.0, 20 mM HEPES, 5 mM $MgCl_2$, 100 mM KCl buffer was used. For pH 5.5, 20 mM cacodylate, 5 mM $MgCl_2$, 100 mM KCl buffer was used. The assay was performed in triplicate (1:1 ratio of RNA:TOPRO, 1 μM each).

The specificity of TARHIY towards H69 was examined by carrying out the binding experiment with $tRNA^{Phe}$. Neomycin was also used as a control, because it is known to bind to $tRNA^{Phe}$. Displacement of fluorescence by the addition of neomycin at both pH 7.0 (**Figures 3.8b** and **3.8c**) and pH 5.5 (**Figure 3.8d** and **3.8e**) conditions, with either 100 mM KCl present (**Figures 3.8c** and **3.8e**) or none (**Figures 3.8b** and **3.8d**). Salt in physiological buffers play an important role in RNA structures and interactions; therefore, binding events of the peptide or neomycin to $tRNA^{Phe}$ in varying ionic strengths was examined. Both $Mg^{2+}$ and $K^+$ play important roles, however, only the concentration of $K^+$ was varied in this study because $Mg^{2+}$ is reported to play important roles in RNA folding.[181] The dye TOPRO is reported to interact with bulges of RNA, therefore,

maintaining the folded structure is important in this assay.[138, 182] For the same reason, although no $Mg^{2+}$ was present in the phage selection at pH 5.5, buffers used at both pH 5.5 and pH 7.0 contained $Mg^{2+}$.

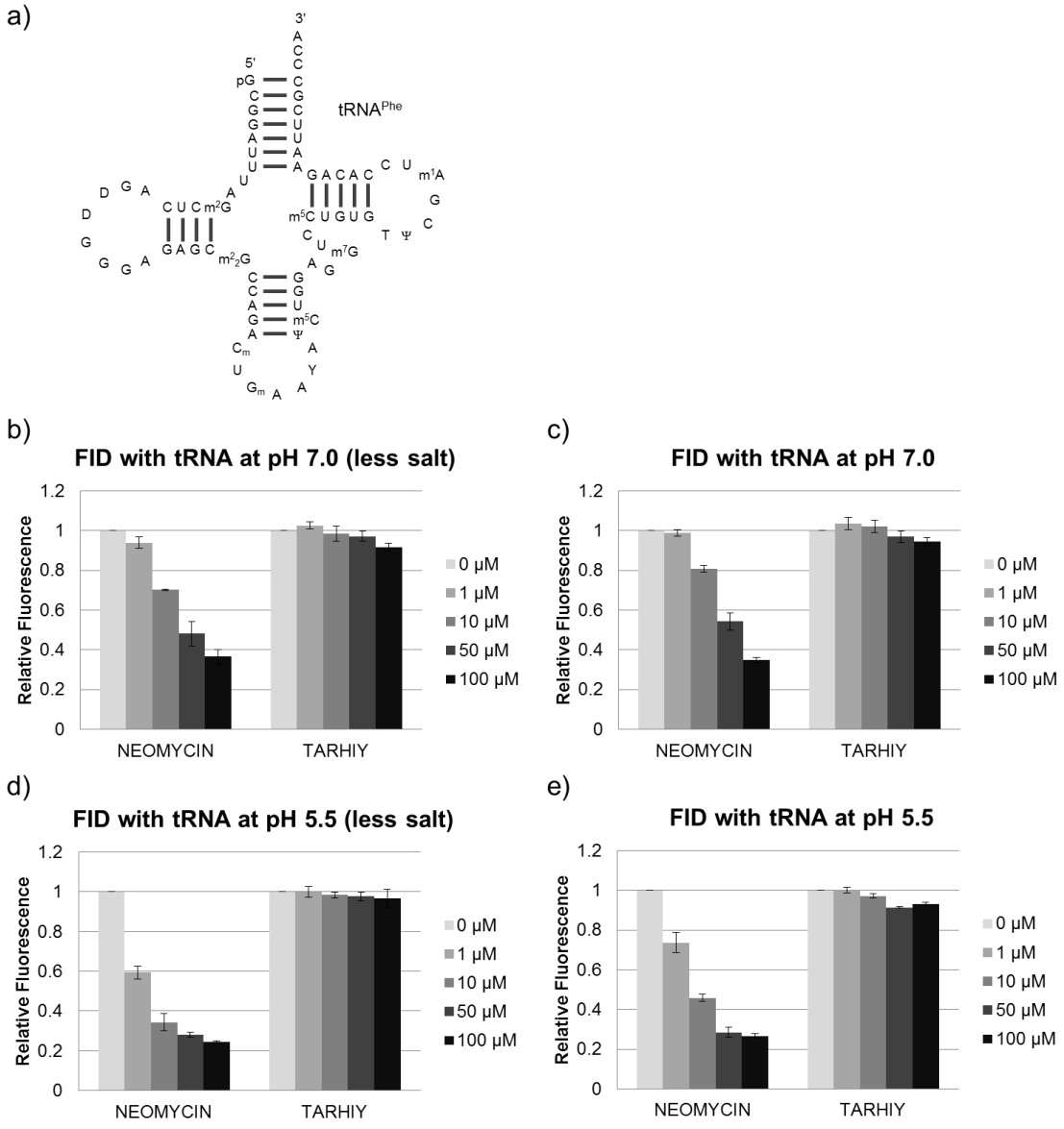


**Figure 3.8.** Salt dependence of neomycin and TARHIY against $tRNA^{Phe}$ at pH 5.5 and pH 7.0. For pH 7.0, 20 mM HEPES, 5 mM $MgCl_2$, 100 mM KCl buffer was used, and for pH 5.5, 20 mM cacodylate, 5 mM $MgCl_2$, 100 mM KCl buffer was used, wherein less salt (b and d) conditions indicate no potassium and regular salt (c and e) conditions indicate 100 mM KCl. The assay was performed in triplicate (1:1 ratio of RNA:TOPRO, 1 µM each). a) The structure of $tRNA^{Phe}$ is shown. b-e) Results of the FID assay with neomycin and TARHIY in the presence of $tRNA^{Phe}$ are shown.

At higher concentrations of the ligands (>50 μM), the salt concentration made little difference (<3%) in displacement of dye at both pH values. At pH 7.0, neomycin exhibited a 1.5-fold lower change of fluorescence compared to studies done at pH 5.5, suggesting less binding to the RNA. At lower concentrations of neomycin (1 and 10 μM), less binding to tRNA was observed when either the salt concentration or pH were raised (up to 20%). The impact of salt on neomycin binding to $tRNA^{Phe}$ is not surprising given that the binding mode involves electrostatic interactions. Unlike neomycin, in less salt conditions without $K^+$ ions present, TARHIY showed little dye displacement (<5% decrease in fluorescence at 100 μM) with addition of the peptide (**Figure 3.9**), and no significant preference for buffer conditions. However, with 100 mM KCl present, upon TARHIY titration at 50 and 100 μM, the dye displacement would increase up to 20 and 28%, respectively. The difference caused by the presence of $K^+$ may be due to the salt playing an important role in folding of the RNA, wherein $K^+$ may stabilize specific RNA structures. This may also provide some information on the binding mode of the peptide. If the peptide binds to H69 through an electrostatic manner, the structure of H69 would be sensitive upon binding of the peptide that would change the secondary structure. This assay is based on TOPRO interacting with the RNA in a certain secondary structure, and if the structure is too flexible, addition of peptide may not impact the structure and cause TOPRO displacement. If the structure is rigid, addition of peptide would be expected to cause displacement of the dye.

A salt dependence study was also performed with H69 ΨΨΨ and H69 UUU (**Figure 3.9**). The salt concentration may impact ligand interactions either directly or indirectly (*i.e.*, RNA structural changes may affect ligand binding). In the absence of potassium, the dye displacement was enhanced with neomycin at all concentrations (up to 25%), but not with TARHIY for both H69 constructs at lower ligand concentrations (<50 μM). The results for neomycin and H69 were consistent with the results for $tRNA^{Phe}$. For

TARHIY, fluorescence quenching was only observed at higher concentrations of the peptide (50 and 100 μM, up to 18%).

A pH dependence study was also performed with H69 ΨΨΨ and H69 UUU (**Figure 3.9**). At pH 5.5, 2-fold enhancement in dye displacement was observed with neomycin (at all concentrations) and TARHIY (at higher concentrations, 50 and 100 μM) compared to pH 7.0. However, no preference for H69 type was observed. At higher concentrations of the peptide (50 and 100 μM, up to 18%) at pH 5.5 conditions, a minor difference was observed upon TARHIY binding. The phage selection was done at pH 5.5 with no $Mg^{2+}$, so the conditions of this assay were different (5 mM $Mg^{2+}$). We hoped to find a peptide that preferred the closed-conformation, and at pH 5.5, the absence of $Mg^{2+}$ was reported to favor this conformation.[67] The presence of $Mg^{2+}$ in this assay may have induced a mixed conformation, resulting in only a small difference between the pH conditions. However, although the peptide did not show selectivity between H69 ΨΨΨ and H69 UUU, a very modest selectivity of H69 over $tRNA^{Phe}$ can be observed if the data in **Figures 3.8** and **3.9** are compared. Lastly, the peptide caused little fluorescence change (up to 28% at 100 μM), while neomycin showed displacement up to 90% at 100 μM.

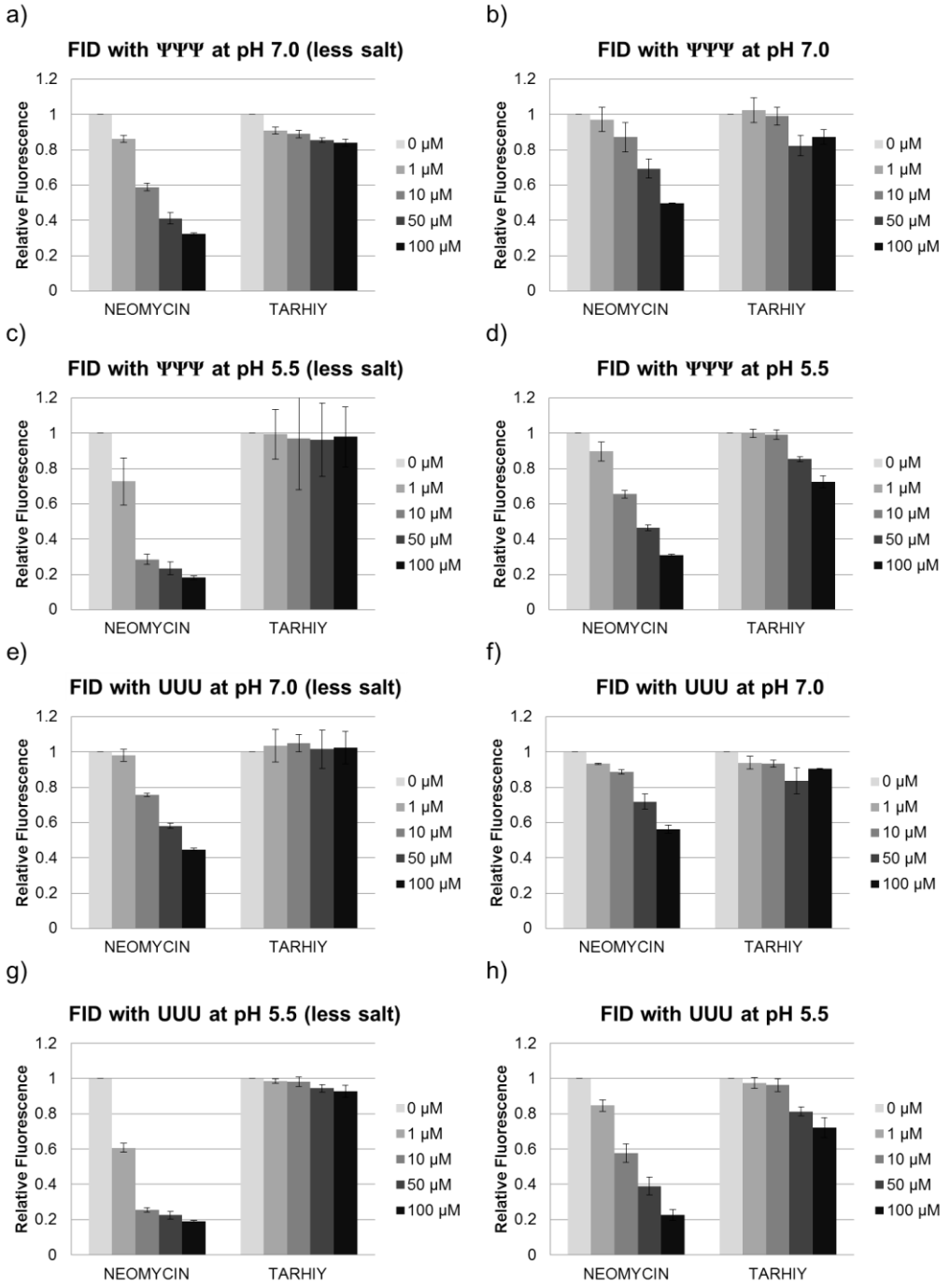


**Figure 3.9.** Salt dependence of neomycin and TARHIY against H69 ΨΨΨ and H69 UUU at pH 5.5 and pH 7.0. For pH 7.0, 20 mM HEPES, 5 mM $MgCl_2$, 100 mM KCl buffer was used, and for pH 5.5, 20 mM cacodylate, 5 mM $MgCl_2$, 100 mM KCl buffer was used, wherein less salt (b and d) conditions indicate no potassium and regular salt (c and e) conditions indicate 100 mM KCl. The assay was performed in triplicate (1:1 ratio of RNA:TOPRO, 1 μM each).

### 3.6. Binding studies with ESI-MS

The goal of ESI-MS experiments was to determine the binding affinity and selectivity of the peptide TARHIY towards H69 ΨΨΨ and H69 UUU at differing buffer conditions (*i.e.*, varying pH), and obtain apparent $K_d$ values and stoichiometries. Previous studies have shown that ESI-MS is a method useful to obtain apparent $K_d$ values for peptide-RNA complexes.[118, 120, 169] The dissociation constant obtained from this study is relative, not absolute, due to the ionization efficiencies being different between RNA and peptide. Furthermore, the decrease of free RNA was not directly related to the increase of the RNA-peptide complex formation (**Figures 3.10 to 3.13**), because the (4-) charge state for the RNA overlapped with the dimer peak of the peptide. In this thesis work, the binding was measured at 10 mM $NH_4OAc$ for both pH 5.5 and pH 7.0 conditions, which is lower than the salt concentration used for selection. The salt concentration employed was lower due to the instrumentation limits; however, the data quality was still poor due to background salt in the samples, which is more apparent in low salt buffers. Despite much effort to purify them, the peptide samples contained residual salt after HPLC. Each experiment was performed in triplicate.

Since the RNA and peptides have different ionization efficiencies, the binding ratios were different for each condition tested. Therefore, conditions were carefully controlled in order to compare and get relative binding information for different RNAs or peptides. The binding ratio was calculated by comparing the (5-) charge states for both RNA and complex. Although the (4-) charge state of H69 showed a stronger signal than other charge states, we were not able to focus on this charge state because it matched the dimer peak of the peptide (**Figures 3.10 to 3.13**). Therefore, the (5-) charge state of the RNA and the complex were used for these studies to determine the peak areas and relative free and bound concentrations.

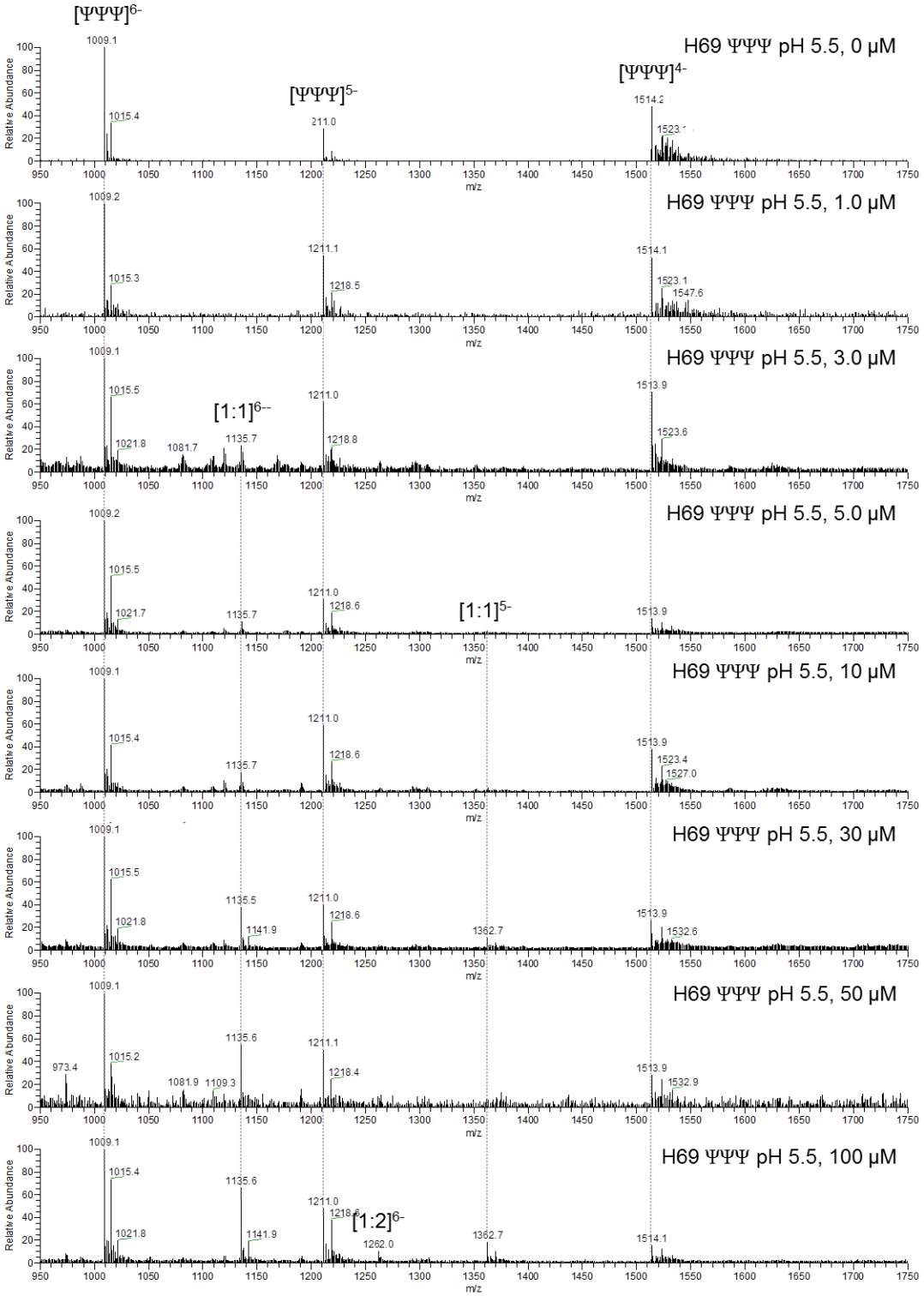


**Figure 3.10.** Representative ESI-MS results for TARHIY titration at pH 5.5 against H69 ΨΨΨ are shown. In the spectra, complexes of 1:1 and 1:2 (H69 ΨΨΨ:peptide) binding ratios are observed. The experiments were performed in triplicate at 10 mM $NH_4OAc$ (pH 5.5).

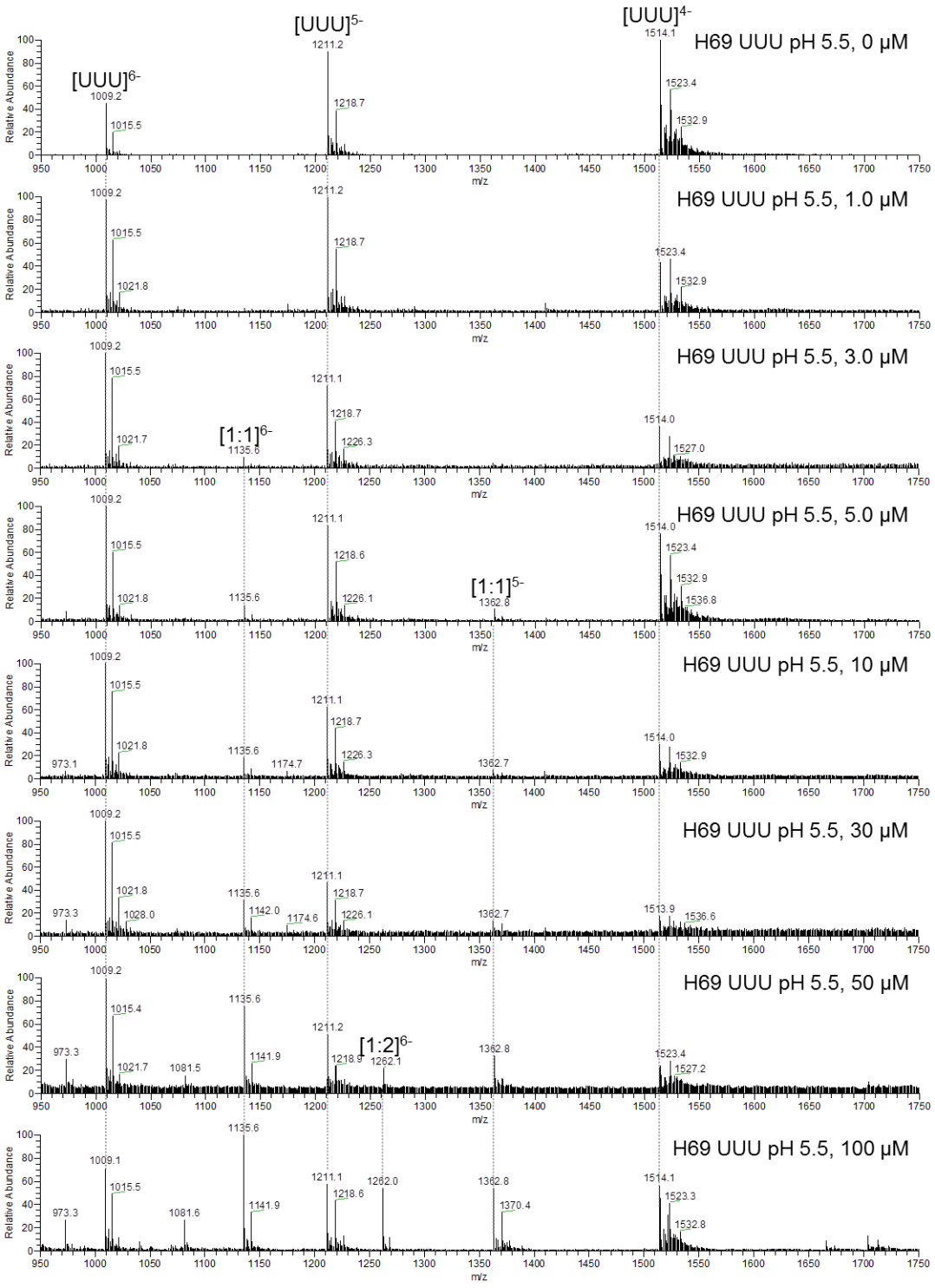


**Figure 3.11.** Representative ESI-MS results for TARHIY titration at pH 5.5 against H69 UUU are shown. In the spectra, complexes of 1:1 and 1:2 (H69 UUU:peptide) binding ratios are observed. The experiments were performed in triplicate at 10 mM $NH_4OAc$ (pH 5.5).

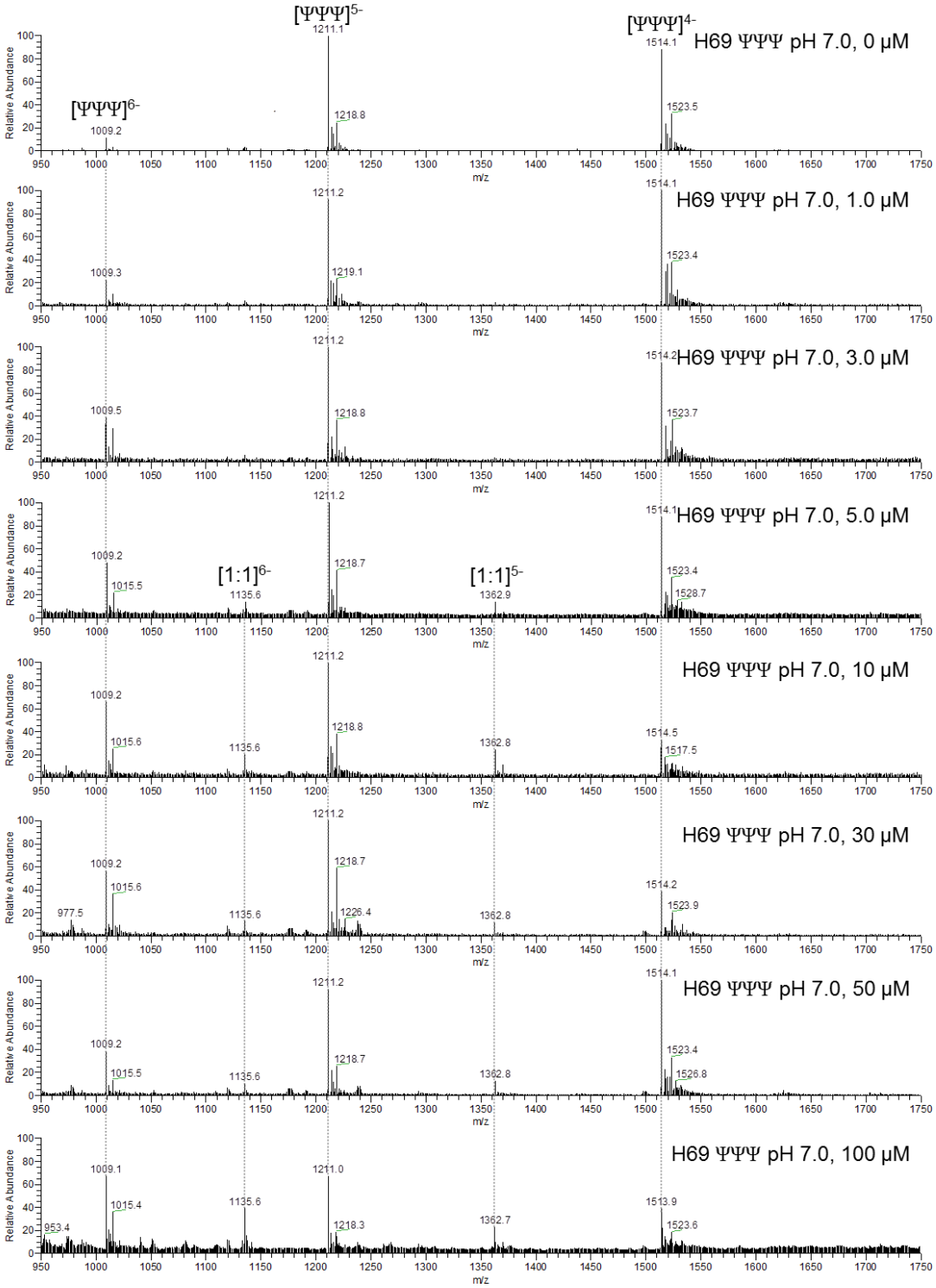


**Figure 3.12.** Representative ESI-MS results for TARHIY titration at pH 7.0 against H69 ΨΨΨ are shown. In the spectra, complexes of 1:1 and 1:2 (H69 ΨΨΨ:peptide) binding ratios are observed. The experiments were performed in triplicate at 10 mM $NH_4OAc$ (pH 7.0).

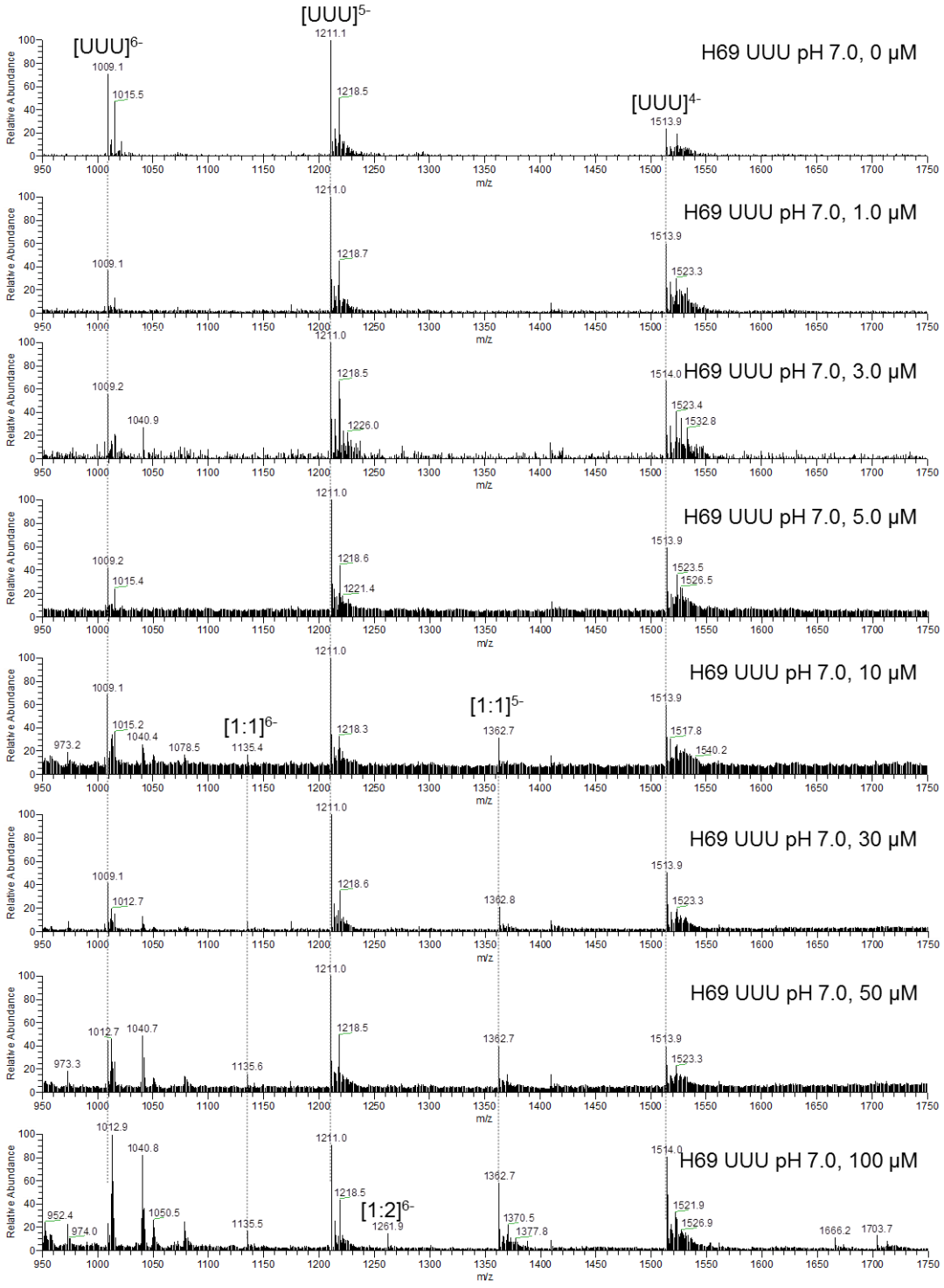


**Figure 3.13.** Representative ESI-MS results for TARHIY titration at pH 7.0 against H69 UUU are shown. In the spectra, complexes of 1:1 and 1:2 (H69 UUU:peptide) binding ratios are observed. The experiments were performed in triplicate at 10 mM $NH_4OAc$ (pH 7.0).

The apparent $K_d$ values as given in **Table 3.4** were obtained using the quadratic equation. The fraction of RNA-peptide complex to free RNA was plotted using GraphPad (**Figure 3.14**). The RNA-peptide complex did not reach saturation most likely because the ionization efficiencies of the RNA-peptide complexes are much lower than that of the free RNA. Despite these limitations, we could gain knowledge about relative binding affinities. The peptides showed moderate (low μM) binding to both H69 ΨΨΨ and H69 UUU. As with the FID studies, no significant selectivity between the modified and unmodified RNA was observed. Although the binding affinity (μM) of the peptide to RNA may appear low compared to protein-drug interactions (nM), it should be pointed out that aminoglycosides, which are effective ribosome-targeting antibiotics, bind with similar affinity to rRNA (low μM) and with very poor selectivity.

When the titrated peptide concentration exceeded 20 μM, a complex of peptide dimer bound to RNA was detected, which may imply an aggregation or more than one binding site of the peptide. These results led to studies of multimeric peptide binding studies with H69 (**Chapter 4**).

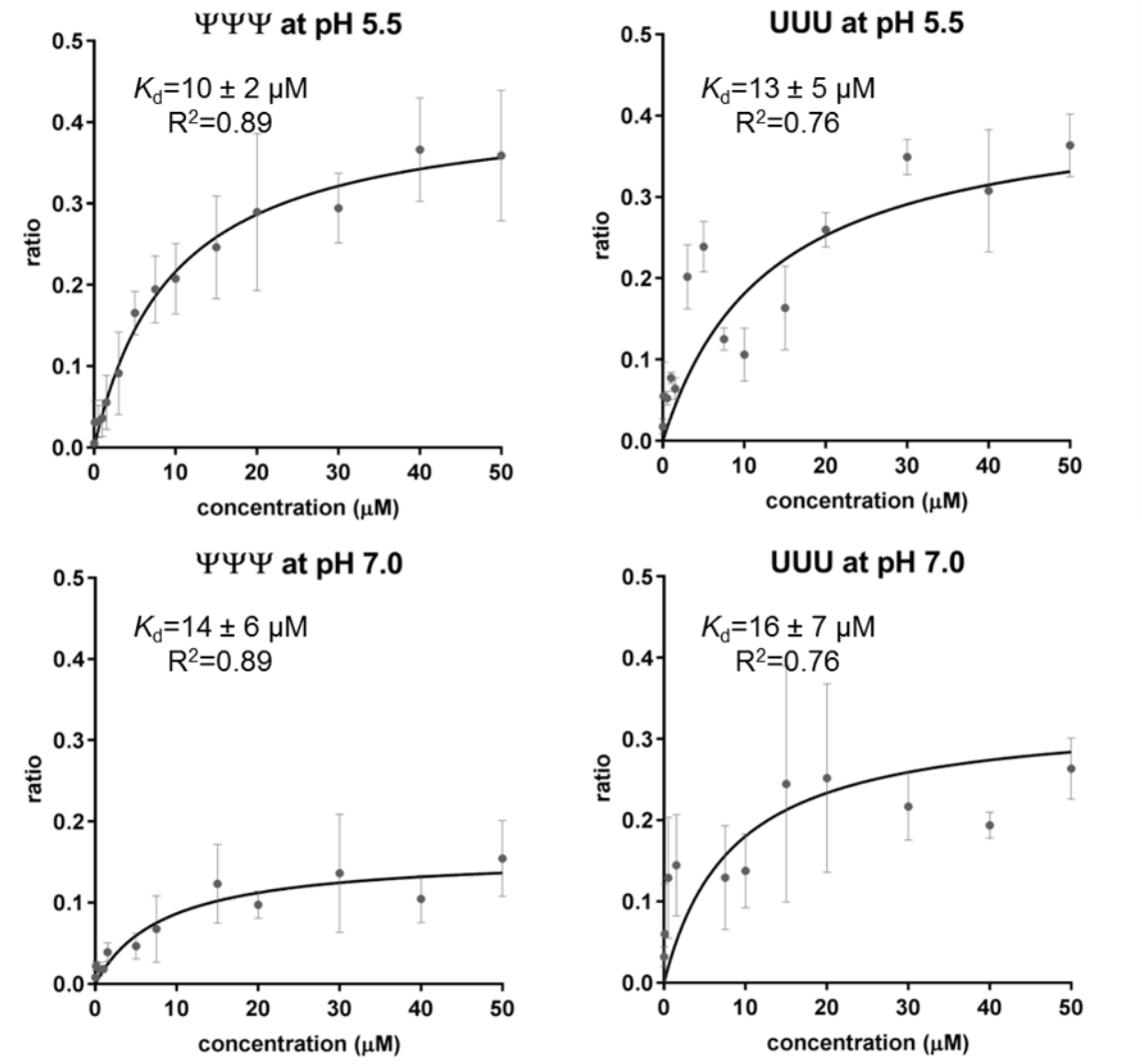


**Figure 3.14.** ESI-MS results for TARHIY at 10 mM $NH_4OAc$ (pH 5.5 and pH 7.0) against H69 ΨΨΨ and H69 UUU. a) The titration curves for TARHIY bound to H69 ΨΨΨ and H69 UUU (y axis: binding ratio of at (5-) charge state) at different buffer conditions (pH 5.5 vs. pH 7.0) are shown.

**Table 3.4.** Apparent dissociation constants ($K_d$s) obtained from ESI-MS. The apparent dissociation constants ($K_d$ values) were obtained by fitting relative binding ratios with a quadratic equation.

| apparent $K_d$ | ΨΨΨ | UUU | UUU/ΨΨΨ |
|---|---|---|---|
| pH 5.5 | 13 ± 3 μM | 19 ± 3 μM | 1.3 |
| pH 7.0 | 14 ± 6 μM | 16 ± 7 μM | 1.1 |

### 3.7. Binding studies with SPR

SPR is a method used to obtain apparent $K_d$ values in solution phase by monitoring interactions of the surface of a CM5 chip.[183] This method does not need a tag on the peptide, and the binding event is detected by monitoring the change in response unit. The response unit is derived from alteration of the refractive index of the chip upon binding. To a CM5 chip was immobilized streptavidin, followed by immobilization of biotinylated H69 ΨΨΨ. To reduce nonspecific binding after immobilization of the biotinylated H69 ΨΨΨ, biotin was passed through the cells to coat any exposed streptavidin sites. Following H69 immobilization, the TARHIY concentration was varied from 0 to 100 μM in both pH 5.5 (20 mM PBS, 100 mM KCl) and pH 7.0 (20 mM HEPES, 100 mM KCl, 5 mM $MgCl_2$) buffers. Each experiment was performed in triplicate. Since the mass of the peptide (758 Da) was smaller compared to H69 (6060 Da), the response unit change was small, but significant. This was the first time in our laboratory that we were able to monitor peptide binding to H69 using SPR. However, the signal was only detectable under pH 5.5 conditions, possibly due to nonspecific charge-charge interactions between the positively charged peptide (pI=9) and negatively charged streptavidin (pI=5) under pH 7.0 conditions. In **Figure 3.15**, curves obtained from streptavidinylated surfaces exhibit a sharp increase immediately after injection followed by a flat line, while curves obtained from avidinylated surfaces exhibit a more gradual increase following the initial injection. Avidin (pI=10.5) was used instead of streptavidin in an attempt to detect binding at pH 7.0, but was unsuccessful (**Figure 3.15**). A binding affinity of 27 μM was obtained with streptavidinylated surfaces, and 11 μM with avidinylated surfaces (2.5-fold tighter binding). Although the phage were selected using streptavidinylated magnetic beads, the $K_d$ value obtained with avidinylated surfaces (11 μM) matched more closely with the $K_d$ value obtained with ESI-MS (10 ± 2 μM).

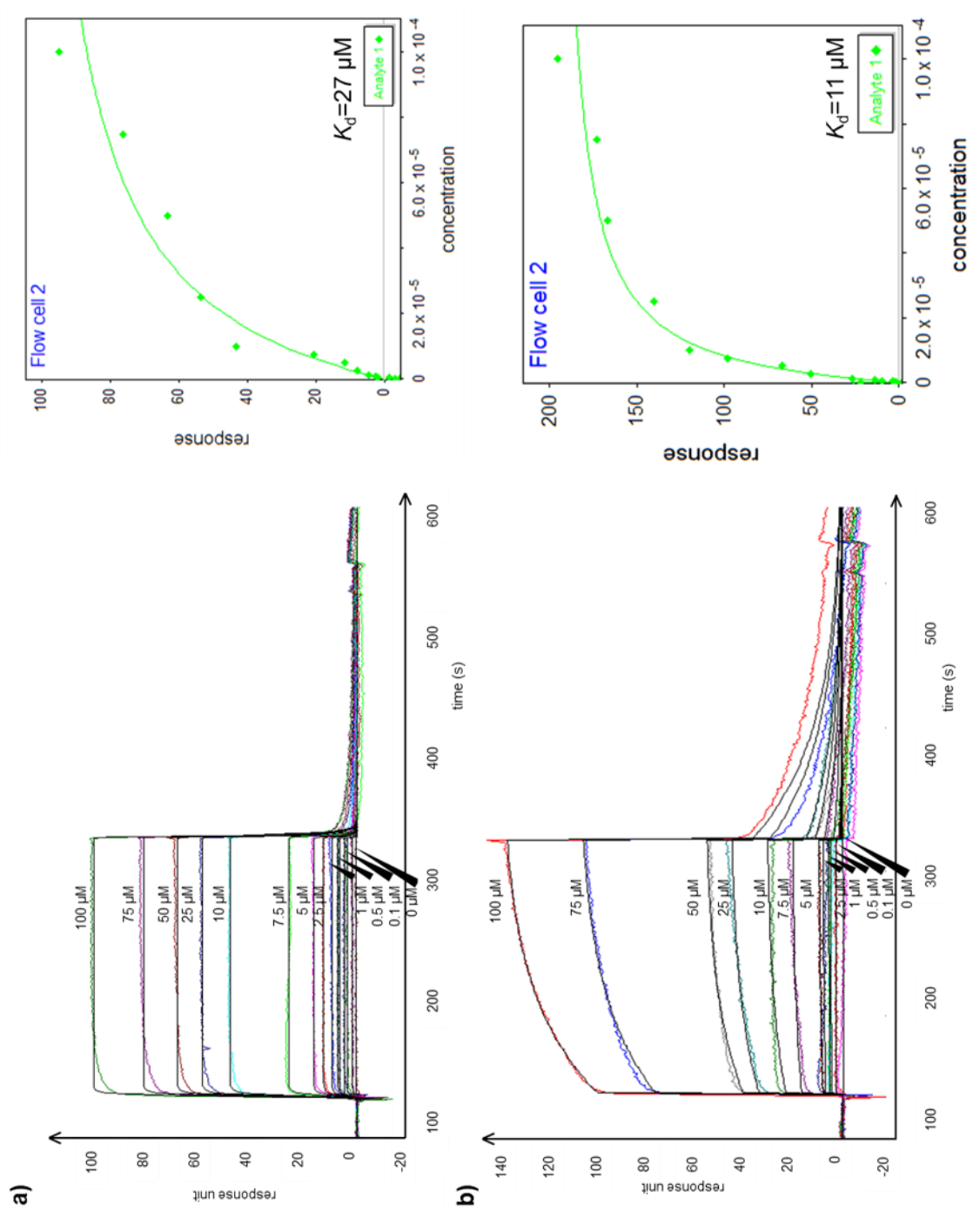


**Figure 3.15.** SPR results for TARHIY at pH 5.5 (20 mM cacodylate, 100 mM KCl, and 0.1% Tween-20) against H69 ΨΨΨ with a) streptavidin or b) avidin. The curves shown in color correspond to measurements of a two-fold serial dilution of the peptide ligands over a concentration range. The curves in black correspond to global fits in 1:1 binding model ($R^2$>0.88).

The kinetics of the binding events with streptavidin or avidin revealed difference between the two proteins immobilized to the CM5 chip. For streptavidin, $k_{on}$ of 4.2e3 $Ms^{-1}$ and $k_{off}$ of 2.7e-5 $s^{-1}$ values were obtained, compared to $k_{on}$ of 13 $Ms^{-1}$ and $k_{off}$ of 0.02 $s^{-1}$ for avidin. A higher $k_{on}$ was observed with streptavidin, implying a fast nonspecific charge-charge binding interaction of the peptide to H69. The apparent binding affinities obtained from $k_{on}$ and $k_{off}$ appeared to be unusually high or low (6.4 nM for streptavidin and 1.4 mM for avidin). Furthermore, poor fitting was observed in both cases, implying that the binding of TARHIY to H69 is not through 1:1 binding.

**3.8. Binding studies with BLItz**

The goal of BLItz studies was to determine the binding affinities of peptide TARHIY to H69 in pH 5.5 and pH 7.0 buffer conditions and compare to other methods. Similar to SPR, this method is useful for monitoring binding events *in situ*, and can be used to obtain kinetic information as well as determining the binding constants.

Previous studies have shown that BLItz results correlate with SPR,[162] likely because of the similar detection method. One major difference between BLItz and SPR is the mode of association and dissociation. SPR has the biosensor immobilized onto a chip and there are flow channels that the ligands and analytes flow through. Therefore, for association and dissociation, a buffer solution containing a target or ligand is constantly flowing over the chip. This process may cause mass transport, but the concentration of the solution stays constant during the process. BLItz uses a biosensor that is immobilized onto a tip that is dipped into a tube containing a buffer solution with a target or ligand. The instrument is designed to constantly shake the tube so that the solution around the biosensor is not just monitoring diffusion.[162, 184] Association and dissociation in this method is done in the same solution into which the biosensor is dipped, with concentrations of the target or ligand increasing or decreasing manually. Therefore, for

binding studies with molecules sensitive to the concentration, it is necessary to use large volumes (250-300 µL) of the solution of interest to minimize error.

In **Figure 3.16**, binding curves obtained from BLItz and dissociation constants are shown. The peptide ligand, which has a mass of 1/8$^{th}$ of the immobilized RNA, produced a small change in signal in SPR. With the use of BLItz, the change in signal was more apparent, as shown in **Figure 3.16**. (Expanded figures are displayed in **Appendix B**)

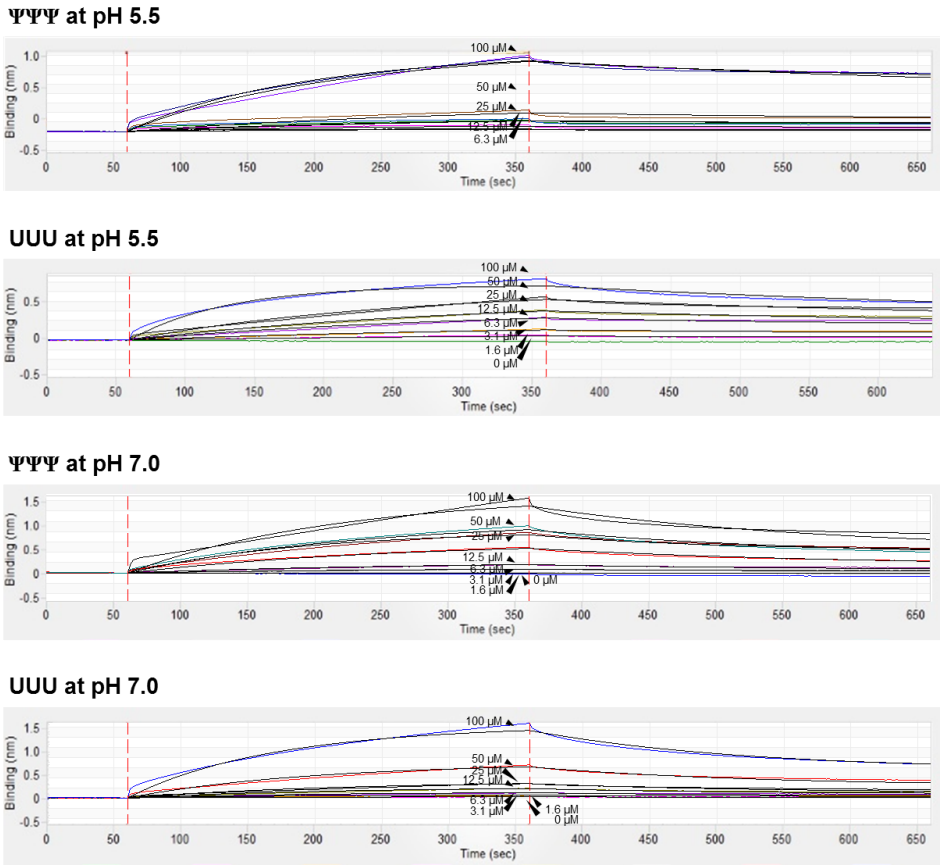


**Figure 3.16.** BLItz binding curves for TARHIY at pH 5.5 (20 mM cacodylate, 100 mM KCl, and 0.1% Tween-20) and pH 7.0 (20 mM HEPES-KOH, 100 mM KCl, 5 mM $MgCl_2$, and 0.1% Tween-20) against H69 ΨΨΨ and H69 UUU. The curves shown in color correspond to measurements of a two-fold serial dilution of the peptide ligands over a concentration range of 0 to 100 µM. The curves in black correspond to global fits in 1:1 binding model. The experiments were performed in triplicate. The expanded figures are displayed in **Appendix B**.

Examining the kinetics of the binding events revealed similar $k_{on}$ and $k_{off}$ values for TARHIY binding to H69 ΨΨΨ and H69 UUU at pH 5.5 and pH 7.0. The average $k_{on}$ and $k_{off}$ values are given in **Table 3.5**. In these cases, poor fitting and large errors were observed, both by the sensogram (**Figure 3.16** and **Appendix B**) and the rate constants (**Table 3.5**), implying that the binding of TARHIY to H69 is probably not through a simple 1:1 binding mode.

**Table 3.5.** Rate constants ($k_{on}$ and $k_{off}$) obtained from BLItz

| | $k_{on}$ ($M^{-1}s^{-1}$) | $k_{off}$ ($s^{-1}$) |
|---|---|---|
| ΨΨΨ at pH 5.5 | $1.7 \times 10^2 \pm 6.3 \times 10^1$ | $2.9 \times 10^{-3} \pm 4.9 \times 10^{-5}$ |
| ΨΨΨ at pH 7.0 | $1.2 \times 10^2 \pm 2.2 \times 10^1$ | $1.8 \times 10^{-3} \pm 7.5 \times 10^{-5}$ |
| UUU at pH 5.5 | $1.3 \times 10^2 \pm 3.5$ | $1.3 \times 10^{-3} \pm 2.5 \times 10^{-5}$ |
| UUU at pH 7.0 | $1.1 \times 10^2 \pm 3.9 \times 10^1$ | $2.0 \times 10^{-3} \pm 3.6 \times 10^{-4}$ |

Association ($k_{on}$) and dissociation ($k_{off}$)rates were determined using global fit, and the average from triplicate measurements are displayed.

The apparent dissociation constants obtained from BLItz are reported in **Table 3.6**. The apparent dissociation constants were ~15 μM, which did not show a significant preference for RNA type or pH value. The binding affinities obtained with this method in physiological buffers, which were used in the phage selection, agree well with the data from ESI-MS. As mentioned earlier these values also demonstrate moderate affinity of the peptide for H69, which matches that of some natural antibiotics that target H69.

**Table 3.6.** Apparent dissociation constants ($K_d$s) obtained from BLItz

| apparent $K_d$ | ΨΨΨ | UUU | UUU/ΨΨΨ |
|---|---|---|---|
| pH 5.5 | 15 ± 1 μM | 15 ± 2 μM | 1.0 |
| pH 7.0 | 15 ± 3 μM | 16 ± 2 μM | 1.1 |

### 3.9. NMR spectroscopy

In this study, 2D $^1$H homonuclear NMR experiments (2D gCOSY) were employed to examine the binding of TARHIY to H69. Crosspeaks between the H5-H6 protons on the

pyrimidines of H69 were observed. If the ligand binds to H69, the local chemical environments of nuclei on H69 may be altered by the ligand directly if it binds in proximity or changes the local H69 RNA conformation upon titration with peptide. Overlays of NMR spectra of H69 obtained with TARHIY are shown in **Figures 3.17** to **3.19**.

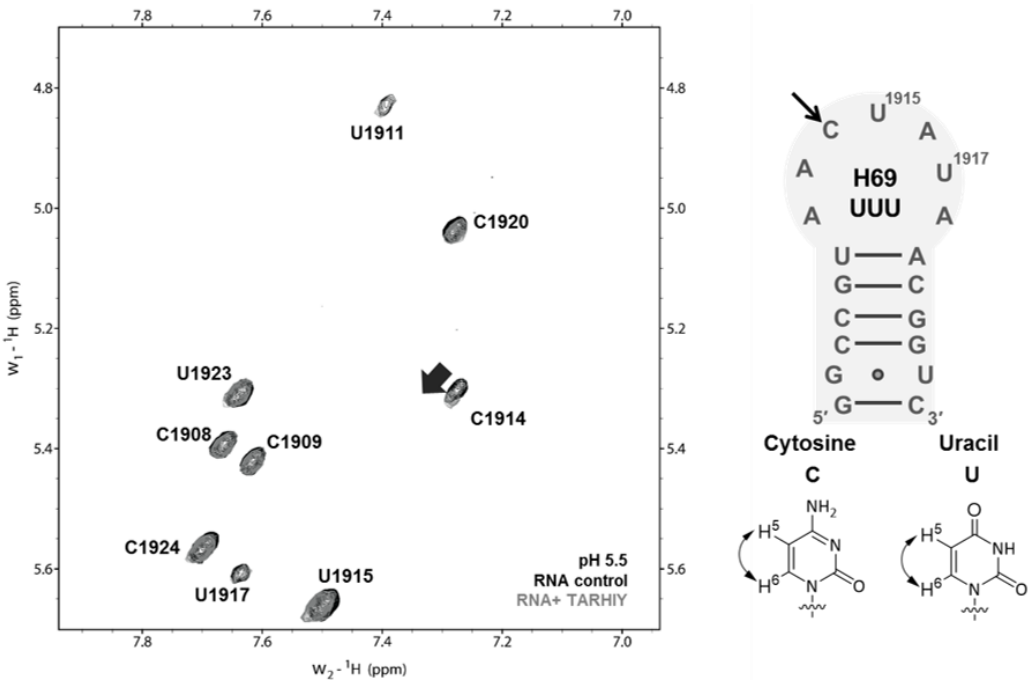


**Figure 3.17.** Overlay of the NMR spectra for H69 UUU in the absence (black) or presence (grey) of TARHIY at pH 5.5. The concentrations of RNA and peptide were 50 and 500 μM, respectively. The arrow indicates the chemical shift change and direction at C1914. The NMR spectra were obtained by Evan Jones.

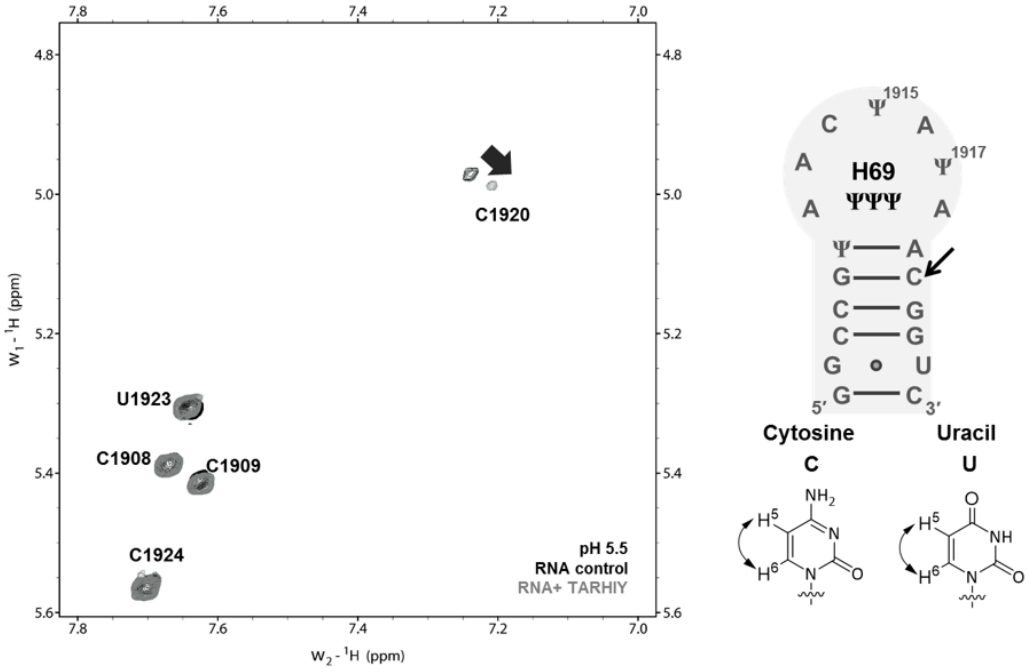


**Figure 3.18.** Overlay of the NMR spectra for H69 ΨΨΨ in the absence (black) or presence (grey) of TARHIY at pH 5.5. The concentrations of RNA and peptide were 50 and 500 μM, respectively. The arrow indicates the chemical shift change and direction at C1914. The NMR spectra were obtained by Evan Jones.

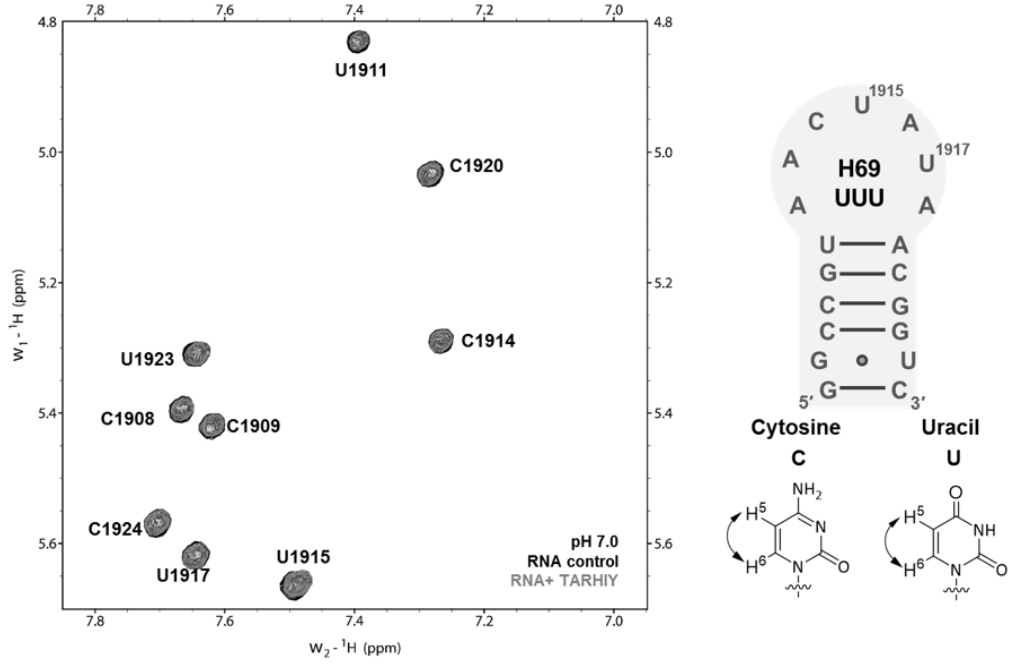


**Figure 3.19.** Overlay of the NMR spectra for H69 UUU in the absence (black) or presence (grey) of TARHIY at pH 7.0. The concentrations of RNA and peptide were 50 and 500 μM, respectively. The arrow indicates the chemical shift change and direction at C1914.The NMR spectra were obtained by Evan Jones.

Upon addition of TARHIY at pH 5.5 conditions, changes in the chemical shifts were observed at C1914 (**Figure 3.17**) and C1920 (**Figure 3.18**) for H69 ΨΨΨ and H69 UUU, respectively. The chemical shift change in H69 UUU at C1914 and U1915 was less than 0.02 ppm (**Figure 3.17**), whereas the change at C1920 for H69 ΨΨΨ was ~0.04 ppm. For H69 ΨΨΨ at pH 5.5, the C1914 crosspeak was not detected, possibly due to structural dynamics (**Figure 3.18**). The changes upon peptide binding imply alterations in the chemical environment around those residues. Residue C1914 is located in the loop region of H69, and C1920 is at the stem-loop transition region. The results imply a direct interaction with TARHIY or an induced conformation change at these regions due to peptide binding. Residue C1914 was shown in previous studies to participate in base stacking with Ψ1915.[48, 185] This is the first time that we observed interactions in the loop region of H69 by a small molecule. Previous studies with DMS probing suggested that the RNA structure involves A1913 existing in a stacked-in (less solvent exposed) conformation at lower pH (pH 5.5) and lower $Mg^{2+}$ concentrations (1 mM).[178] The buffer conditions for the selection experiment was at pH 5.5 with no $Mg^{2+}$ (20 mM $KH_2PO_4$, 100 mM KCl, 1 mM EDTA, pH 5.5 or pH 7.0).[178] The concentrations of RNA and peptide were 50 and 500 μM, respectively.

The spectrum of H69 UUU with TARHIY at pH 7.0 is shown in **Figure 3.19**. No change in the chemical shifts were observed in this case. The binding studies discussed in previous sections revealed that there was no apparent difference in binding affinity to H69 ΨΨΨ or H69 UUU regardless of the solution pH. The NMR results suggest that binding of the peptide to H69 UUU at pH 7.0 changes the local RNA conformation which was not observed for H69 ΨΨΨ. From previous studies, it was shown that a decrease in the pH value may induce increased stacking of the loop region in H69 ΨΨΨ.[67, 178] The peptide may bind to the loop, but the stacking interactions may not be impacted enough to observe a change in the NMR spectrum.

### 3.10. Growth assay

To determine whether the selected phage have effects on survival of *E. coli*, a growth assay was performed. Custom phage displaying peptides TARHIY and TPARHIY were prepared to determine whether there is a difference between the two sequences with respect to bacterial growth. A known artifact sequence SILPYPY, which was found in this study and previous studies, was used as a negative control.[175] The custom phage is *Kan*$^R$, and since kanamycin does not interfere with H69 function, the growth was predicted to be dependent on the phage present. The custom phage were grown with kanamycin at 60 mg/L in LB media. The bacterial strain ER2738 used for phage display was *Tet*$^R$, therefore the custom phage would not grow in ER2738. Instead, ER2267, a phage strain that is *Kan*$^R$, was used for the growth assay.

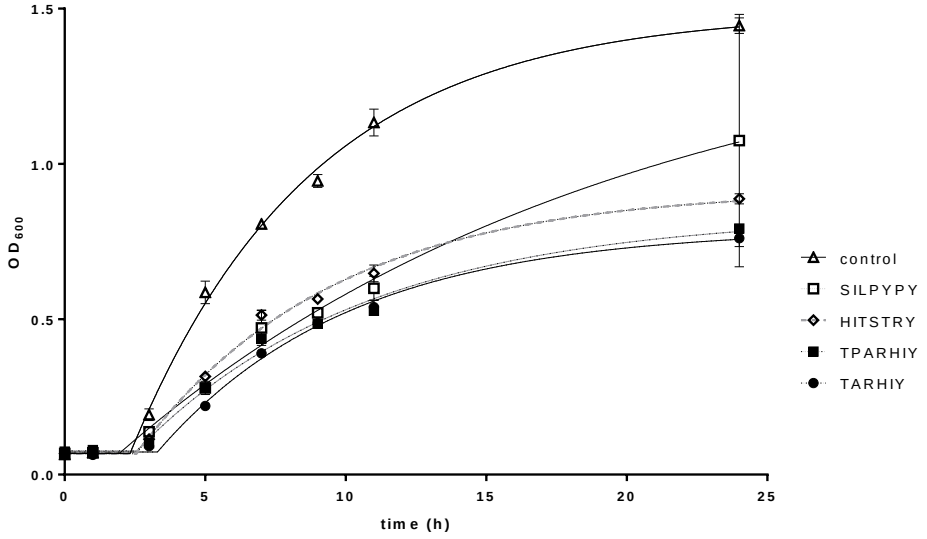


**Figure 3.20.** Growth assay results are shown. To media containing ER2267, ~$10^{10}$ virions of phage were added and their effect on growth was monitored. Values are average values of three measurements. Except for the measurement with SILPYPY (18% error) at 24 h, each measurement exhibited a small difference (<3%). The data were fitted with GraphPad.

The goal of this assay was to examine growth impact of the selected phage. The selected phage (TARHIY) reduce the growth at 24 h by 40% compared to the control

with no phage infection. However, for the other phage studied (TARHIY, TPARHIY, HITSTRY, and SILPYPY), a decrease (<20% at 24 h) in growth was observed. At 24 h, compared to SILPYPY, a peptide that was selected in previous studies to be a fast grower, peptides TPARHIY and TARHIY showed 20% decrease in growth. Compared to HITSTRY, another peptide that was selected during this selection, peptides TPARHIY and TARHIY showed 10% decrease in growth. However, the difference was not significant, and no phage showed more than 40% decrease in growth, which may reveal some information of the selected phage. As discussed in **Sections 3.1** and **3.2**, the phages selected through phage display may be fast growers in general, because phage causing complete growth inhibition would never be selected. The phage encoding TARHIY and TPARHIY showed similar growth, implying that the proline may not impact the peptide activity. The TPARHIY peptide was selected from phage display and appeared 38 times out of 105 sequences, indicating that it overpowered other fast-growing phage. In contrast, the TARHIY peptide was discovered through the binding analysis following selection. Nonetheless, they appear to have similar activity in the growth assay.

### 3.11. Competition studies of peptide TARHIY and neomycin to H69 using BLItz

Previous studies have shown that neomycin interacts with the stem region of H69.[186-187] For ribosome recycling, RRF interacts with H69, which then separates H69 from forming B2a intersubunit of the 70S ribosome.[32, 61, 186, 188] Rings I and II of neomycin was shown to be bound to H69 at residues G1921-C1924 and G1906 (**Figure 3.21**), which alters the conformation of H69.[186] The interaction between H69 and RRF was shown to be disrupted upon binding of 2-DOS, leading to inhibition of ribosome recycling.[186]

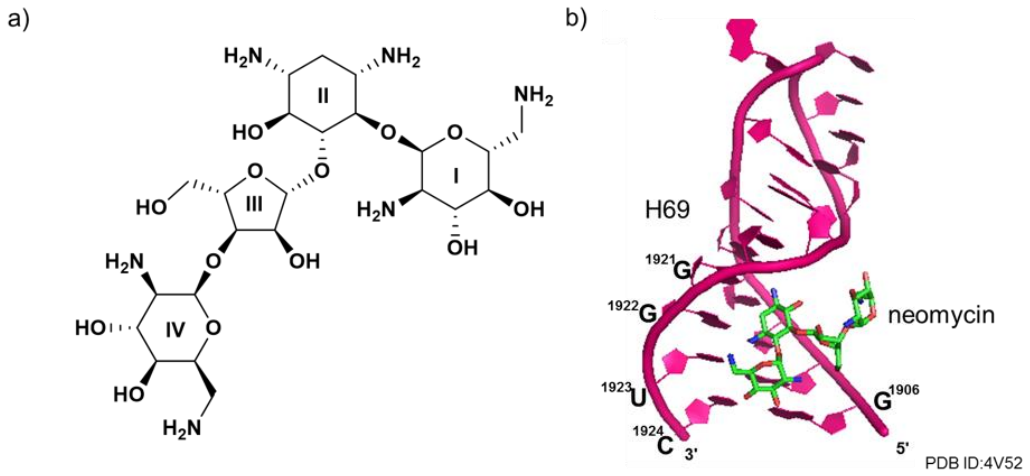


**Figure 3.21.** A chemical structure of neomycin and crystal structure (PDB ID: 4V52) of H69 and neomycin is shown.

In previous sections, a peptide TARHIY was derived from a sequence selected from phage display, which exhibited a moderate binding to the loop region of H69. Through ESI-MS and BLItz, the peptide exhibited moderate binding to H69. A Scatchard analysis of ESI-MS data implied there is cooperative binding of the peptides to H69. The primary binding site was the H69 loop region. Therefore, peptide TARHIY binding to H69 in the presence of neomycin was explored. The peptide, TARHIY was shown to have binding to the loop region of H69, while neomycin was shown in previous studies to bind to the stem region of H69, so we were curious to know if both ligands could bind simultaneously to H69.

### 3.11.1. Design of binding assay of neomycin and TARHIY to H69 using BLItz

In previous chapters, biotinylated H69 was immobilized to a streptavidinylated surface to select peptide ligands and to monitor the binding of ligands, such as monomer peptides or dimeric peptides in buffer, using SPR or BLItz. However, to monitor dual binding of neomycin and peptide TARHIY, immobilization of the RNA followed by binding of ligands (neomycin or peptide TARHIY) may not be able to show dual binding modes. Therefore, to monitor dual binding of neomycin and peptide TARHIY to H69, instead of

immobilizing the target, H69, a biotinylated peptide TARHIY was immobilized onto the tip, followed by association of free H69. After the H69 association step, we monitored the biosensor in a secondary association step in buffer, then solutions containing neomycin or peptide TARHIY, or the free RNA (**Figure 3.22**).

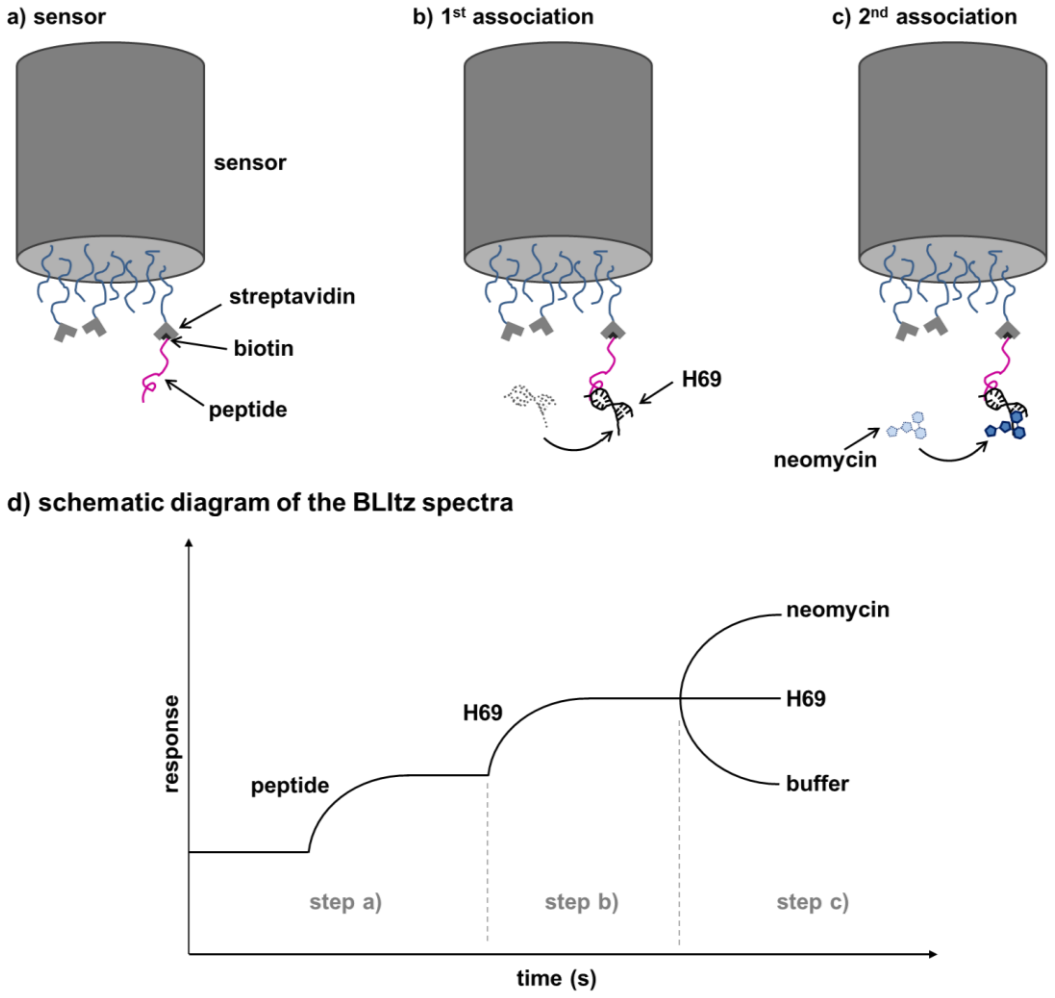


**Figure 3.22.** A schematic design of a BLItz experiment to monitor dual binding of peptide and neomycin to H69 is shown. a) Sensor preparation with peptide immobilization is illustrated. b) The first association of H69 is represented. c) The second association of neomycin is shown. d) A schematic sensogram of steps a) to c) is shown.

To immobilize the peptide onto a streptavidinylated biosensor, a biotinylated peptide TARHIY was synthesized. A schematic description of the synthesis is shown in **Scheme**

**3.1.** By utilizing a orthogonally protected Fmoc-Lys(ivDde)-OH, peptide TARHIY was synthesized onto the α-amino group, followed by attachment of biotin onto the ε-amino group. The peptide was then cleaved with a cleavage cocktail described in **Chapter 2**, followed by purification with HPLC. The structure and MALDI-TOF spectrum of the purified biotinylated peptide TARHIY is shown in **Figure 3.23**.

**Scheme 3.1.** Scheme of synthesis of biotinylated peptide TARHIY

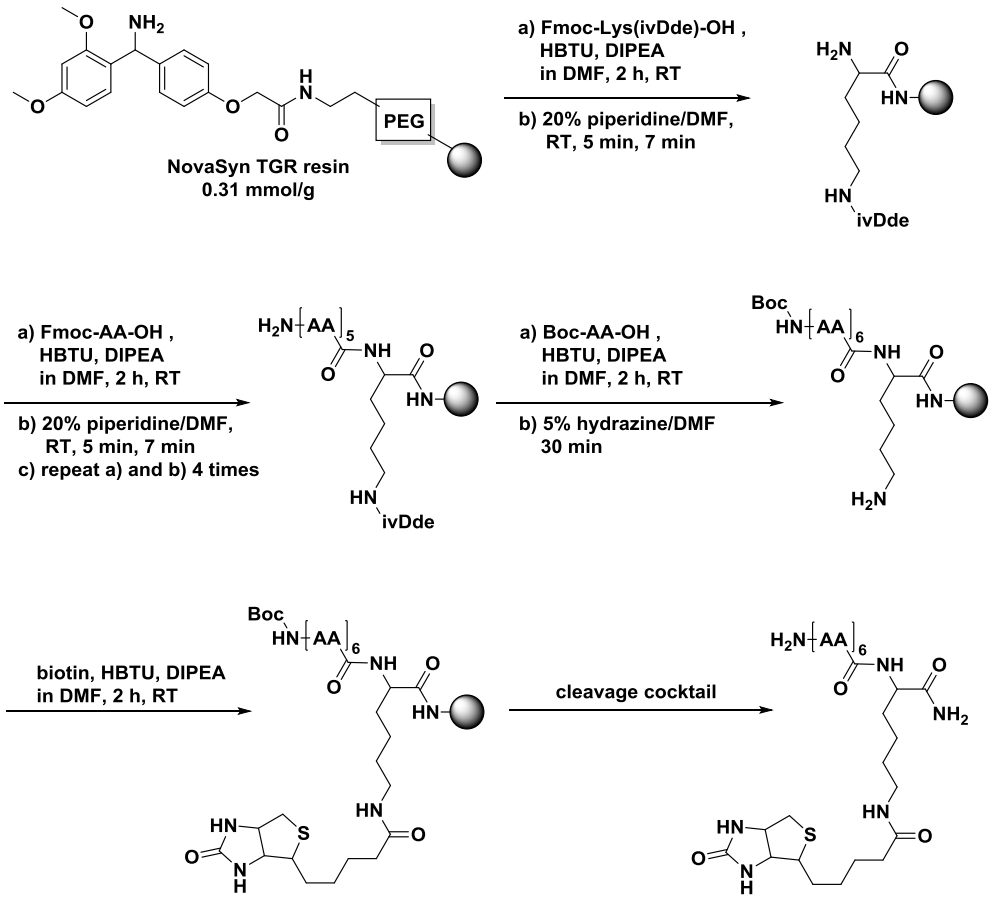

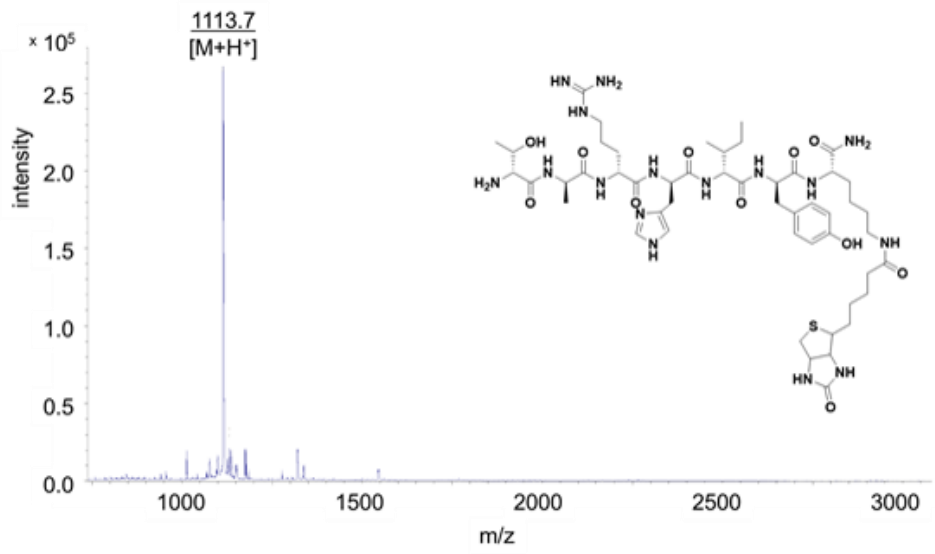


**Figure 3.23.** MALDI-TOF spectrum of biotinylated peptide TARHIY is shown.

### 3.11.2. Binding of neomycin and TARHIY to H69 using BLItz

To monitor possible dual binding of neomycin and TARHIY to H69, BLItz was used. To a streptavidinylated sensor, biotinylated peptide TARHIY (Bi-TARHIY) was immobilized, followed by binding events at pH 5.5. The RNA H69 UUU (1 μM) in 20 mM PBS, 100 KCl was then added, followed by incubation with buffer, neomycin (1 μM), or free peptide TARHIY (10 μM) in buffer. The concentration of neomycin solution and peptide TARHIY was based on the $K_d$s observed in previous studies. The sensogram is shown in **Figure 3.24.** In theory, if the binding sites of neomycin and peptide TARHIY are independent from each other, one would expect to see a sensogram such as **Figure 3.24b**, which shows increase in signal when neomycin binds, and decrease in signal in buffer. However, the buffer showed similar dissociation curve compared to the free peptide, while neomycin showed a steep decrease in dissociation. This result indicates that although the primary binding sites are different, the binding modes of the two molecules to H69 UUU are not independent. In this case, neomycin and TARHIY appear to have

competitive binding to H69, or allosteric binding of one ligand impacts binding by the second ligand.

a)

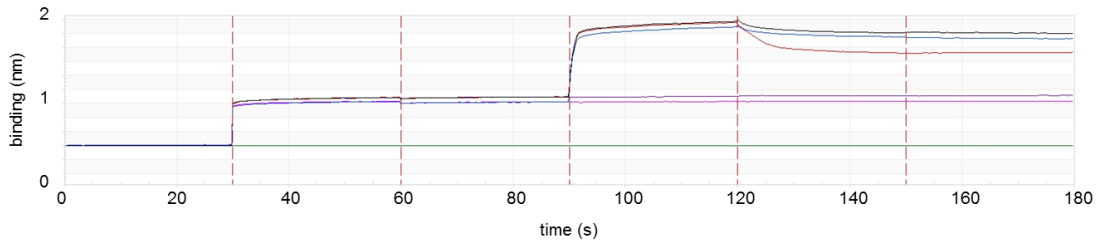


b)

| | color code | 1 | 2 | 3 | 4 | 5 | 6 |
|---|---|---|---|---|---|---|---|
| buffer | | buffer | buffer | buffer | buffer | buffer | buffer |
| peptide TARHIY + buffer | | buffer | Bi-TARHIY | buffer | buffer | buffer | buffer |
| peptide TARHIY + neomycin | | buffer | Bi-TARHIY | buffer | buffer | neomycin | buffer |
| peptide TARHIY + H69 UUU + neomycin | | buffer | Bi-TARHIY | buffer | H69 UUU | neomycin | buffer |
| peptide TARHIY + H69 UUU + free TARHIY | | buffer | Bi-TARHIY | buffer | H69 UUU | TARHIY | buffer |
| peptide TARHIY + H69 UUU + buffer | | buffer | Bi-TARHIY | buffer | H69 UUU | buffer | buffer |

**Figure 3.24.** BLItz sensogram and table indicating each step incubation of peptide biotinylated TARHIY, RNA H69 UUU, and neomycin are shown. a) Overlay of sensograms are shown. b) A description of each sensogram is shown with the incubation conditions for each step.

Another BLItz sensogram indicating the correlation of the binding sites of the ligands towards H69 is shown in **Figure 5.6**. This sensogram shows a binding event of H69 with the two ligands differently from **Figure 5.5**. In **Figure 5.6**, Bi-UUU is immobilized to the bionsensor prior to the ligands binding. At step 4, either neomycin or peptide TARHIY was added, and in step 5, a different ligand was added. The data shown do not reveal a $K_d$ or total displacement that can show the binding sites overlap. However, the final equilibrium response of the binding curves shows different levels when neomycin is added relevant to the order of addition. When the peptide is added first followed by addition of neomycin, the equilibrium response is lower compared to *vice versa*.

### 3.12. Conclusions

In this chapter, phage display was done to find a peptide that has selective binding to H69 ΨΨΨ at pH 5.5. The peptides selected did not reveal a preference for H69 ΨΨΨ over UUU as hoped, but the peptide TPARHIY revealed a moderate preference for H69 over $tRNA^{Phe}$. A truncated version, TARHIY was shown in the FID assay to have better affinity for H69 than the selected peptide TPARHIY. Several binding studies were performed, namely ESI-MS, BLItz, and NMR. Each study was performed at both pH 5.5 and pH 7.0 with H69 ΨΨΨ and H69 UUU. These studies revealed TARHIY binding to H69, and gave the apparent $K_d$ values. The peptide showed moderate binding affinity (10-20 μM) with a $K_d$ value close to that of a natural antibiotic, neomycin, binding to H69.[187] However, curve fits for $K_d$ determination were poor and our results imply more complex binding events than 1:1 interactions.

The binding site was examined by 2D NMR, which suggested binding near C1914 and C1920. To the best of our knowledge, this is the first example of a small molecule interacting with the loop region of H69 for the isolated RNA. All of the methods complement each other, and the observed trends in $K_d$ values were consistent. ESI-MS and BLItz studies showed there was no apparent selectivity between H69 ΨΨΨ and H69 UUU.

Growth assays showed that the phage with TARHIY decrease *E. coli* amplification, however, the difference from other sequences that are known fast growers was not significant, leaving the possibility of the selected peptide being a fast grower with moderate binding to the target. However, if complete growth inhibition is achieved, the peptides would never be selected. Therefore, TARHIY may further be optimized to enhance its binding affinity.

Peptide TARHIY exhibited moderate binding affinity with $K_d$ values comparable to those observed with neomycin binding to H69. Although selectivity was not achieved, the

peptide could be used to screen for ligands binding to the H69 loop region with higher affinity. In order to find a peptide selective for H69 ΨΨΨ, one may alter the selection conditions. Specific elution may be useful, but, for a target with a flexible structure such as H69, the resulting peptide may not be that selective. Another method that could be useful for improving the peptide selectivity is counter-selection by performing biopanning with H69 ΨΨΨ, followed by a secondary selection with H69 UUU or *vice versa*. Phage expressing TPARHIY was obtained 38 times out of 105 sequences from round 3. This sequence was dominant in the selection, suggesting that it is a fast grower, which was supported by the growth assay results.

In this study, we used pH 5.5 buffer conditions, which was acidic compared to physiological buffers commonly used in phage display. The yield obtained at each round was significantly smaller (>10-fold) compared to selections from pH 7.0 conditions. Other than the pH, we used biopanning conditions corresponding to previous studies.[118] At rounds 3 and 4, the incubation time was decreased from 2 to 0.5 h. Tight binders have high $k_{off}$ values, which means the dissociation takes longer than weak binders. Therefore, increasing the incubation time may help increase the affinity.

In this study, ESI-MS and SPR results suggested the possibility of 1:2 stoichiometry of RNA:peptide binding. Also, NMR results showed binding at the loop region, which was not seen previously with neomycin, and may imply a different binding mode than the aminoglycosides. There is a possibility of multimeric binding, which leaves questions regarding selection of monomer peptides from phage display. The binding mode of the peptide to H69 was still not clear, which led to the following studies in **Chapter 4**, in which multimeric binding of the peptides was explored.

# CHAPTER 4 – EXPLORING MULTIMERIC BINDING EFFECTS OF PEPTIDES

## 4.1. Design of branched peptides

In **Chapter 3**, peptide TPARHIY was selected from phage display, and a truncated variant TARHIY exhibited moderate binding affinity for the desired target H69. As mentioned in the previous section, a 2:1 binding stoichiometry of the peptide to H69 was observed in ESI-MS studies, which led us to the design of a dimer peptide. Also, the NMR spectra for H69 ΨΨΨ with TARHIY indicated two sites of H69 undergoing chemical environment changes, namely C1914 in the loop, and C1920 in the stem near the loop. An approximate distance between C1914 and C1920 using PyMOL is 2.5 nm, while the monomer peptide length using Chem3D is 2 nm. Phage from the Ph.D.-7 library have five copies of the peptide expressed on the pIII coat protein, leaving the possibility for multimeric binding of the peptide to H69. Previous studies showed that branched peptides could accommodate cell-penetrating ligands, thus increasing their potential antibacterial activity.[132, 189-190] Previous studies have also shown that peptides may bind to their targets in a multimeric fashion,[191] especially those identified from phage display.[190] These studies demonstrated that peptides found from phage display had weaker binding affinity as a monomer compared to that of a multimer.[132, 189, 191]

Scatchard analysis on monomer binding was performed to determine whether multimeric binding takes place (**Figure 4.1**). The binding ratio (Y) over peptide concentration ([L]) was plotted against the binding ratio (Y) of the bound RNA over total RNA concentration. For 1:1 binding mode, a linear plot is shown, which was not observed with our ESI-MS data. Two linear slopes were observed, indicating two binding modes. This could possibly explain the poor fitting for ESI-MS binding curves in **Figure 3.14.** Scatchard analysis revealed possible 2:1 binding or >1 binding mode of monomer.

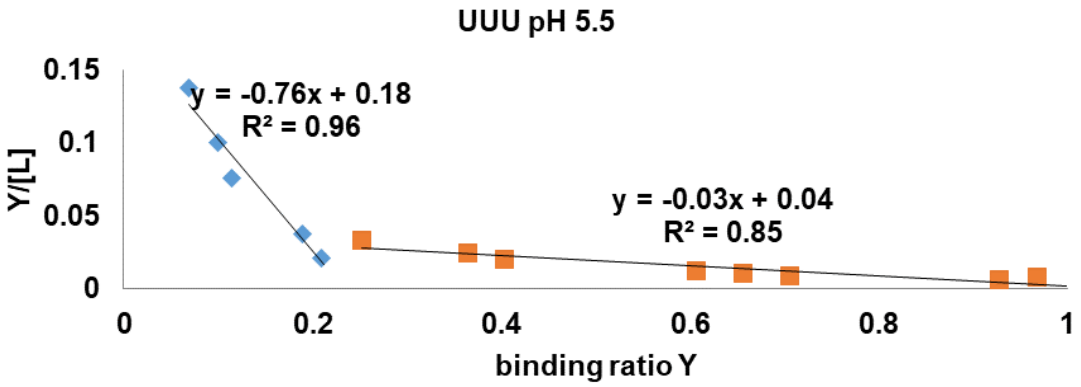


**Figure 4.1.** A Scatchard plot of H69 UUU binding to TARHIY is shown.

Based on this idea discussed above, we designed a dimeric peptide (**Figure 4.2**). The peptide selected in **Chapter 3** appeared 38 times out of 105 from sequencing analysis. The binding affinity of the peptide to H69 was moderate (10-20 μM), with little selectivity for modification status of H69. Our goal was to test if there is a multimeric binding effect of the peptide. The phage has a Ser-Gly-Gly-Gly linker that is connected to the randomized peptide on the *N*-terminus. In our study, we used β-Ala-β-Ala-β-Ala as a linker, which provides the same number of carbons in between the monomer and the branch, and one less amide group, allowing enhanced flexibility. A lysine residue was used as the branch point, because of the ability to continue peptide synthesis off the side chain.

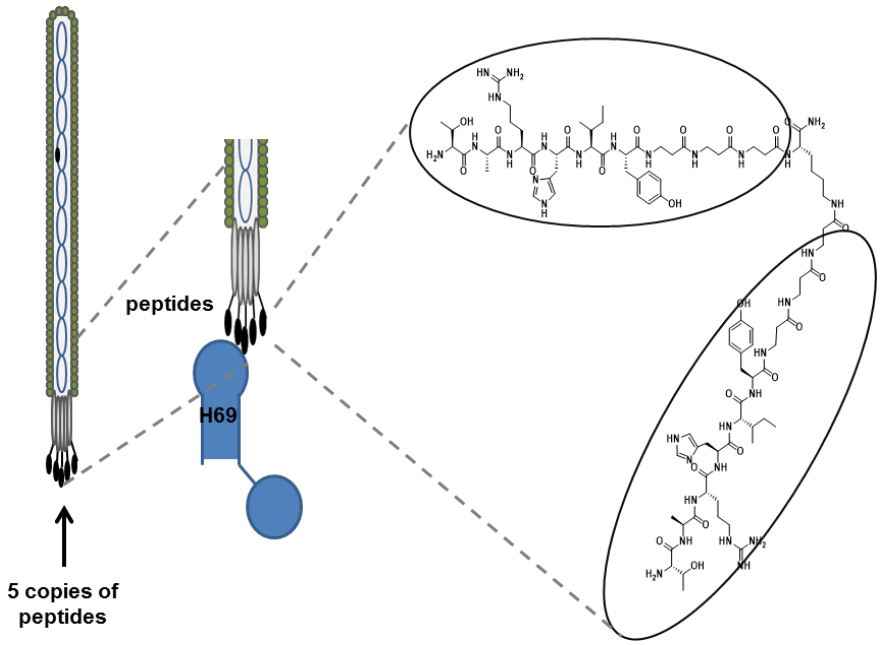


**Figure 4.2.** An image showing the rationale of the project and the structure of the dimer peptide is given.

### 4.2. Synthesis of branched peptides

To synthesize a dimer peptide, lysine was selected as the branch point. Lysine has an ε-amino group from the side chain, allowing addition of the same or different amino acids onto each amino group by utilizing specific protecting groups on each amino group. For this part of the study, Fmoc-Lys(Fmoc)-OH was used to add on identical peptide sequences to the branch. Two sequences, TARHIY, the phage-selected sequence, and AAAAAA, a control sequence, were the peptide monomers used to generate the dimer. On the phage, there are three glycines and a serine at the C-terminus of the peptide connected to the pIII coat protein, which works as a spacer.[192] In this study, I added three β-alanines (B), which are commonly used spacers (**Scheme 4.1**). Even with the spacers after the branch, the surface of the resin was likely too crowded, leading to a failed synthesis. After using a low-loading resin NovaSynTGR resin (0.31 mmol/g), I was able to obtain the desired products in good yield and purity (**Figure 4.3**). The peptides, $(TARHIYBBB)_2$-K-$NH_2$ (branched TARHIY, B1T) and $(AAAAAABBB)_2$-K-$NH_2$ (branched

AAAAAA, B1A), were generated by using standard Fmoc-solid phase peptide synthesis (SPPS).[132] The synthesized peptides were purified with HPLC and characterized by MALDI-TOF MS.

**Scheme 4.1.** Synthesis of branched peptides with the same side chains

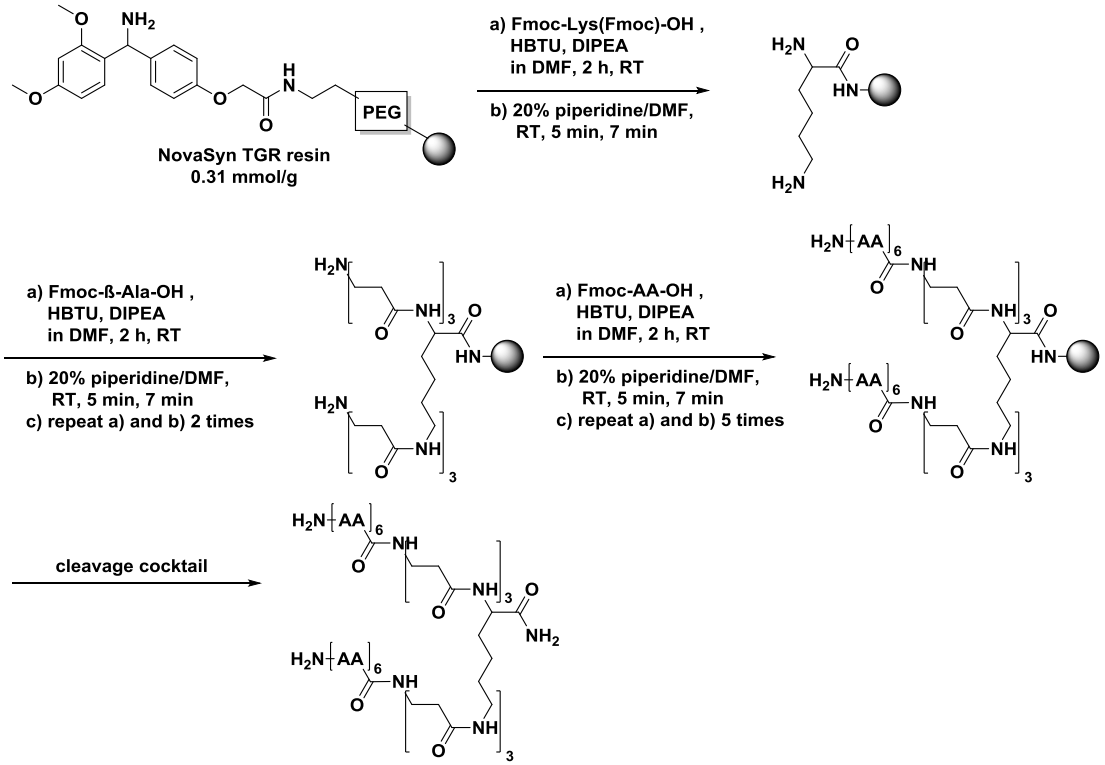

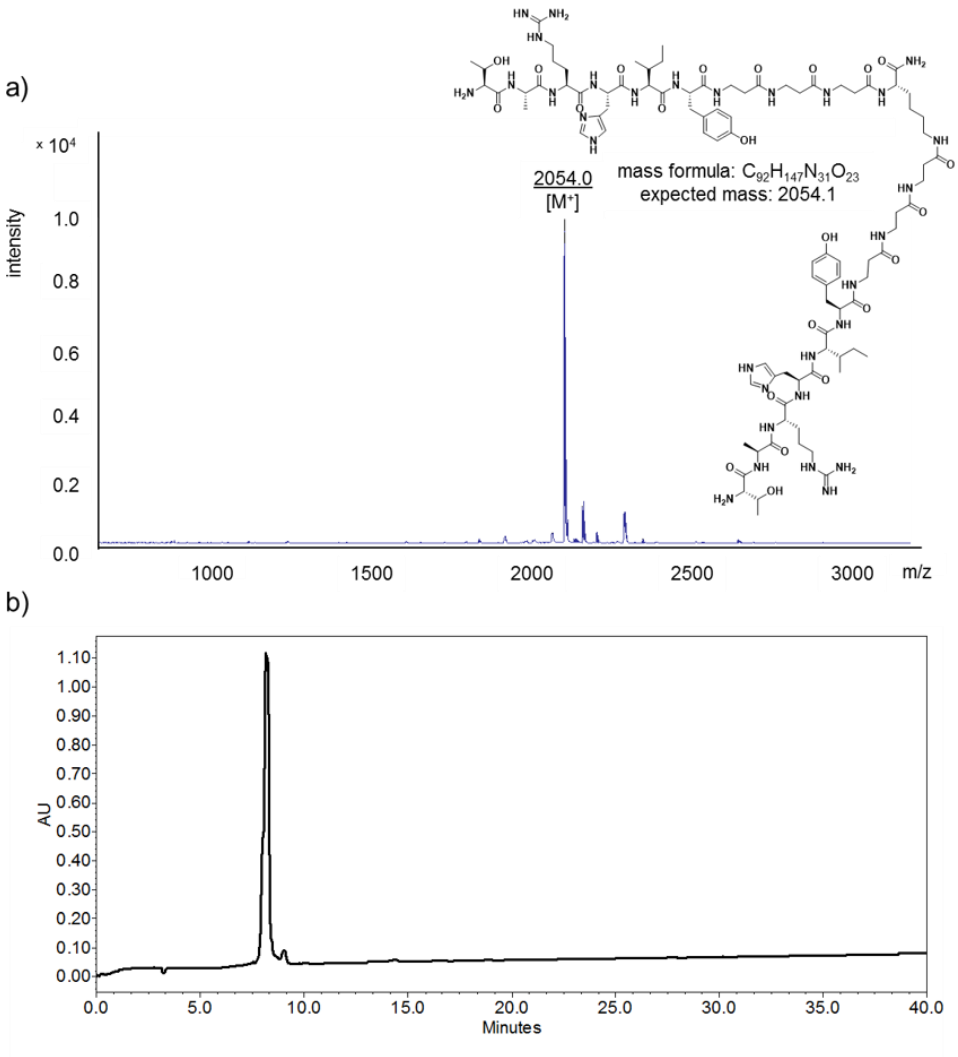


**Figure 4.3.** MALDI-TOF spectrum (a) and HPLC trace (b) of B1T is shown.

Also, to examine whether the *N*-terminus of the peptide is important for activity (*i.e.*, RNA binding), we designed branched TARHIY analogues. The sequences that were designed are shown in **Figure 4.4**. For a) and b), Fmoc-Lys(Fmoc)-OH was used as the branch point, and for c) and d), Fmoc-Lys(ivDde)-OH was employed. The protecting group ivDde allowed attaching a different side chain (*i.e.*, AAAAAABBB or YIHRATBBB) onto the ε-amino group (**Scheme 4.2**). The peptides were synthesized with standard Fmoc-solid phase peptide synthesis (SPPS) using NovaSynTGR resin, and three β-alanines (B) were added as spacers. To determine the role of peptide monomer

orientation, (TARHIYBBB)(YIHRATBBB)-K-prG-$NH_2$ (reverse dimer TY) was designed. Also, a propargylglycine (prG) was added on the *C*-terminus to facilitate further modification on structures of the peptide, such as addition of a dye or small molecule for further studies. For c) and d), the sequence TARHIYBBB was synthesized first with Boc-Thr(Bzl)-OH on the α-amino group, followed by ivDde deprotection with 5% hydrazine, followed by Fmoc synthesis to add AAAAABBB or YIHRATBBB on the ε-amino group. The synthesis was followed by purification by HPLC and characterization by MALDI-TOF MS.

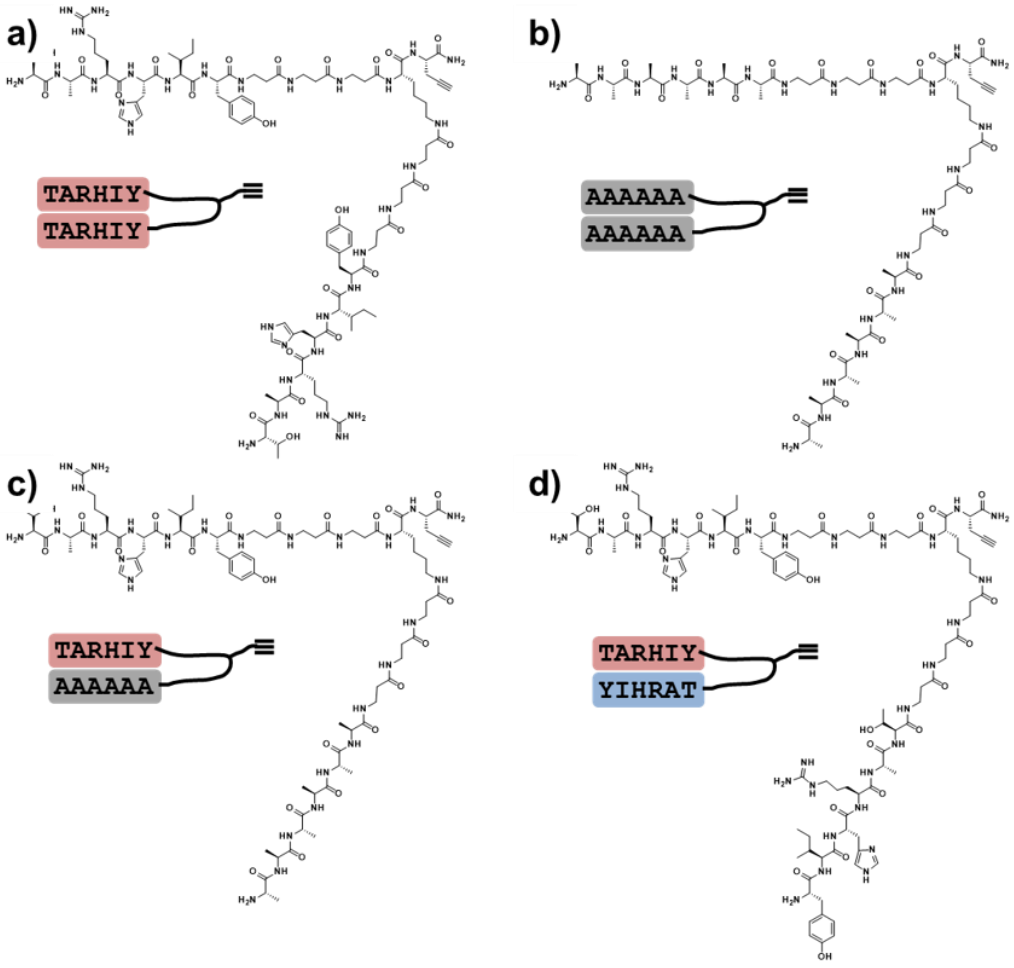


**Figure 4.4.** Structures of branched peptides with alkynyl groups are shown. The following peptides were generated: a) $(TARHIYBBB)_2$-K-prG-$NH_2$ (dimer TT), b) (TARHIYBBB)(AAAAAABBB)-K-prG-$NH_2$ (dimer TA), c) $(AAAAAABBB)_2$-K-prG-$NH_2$ (dimer AA), and d) (TARHIYBBB)(YIHRATBBB)-K-prG-$NH_2$ (reverse dimer TY).

**Scheme 4.2.** Scheme of synthesis of branched peptides with different side chains

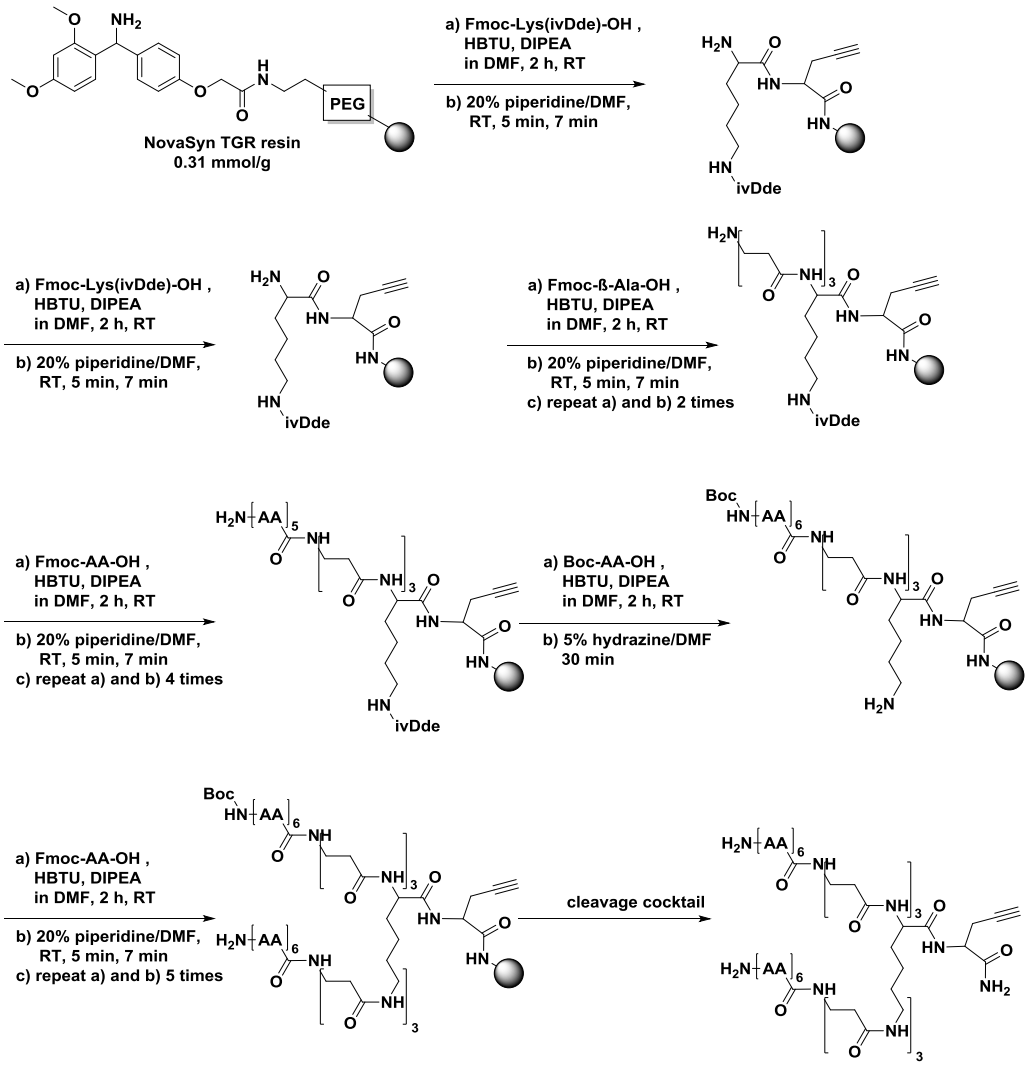


## 4.3. Binding of RNA with branched peptides using MALDI-TOF

To examine complex formation of branched peptides, binding studies with H69 were carried out. The complex was detected by MALDI-TOF although this method is only qualitative. To 2 μM of H69 in water was added 2 μM of peptide solution, and the mixture was spotted on a MALDI plate using 3-hydroxypicolinic acid (HPA) as a matrix. The branched peptides described above were tested, with both H69 ΨΨΨ and H69 UUU.

Although not quantitative, this method does provide evidence for formation of complexes with the dimer TT, dimer TA, and reverse dimer TY with H69 (**Figure 4.5**). Complexes with the control dimer AA were not observed. Further studies were required to confirm the binding.

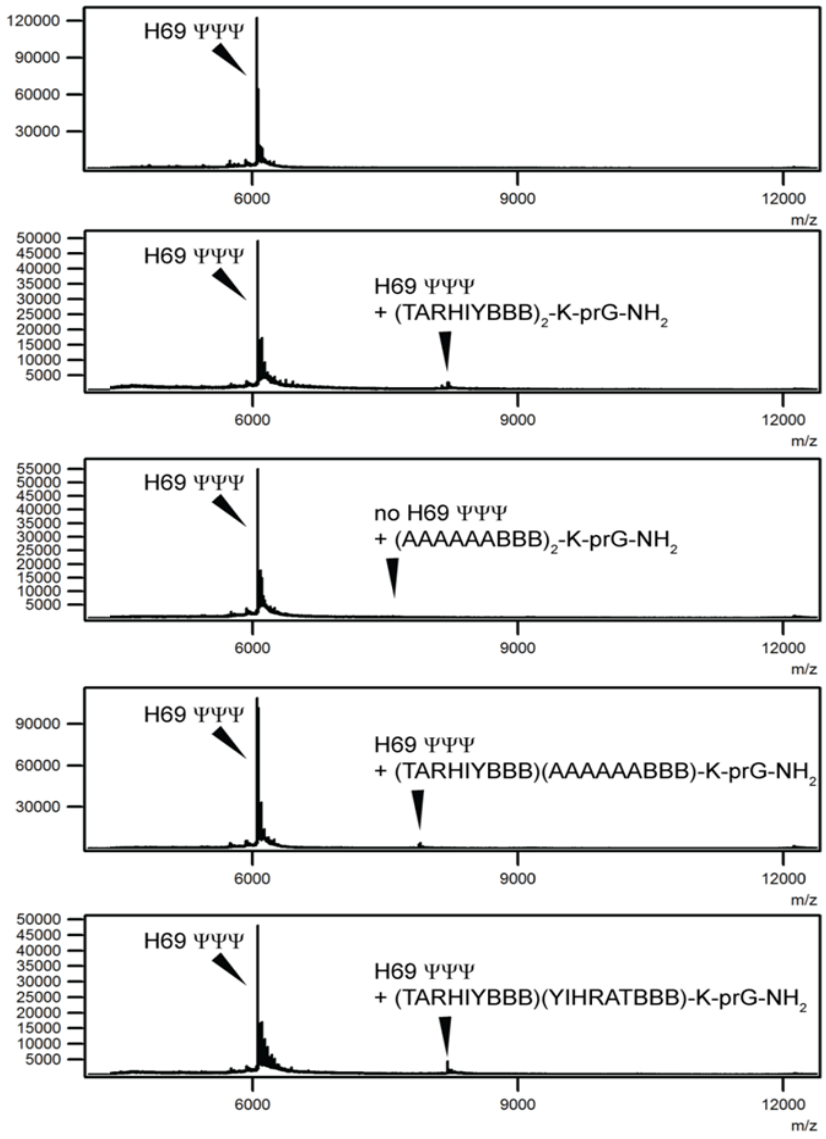


**Figure 4.5.** MALDI-TOF results for binding of dimer TT, dimer AA, dimer TA, and reverse dimer TY with H69 ΨΨΨ are shown. While complexes of dimer, dimer TA, and reverse dimer TY with H69 were observed, complexes of dimer AA with H69 ΨΨΨ were not detected by MALDI-TOF.

### 4.4. Binding of RNA with branched peptides using ESI-MS

To determine the binding affinity of peptide $(TARHIYBBB)_2$-K-$NH_2$ (branched peptide, B1T), ESI-MS was used. In this study, the binding was measured at 10 mM $NH_4OAc$ for both pH 5.5 and pH 7.0 conditions, 1 μM of H69 ΨΨΨ and H69 UUU, and the concentration of peptide varied from 0 to 100 μM. Unlike the monomer, there was no overlap between the peptide and RNA peaks (**Figures 4.6** to **4.9**). In this case, intensity of the (5-) charge state, which was highest, was used for quantification. In the previous chapter in which monomers were examined, (5-) charge state was used. From the apparent $K_d$ values (**Table 4.1**) obtained from plots shown in **Figure 4.10**, it is found that the binding affinities towards H69 ΨΨΨ and H69 UUU have both increased at least 10-fold, but no apparent selectivity was observed.

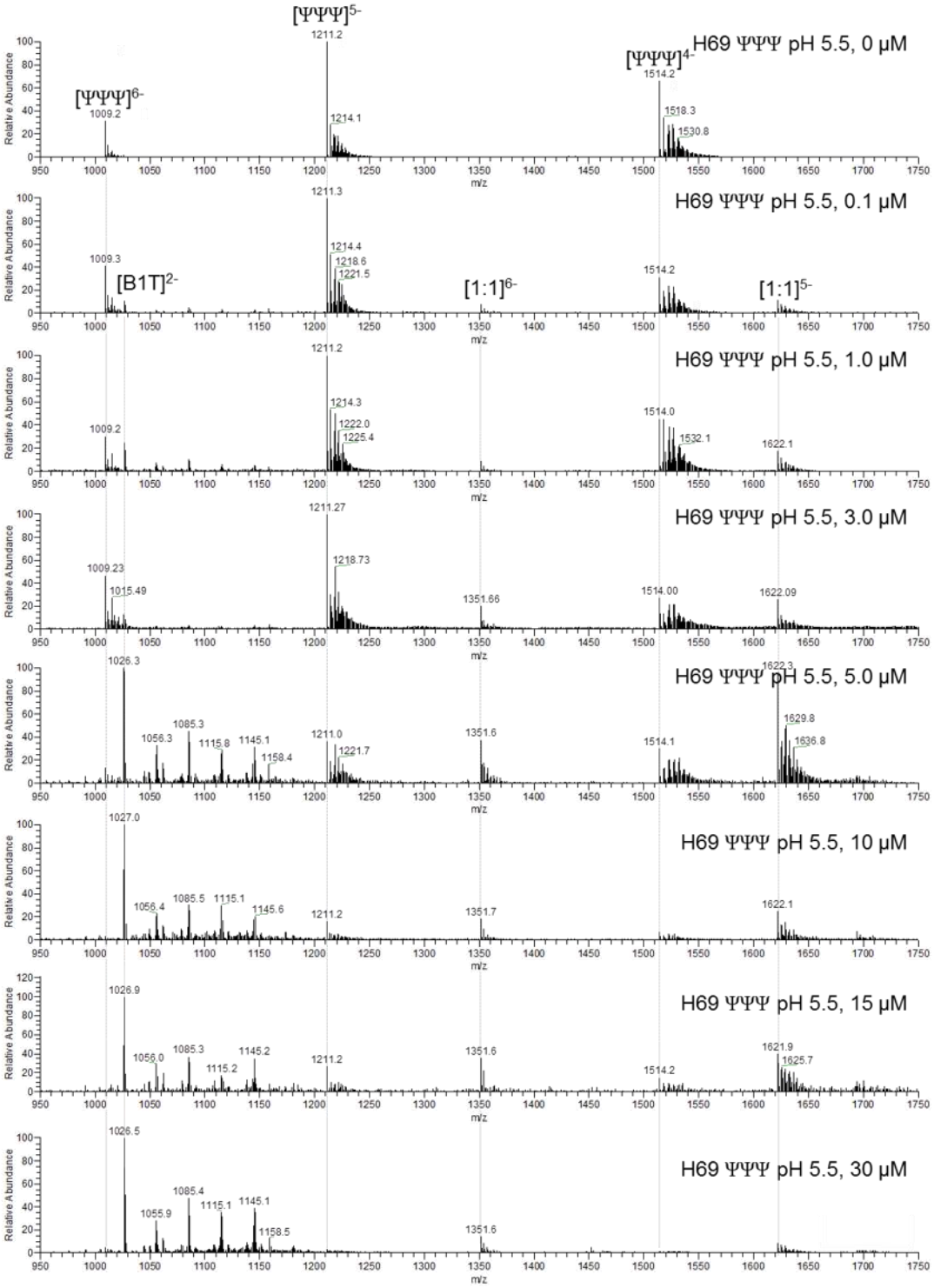


**Figure 4.6.** Representative ESI-MS results for B1T titration (pH 5.5) against H69 ΨΨΨ are shown. In the spectra, complexes of 1:1 (H69 UUU:peptide) binding ratios are observed. The experiments were performed in duplicate at 10 mM $NH_4OAc$ (pH 5.5). The expanded figures are displayed in **Appendix E**.

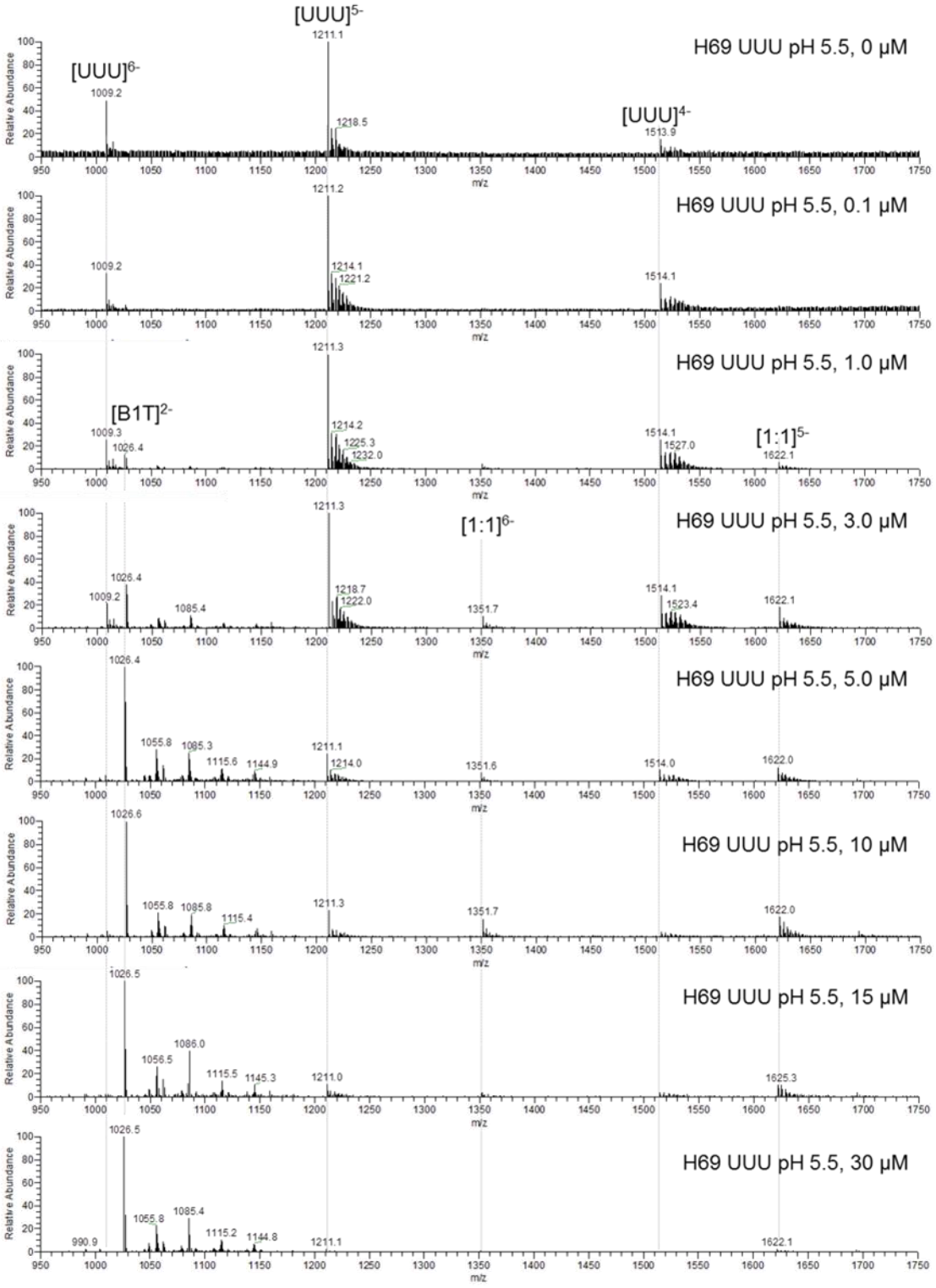


**Figure 4.7.** Representative ESI-MS results for B1T titration (pH 5.5) against H69 UUU are shown. In the spectra, complexes of 1:1 (H69 UUU:peptide) binding ratios are observed. The experiments were performed in duplicate at 10 mM $NH_4OAc$ (pH 5.5). The expanded figures are displayed in **Appendix E**.

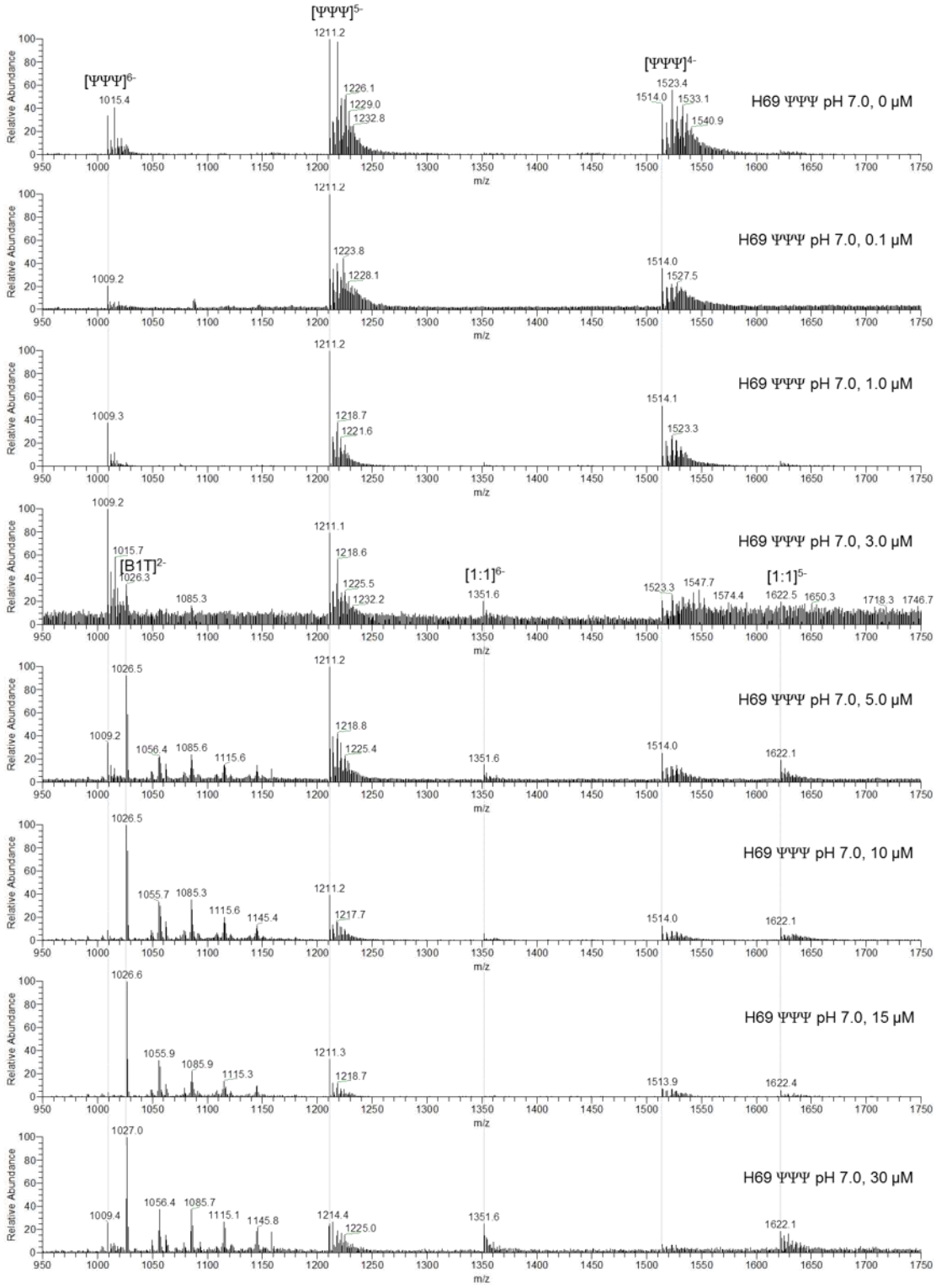


**Figure 4.8.** Representative ESI-MS results for B1T titration (pH 7.0) against H69 ΨΨΨ are shown. In the spectra, complexes of 1:1 (H69 UUU:peptide) binding ratios are observed. The experiments were performed in duplicate at 10 mM $NH_4OAc$ (pH 7.0). The expanded figures are displayed in **Appendix E**.

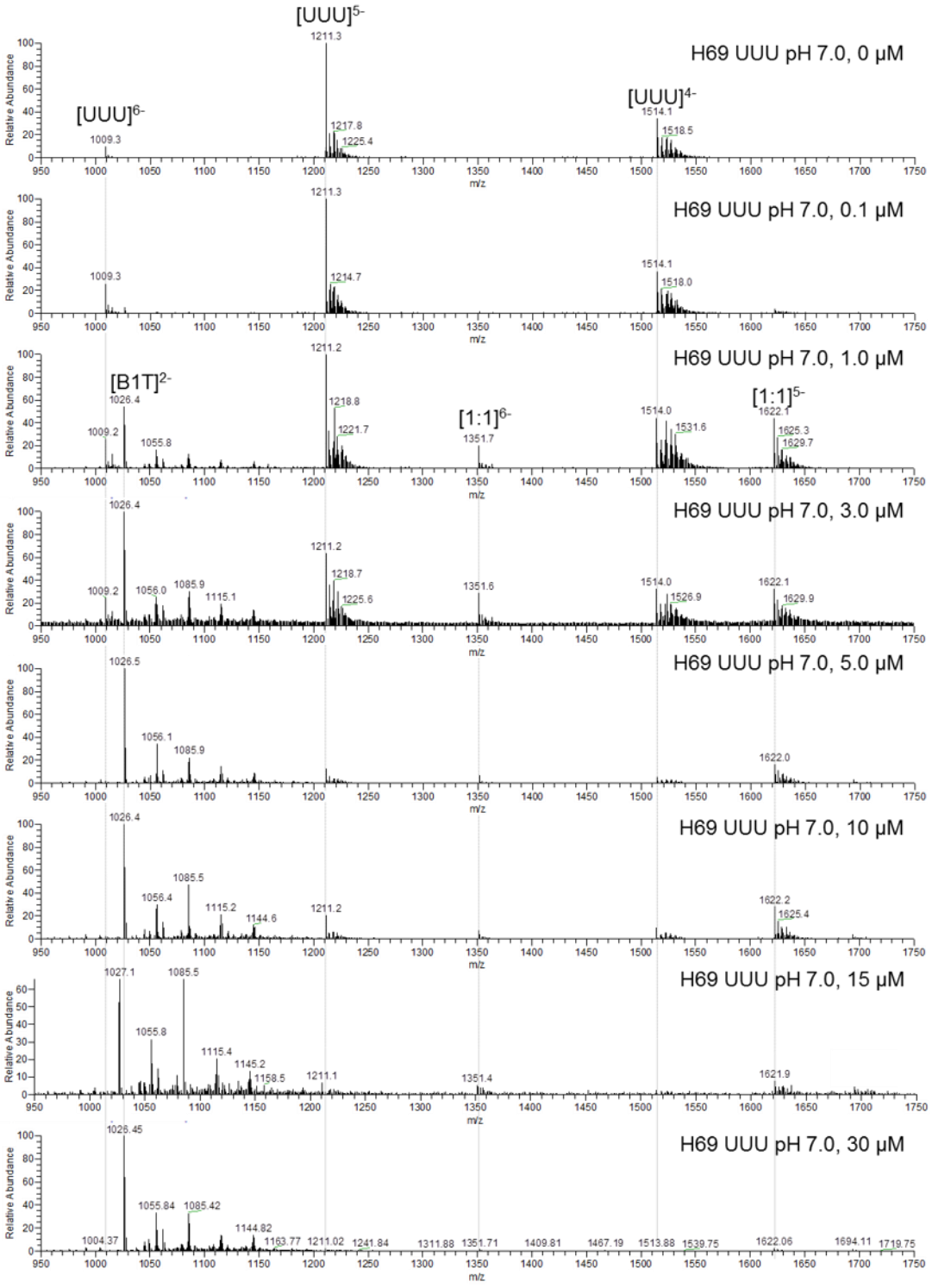


**Figure 4.9.** Representative ESI-MS results for B1T titration (pH 7.0) against H69 UUU are shown. In the spectra, complexes of 1:1 (H69 UUU:peptide) binding ratios are observed. The experiments were performed in duplicate at 10 mM $NH_4OAc$ (pH 7.0). The expanded figures are displayed in **Appendix E**.

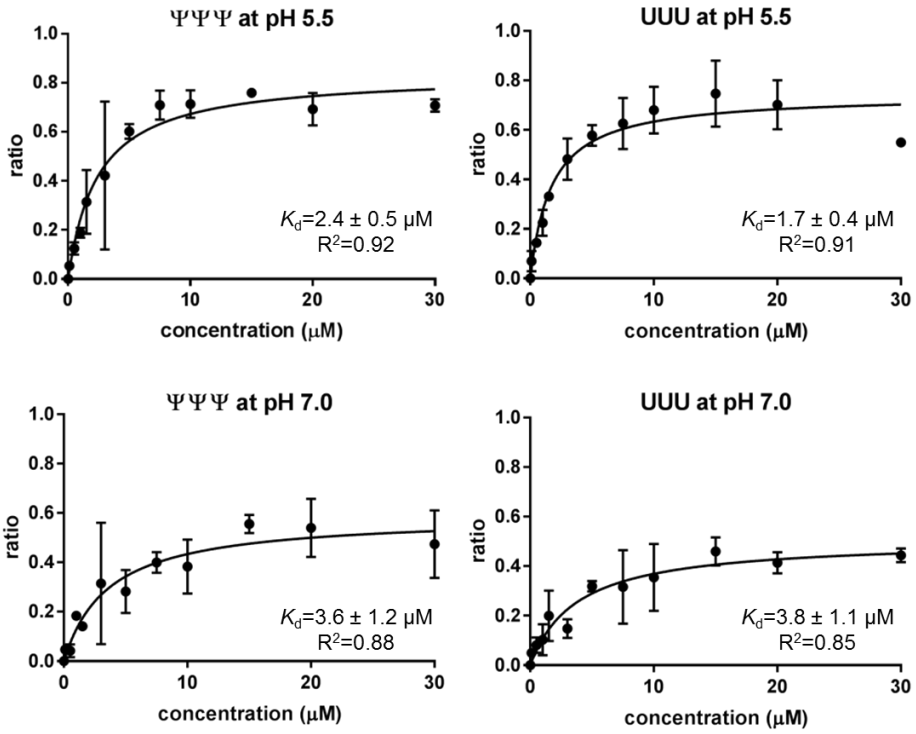


**Figure 4.10.** ESI-MS results for branched peptide B1T at 10 mM $NH_4OAc$ (pH 5.5 and pH 7.0) against H69 ΨΨΨ and H69 UUU. a) The titration curves for TARHIY bound to H69 ΨΨΨ and H69 UUU (y axis: binding ratio of at (5-) charge state) at different buffer conditions (pH 5.5 vs. pH 7.0) are shown.

**Table 4.1.** Apparent dissociation constants ($K_d$s) obtained from ESI-MS.

| apparent $K_d$ | ΨΨΨ | UUU | UUU/ΨΨΨ |
|---|---|---|---|
| pH 5.5 | 2.4 ± 0.5 μM | 1.7 ± 0.4 μM | 1.4 |
| pH 7.0 | 3.6 ± 1.2 μM | 3.8 ± 1.1 μM | 0.9 |

Scatchard analysis on dimer binding was performed (**Figure 4.11**). The binding ratio (Y) over peptide concentration ([L]) was plotted against the binding ratio (Y) of the bound RNA over total RNA concentration. For the monomer, two linear slopes were observed, indicating two binding modes. Scatchard analysis revealed possible 2:1 binding or >1 binding mode of monomer. For the dimer, one linear slope was observed, which indicates 1:1 binding mode.

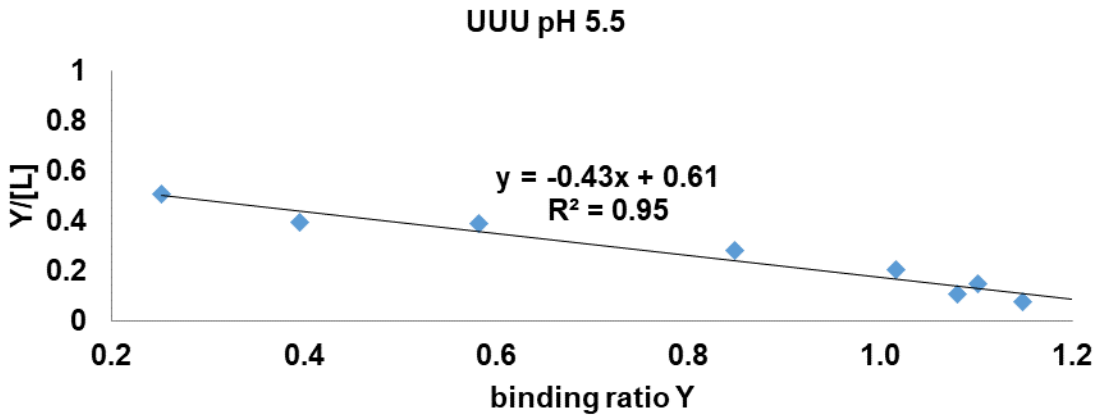


**Figure 4.11.** A Scatchard plot of H69 UUU binding to dimer peptide is shown.

### 4.5. Binding of RNA with branched peptides using BLItz

As a label-free method to monitor binding interactions, BLItz was used for dimer studies. The dimer exhibited binding to H69, while the control dimer AA did not show binding. For dimer TT, the apparent dissociation constant obtained was comparable to that obtained by ESI-MS, which was 2.2 ± 0.1 μM for H69 ΨΨΨ and 3.9 ± 0.2 μM H69 UUU at pH 7.0. In contrast, SPR experiments were not successful with the dimer. Apparent $K_d$ values using steady state response units were obtained, but the dissociation curves had very poor fits. Representative data are shown in **Figures 4.12** to **4.14**. By using BLItz, we were able to obtain the apparent $K_d$ values for the fits. Dimer peptide concentrations varying from 0 to 100 μM in buffers were studied.

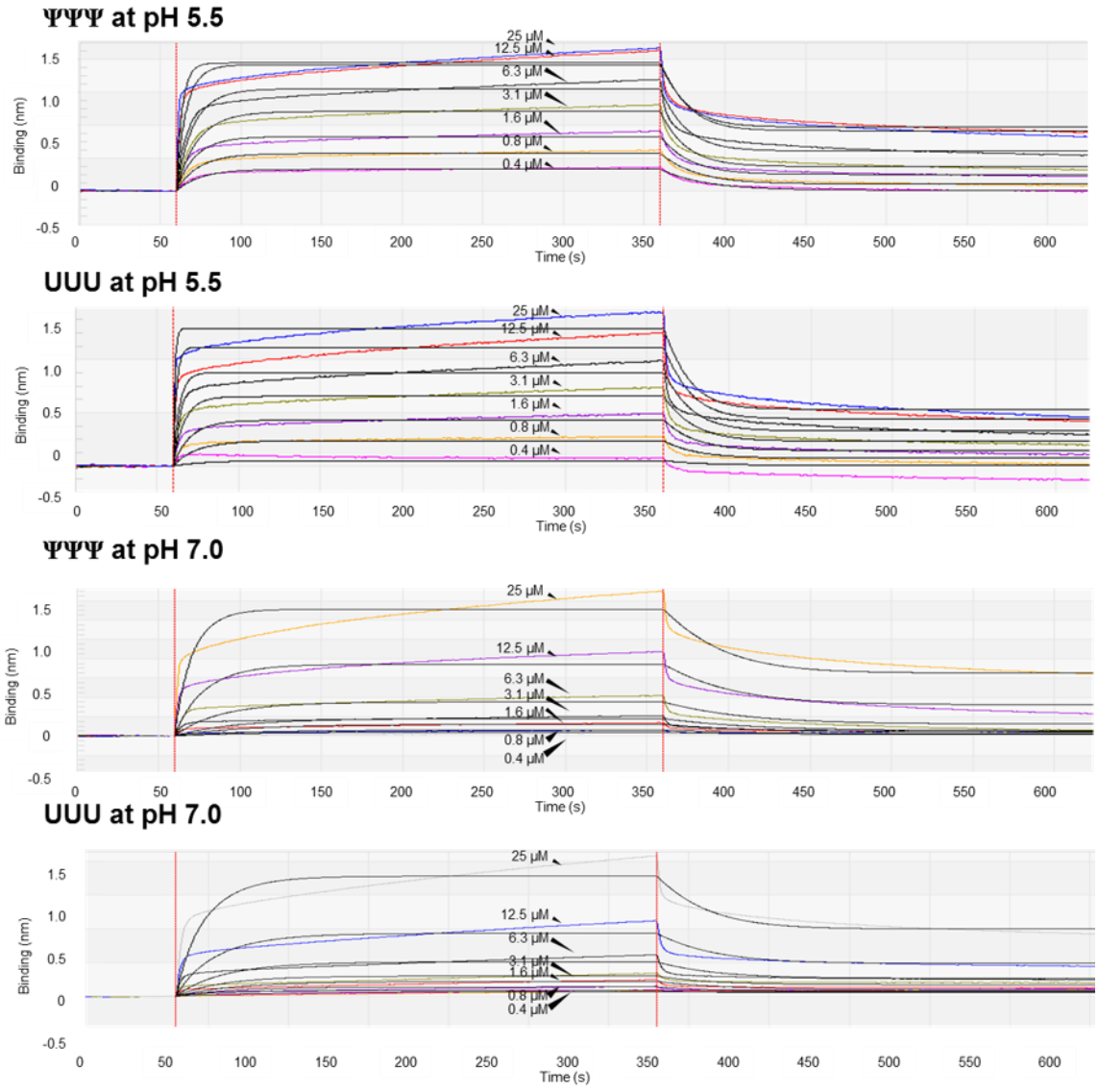


**Figure 4.12.** Representative BLItz results for branched peptide dimer TT titration at pH 5.5 (20 mM cacodylate, 100 mM KCl, and 0.1% Tween-20) and pH 7.0 (20 mM HEPES-KOH, 100 mM KCl, 5 mM $MgCl_2$, and 0.1% Tween-20) against H69 ΨΨΨ and H69 UUU. The curves shown in color correspond to measurements of a two-fold serial dilution of the peptide ligands over a concentration range of 0 to 100 μM. The curves in black correspond to global fits in 1:1 binding model. The experiments were performed in triplicate. The expanded figures are displayed in **Appendix B**.

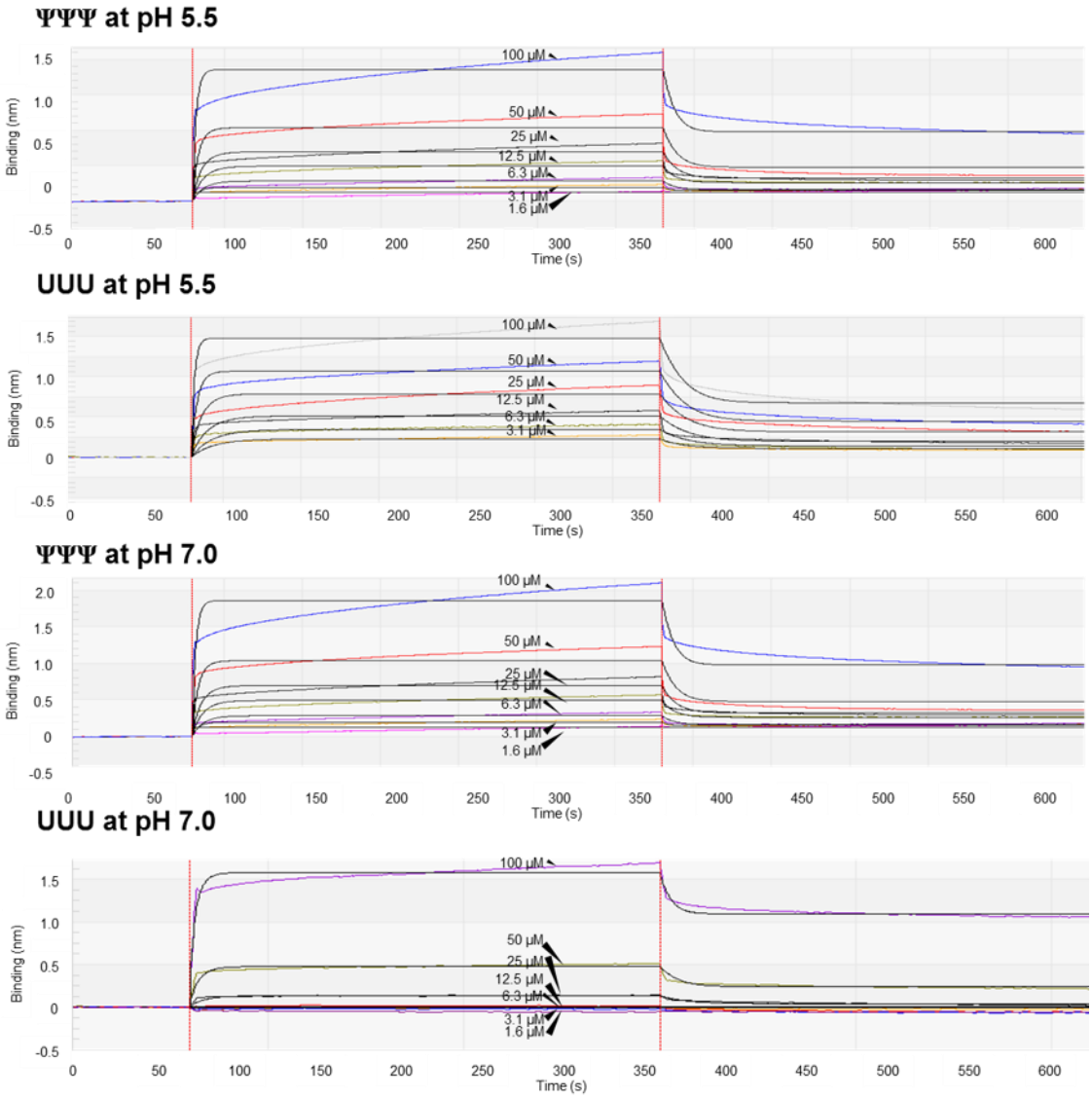


**Figure 4.13.** Representative BLItz results for branched peptide dimer TA titration at pH 5.5 (20 mM cacodylate, 100 mM KCl, and 0.1% Tween-20) and pH 7.0 (20 mM HEPES-KOH, 100 mM KCl, 5 mM $MgCl_2$, and 0.1% Tween-20) against H69 ΨΨΨ and H69 UUU. The curves shown in color correspond to measurements of a two-fold serial dilution of the peptide ligands over a concentration range of 0 to 100 µM. The curves in black correspond to global fits in 1:1 binding model. The experiments were performed in duplicate. The expanded figures are displayed in **Appendix B**.

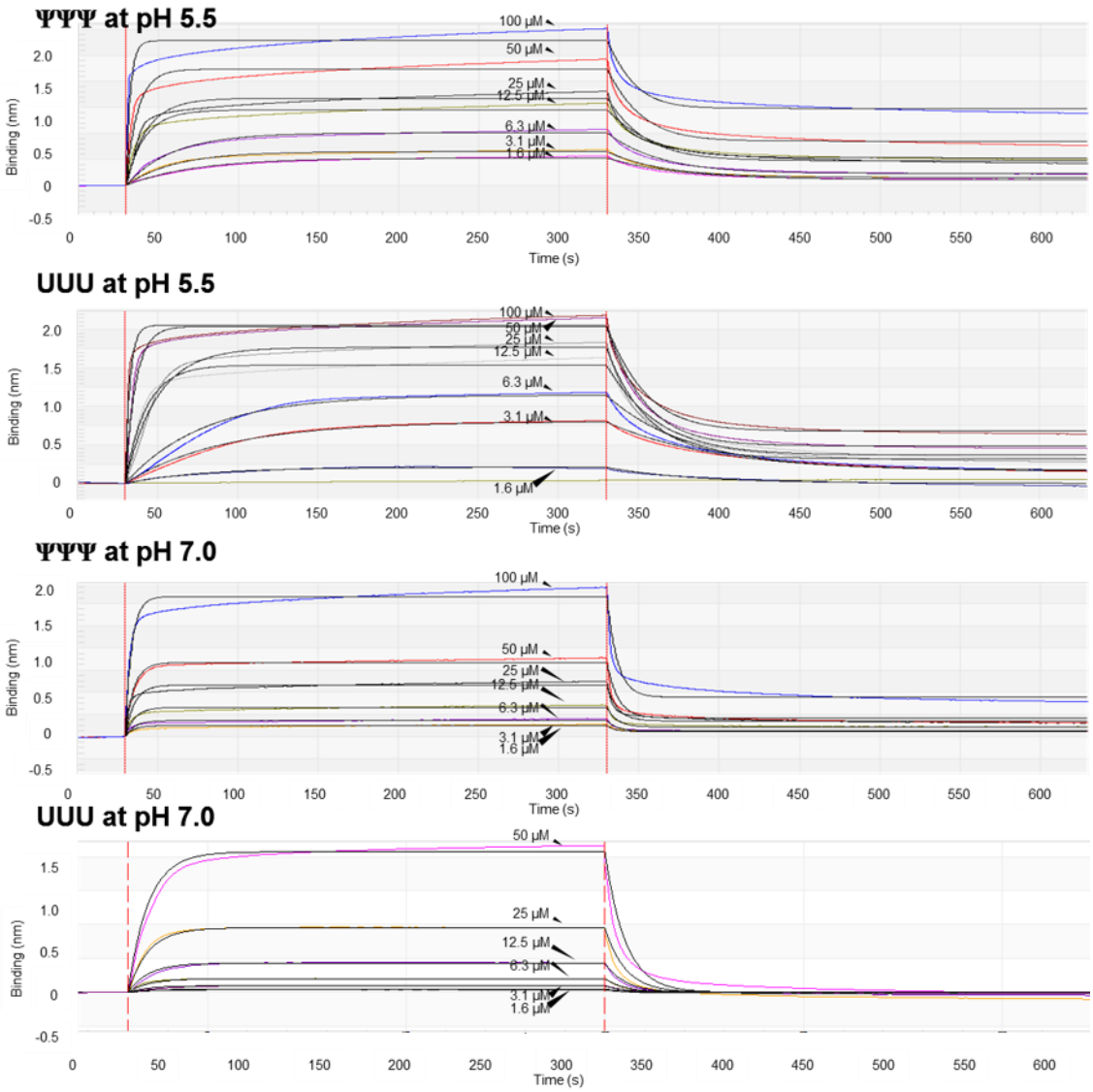


**Figure 4.14.** Representative BLItz results for branched peptide reverse dimer TY titration at pH 5.5 (20 mM cacodylate, 100 mM KCl, and 0.1% Tween-20) and pH 7.0 (20 mM HEPES-KOH, 100 mM KCl, 5 mM $MgCl_2$, and 0.1% Tween-20) against H69 ΨΨΨ and H69 UUU. The curves shown in color correspond to measurements of a two-fold serial dilution of the peptide ligands over a concentration range of 0 to 100 µM. The curves in black correspond to global fits in 1:1 binding model ($R^2$>0.98). The experiments were performed in duplicated. The expanded figures are displayed in **Appendix B**.

**Table 4.2.** Rate constants ($k_{on}$ and $k_{off}$) obtained from BLItz

| dimer TT‡ | $k_{on}$ ($M^{-1}s^{-1}$) | $k_{off}$ ($s^{-1}$) |
|---|---|---|
| ΨΨΨ at pH 5.5 | $2.7 \times 10^4 \pm 1.2 \times 10^3$ | $3.7 \times 10^{-2} \pm 6.4 \times 10^{-4}$ |
| UUU at pH 5.5 | $3.7 \times 10^4 \pm 3.9 \times 10^3$ | $3.3 \times 10^{-3} \pm 2.1 \times 10^{-4}$ |
| ΨΨΨ at pH 7.0 | $3.3 \times 10^3 \pm 2.6 \times 10^2$ | $1.3 \times 10^{-2} \pm 8.3 \times 10^{-4}$ |
| UUU at pH 7.0 | $1.6 \times 10^3 \pm 1.3 \times 10^2$ | $1.3 \times 10^{-2} \pm 6.1 \times 10^{-4}$ |
| **dimer TA*** | **$k_{on}$ ($M^{-1}s^{-1}$)** | **$k_{off}$ ($s^{-1}$)** |
| ΨΨΨ at pH 5.5 | $4.3 \times 10^3 \pm 4.7 \times 10^2$ | $5.6 \times 10^{-2} \pm 5.4 \times 10^{-3}$ |
| UUU at pH 5.5 | $9.9 \times 10^3 \pm 7.2 \times 10^2$ | $3.3 \times 10^{-2} \pm 1.8 \times 10^{-3}$ |
| ΨΨΨ at pH 7.0 | $7.4 \times 10^3 \pm 6.8 \times 10^2$ | $8.0 \times 10^{-2} \pm 6.2 \times 10^{-3}$ |
| UUU at pH 7.0 | $7.0 \times 10^3 \pm 1.5 \times 10^2$ | $9.8 \times 10^{-2} \pm 1.1 \times 10^{-3}$ |
| **dimer TY*** | **$k_{on}$ ($M^{-1}s^{-1}$)** | **$k_{off}$ ($s^{-1}$)** |
| ΨΨΨ at pH 5.5 | $8.1 \times 10^2 \pm 6.3 \times 10^1$ | $2.3 \times 10^{-2} \pm 1.6 \times 10^{-4}$ |
| UUU at pH 5.5 | $6.8 \times 10^2 \pm 2.1 \times 10^1$ | $1.9 \times 10^{-2} \pm 1.8 \times 10^{-4}$ |
| ΨΨΨ at pH 7.0 | $2.6 \times 10^3 \pm 1.9 \times 10^2$ | $1.1 \times 10^{-1} \pm 3.5 \times 10^{-3}$ |
| UUU at pH 7.0 | $4.9 \times 10^3 \pm 1.4 \times 10^3$ | $1.8 \times 10^{-1} \pm 8.2 \times 10^{-3}$ |

‡: Association and dissociation rates were determined using global fit, and the average from triplicate measurements are displayed.
*: Association and dissociation rates were determined using global fit, and the average from duplicate measurements are displayed.

Evaluation of the kinetics of the binding events revealed similar $k_{on}$ and $k_{off}$ values of the dimers binding to H69 ΨΨΨ and H69 UUU at pH 5.5 and pH 7.0. The $k_{on}$ and $k_{off}$ values are given in **Table 4.2**. For all of the dimers, compared to the monomer, ~10-fold faster association and dissociation was observed. Dimer TT revealed ~100-fold faster association to H69 and ~10-fold slower dissociation at pH 5.5 compared to the monomer. If the binding interaction is through charge-charge interactions, it makes sense that the association rate would be higher compared to the monomer due to increased charge on the dimer. However, similar to the binding of TARHIY, poor fitting was observed, both for the sensograms (**Figures 4.10** to **4.12** and **Appendix B**) and the rate constants (**Table 4.2**), possibly implying the binding of TARHIY to H69 is not through 1:1 binding mode.

**Table 4.3.** Apparent dissociation constants ($K_d$s) obtained from BLItz

| **dimer TT** | **ΨΨΨ** | **UUU** | **UUU/ΨΨΨ** |
|---|---|---|---|
| pH 5.5 | 1.4 ± 0.4 μM | 2.6 ± 0.7 μM | 1.9 |
| pH 7.0 | 4.1 ± 1.2 μM | 2.0 ± 0.7 μM | 0.5 |
| **dimer TA** | **ΨΨΨ** | **UUU** | **UUU/ΨΨΨ** |
| pH 5.5 | 13 ± 1 μM | 16 ± 2 μM | 1.2 |
| pH 7.0 | 10 ± 1 μM | 14 ± 0 μM | 1.4 |
| **reverse dimer TY** | **ΨΨΨ** | **UUU** | **UUU/ΨΨΨ** |
| pH 5.5 | 35 ± 1 μM | 36 ± 2 μM | 1.0 |
| pH 7.0 | 37 ± 6 μM | 35 ± 4 μM | 0.9 |
| **monomer** | **ΨΨΨ** | **UUU** | **UUU/ΨΨΨ** |
| pH 5.5 | 15 ± 1 μM | 15 ± 2 μM | 1.0 |
| pH 7.0 | 15 ± 3 μM | 16 ± 2 μM | 1.1 |

The apparent $K_d$ value obtained for dimer TT binding to H69 was 2.5 ± 0.8 μM on average, which is in agreement with that obtained from ESI-MS (2.9 ± 0.8 μM on average). The apparent $K_d$ value obtained with dimer TA was 13 ± 1 μM, which was comparable to the value of TARHIY obtained with other methods (16 ± 5 μM with ESI-MS and 15 ± 2 μM with BLItz). The apparent $K_d$ value obtained for the reverse dimer TY and H69 UUU was 36 ± 3 μM on average, which is 10-fold less than that of dimer TT, and 3-fold lower than dimer TA or monomer peptide TARHIY towards H69 UUU. For the dimer studies, dimer TA and reverse dimer were generated to see if the orientation of the monomer units was important. The decrease in apparent $K_d$ value obtained with reverse dimer TY compared to dimer TT may indicate that the orientation of the peptide is likely important, and also suggests multimeric binding.

From previous Scatchard analysis of the ESI-MS results, the monomer exhibited 2 different slopes, while the dimer exhibited 1 slope. This result implied that the dimer may go through a 1:1 binding mode with H69. Apparent dissociation constants obtained from ESI-MS or BLItz both showed improved binding with dimer TT, suggesting the dimer TT binds to H69 tighter than the monomer up to 10-fold. However, in the expanded BLItz binding curves in **Appendix B**, dimer TT also does not show a good 1:1 fitting. This may suggest that although 1 slope was obtained from Scatchard analysis for dimer TT, the binding may not be through a 1:1 binding mode. Possibly adding more data points may provide a better understanding of the data. Also, for the BLItz binding curves, for dimer TT against H69 ΨΨΨ at pH 5.5, when the peptide concentration is lower than 6.3 μM, the curves exhibited better fitting, while the curves did not exhibit decent fitting with H69 UUU or H69 ΨΨΨ at pH 7.0. Dimer TY also exhibited better fitting for both H69 and buffer conditions at lower concentration, suggesting the peptide goes through a 1:1 binding. However, a better binding analysis may be required to understand the binding mode. Also, molecular docking experiments may provide better understanding of the binding mode as well.

**4.6. NMR spectroscopy**

In **Chapter 3**, binding of peptide TARHIY to H69 was examined by NMR. Small changes in chemical shifts at C1914 and C1920 were observed in pH 5.5 buffer conditions. In **Sections 4.4** and **4.5**, binding of these dimer analogues to H69 was examined, and relative binding affinities were determined. In this section, binding of dimer TT, dimer TA, and reverse dimer TY to H69 UUU (at pH 5.5 and pH 7.0) and H69 ΨΨΨ was examined by NMR, and ge-2D COSY was used to analyze $J_{H5\text{-}H6}$ of the pyrimidines. Peaks were assigned based on previously reported values.[47, 166] Through such studies, the binding site(s) of the peptides can be deduced. The samples were prepared as mentioned in **Chapter 2.8**. The samples were then given to Evan Jones

who obtained the NMR spectra on Bruker ADVANCE 700 MHz NMR (Billerica, MA) equipped with a TXI cryoprobe at 298K.

Dimer TT binding to H69 was examined first since it is derived from two copies of the parent monomer peptide. For H69 UUU at pH 5.5, chemical shift changes were observed at C1909, C1914, U1917, C1920, and C1924, which suggests an overall conformational change of the RNA, not just the loop region as we observed with the monomer (**Figure 4.15**). For H69 ΨΨΨ at pH 5.5, the loop region was not resolved well, however, we were able to observe a change at C1924 in the stem region (**Figure 4.16**). This result was different from that obtained with the monomer, which showed a chemical shift change at C1920. For H69 UUU at pH 7.0, changes at C1914 and C1920 were observed, which was not observed with the monomer (**Figure 4.17**).

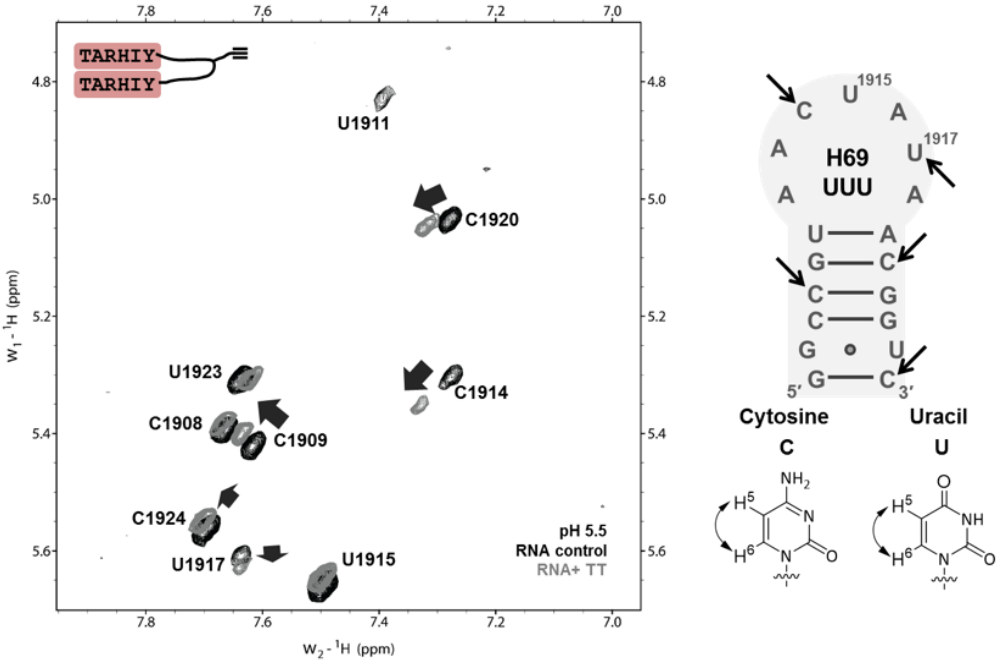


**Figure 4.15.** Overlay of the NMR spectra for H69 UUU in the absence (black) or presence (grey) of dimer TT at pH 5.5. The concentrations of RNA and peptide were 50 and 500 μM, respectively. The arrow indicates the chemical shift change and direction at C1914. The NMR spectra were obtained by Evan Jones.

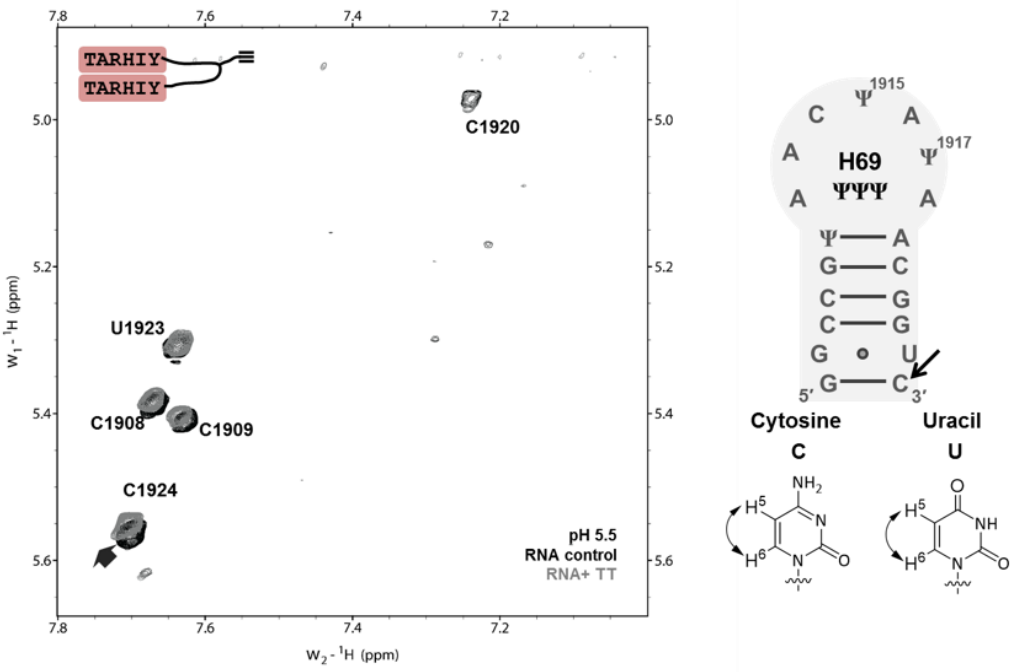


**Figure 4.16.** Overlay of the NMR spectra for H69 ΨΨΨ in the absence (black) or presence (grey) of dimer TT at pH 5.5. The concentrations of RNA and peptide were 50 and 500 μM, respectively. The arrow indicates the chemical shift change and direction at C1914. The NMR spectra were obtained by Evan Jones.

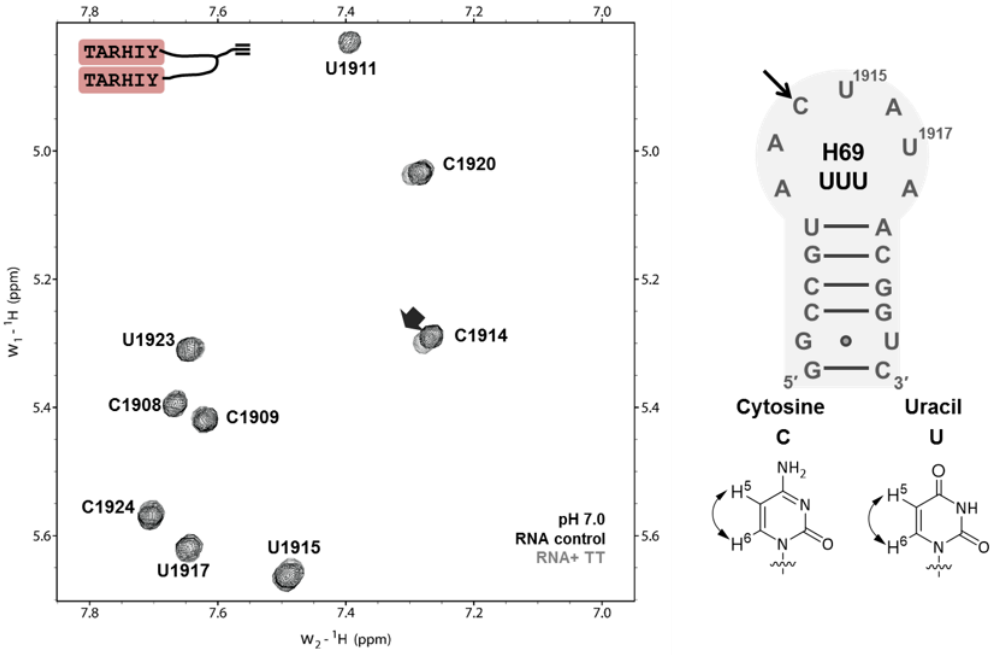


**Figure 4.17.** Overlay of the NMR spectra for H69 UUU in the absence (black) or presence (grey) of dimer TT at pH 7.0. The concentrations of RNA and peptide were 50 and 500 μM, respectively. The arrow indicates the chemical shift change and direction at C1914. The NMR spectra were obtained by Evan Jones.

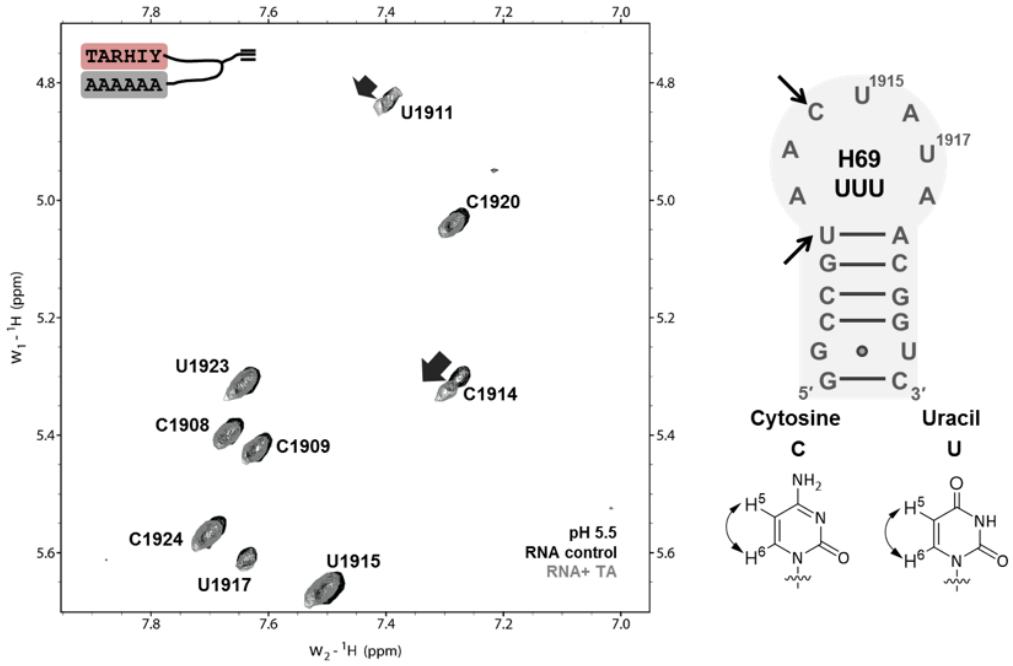


**Figure 4.18.** Overlay of the NMR spectra for H69 UUU in the absence (black) or presence (grey) of dimer TA at pH 5.5. The concentrations of RNA and peptide were 50 and 500 μM, respectively. The arrow indicates the chemical shift change and direction at C1914. The NMR spectra were obtained by Evan Jones.

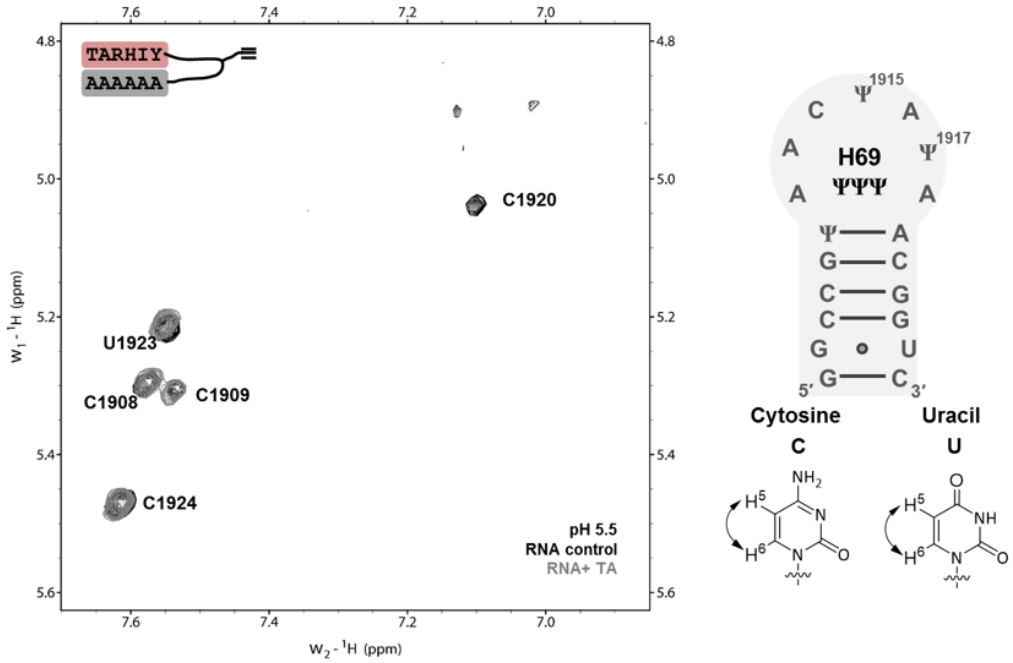


**Figure 4.19.** Overlay of the NMR spectra for H69 ΨΨΨ in the absence (black) or presence (grey) of dimer TA at pH 5.5. The concentrations of RNA and peptide were 50 and 500 μM, respectively. The NMR spectra were obtained by Evan Jones.

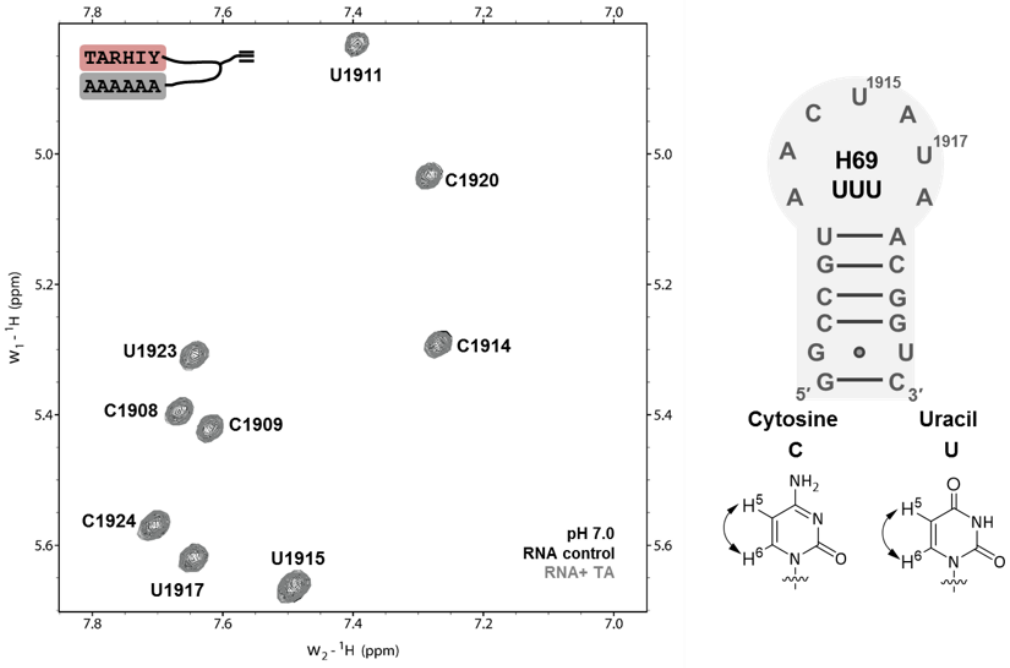


**Figure 4.20.** Overlay of the NMR spectra for H69 UUU in the absence (black) or presence (grey) of dimer TA at pH 7.0. The concentrations of RNA and peptide were 50 and 500 μM, respectively. The NMR spectra were obtained by Evan Jones.

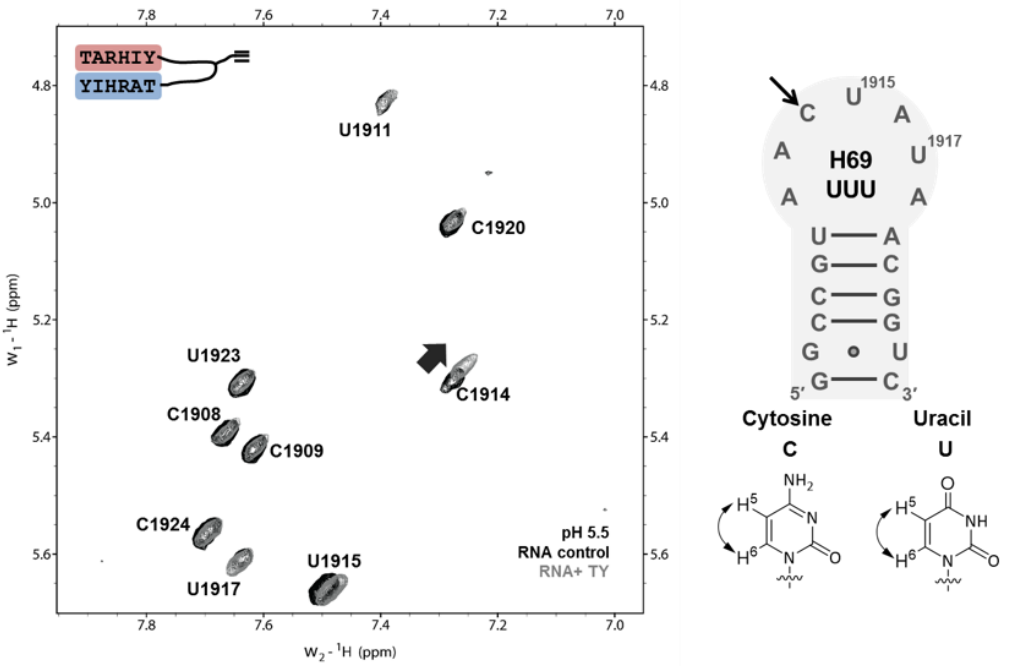


**Figure 4.21.** Overlay of the NMR spectra for H69 UUU in the absence (black) or presence (grey) of reverse dimer TY at pH 5.5. The concentrations of RNA and peptide were 50 and 500 μM, respectively. The arrow indicates the chemical shift change and direction at C1914. The NMR spectra were obtained by Evan Jones.

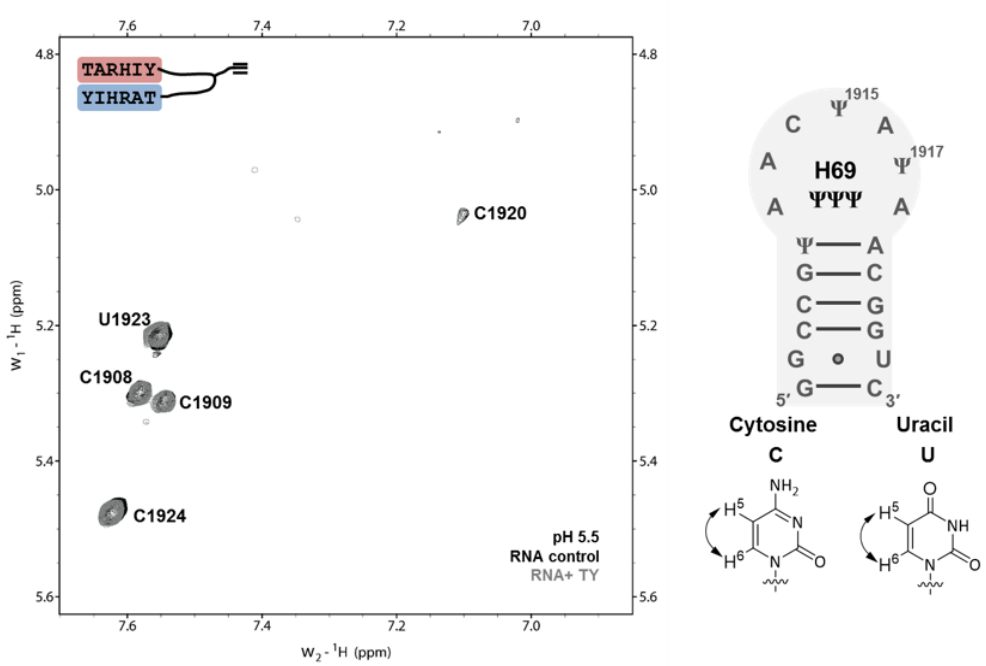


**Figure 4.22.** Overlay of the NMR spectra for H69 ΨΨΨ in the absence (black) or presence (grey) of reverse dimer TY at pH 5.5. The concentrations of RNA and peptide were 50 and 500 μM, respectively. The NMR spectra were obtained by Evan Jones.

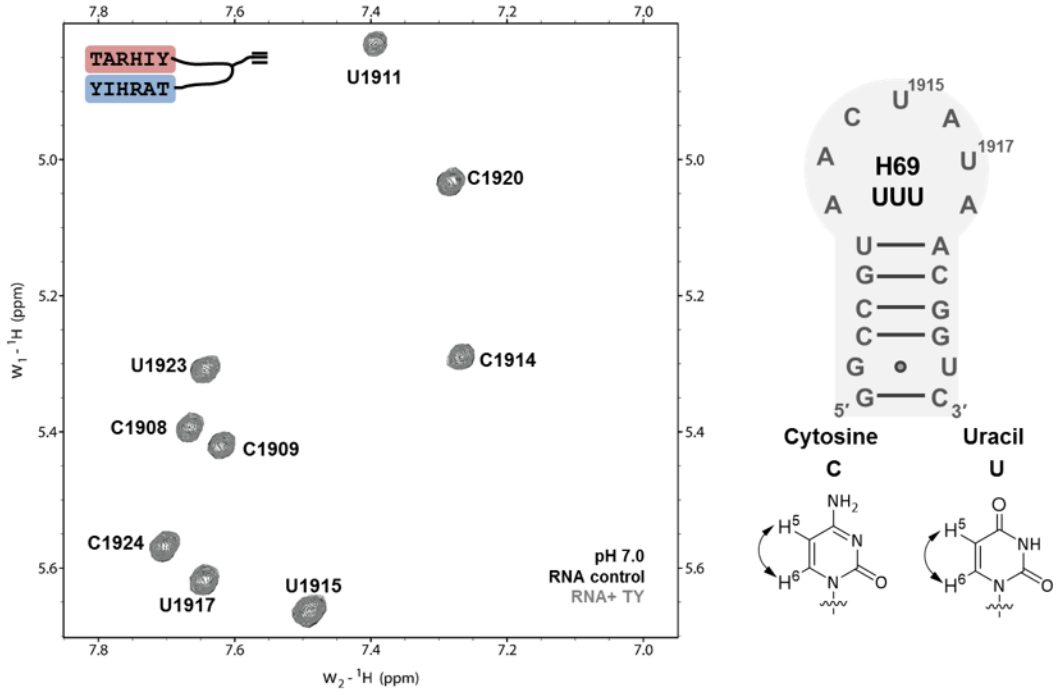


**Figure 4.23.** Overlay of the NMR spectra for H69 UUU in the absence (black) or presence (grey) of dimer TA at pH 7.0. The concentrations of RNA and peptide were 50 and 500 μM, respectively. The NMR spectra were obtained by Evan Jones.

The dimer TT binding to H69 UUU exhibited different chemical shift patterns at pH 5.5 and pH 7.0. It has been reported previously that Ψ enhances base stacking, although the global stabilities of H69 UUU and H69 ΨΨΨ are similar.[185] Considering that all of the dissociation constants are similar at both buffer conditions, this difference implies that the binding modes of the peptides may differ. However, the overall change in H69 UUU at pH 5.5 with dimer TT implies that the binding of the dimer TT compared to the monomer may be more extensive, involving more contacts with the RNA. This result is also consistent with the tighter affinity relative to monomer, as determined by ESI-MS and BLItz.

Dimer TA binding to H69 was examined next to determine the role of the dimer identity. For H69 UUU at pH 5.5, a small chemical shift change was observed at C1914 (0.02 ppm) and U1915 (0.01 ppm) upon addition of the peptide, which was similar to that of the monomer (**Figure 4.18**). For H69 ΨΨΨ at pH 5.5, the loop region was not well resolved, however, we were able to observe a slight (0.01 ppm) chemical shift change at U1923, which is in the stem region (**Figure 4.19**). This was different from the result obtained with the monomer, which only showed a chemical shift change at C1920. For H69 UUU at pH 7.0, no change was observed, which was similar to the result with the monomer (**Figure 4.20**). Similarity of the binding affinities of dimer TA and monomer binding to H69 were observed in previous ESI-MS and BLItz studies as well, implying the branch moiety (AAAAAA) does not impact the interactions with the RNA.

Reverse dimer TY binding to H69 was examined to determine whether the sequence orientation was important. For H69 UUU at pH 5.5, a chemical shift upfield was observed at C1914 (0.02 ppm), which was in a different direction from the monomer or dimer TT changes (**Figure 4.21**). This shows that the orientation of the peptide is important in the peptide binding to H69. For H69 ΨΨΨ at pH 5.5 (**Figure 4.22**) or H69 UUU at pH 7.0 (**Figure 4.23**), no change was observed.

In **Sections 4.4** and **4.5**, binding studies have shown that in comparison to the monomer, affinity of dimer TT increased up to 10-fold, but the dimer TA was similar, and the reverse dimer TY had 3-fold lower binding. Although the binding affinities of the monomer to H69 under different buffer conditions were similar, the NMR studies have shown that H69 ΨΨΨ at pH 5.5 or H69 UUU at pH 7.0 spectra had little or no changes in the chemical shifts upon peptide binding. Previous NMR studies revealed that for H69 ΨΨΨ, local base-stacking interactions exist with Ψ1911-A1919-A1918-Ψ1917-A1916-Ψ1915, while in H69 UUU only A1916 and U1917 participate in base stacking.[48, 166] These results also agreed well with DMS probing and SHAPE analysis.[178, 193] For H69 ΨΨΨ, Ψ modifications were shown to enhance base stacking, yet through the modifications the global structure is altered compared to the unmodified RNA, which is overall thermodynamically destabilizing due to constraints on the loop structure.[185]

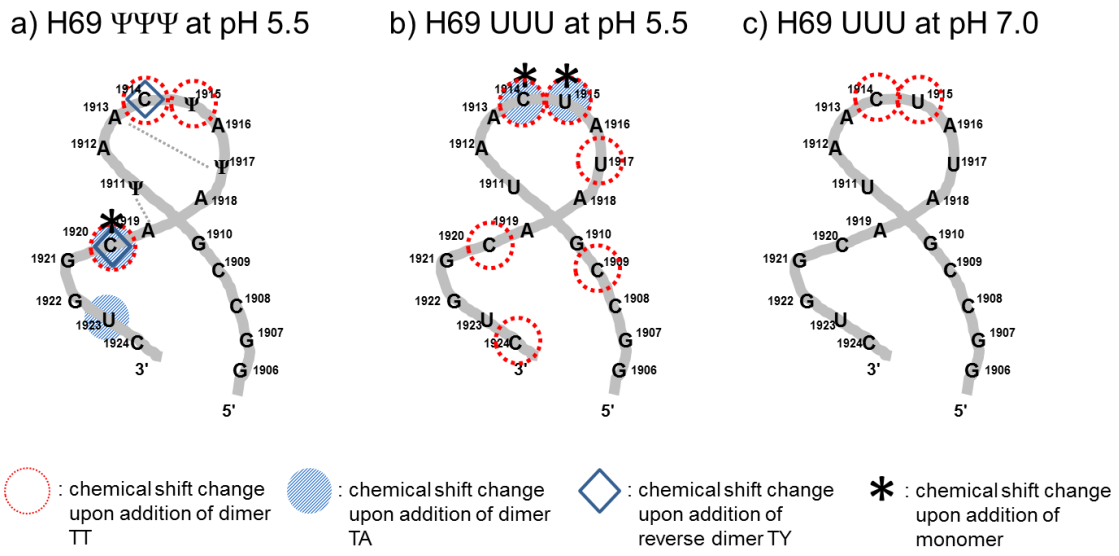


**Figure 4.24.** A schematic description of residues of H69 that showed a change upon peptide binding are marked.

Upon binding of dimer TT, both H69 ΨΨΨ and H69 UUU have shown changes in chemical shifts for C1914 and Ψ/U1915, which implies binding to the loop region. Also,

for both H69 ΨΨΨ and H69 UUU at pH 5.5, change at C1920, and C1924 were observed, which may imply that there is a change in the overall conformation upon binding. The differences between H69 ΨΨΨ and H69 UUU in binding to the dimer TT were the additional changes in chemical shift observed in H69 UUU. However, residues in the loop region of H69 ΨΨΨ did not resolve well (C1914 and Ψ1915), possibly due to the flexible structure on the 5'-side of the loop. Residue Ψ1917 was shown to have an interaction with A1912, which protects that residue from solvent exposure.[185] At pH 5.5, the stem-closing base pairing of Ψ/U1911 and C1920 was shown to be destabilized for both H69 ΨΨΨ and H69 UUU.[166] In contrast, H69 UUU displayed a continuous base-stacking interaction at U1911-A1912-C1914-U1915. With H69 at pH 7.0, the dimer TT showed interaction to the loop residues C1914 and U1915. Although the binding studies with ESI-MS and BLItz have shown the binding affinities to be similar to each other, the binding patterns in NMR studies were different. It is possible that the relaxed structure of H69 UUU at pH 7.0 plays a role in the different binding interactions with the peptides.

**4.7. Conclusions**

Multivalent effects of the peptide were explored by synthesizing dimer TARHIY and derivatives. By designing a dimeric peptide utilizing lysine as a branching point and β-alanine as a linker, we were able to synthesize a dimeric peptide. Binding studies with ESI-MS and BLItz showed that the dimer TT peptide has enhanced binding compared to the monomer, which was also shown through Scatchard analysis. The peptide dimer derivatives with AAAAAA exhibited similar binding to the monomer. Reverse dimer TY with reverse sequence YIHRAT instead of TARHIY showed decreased binding. Studies with reverse dimer TY support the idea that there may be multivalent binding of the peptide to H69 as well as the importance of the orientation of the peptide. However, there is room for improvement for the design of the peptides. The branching point and linkers do not exactly match the original design of the phage library, which raise some

questions on the dimeric peptide studies. The linker can also be modified by using PEGylated linkers, which would add more flexibility to the peptides, and also will be resistant to degradation.

One important fact we learned from BLItz studies was that the binding of the dimer TT to H69 was ~100-fold faster in association and ~10-fold faster in dissociation compared to the monomer TARHIY. The binding mode of TARHIY to H69 was not very clear from **Chapter 3**. With the increase of charge with the dimeric structure, the faster association/dissociation may support the binding to be through charge-charge interactions. Although the dimer TT and reverse dimer TY have the same amino acid composition, the orientation of the charges make a difference in both binding affinity and rate constants, also supporting the importance of orientation. The data obtained with ESI-MS or BLItz studies showed poor fitting, which suggests the peptide interaction to H69 may not be through a simple 1:1 binding or conditions for the experiments may need optimization.

The NMR spectra obtained with NMR have shown changes in the chemical shifts for the stem region residues, which indicate an overall conformation change of the RNA upon peptide binding (**Figure 4.23**). In the NMR studies, the orientation of the peptide was important for the dimeric peptide binding. Overall, the work in this chapter has revealed the importance of the orientation of peptide binding to H69, along with the multimeric binding.

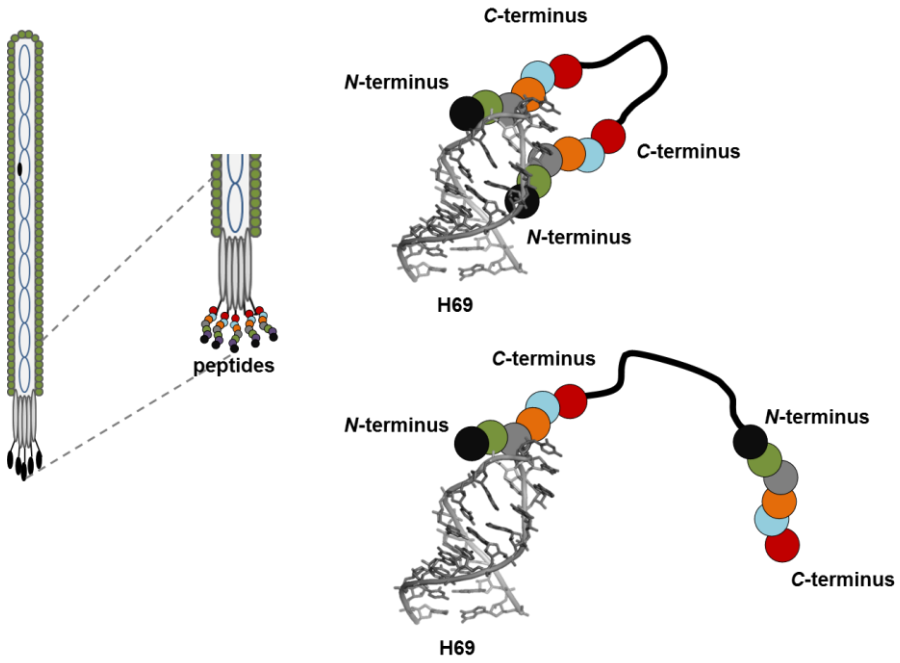


**Figure 4.25.** A schematic figure of dimer TT and reverse dimer is shown.

# CHAPTER 5 – Future directions and Summary

## 5.1. Future directions

### 5.1.1. Optimization of the branched peptide binding

In **Chapter 4**, dimeric peptides were synthesized, and binding studies revealed enhanced binding of those peptides compared to the monomer. However, the design of the peptide can be improved by optimization of the structure. We used lysine as a branching point, which was also used in previous studies involving multimeric peptide syntheses.[132, 189] However, these studies can only explore dimeric binding, while studies from Bastings *et al*. have shown studies with multimers including dimers, teteramers, and pentamers. [190] In their study, the dendrimeric branch was synthesized, followed by attaching the peptide of interest *via* native chemical ligation (NCL). Dendrimeric branches will help explore multimeric binding. Also, by adding a clickable moiety such as an azide or alkyne, along with multimers, other molecules can be attached to the peptide (*i.e.*, fluorescent dyes or potent molecules with binding affinity or cell-penetrating activity).

Also, the distance between the branch and peptide can be optimized. In our study, β-alanine was incorporated as a linker. However, previous studies have used different linkers in between, such as polyethyleneglycol (PEG), aminohexanoic acid (Ahx), β-alanine (β-Ala), or 2-(2-aminoethoxy)ethoxy (AEEAc).[132, 189-190] Also, in the study by Hooks *et al.*, methionine, lysine, and D-lysine were used as spacers that can avoid aggregation of the peptide sequences.[132] Optimization of the linker length along with chemical properties may enhance binding affinity to H69. In order to find an optimal distance, PEGylated amino acids can be incorporated as linkers, with structures shown in **Figure 5.1**. Also, by changing the linker length between the branching point and TARHIY, the optimal linker length can be found, by adding PEG groups as spacers.[194-195] Addition of PEG or propargylglycine onto either *C*- or *N*-terminus will allow observation

of the effect of the functional groups on each terminus. Synthesis of TARHIY peptides with PEG linkers was completed.

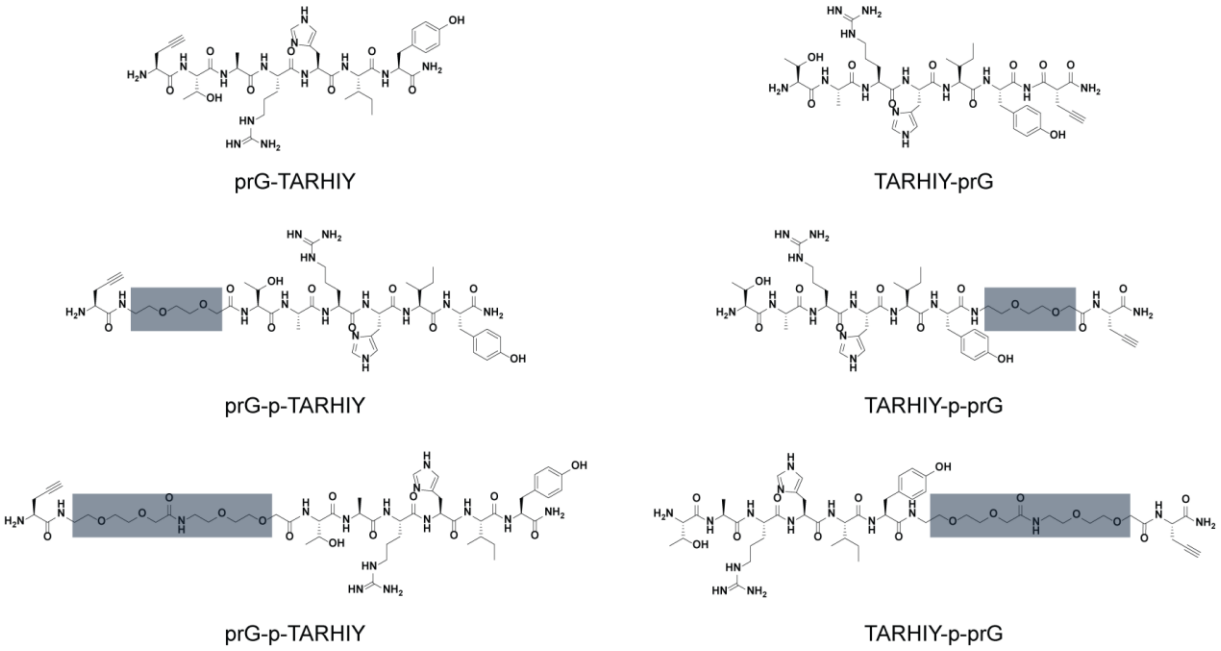


**Figure 5.1.** Structure of TARHIY peptides with PEG spacers is shown. The propargylglycines and PEG groups were added to either the *N*-terminus or the *C*-terminus.

### 5.1.2. Developing TARHIY as a probe for H69 loop region binding studies

In **Chapter 3**, TARHIY exhibited binding for H69 in the loop region. This was not seen previously, which may lead to the development of a probe targeting the loop region of H69. Also, dimer TT exhibited enhanced binding to H69. The binding sites of dimer TT was determined by NMR in **Chapter 4**. Dimer TT was shown to primarily bind to the loop region with H69 UUU at pH 7.0 and H69 ΨΨΨ at pH 5.5, and to change the overall chemical shifts with H69 UUU at pH 5.5. Previous studies have shown that RRF interacts with H69 in the loop region, which then reduces H69 interactions important for the B2a intersubunit bridge of the 70S ribosome.[32, 61, 186, 188] Aminoglycosides primarily

bind to H69 in the stem region, and the overall conformation changes upon binding. The interaction between H69 and RRF was shown to be disrupted upon binding of aminoglycosides, leading to inhibition of ribosome recycling.[186] In this thesis work, peptide TARHIY was shown to bind to the loop region with moderate affinity. Attaching fluorescent labels to the peptide TARHIY or dimer TT will enable screening molecules binding to H69 in the loop region. Also, fluorescence resonance energy transfer (FRET) assays may be employed to monitor changes in H69 and RRF interactions upon molecule binding.

### 5.1.3. Mapping of H69 with TARHIY analogues using ESI-MS

A 29-nucleotide hairpin structured RNA, trans-activating response element (TAR) RNA (5′-GGCAGAUCUGAGCCUGGGAGCUCUCUGCC-3′), is found in 5'-end of nascent HIV-1 transcripts, which has an extinction coefficient of 268,900 L/mol•cm.[195] Trans-activating (Tat) protein ($H_2N$-GRKKRRQRRRPP-$NH_2$) is an arginine-rich motif, which has tight binding to TAR RNA, reported to bind to the bulge and loop region.[195] The binding affinity is 0.7 μM, and this is a well-established system for RNA-protein binding studies.[195] Rana *et al.* have selected heterochiral tripeptides binding to the bulge region using TAR lacking the bulge as a competitor using one-bead-one-compound (OBOC) assay.[196] The tripeptide KkN exhibited tighter binding than Tat protein (0.4 μM), and Rkv exhibited weaker binding (10 μM).[196] To find the binding region at the molecular level, ESI-MS mapping would be ideal. Among other biophysical methods used in this study, only NMR spectroscopy and ESI-MS only can monitor ligand binding sites on RNA at a molecular level. While NMR spectroscopy has a limitation of requiring a large amounts of the sample, ESI-MS only requires small amount of sample. In our NMR studies, although the binding affinities appeared to be similar, H69 ΨΨΨ and H69 UUU showed different patterns for binding dimer peptides. Furthermore, some peaks were difficult to observe due to the flexible nature of the H69 loop region. ESI-MS mapping may allow monitoring

of these flexible regions upon binding to peptides. Since the binding region is known for TAR RNA to Tat peptide, employing ESI-MS and establishing mapping methods with the tripeptides (KkN and Rkv) would be valuable. This approach could be used to detect binding regions of other peptides to target RNAs, such as H69. We could monitor binding of TARHIY or neomycin towards modified or unmodified variants of H69.[197] Currently, the mapping studies using ESI-MS are being done in the Rodgers' lab. TAR RNA was prepared using T7 polymerase *in vitro* transcription, and the peptides were prepared using solid-phase peptide synthesis.

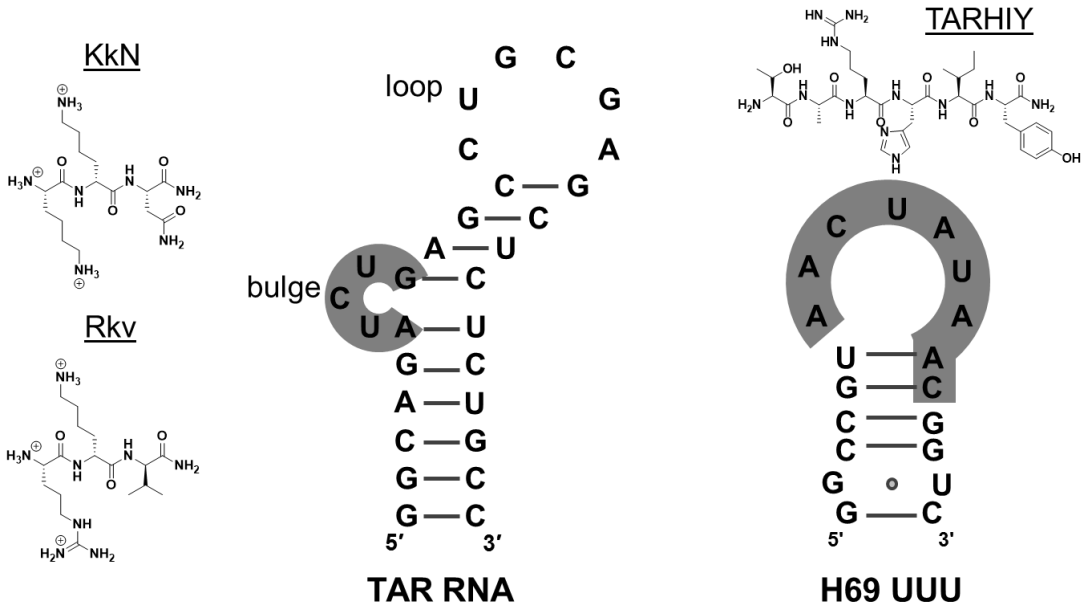


**Figure 5.2.** Structures of TAR RNA and H69 UUU and peptides that can be employed for mapping studies are shown.

### 5.2. Summary

In order to find a ligand that can target H69 of the bacterial ribosome, in **Chapter 3**, phage display was performed in pH 5.5, and several peptides were selected. The selected peptides were synthesized, and a peptide TARHIY was selected by FID assay for further binding studies. The peptide TARHIY showed moderate binding to H69

employing ESI-MS and BLItz. However, the selected peptide TARHIY did not show selectivity towards a certain conformation or type of H69, although the peptide showed selectivity towards H69 over $tRNA^{Phe}$. The binding site of peptide TARHIY was determined to be in the loop region of H69 employing NMR, which was not observed previously.

In **Chapter 4**, analogues of dimers were synthesized and the binding of those to H69 were studied. These studies have shown that the peptide TARHIY may be binding to H69 in a cooperative manner, shown in increased binding affinity with ESI-MS and BLItz, and change in conformation with a dimer that was monitored with NMR. Also, The dimer exhibited improved binding comparable to the binding affinity of neomycin. Based on our NMR studies, H69 UUU showed conformational changes upon dimeric binding, which were similar to that of neomycin binding to H69.

In **Chapter 5**, dual binding of neomycin and peptide TARHIY were examined with MALDI-TOF and BLItz studies. Neomycin, a well-known aminoglycoside binds to H69 at the stem region. It was shown that there is a complex of neomycin, peptide TARHIY, and H69. However, although the primary binding sites have been shown to be different for the two ligands, when they are incubated together with H69, the binding events may not be independent from each other. Previous studies of Agris *et al.*[187] have shown that neomycin may bind to H69 in a cooperative manner by changing the conformation of H69. The BLItz experiment has shown that the binding of neomycin and peptide TARHIY may not be independently binding to H69. This may imply although the primary binding sites are different, neomycin and peptide TARHIY may bind to H69 in a similar fashion by altering the conformation.

Overall, a peptide sequence targeting H69 was identified from phage display, and using various methods, the peptide exhibited moderate binding. The peptide showed binding to the loop region of H69, which was not observed previously. A known

aminoglycoside neomycin binds to the stem region of H69, therefore, dual binding was explored by monitoring a complex formation with MALDI-TOF. Serial incubation then left dual binding of neomycin or peptide TARHIY to be questionable. Also, multimeric binding was observed with the peptide TARHIY, which was then studied with dimeric peptides, which showed enhanced binding. This result indicates that peptides selected using phage display may be useful parent sequences, however, whether the monomer is a tight binder itself or multimeric effects enhance the binding need to be considered.

# APPENDIX A. MALDI-TOF RESULTS AND HPLC TRACES OF PEPTIDES USED IN THIS THESIS

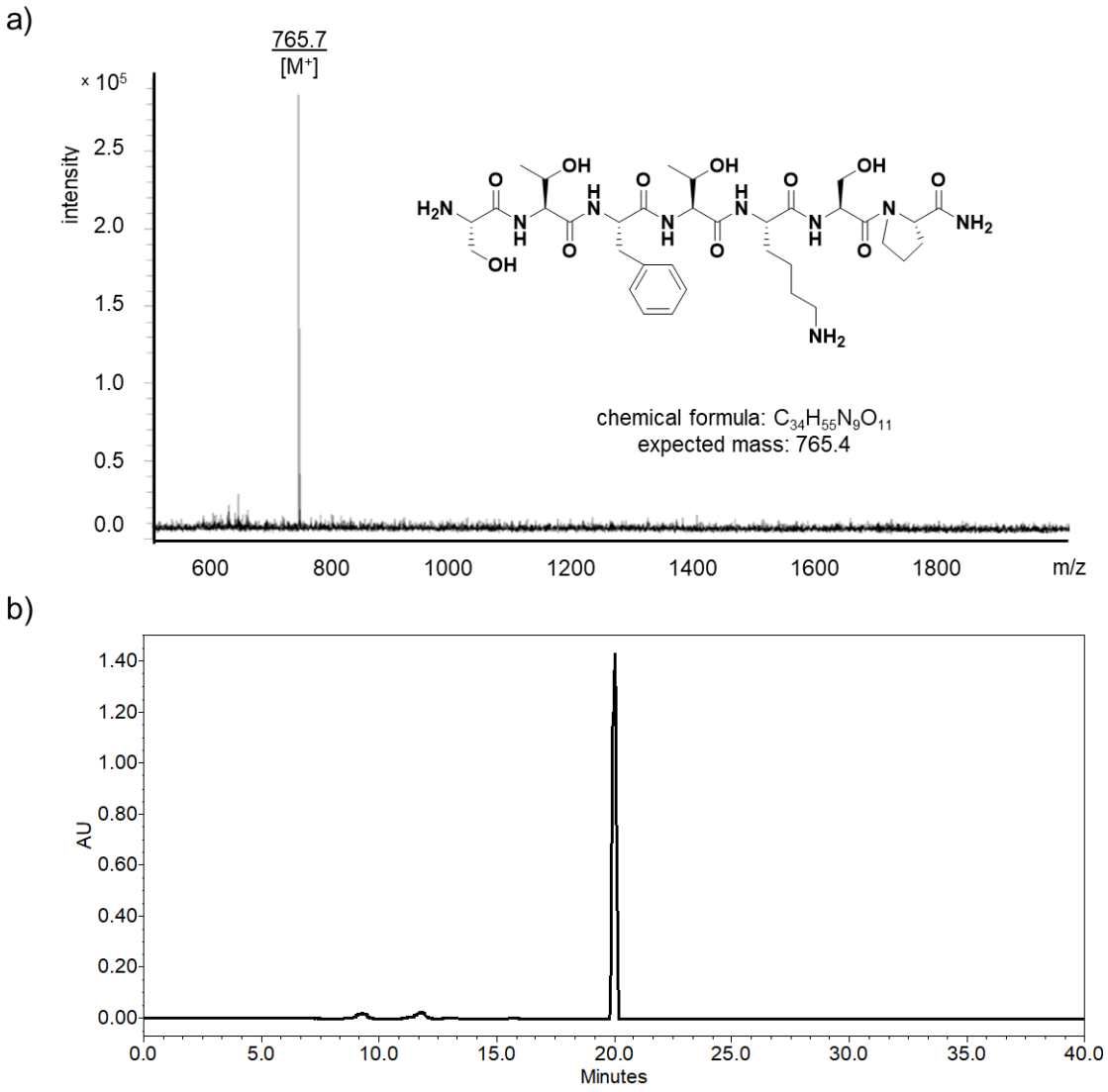


**Figure A1**. MALDI-TOF spectrum (a) and HPLC trace (b) of STFTKSP is shown.

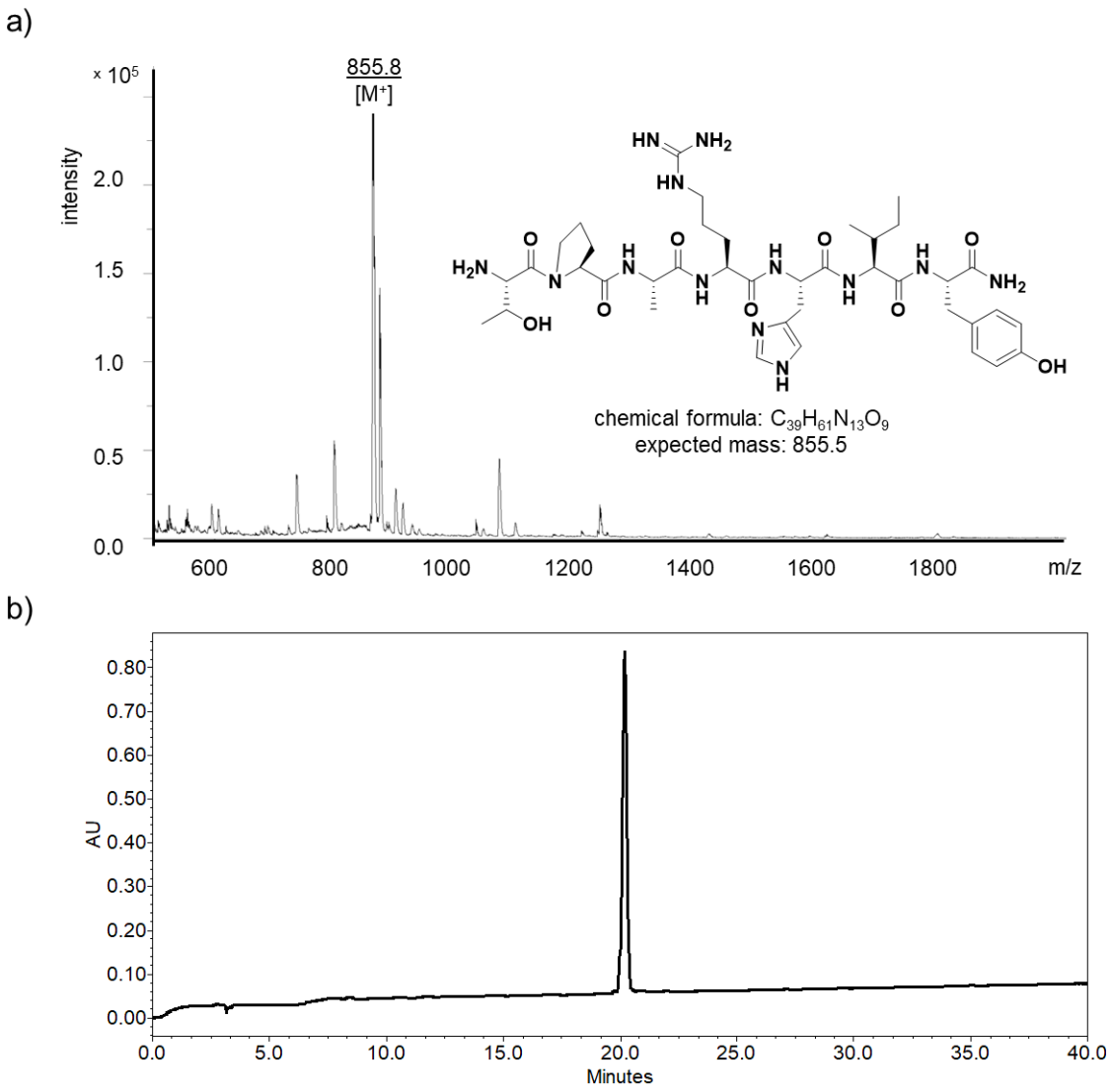


**Figure A2**. MALDI-TOF spectrum (a) and HPLC trace (b) of TPARHIY is shown.

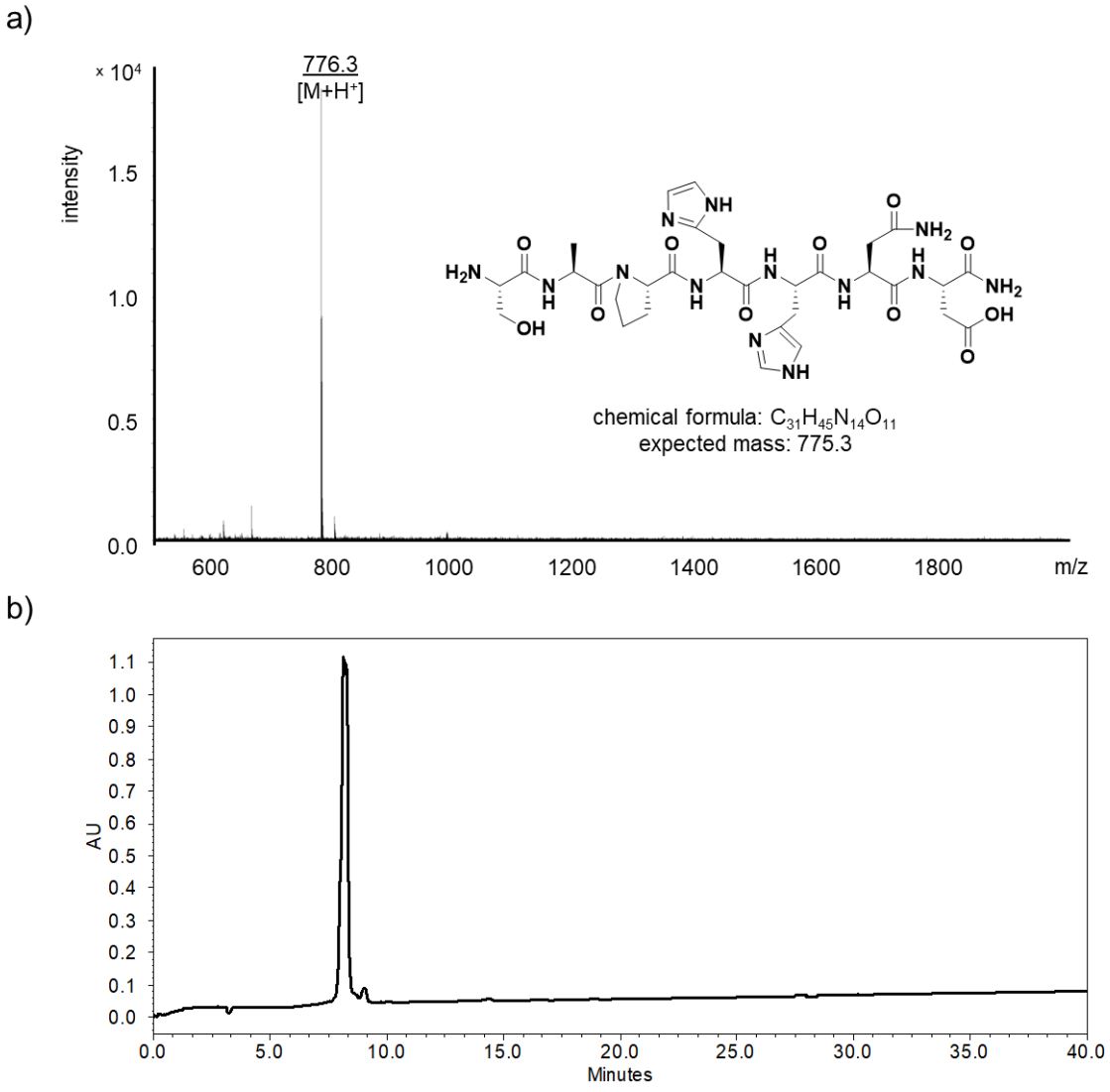


**Figure A3**. MALDI-TOF spectrum (a) and HPLC trace (b) of SAPHHND is shown.

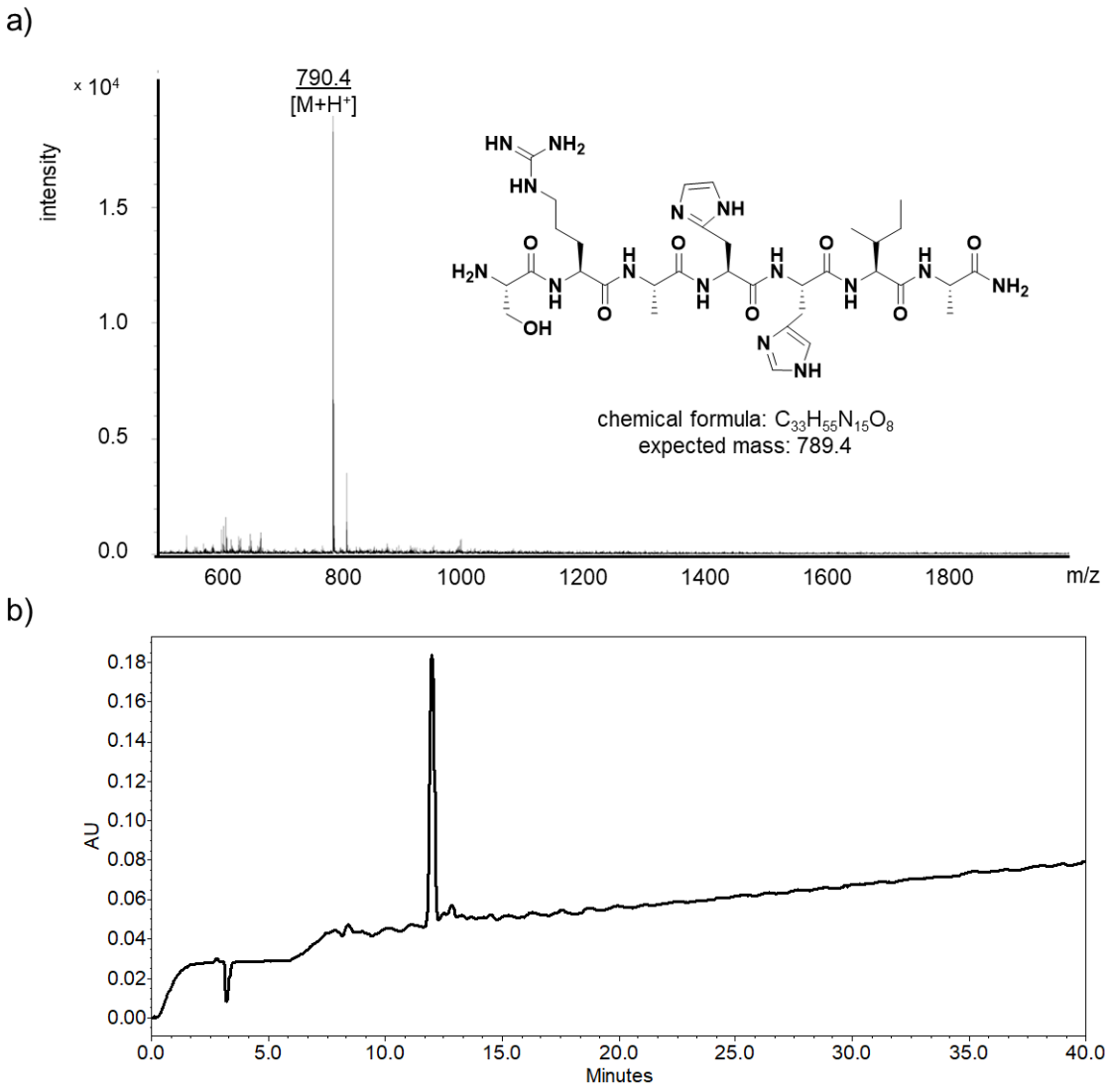


**Figure A4**. MALDI-TOF spectrum (a) and HPLC trace (b) of SRAHHIA is shown.

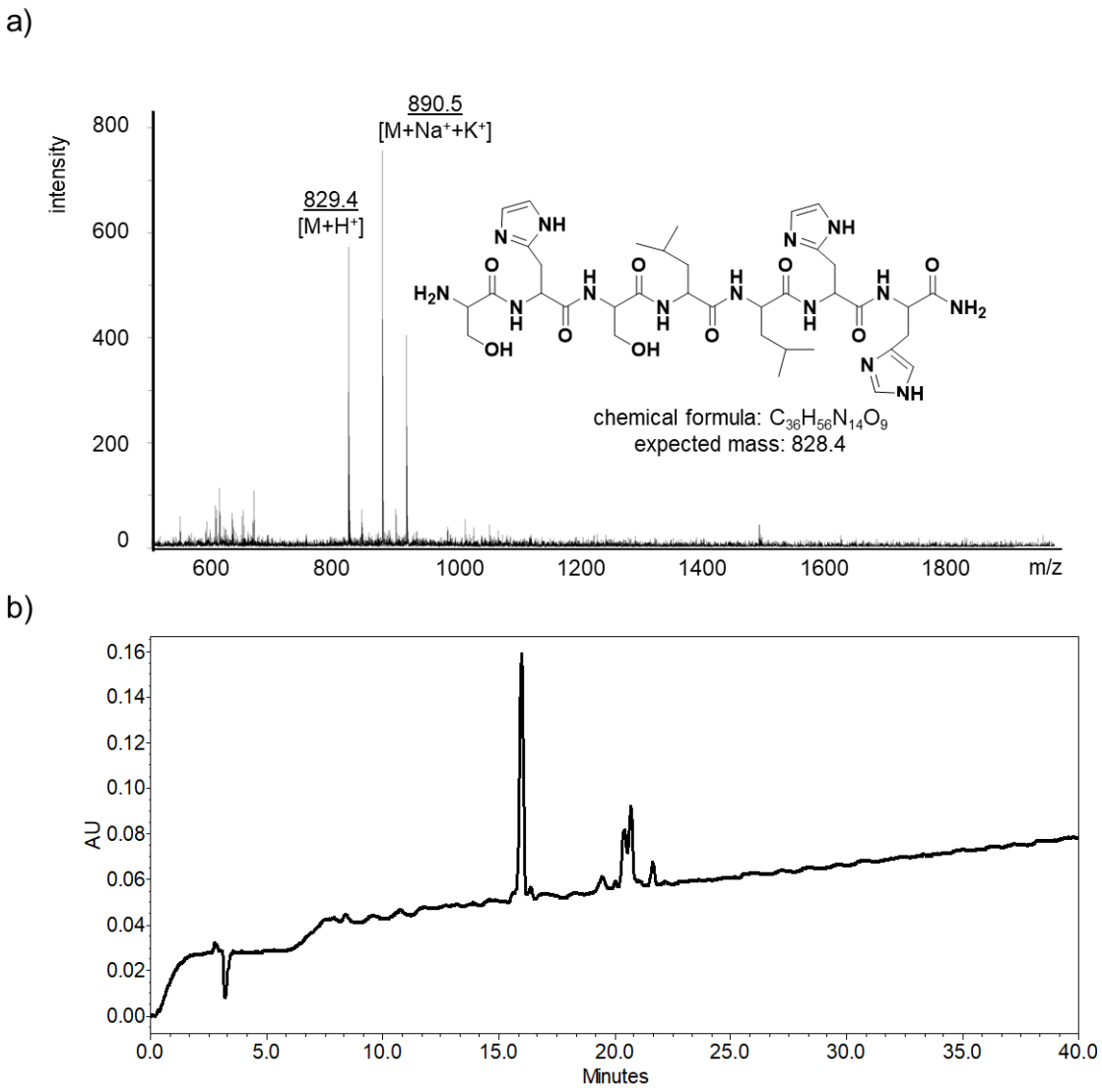


**Figure A5**. MALDI-TOF spectrum (a) and HPLC trace (b) of SHSLLHH is shown.

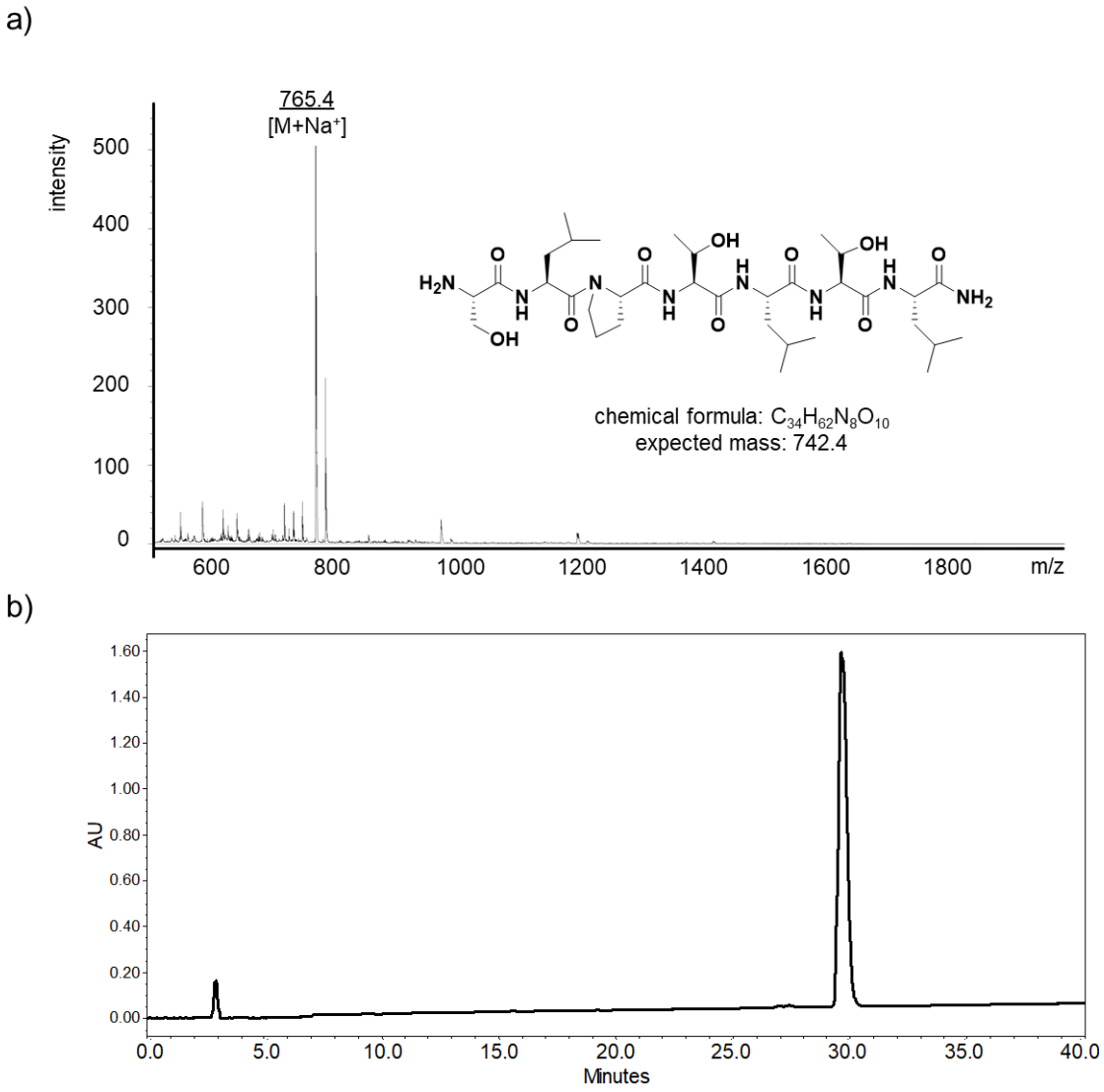


**Figure A6**. MALDI-TOF spectrum (a) and HPLC trace (b) of SLPTLTL is shown.

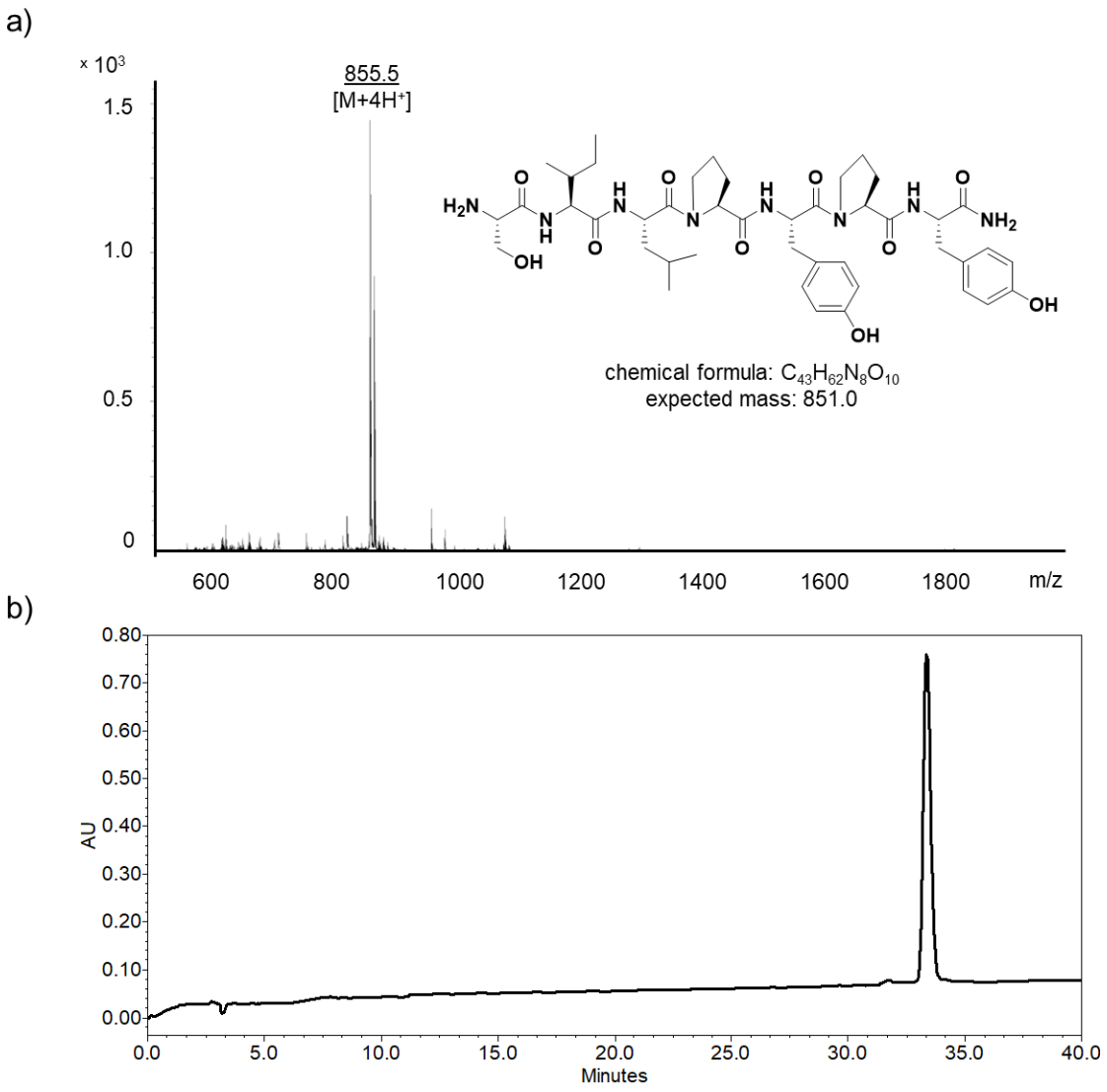


**Figure A7**. MALDI-TOF spectrum (a) and HPLC trace (b) of SILPYPY is shown.

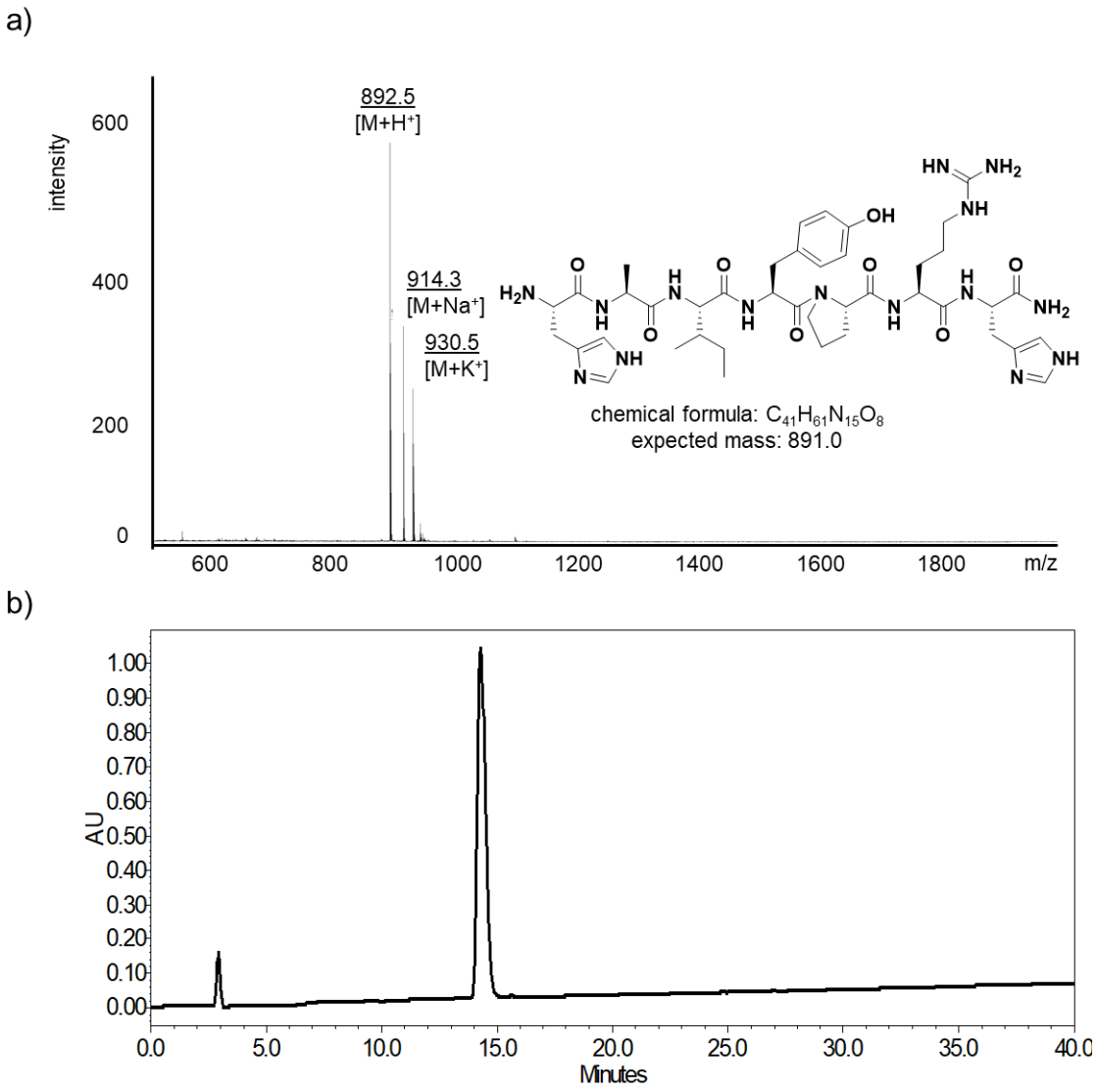


**Figure A8**. MALDI-TOF spectrum (a) and HPLC trace (b) of HAIYPRH is shown.

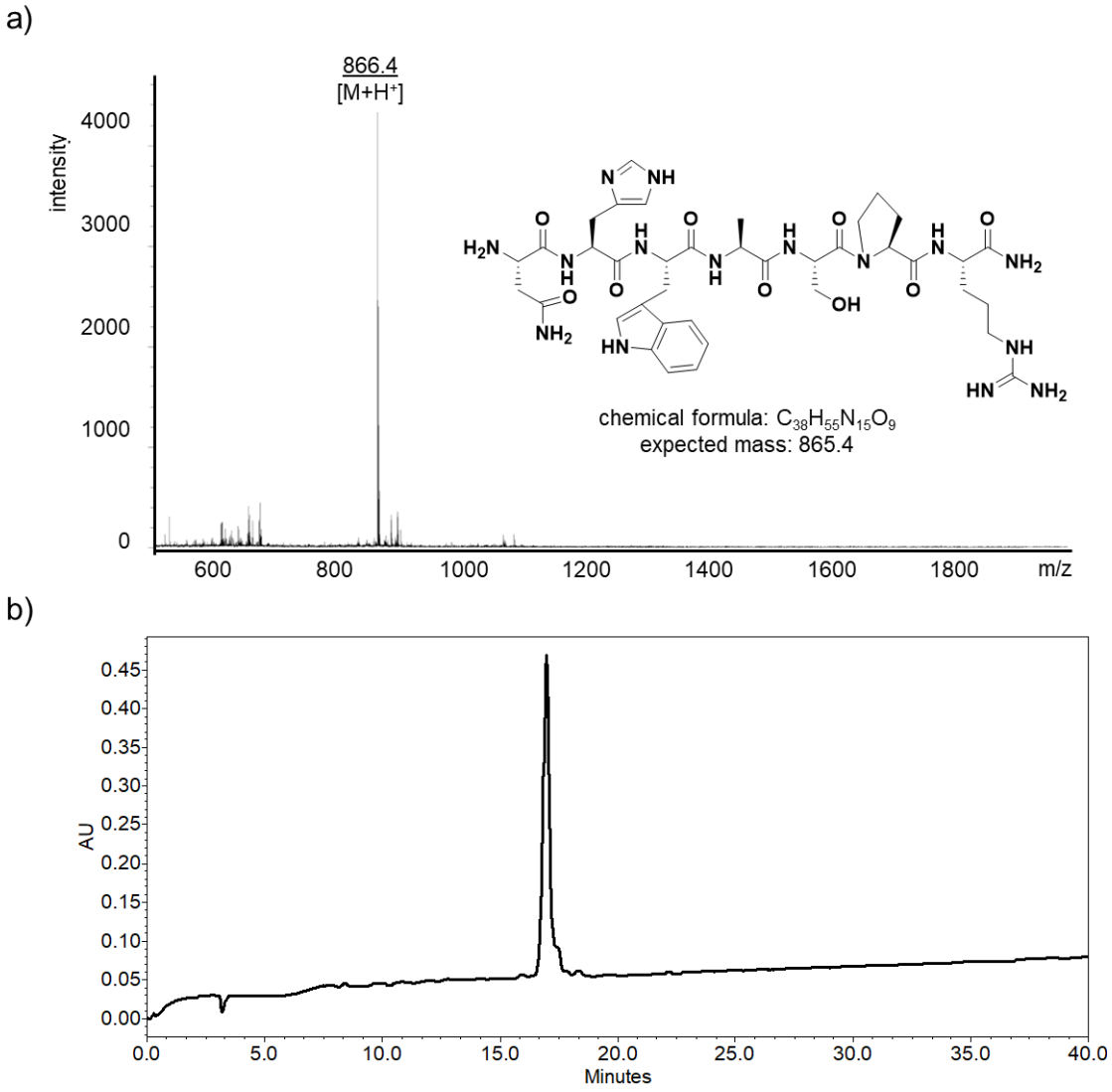


**Figure A9**. MALDI-TOF spectrum (a) and HPLC trace (b) of NHWASPR is shown.

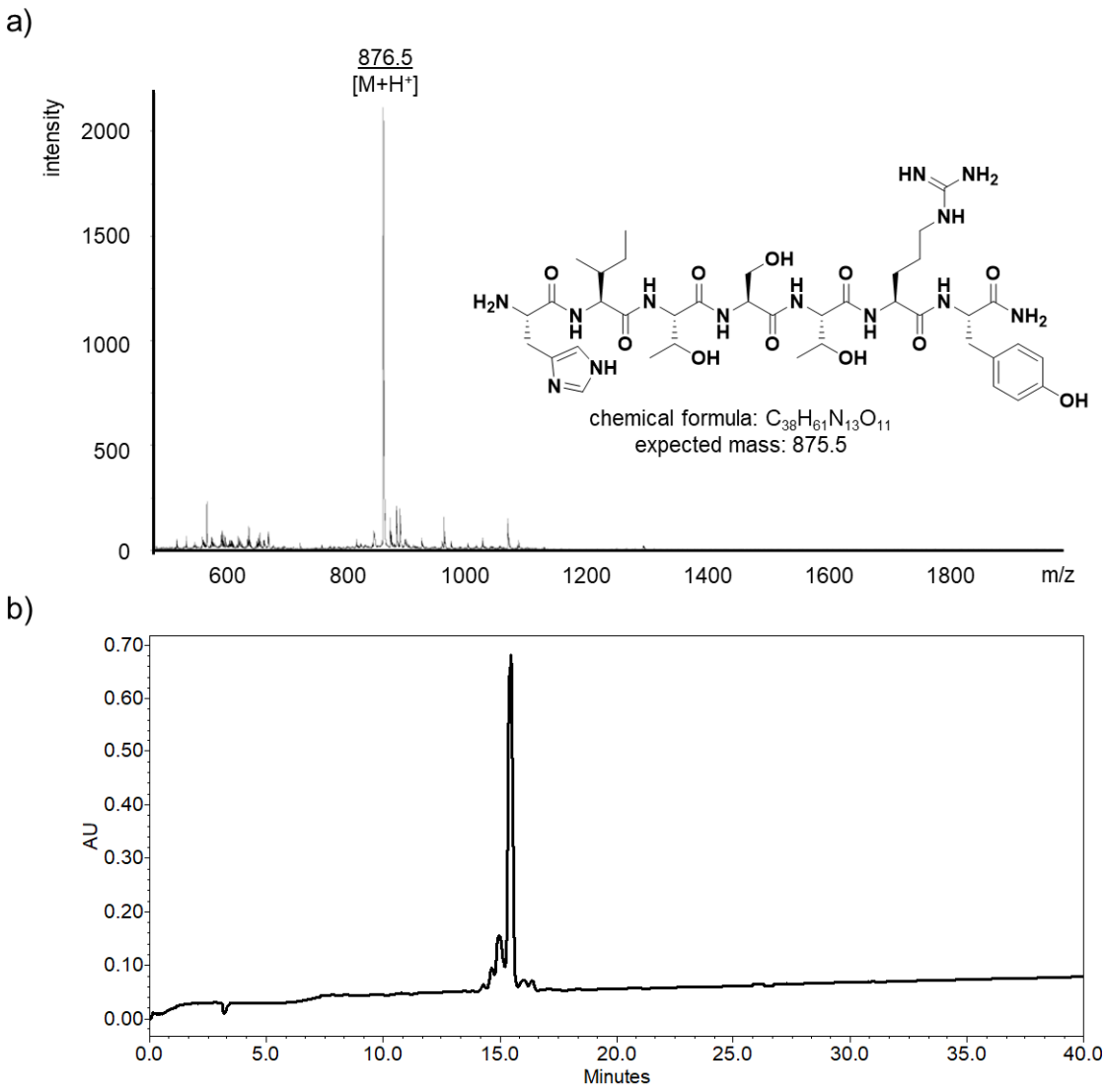


**Figure A10**. MALDI-TOF spectrum (a) and HPLC trace (b) of HITSTRY is shown.

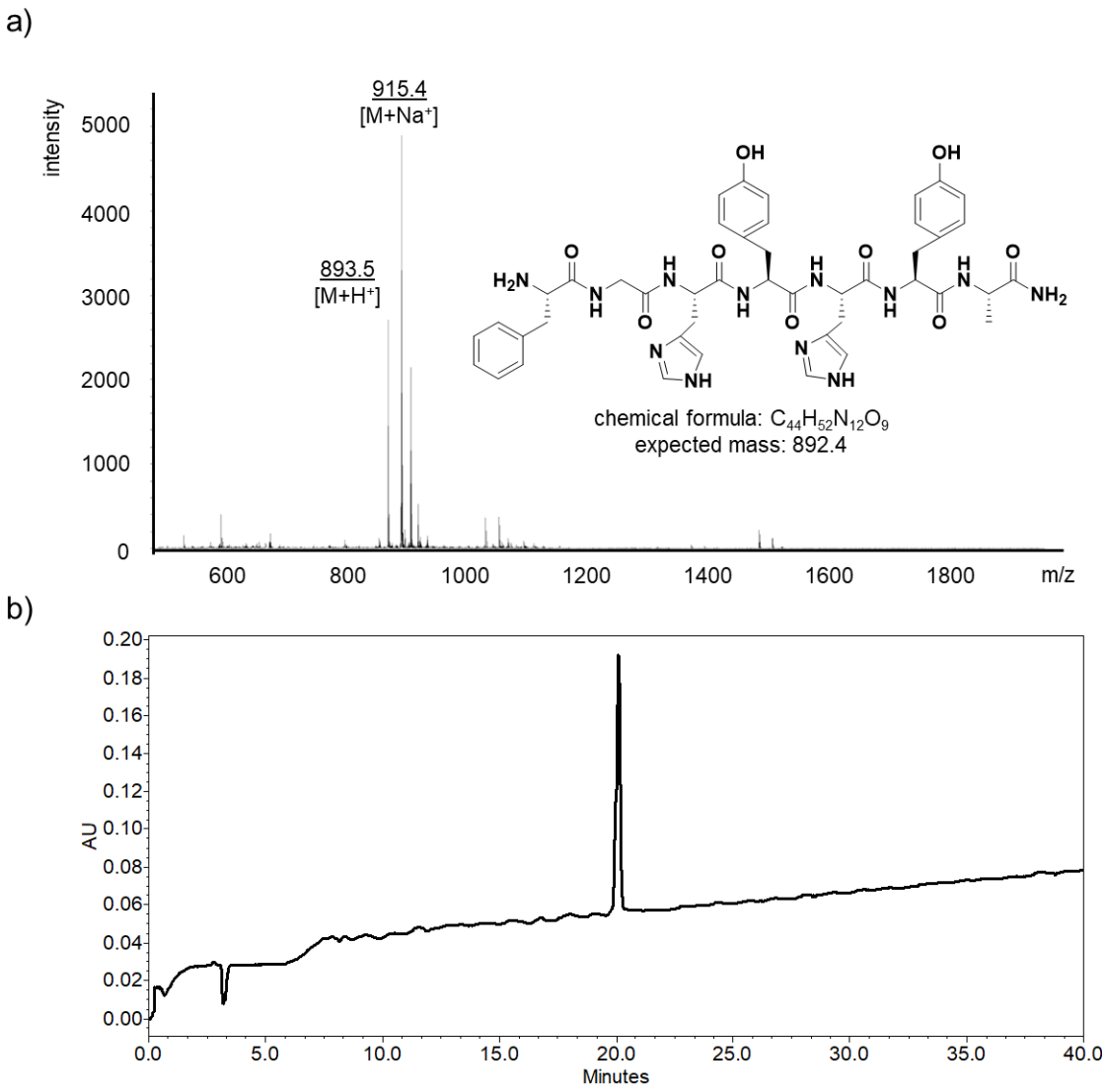


**Figure A11**. MALDI-TOF spectrum (a) and HPLC trace (b) of FGHYHYA is shown.

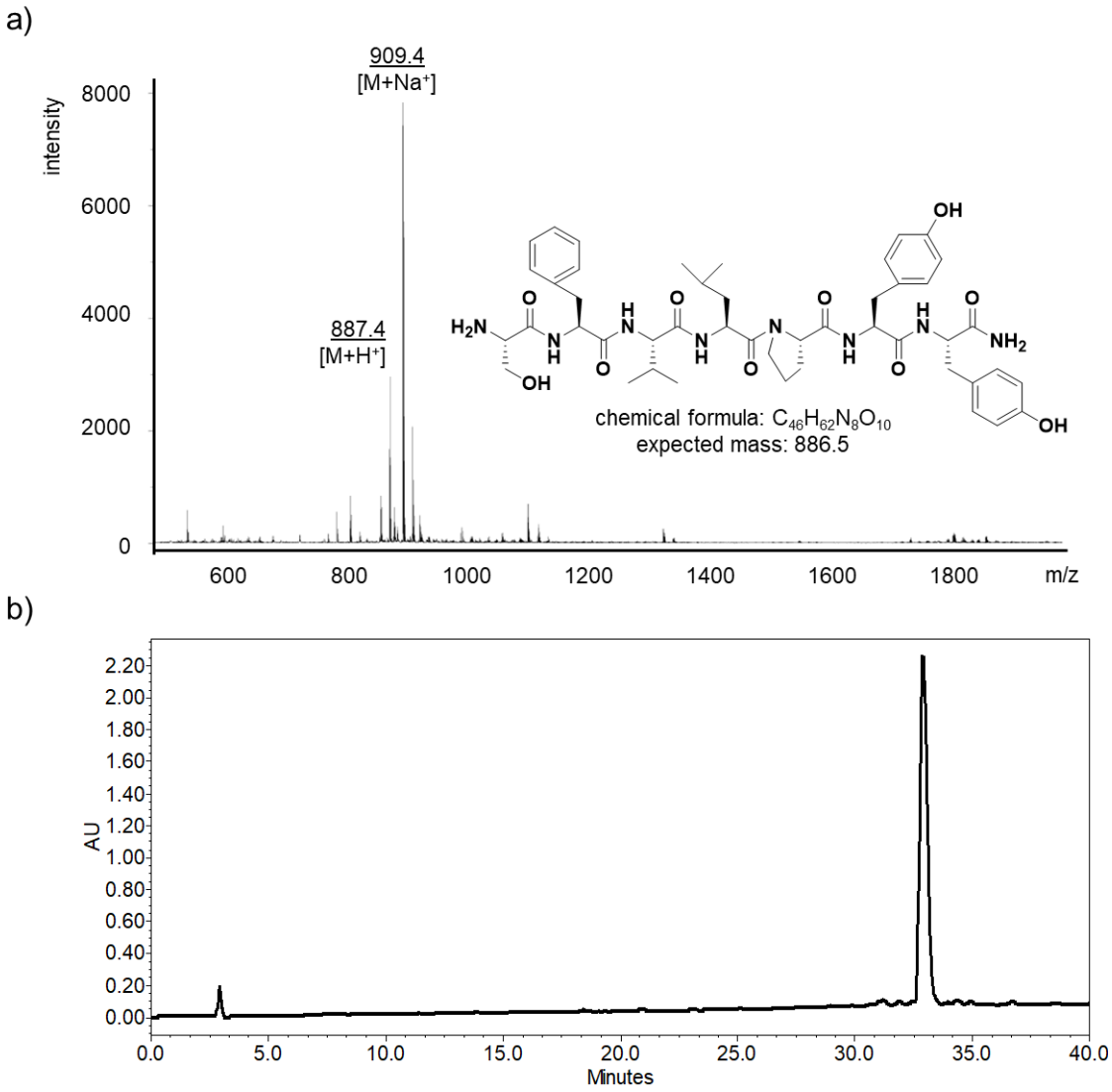


**Figure A12**. MALDI-TOF spectrum (a) and HPLC trace (b) of SFVLPYY is shown.

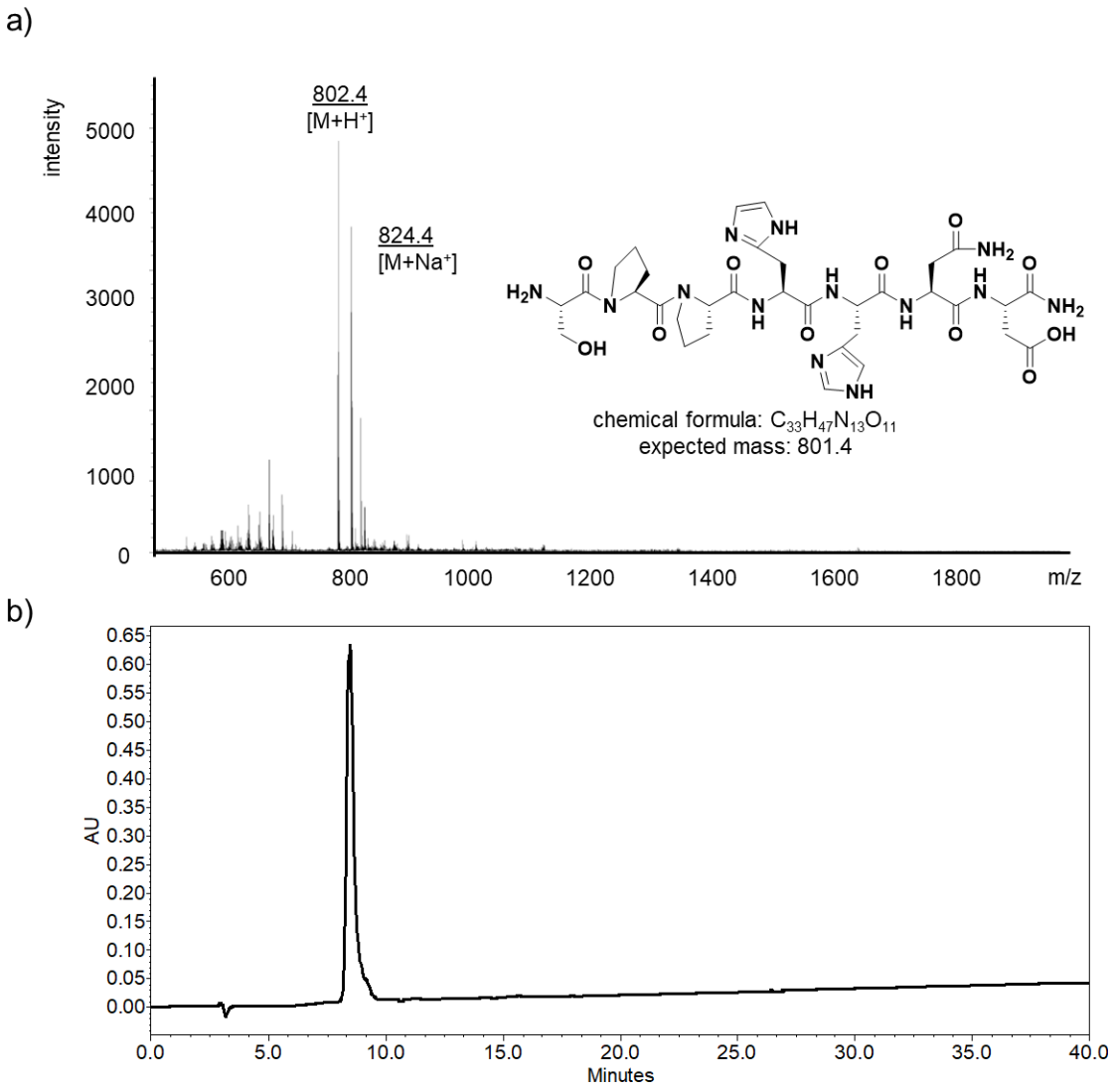


**Figure A13**. MALDI-TOF spectrum (a) and HPLC trace (b) of SPPHHND is shown.

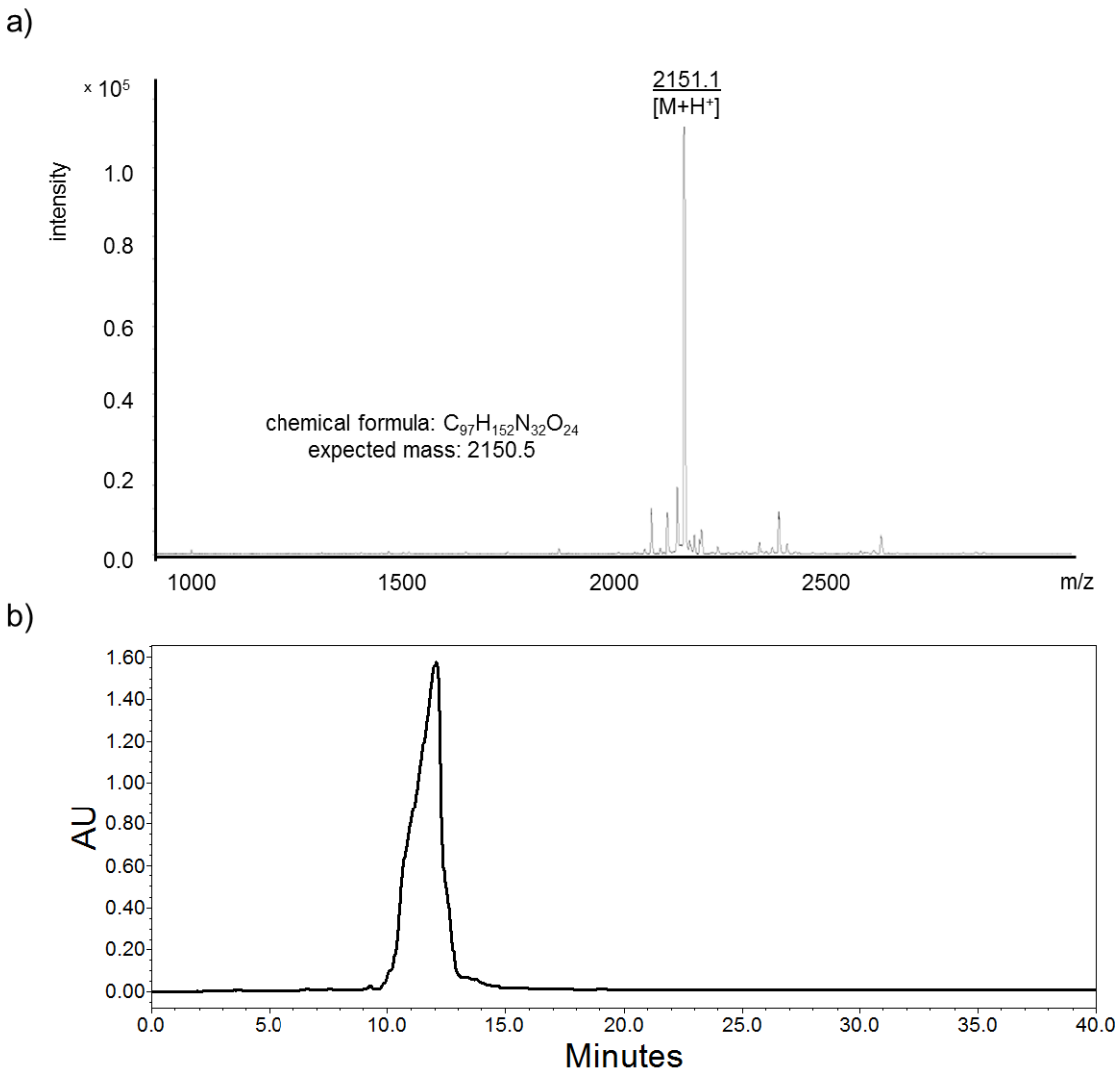


**Figure A14.** MALDI-TOF spectrum (a) and HPLC trace (b) of dimer TT is shown.

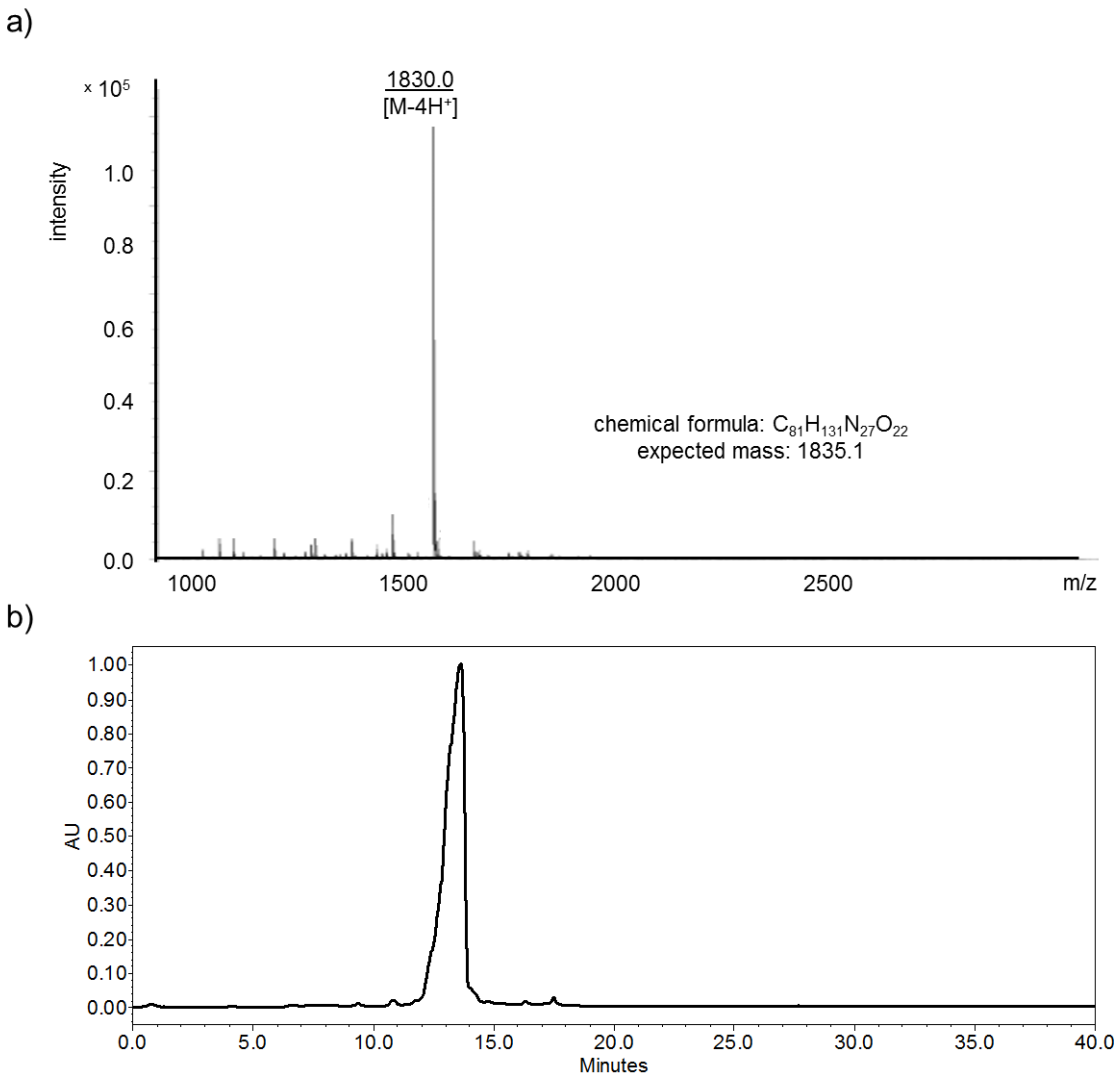


**Figure A15**. MALDI-TOF spectrum (a) and HPLC trace (b) of dimer TA is shown.

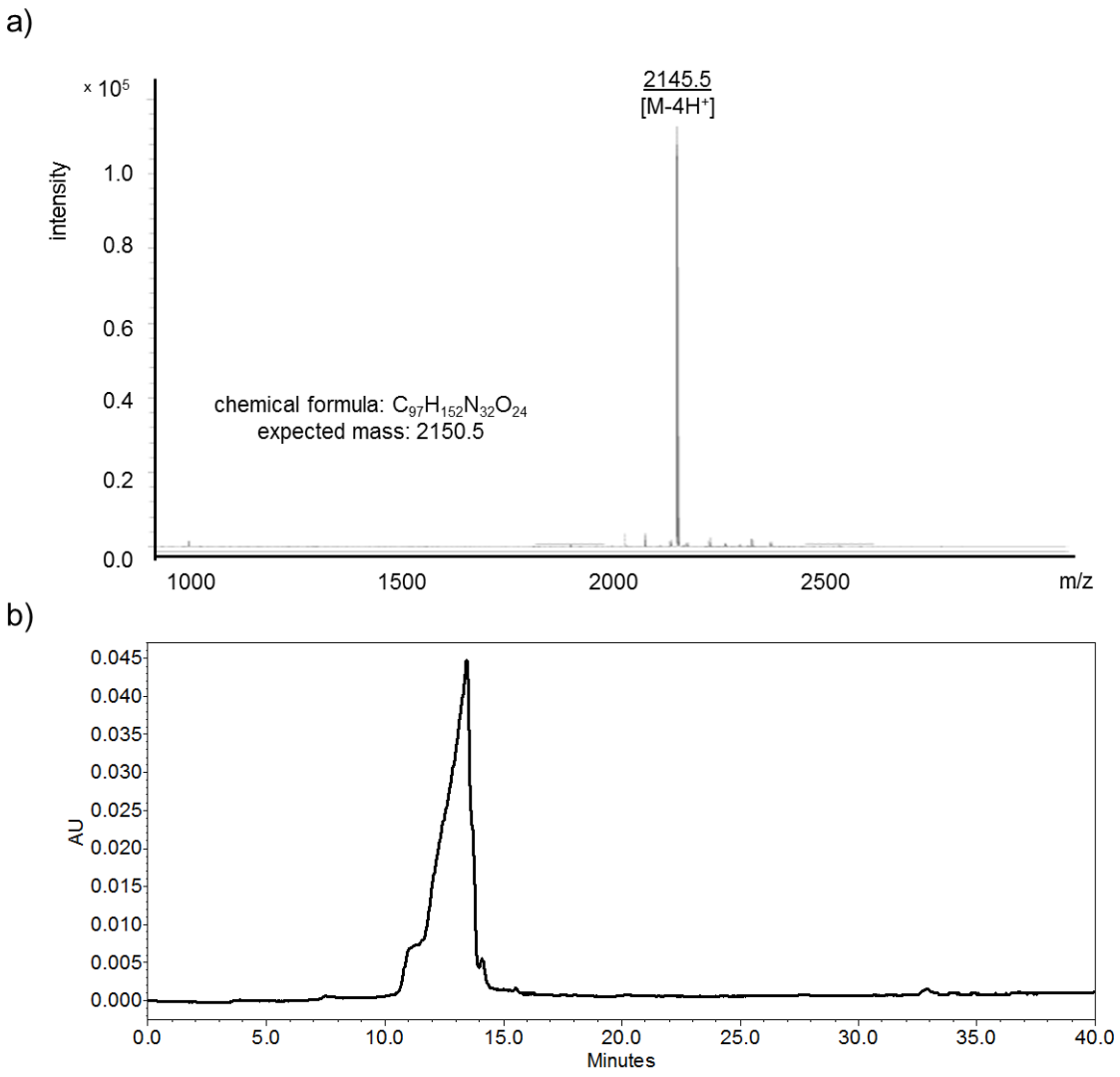


**Figure A16**. MALDI-TOF spectrum (a) and HPLC trace (b) of reverse dimer TY is shown.

## APPENDIX B. EXPANDED BLITZ SPECTRA OF PEPTIDE TITRATION TO H69

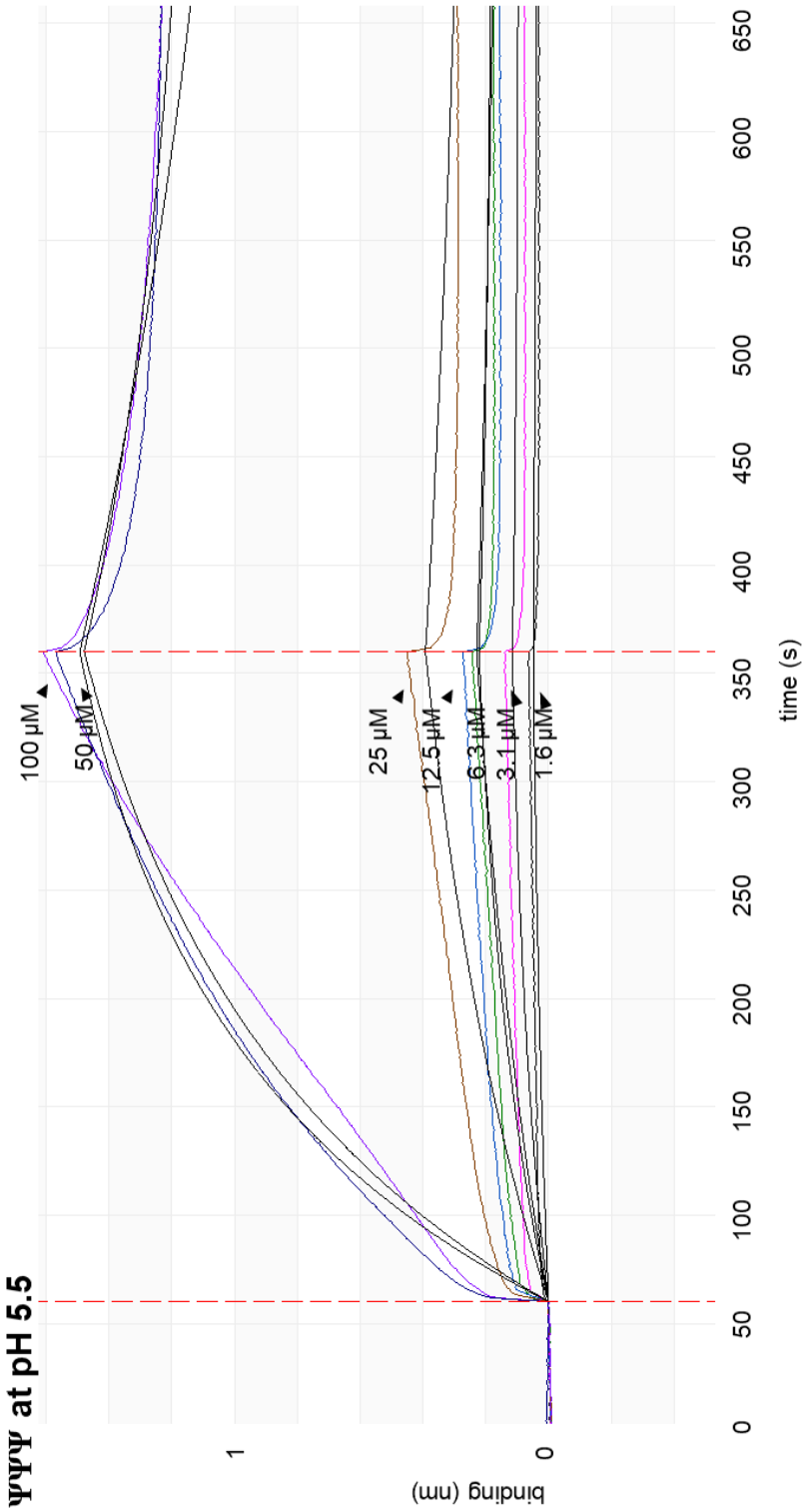


**Figure B1**. Representative BLItz results for TARHIY titration at pH 5.5 (20 mM cacodylate, 100 mM KCl, and 0.1% Tween-20) against H69 ΨΨΨ. Black lines represent the 1:1 fitting curve.

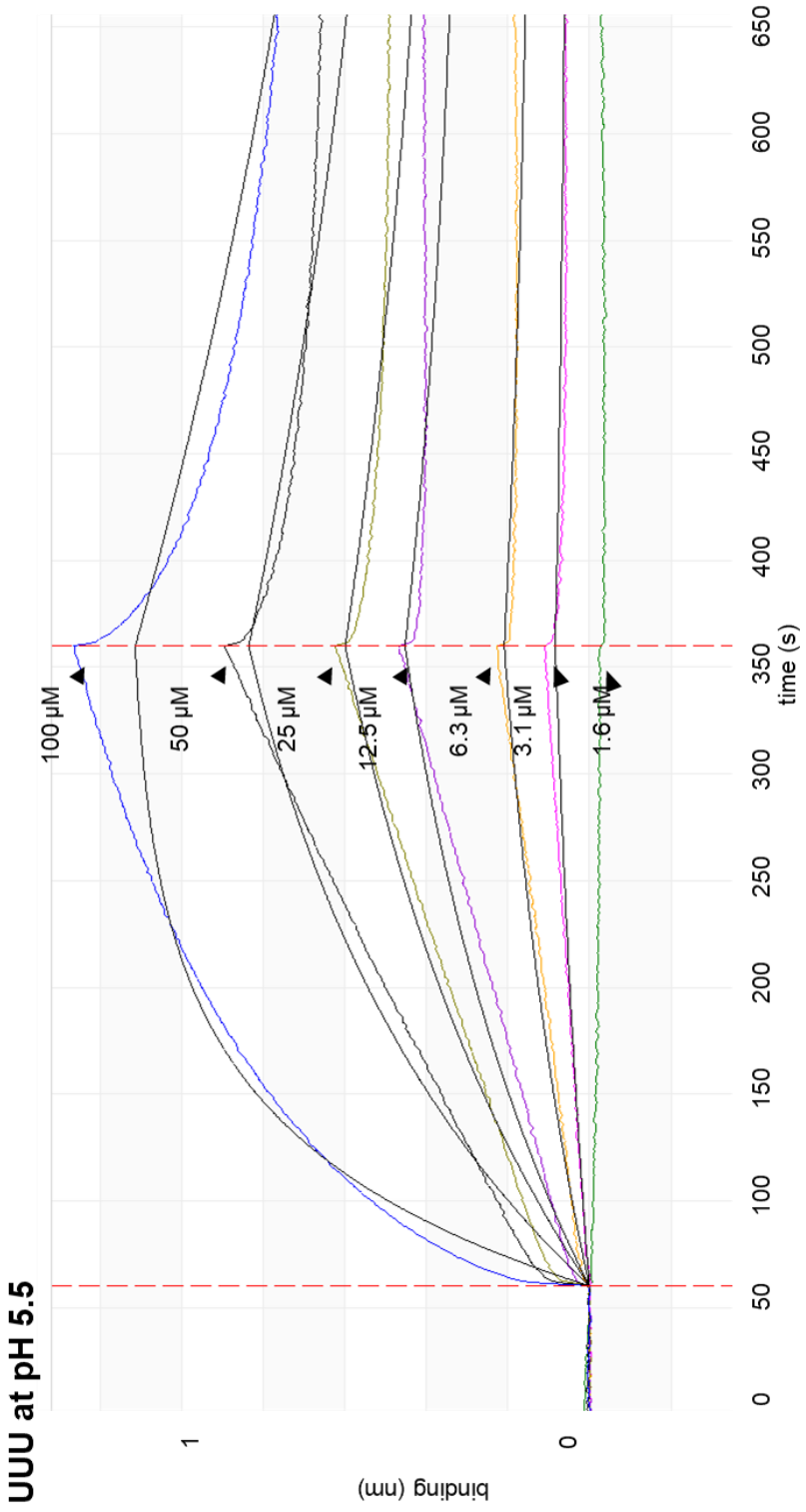


**Figure B2**. Representative BLItz results for TARHIY titration at pH 5.5 (20 mM cacodylate, 100 mM KCl, and 0.1% Tween-20) against H69 UUU. Black lines represent the 1:1 fitting curve.

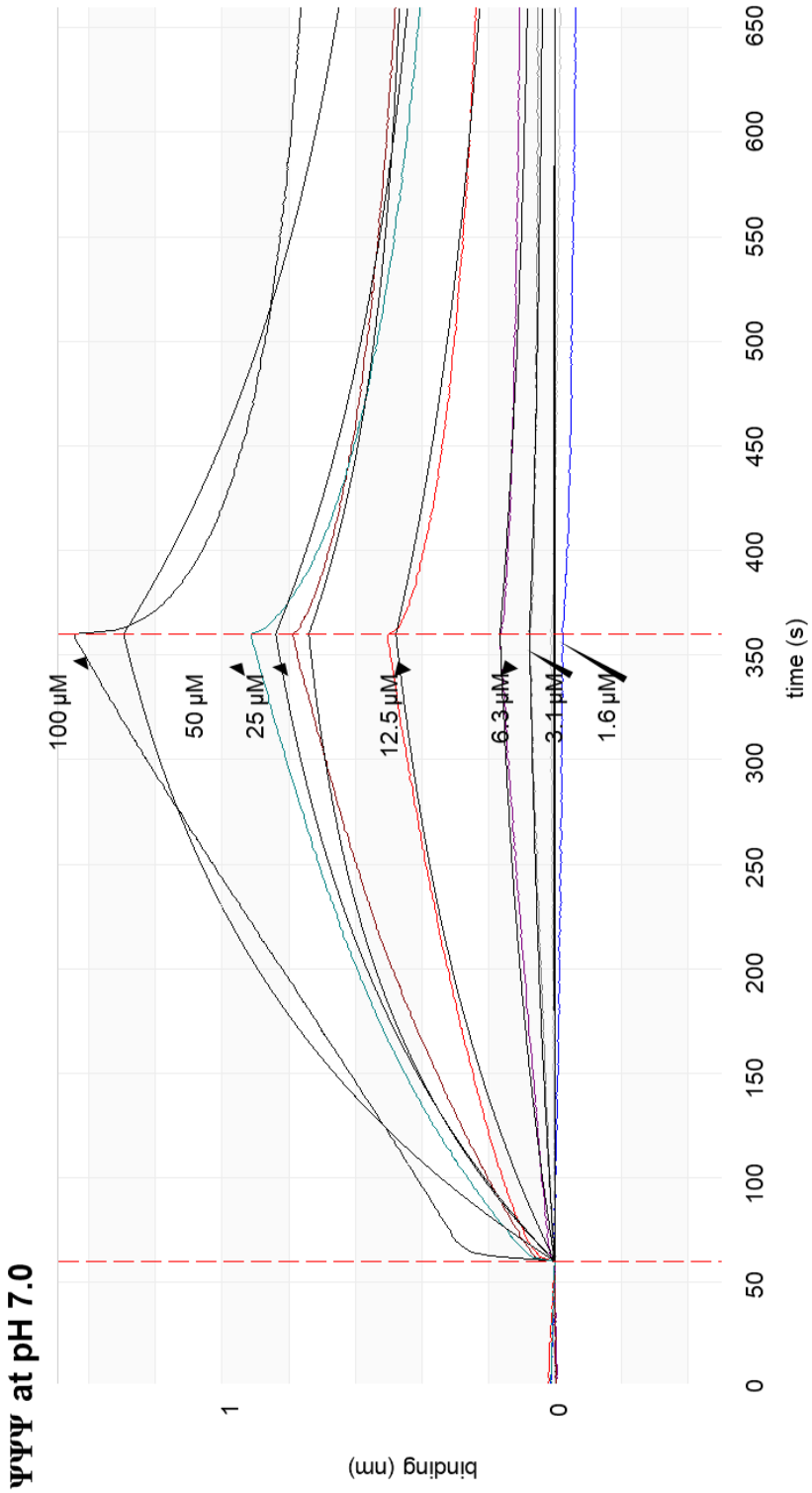


**Figure B3**. Representative BLItz results for TARHIY titration at pH 7.0 (20 mM HEPES-KOH, 100 mM KCl, 5 mM $MgCl_2$, and 0.1% Tween-20) against H69 ΨΨΨ. Black lines represent the 1:1 fitting curve.

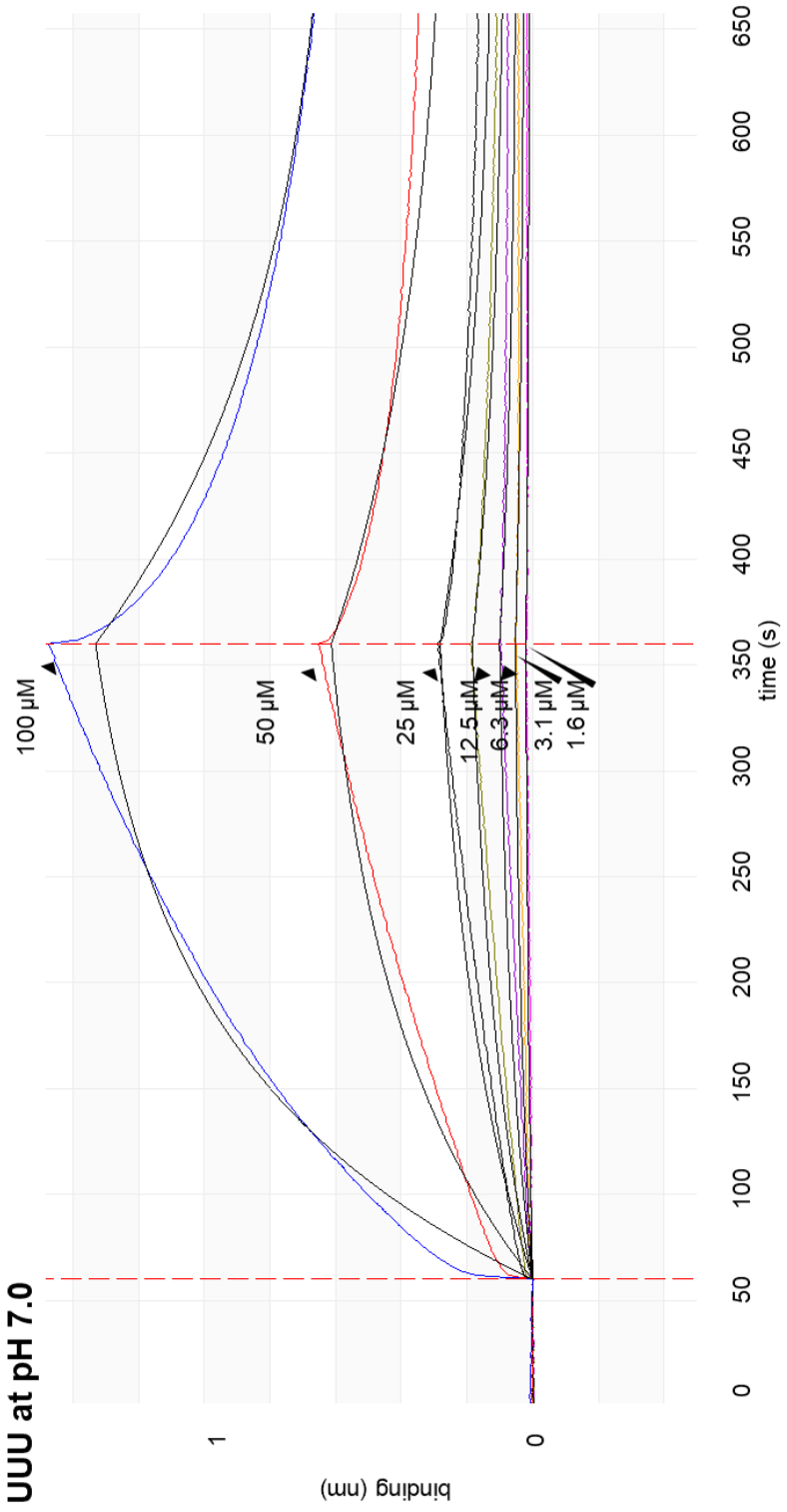


**Figure B4**. Representative BLItz results for TARHIY titration at pH 7.0 (20 mM HEPES-KOH, 100 mM KCl, 5 mM $MgCl_2$, and 0.1% Tween-20) against H69 UUU. Black lines represent the 1:1 fitting curve.

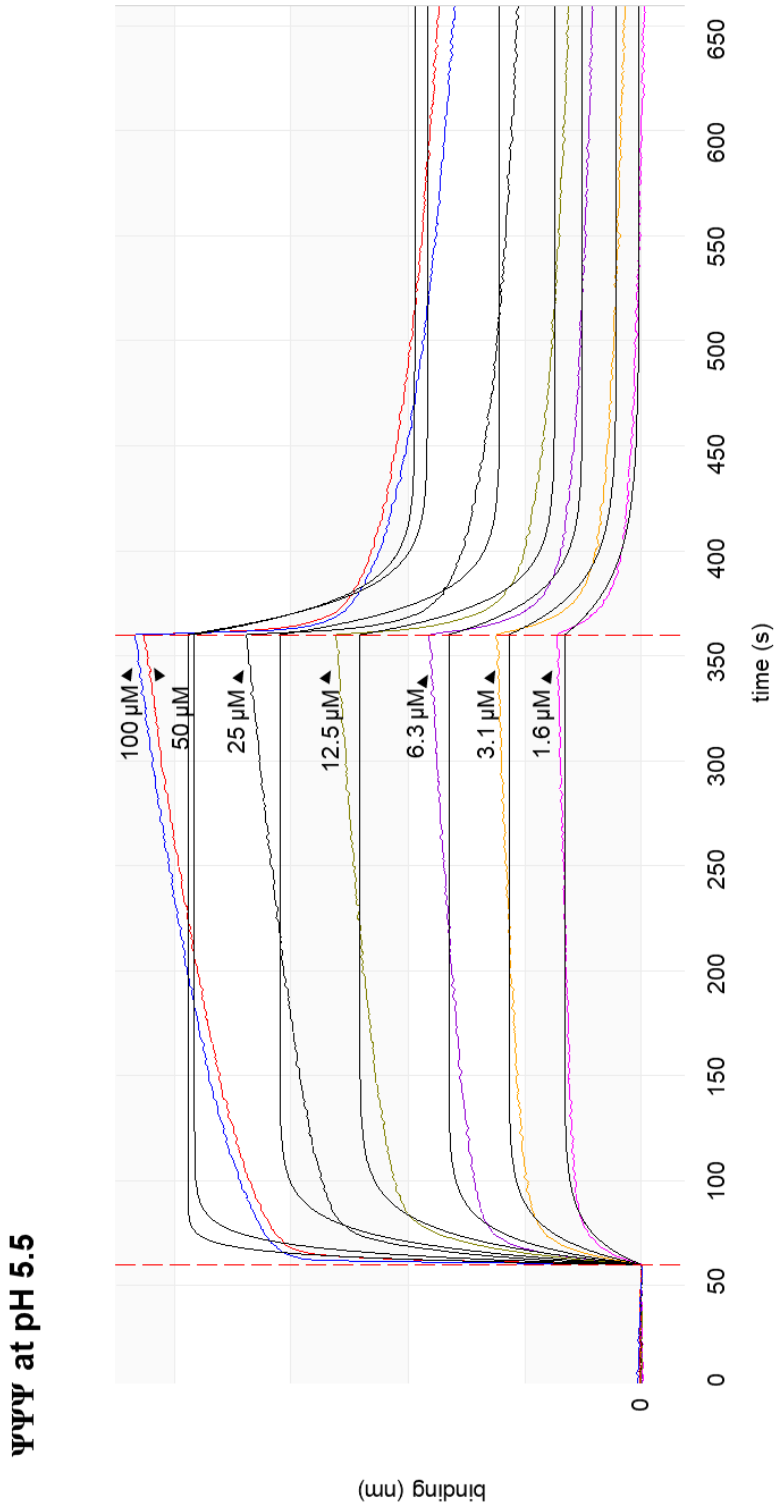


**Figure B5**. Representative BLItz results for dimer TT titration at pH 5.5 (20 mM cacodylate, 100 mM KCl, and 0.1% Tween-20) against H69 ΨΨΨ. Black lines represent the 1:1 fitting curve.

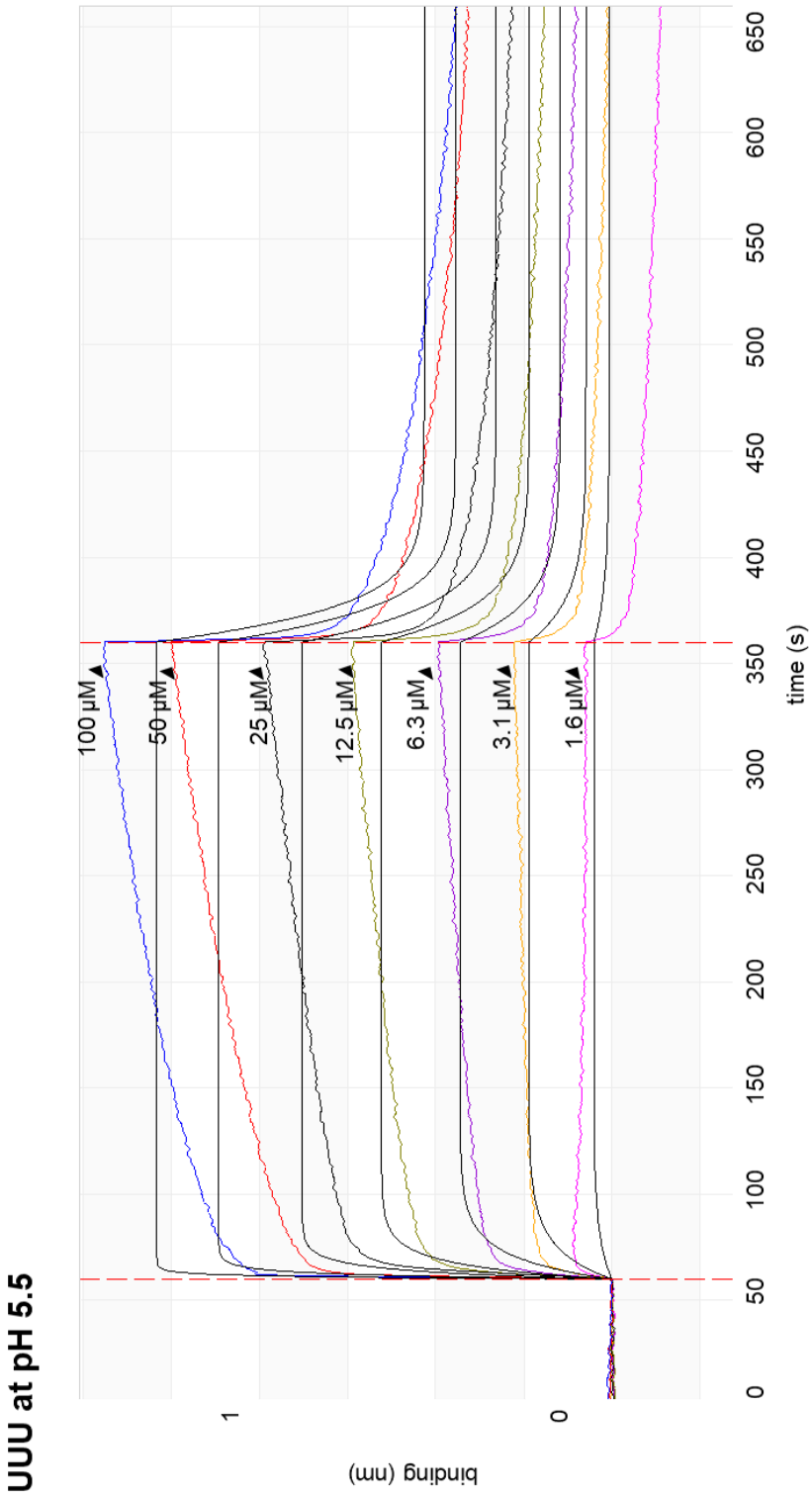


**Figure B6**. Representative BLItz results for dimer TT titration at pH 5.5 (20 mM cacodylate, 100 mM KCl, and 0.1% Tween-20) against H69 UUU. Black lines represent the 1:1 fitting curve.

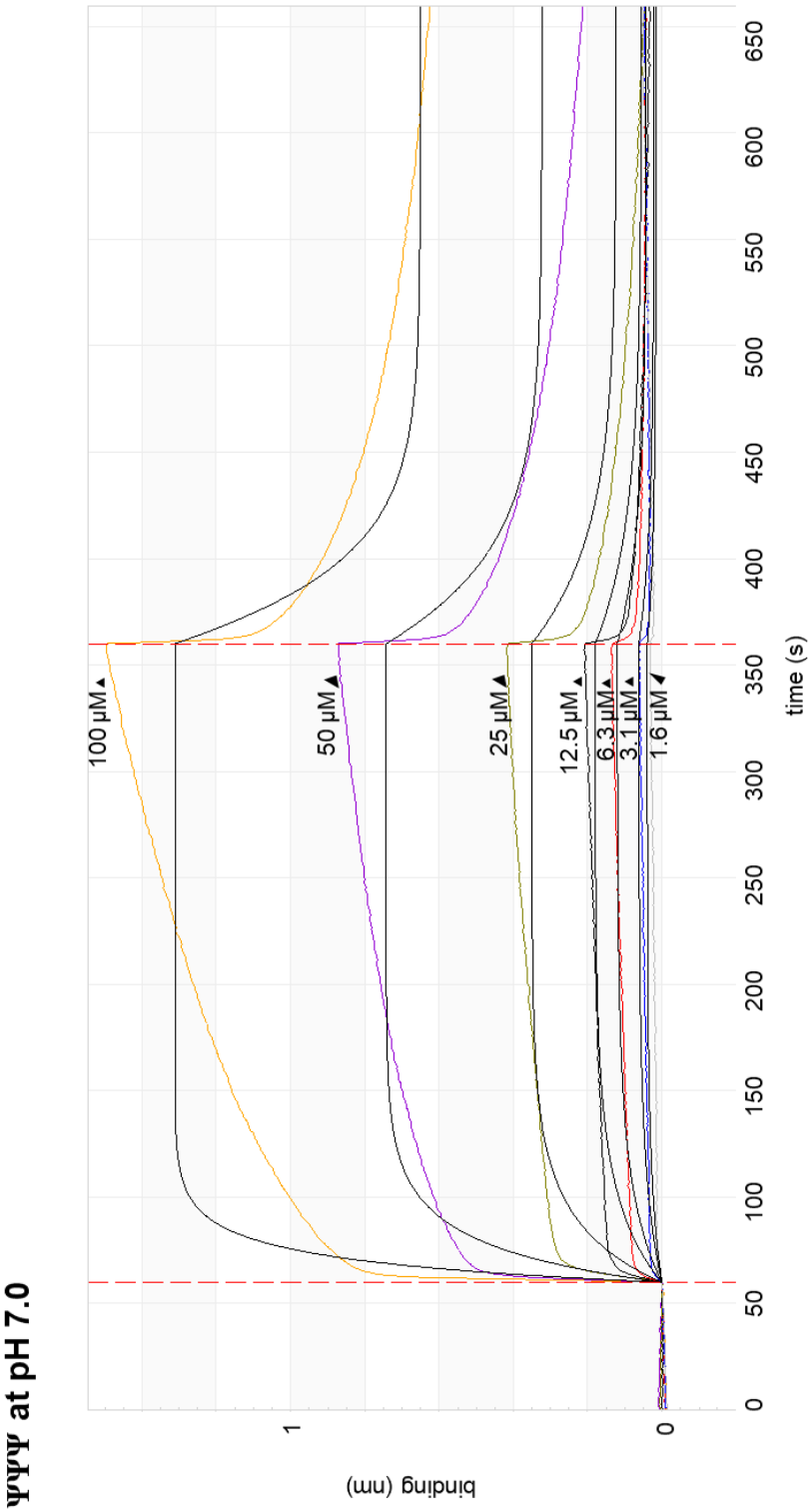


**Figure B7**. Representative BLItz results for dimer TT titration at pH 7.0 (20 mM HEPES-KOH, 100 mM KCl, 5 mM $MgCl_2$, and 0.1% Tween-20) against H69 ΨΨΨ. Black lines represent the 1:1 fitting curve.

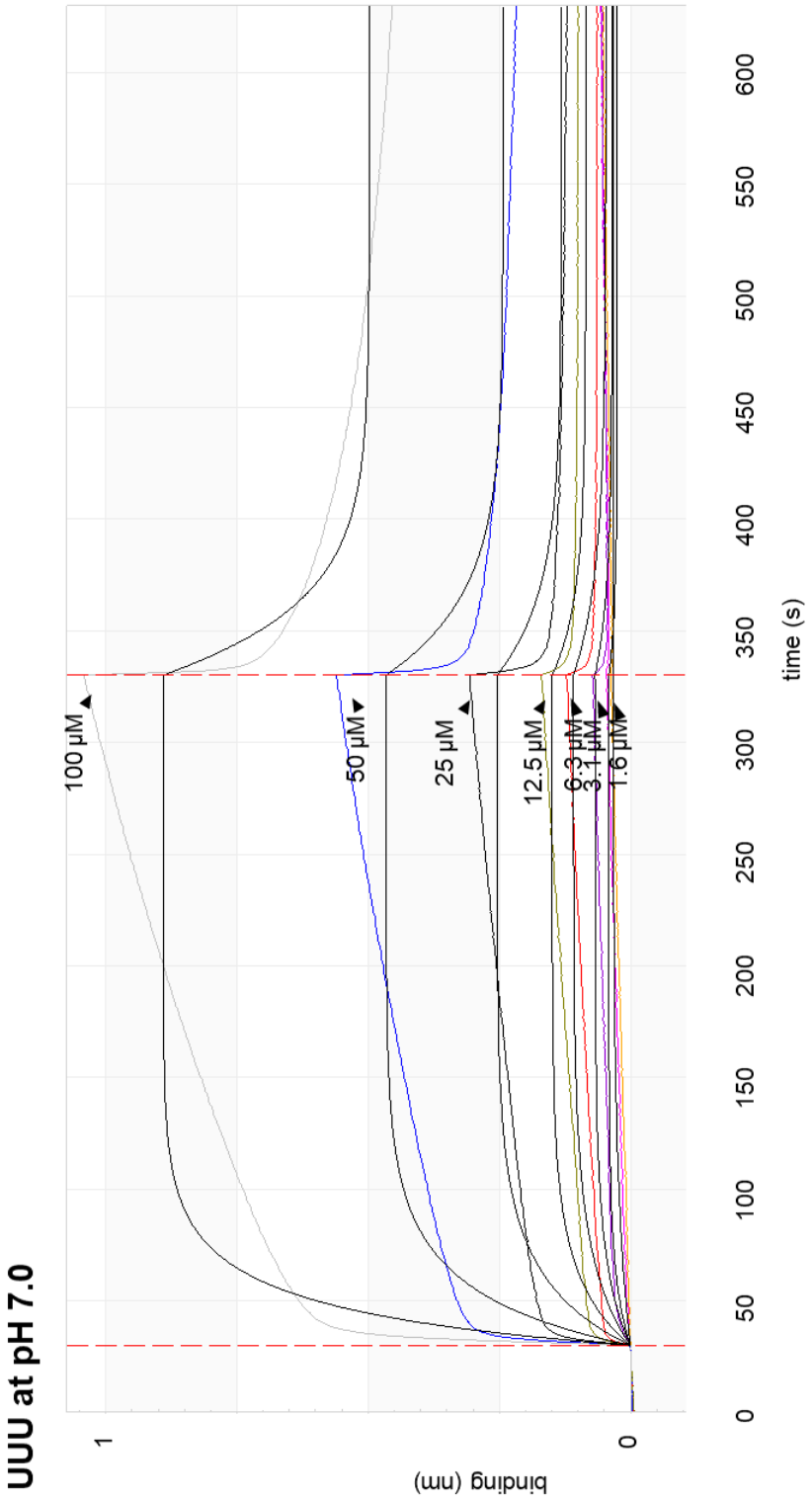


**Figure B8**. Representative BLItz results for dimer TT titration at pH 7.0 (20 mM HEPES-KOH, 100 mM KCl, 5 mM $MgCl_2$, and 0.1% Tween-20) against H69 UUU. Black lines represent the 1:1 fitting curve.

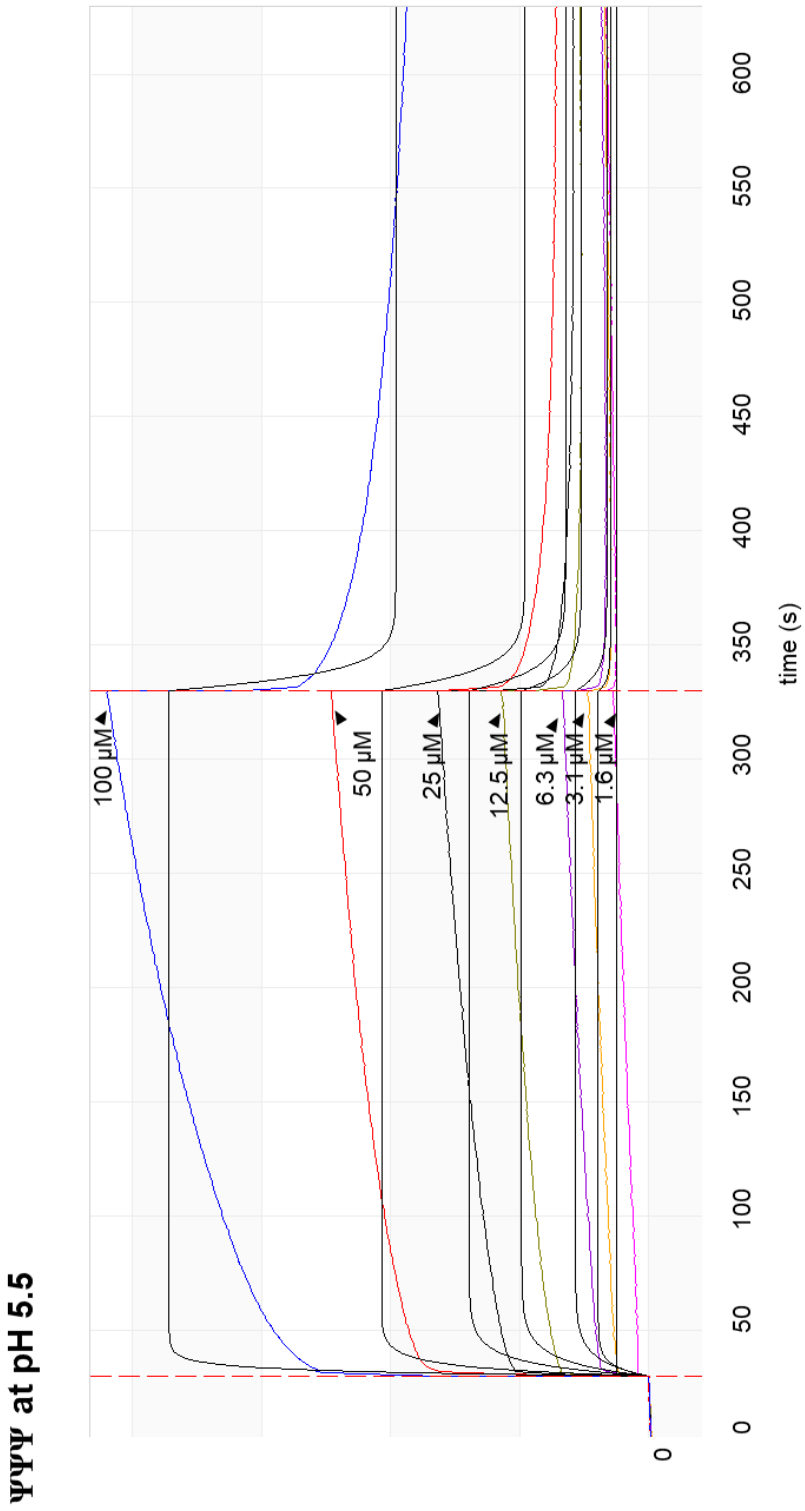


**Figure B9**. Representative BLItz results for dimer TA titration at pH 5.5 (20 mM cacodylate, 100 mM KCl, and 0.1% Tween-20) against H69 ΨΨΨ. Black lines represent the 1:1 fitting curve.

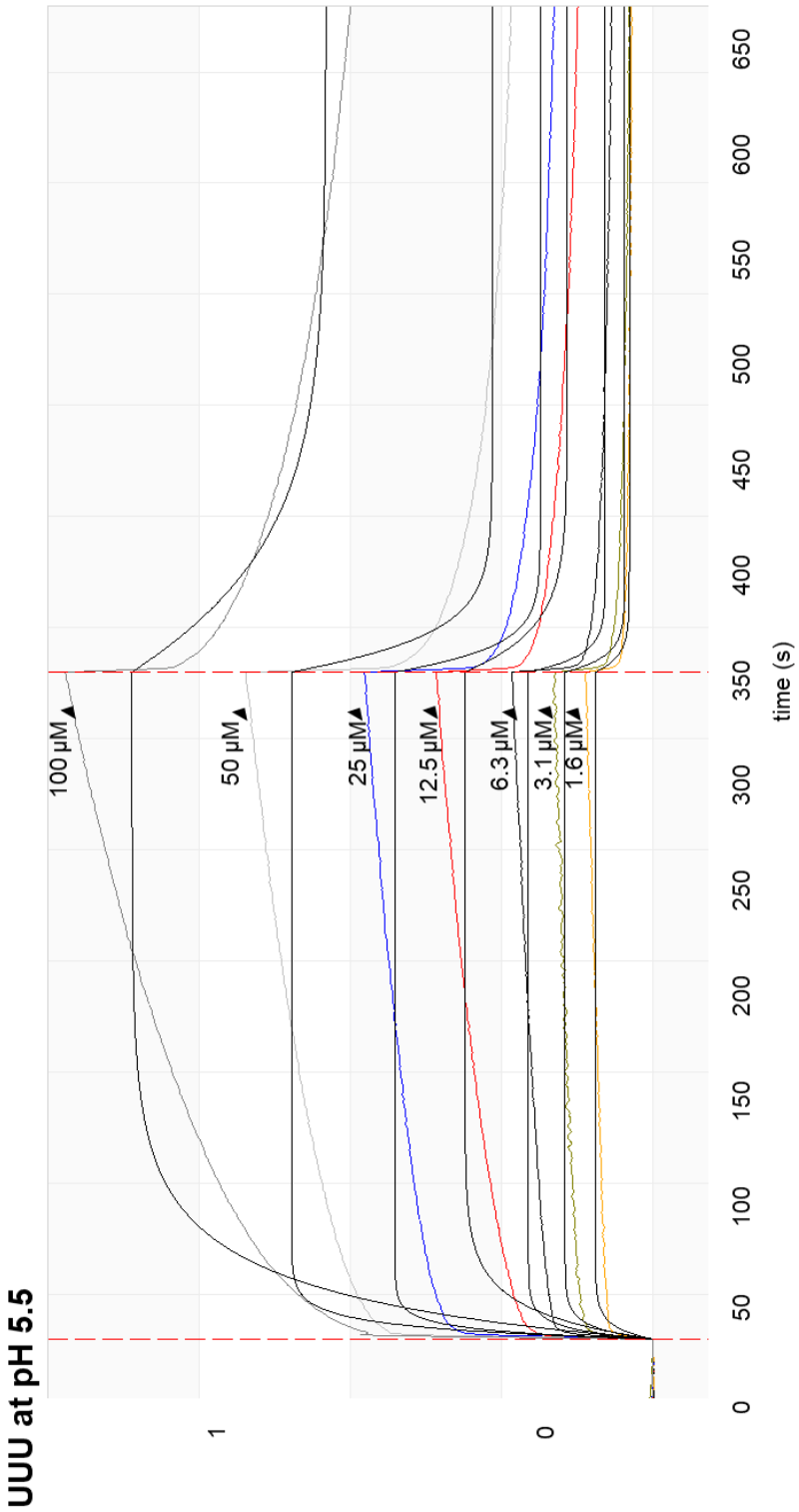


**Figure B10**. Representative BLItz results for dimer TA titration at pH 5.5 (20 mM cacodylate, 100 mM KCl, and 0.1% Tween-20) against H69 UUU. Black lines represent the 1:1 fitting curve.

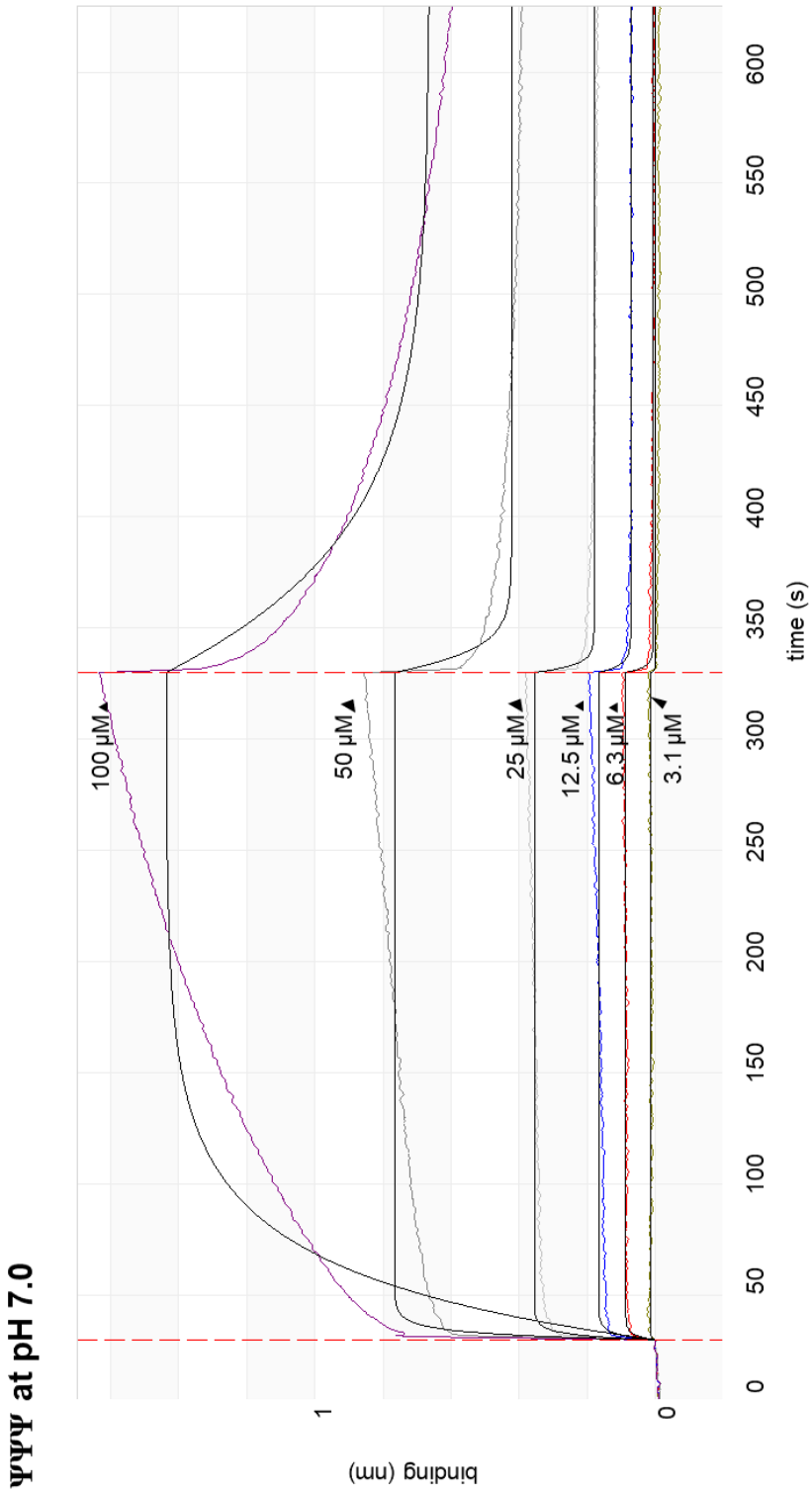


**Figure B11**. Representative BLItz results for dimer TA titration at pH 7.0 (20 mM HEPES-KOH, 100 mM KCl, 5 mM $MgCl_2$, and 0.1% Tween-20) against H69 ΨΨΨ. Black lines represent the 1:1 fitting curve.

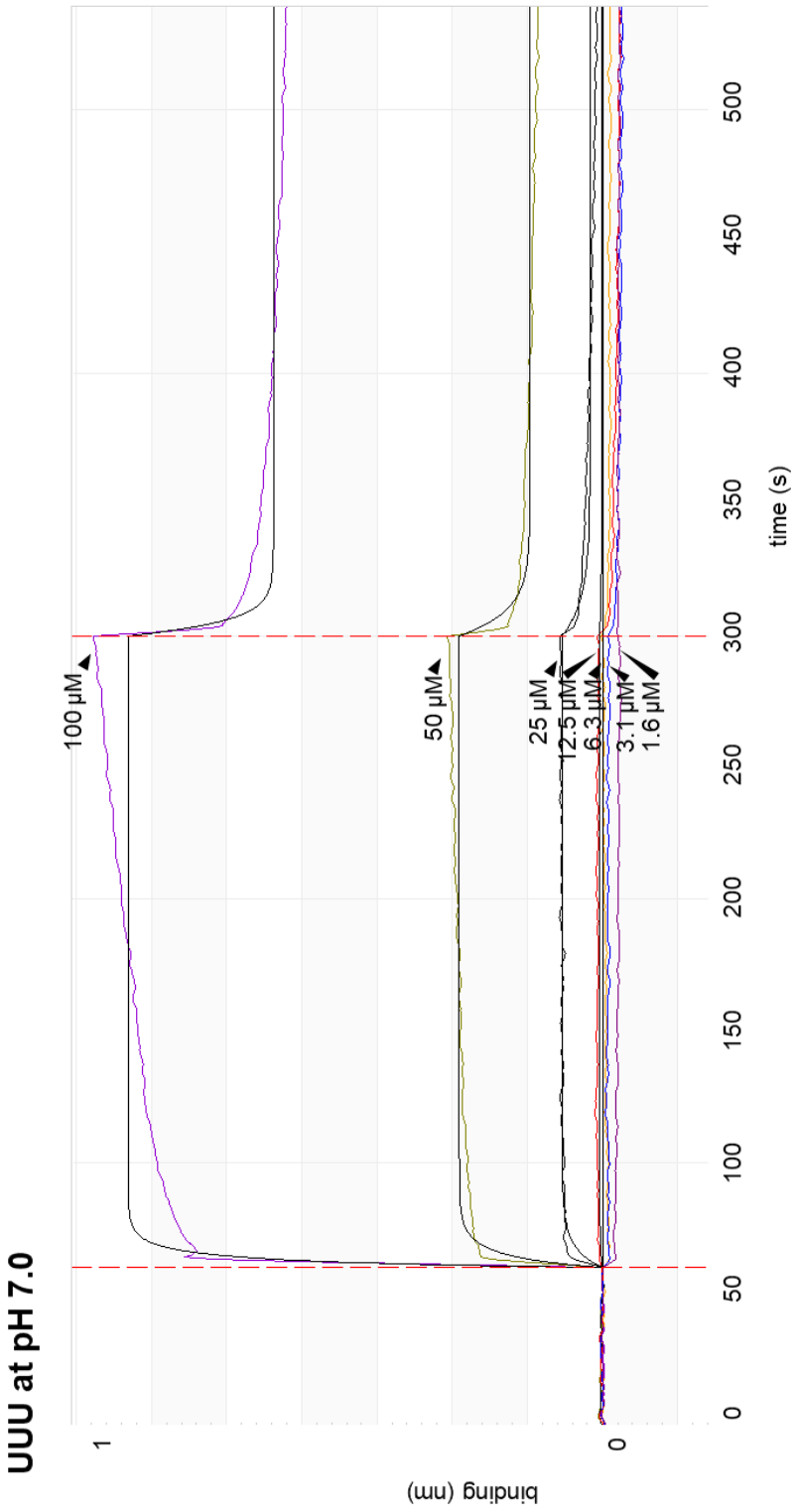


**Figure B12**. Representative BLItz results for dimer TA titration at pH 7.0 (20 mM HEPES-KOH, 100 mM KCl, 5 mM $MgCl_2$, and 0.1% Tween-20) against H69 UUU. Black lines represent the 1:1 fitting curve.

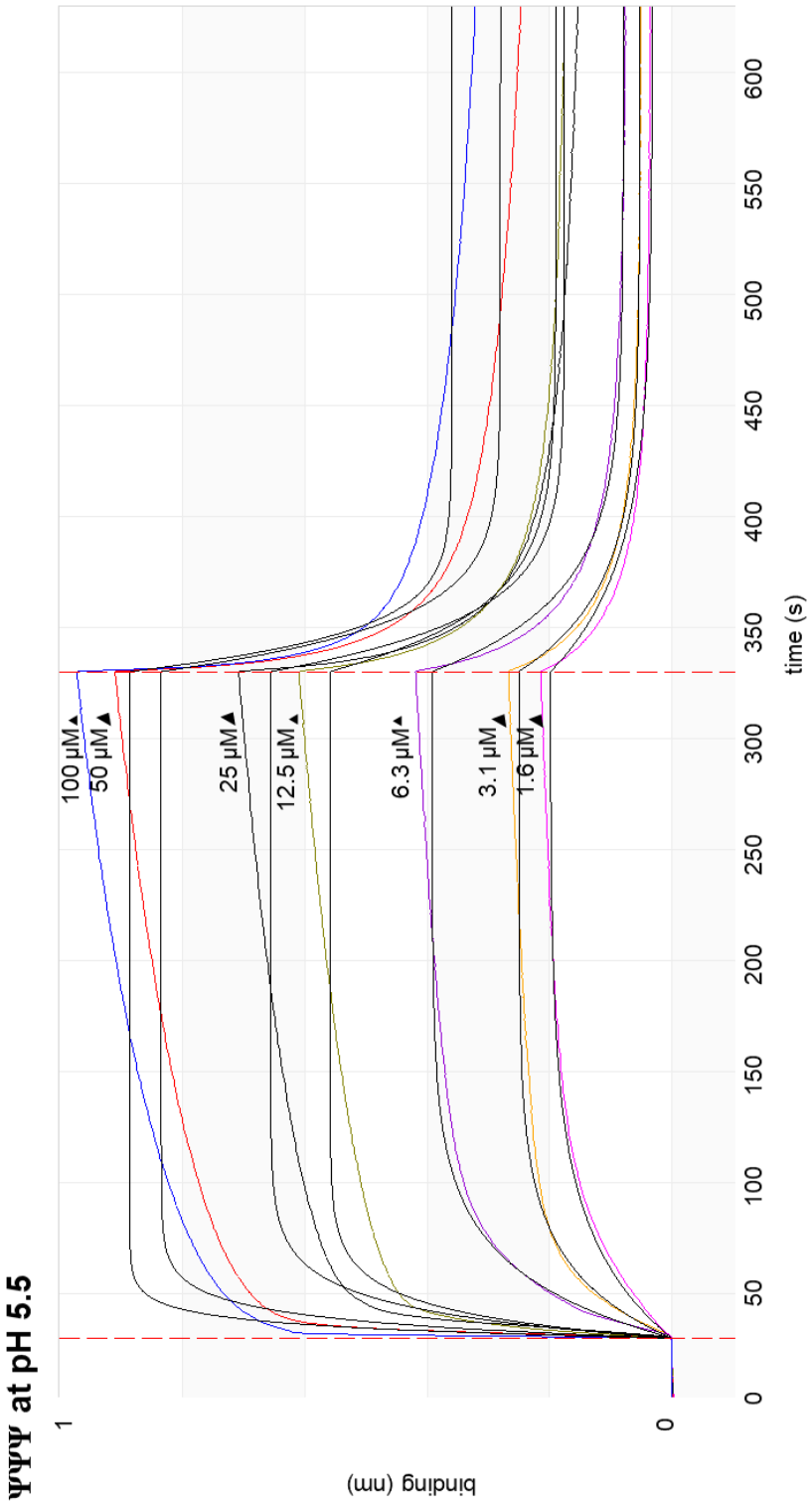


**Figure B13**. Representative BLItz results for dimer TY titration at pH 5.5 (20 mM cacodylate, 100 mM KCl, and 0.1% Tween-20) against H69 ΨΨΨ. Black lines represent the 1:1 fitting curve.

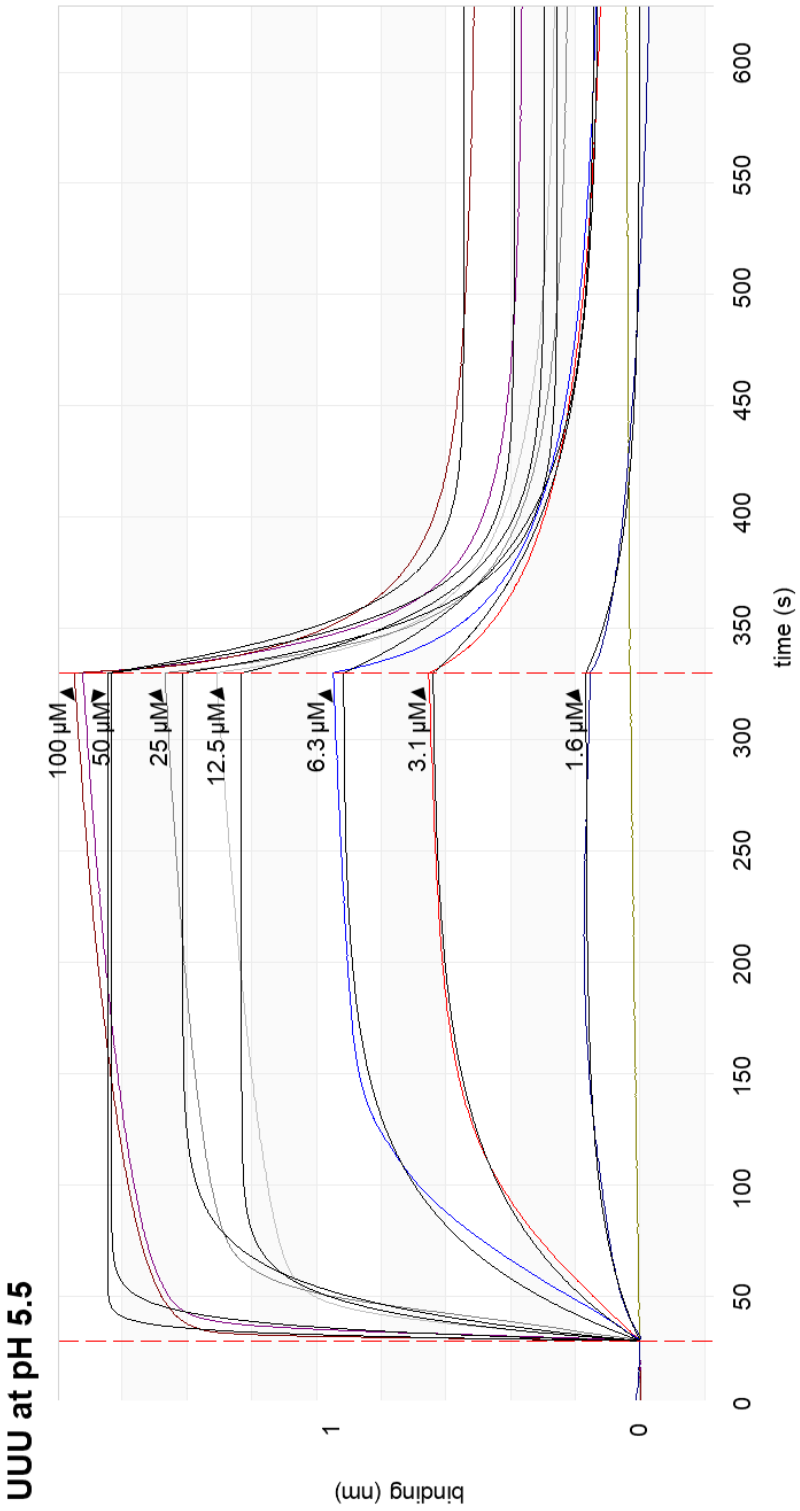


**Figure B14**. Representative BLItz results for dimer TY titration at pH 5.5 (20 mM cacodylate, 100 mM KCl, and 0.1% Tween-20) against H69 UUU. Black lines represent the 1:1 fitting curve.

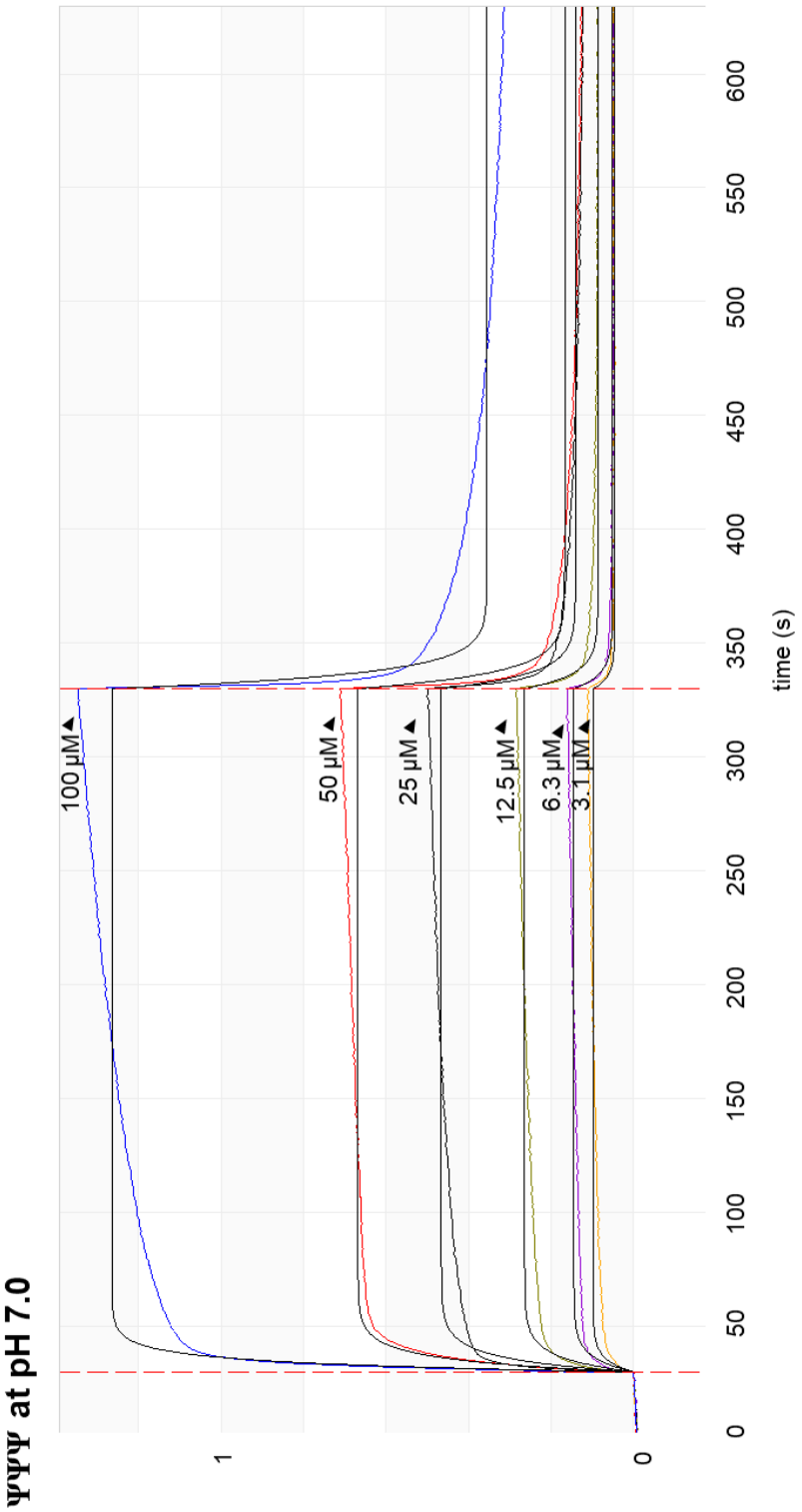


**Figure B15**. Representative BLItz results for dimer TY titration at pH 7.0 (20 mM HEPES-KOH, 100 mM KCl, 5 mM $MgCl_2$, and 0.1% Tween-20) against H69 ΨΨΨ. Black lines represent the 1:1 fitting curve.

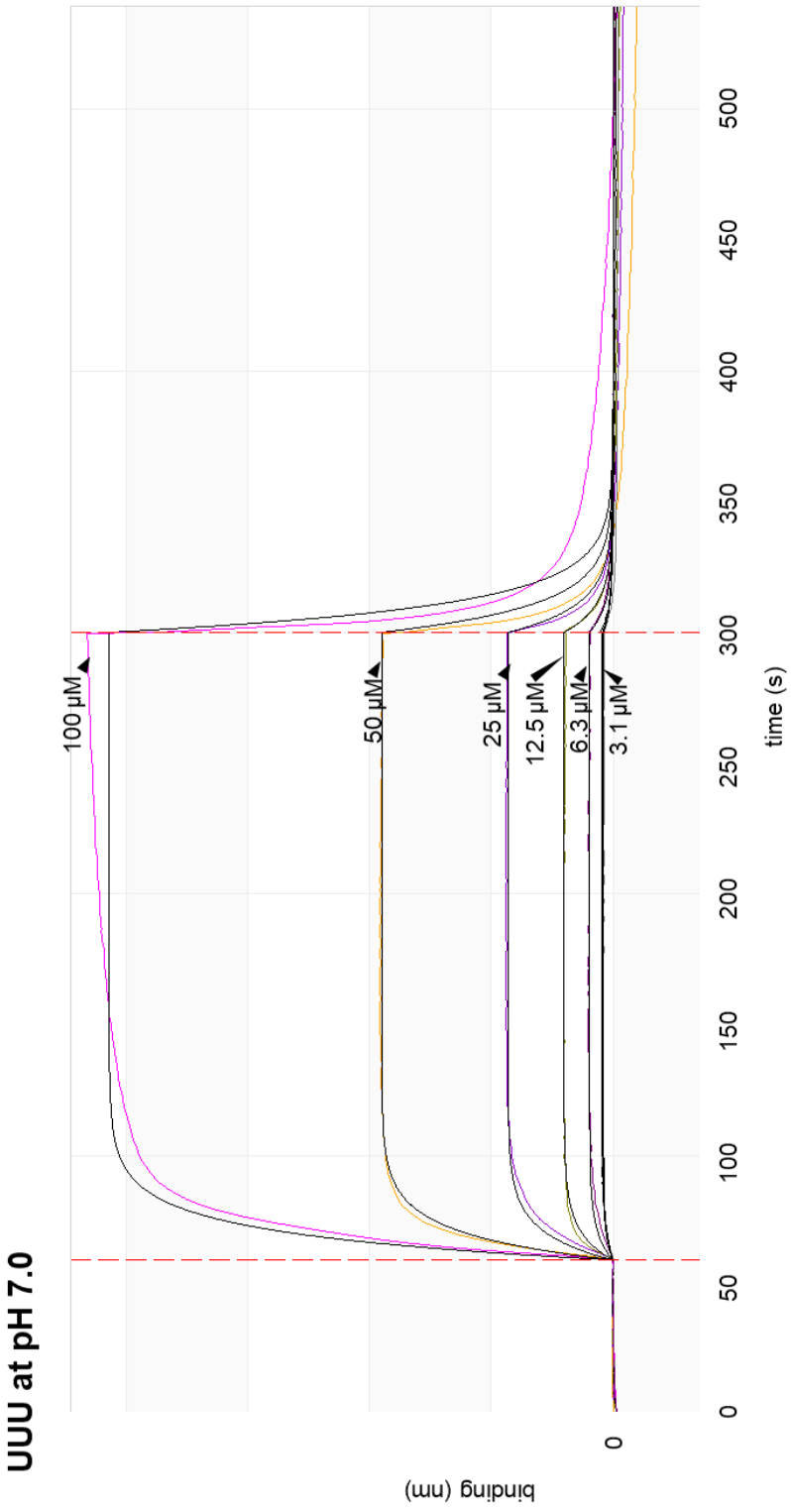


**Figure B16**. Representative BLItz results for dimer TY titration at pH 7.0 (20 mM HEPES-KOH, 100 mM KCl, 5 mM $MgCl_2$, and 0.1% Tween-20) against H69 UUU. Black lines represent the 1:1 fitting curve.

## APPENDIX C. CHEMICAL SHIFT CHANGES OF H69 UPON PEPTIDE TITRATION

| | UUU at pH 5.5 | | | | ΨΨΨ at pH 5.5 | | | | UUU at pH 7.0 | | | | |
|---|---|---|---|---|---|---|---|---|---|---|---|---|---|
| residues | monomer | dimer TT | dimer TA | reverse dimer TY | monomer | dimer TT | dimer TA | reverse dimer TY | monomer | dimer TT | dimer TA | reverse dimer TY | |
| C1908 | 0 | 0.01 | 0.01 | 0 | 0 | 0.01 | 0 | 0 | 0 | 0 | 0 | 0 | stem |
| C1909 | 0 | 0.02 | 0.01 | 0 | 0 | 0.01 | 0 | 0 | 0 | 0 | 0 | 0 | stem |
| U/Ψ1911 | 0 | 0 | 0.01 | 0 | N/A | N/A | N/A | N/A | 0 | 0 | 0 | 0 | stem |
| C1914 | 0.02 | 0.05 | 0.02 | 0.02 | x | x | x | x | 0 | 0.01 | 0 | 0 | loop |
| U/Ψ1915 | 0.01 | 0.01 | 0.01 | 0.02 | N/A | N/A | N/A | N/A | 0 | 0 | 0 | 0 | loop |
| U/Ψ1917 | 0 | 0.01 | 0.01 | 0 | N/A | N/A | N/A | N/A | 0 | 0 | 0 | 0 | loop |
| C1920 | 0 | 0.04 | 0.01 | 0 | 0.04 | 0 | 0 | 0 | 0 | 0.01 | 0 | 0 | stem |
| U1923 | 0 | 0.01 | 0.01 | 0 | 0 | 0 | 0 | 0 | 0 | 0 | 0 | 0 | stem |
| C1924 | 0 | 0.01 | 0.01 | 0 | 0 | 0.02 | 0 | 0 | 0 | 0 | 0 | 0 | stem |

x : no peak was resolved

## APPENDIX D. BUFFERS USED IN THIS THESIS STUDY

**Buffer A**

20 mM HEPES-KOH, pH 7.0, 100 mM KCl, 5 mM $MgCl_2$, 5% glycerol, 0.1 mg/mL BSA with 0.1% (v/v) Tween-20

**Buffer B**

20 mM PBS, pH 5.5, 100 mM KCl, 5% glycerol, 0.1 mg/mL BSA with 0.1% (v/v) Tween-20 (buffer B)

**Binding buffer (pH 7.0)**

20 mM HEPES-KOH, pH 7.0, 100 mM KCl, 5 mM $MgCl_2$, 5% glycerol, 0.1 mg/mL BSA

**Binding buffer (pH 5.5)**

20 mM PBS, pH 5.5, 100 mM KCl, 5% glycerol, 0.1 mg/mL BSA with 0.1% (v/v)

**ESI-MS buffer (pH 5.5 or pH 7.0)**

10 mM $NH_4OAc$, 50% isopropanol

## APPENDIX E. EXPANDED VIEW OF THE ESI-MS SPECTRA IN THIS STUDY

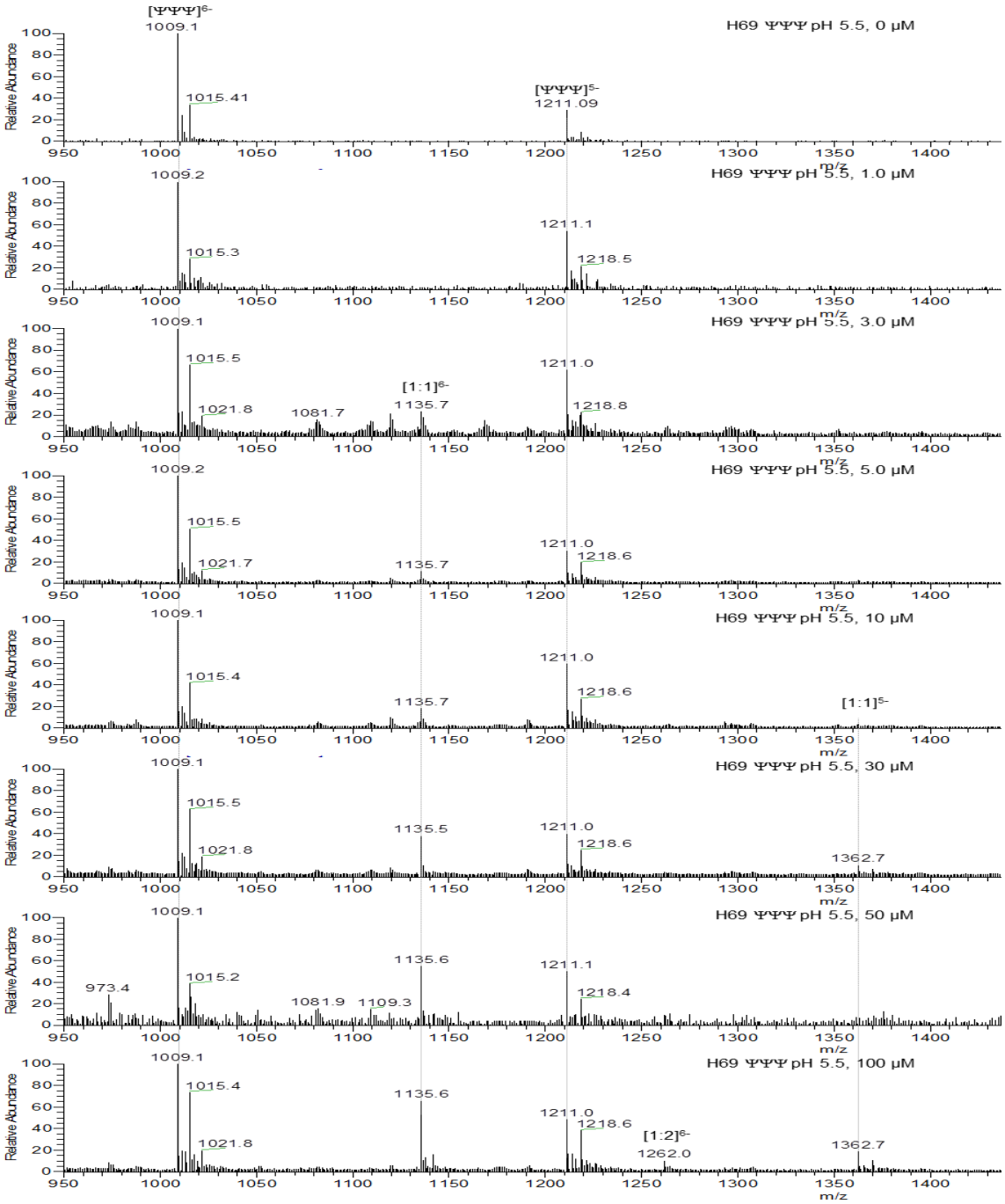


**Figure E1**. Expanded view of representative ESI-MS results for TARHIY titration (pH 5.5) against H69 ΨΨΨ.

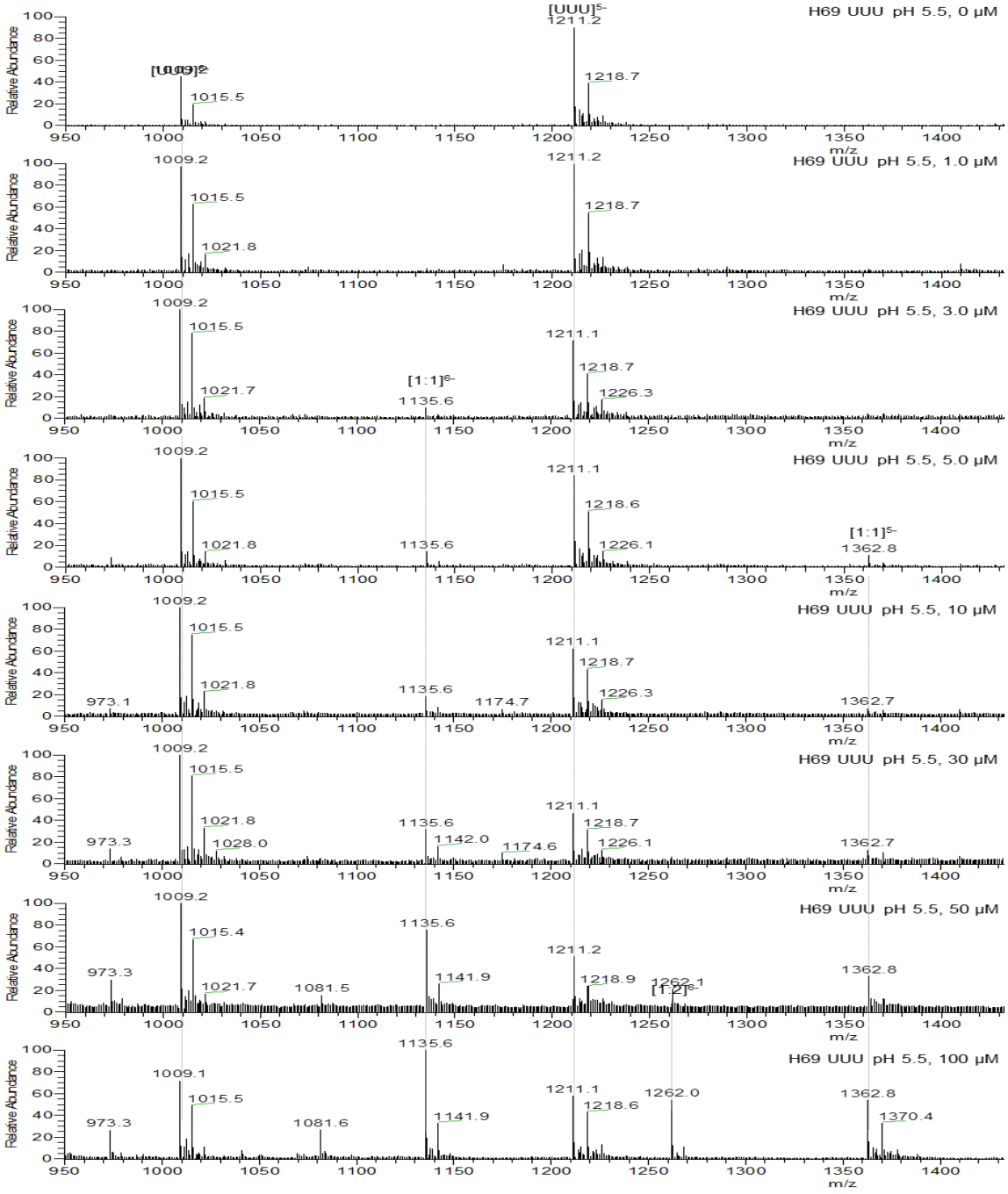


**Figure E2**. Expanded view of representative ESI-MS results for TARHIY titration (pH 5.5) against H69 UUU.

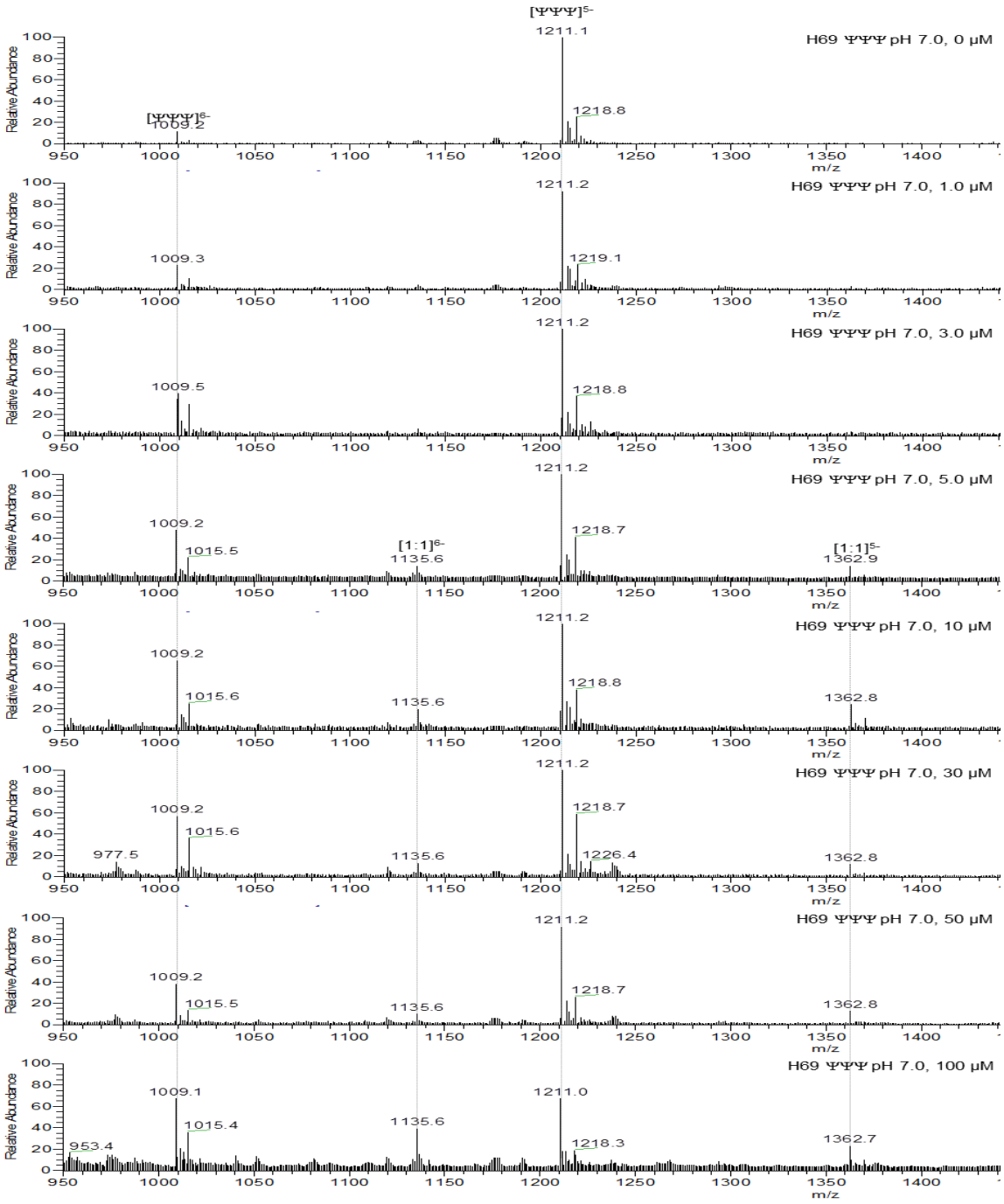


**Figure E3**. Expanded view of representative ESI-MS results for TARHIY titration (pH 7.0) against H69 ΨΨΨ.

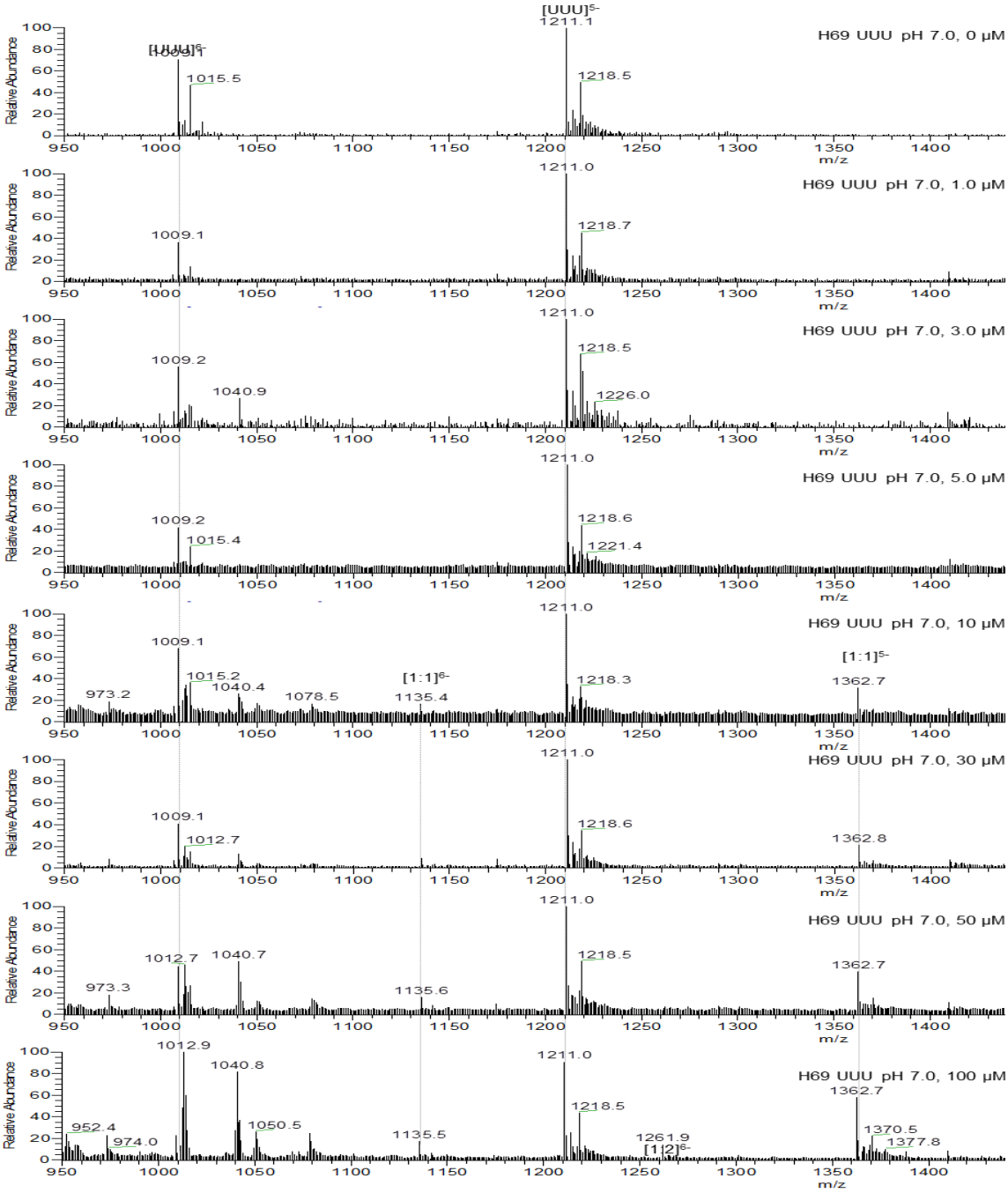


**Figure E4**. Expanded view of representative ESI-MS results for TARHIY titration (pH 7.0) against H69 UUU.

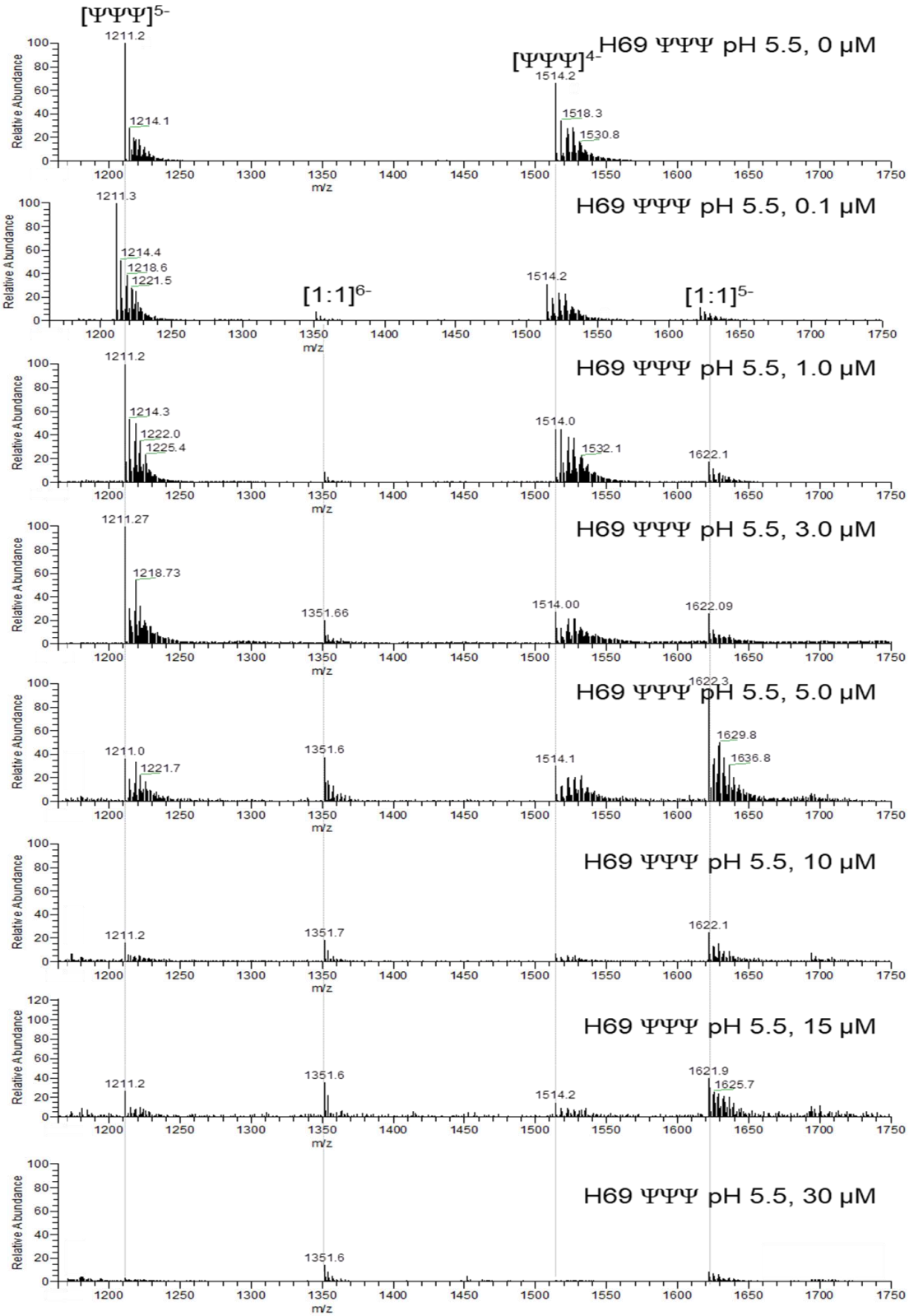


**Figure E5**. Expanded view of representative ESI-MS results for B1T titration (pH 5.5) against H69 ΨΨΨ.

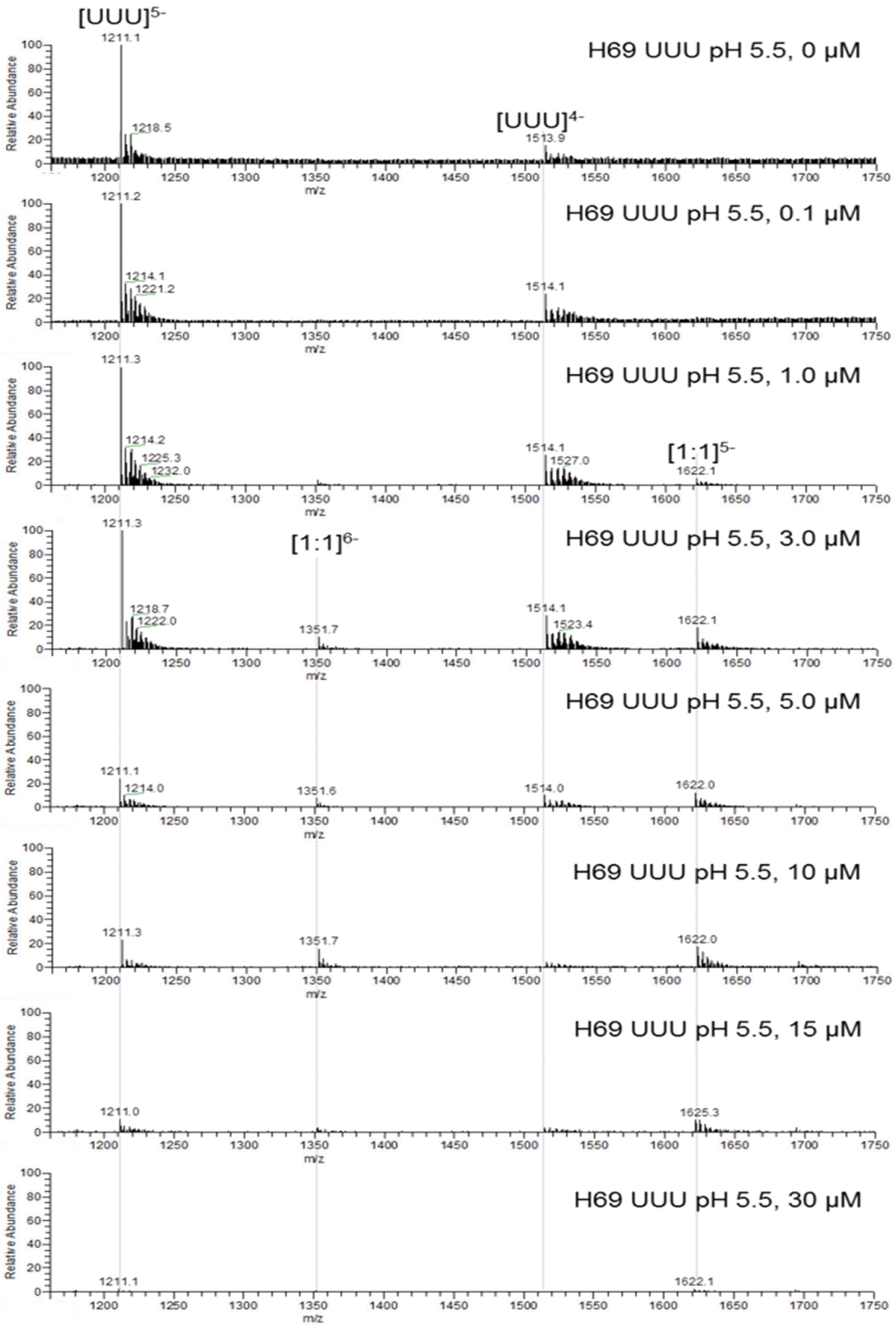


**Figure E6**. Expanded view of representative ESI-MS results for B1T titration (pH 5.5) against H69 UUU.

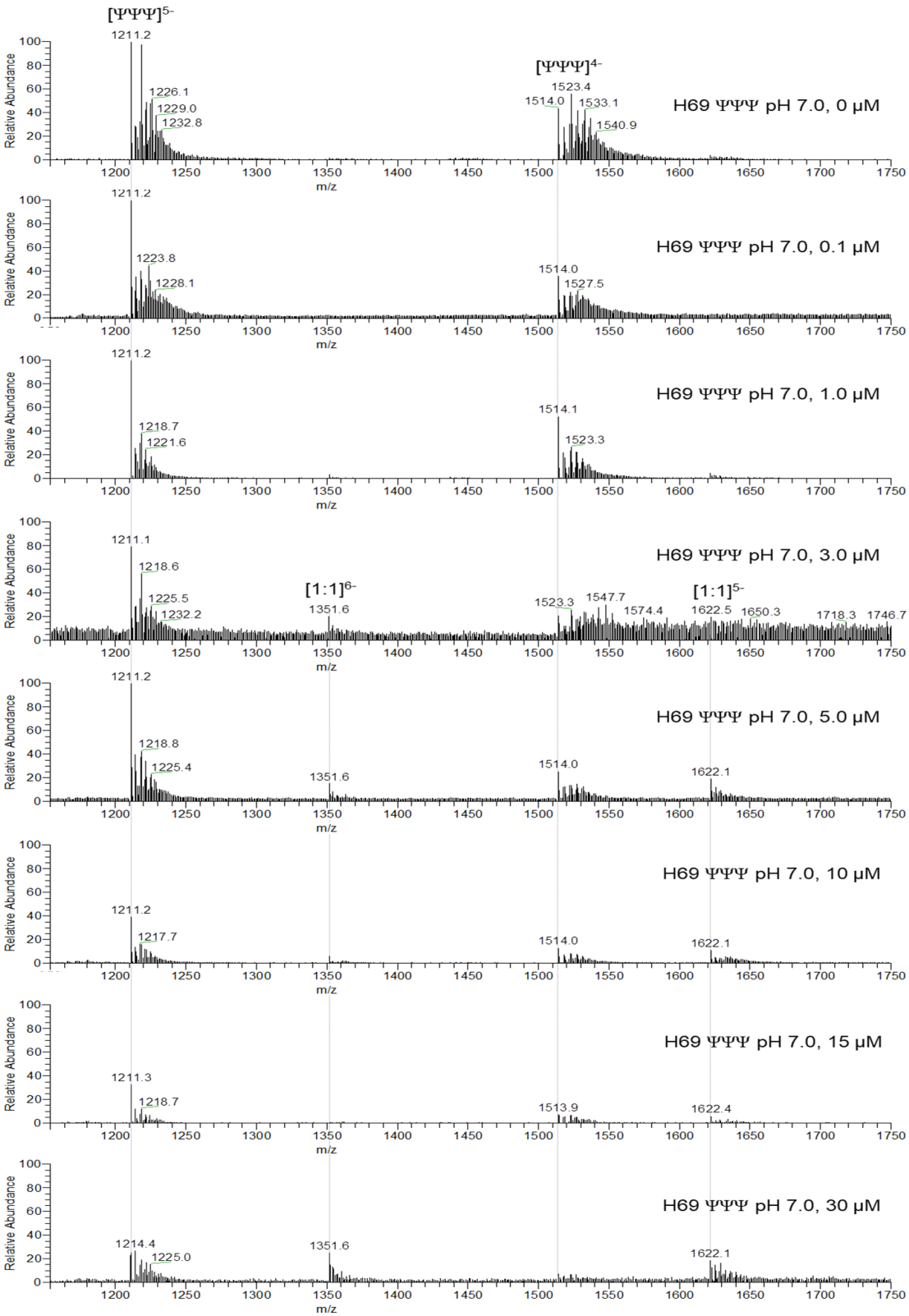


**Figure E7**. Expanded view of representative ESI-MS results for B1T titration (pH 7.0) against H69 ΨΨΨ.

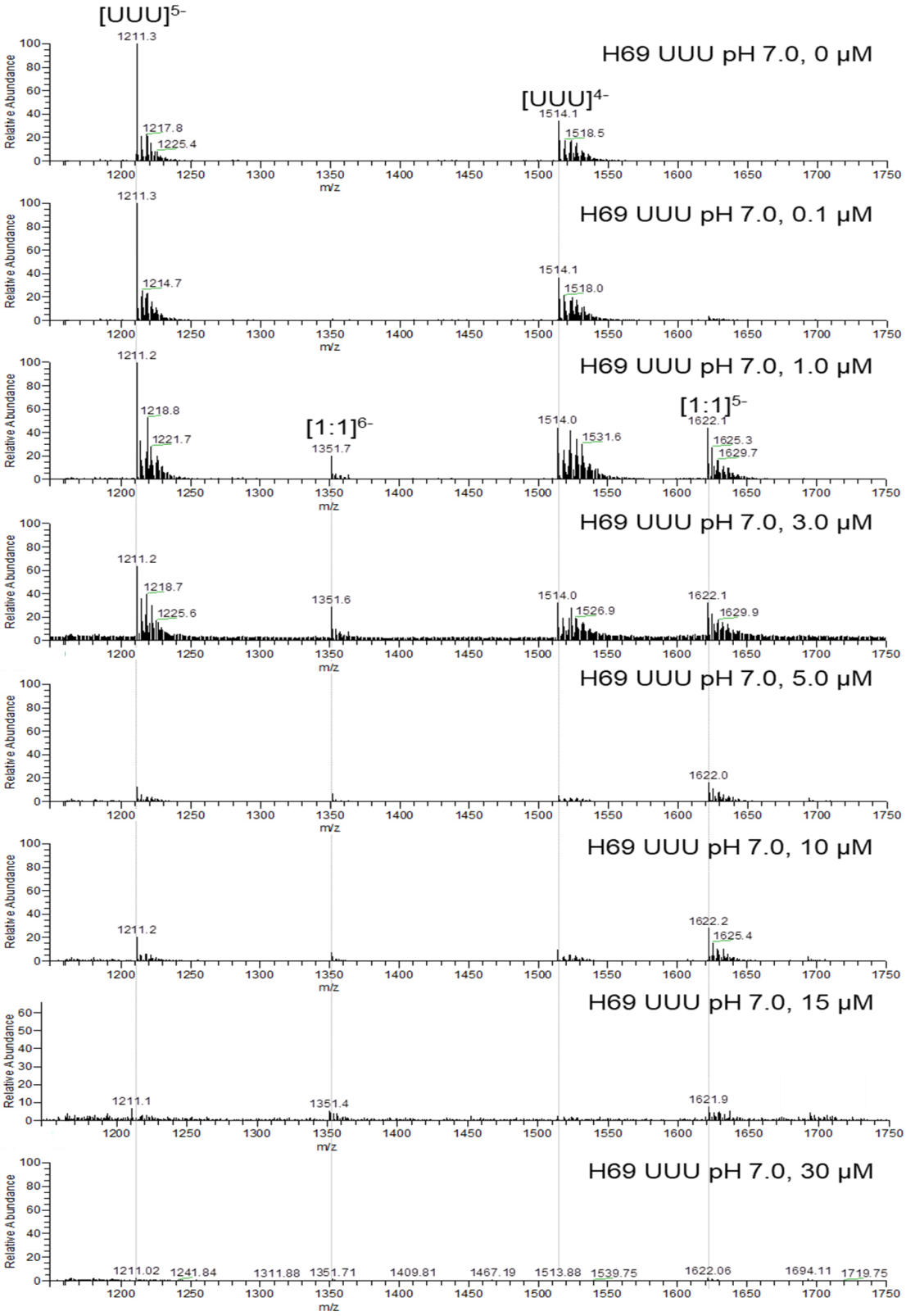


**Figure E8**. Expanded view of representative ESI-MS results for B1T titration (pH 7.0) against H69 UUU.

## REFERENCES

1. Fleming, A., The development and use of penicillin. *Chic Med Sch Q* **1946,** *7* (2), 20-8.

2. Tomasz, A.; Waks, S., Mechanism of action of penicillin: triggering of the pneumococcal autolytic enzyme by inhibitors of cell wall synthesis. *Proc Natl Acad Sci U S A* **1975,** *72* (10), 4162-6.

3. Wilson, D. N., Ribosome-targeting antibiotics and mechanisms of bacterial resistance. *Nat Rev Microbiol* **2014,** *12* (1), 35-48.

4. Henry, R. J., The mode of action of sulfonamides. *Bacteriol Rev* **1943,** *7* (4), 175-262.

5. Howard, B. M.; Pinney, R. J.; Smith, J. T., 4-Quinolone bactericidal mechanisms. *Arzneimittelforschung* **1993,** *43* (10), 1125-9.

6. Pioletti, M.; Schlunzen, F.; Harms, J.; Zarivach, R.; Gluhmann, M.; Avila, H.; Bashan, A.; Bartels, H.; Auerbach, T.; Jacobi, C.; Hartsch, T.; Yonath, A.; Franceschi, F., Crystal structures of complexes of the small ribosomal subunit with tetracycline, edeine and IF3. *EMBO J* **2001,** *20* (8), 1829-39.

7. Connell, S. R.; Tracz, D. M.; Nierhaus, K. H.; Taylor, D. E., Ribosomal protection proteins and their mechanism of tetracycline resistance. *Antimicrob Agents Chemother* **2003,** *47* (12), 3675-81.

8. Garza-Ramos, G.; Xiong, L.; Zhong, P.; Mankin, A., Binding site of macrolide antibiotics on the ribosome: new resistance mutation identifies a specific interaction of ketolides with rRNA. *J Bacteriol* **2001,** *183* (23), 6898-907.

9. Fourmy, D.; Recht, M. I.; Blanchard, S. C.; Puglisi, J. D., Structure of the A site of *Escherichia coli* 16S ribosomal RNA complexed with an aminoglycoside antibiotic. *Science* **1996,** *274* (5291), 1367-71.

10. Fourmy, D.; Recht, M. I.; Puglisi, J. D., Binding of neomycin-class aminoglycoside antibiotics to the A site of 16S rRNA. *J Mol Biol* **1998,** *277* (2), 347-62.

11. Walter, F.; Vicens, Q.; Westhof, E., Aminoglycoside-RNA interactions. *Curr Opin Chem Biol* **1999,** *3* (6), 694-704.

12. Vicens, Q.; Westhof, E., Crystal structure of paromomycin docked into the eubacterial ribosomal decoding A site. *Structure* **2001,** *9* (8), 647-58.

13. Mingeot-Leclercq, M. P.; Glupczynski, Y.; Tulkens, P. M., Aminoglycosides: activity and resistance. *Antimicrob Agents Chemother* **1999,** *43* (4), 727-37.

14. Wright, G. D.; Berghuis, A. M.; Mobashery, S., Aminoglycoside antibiotics. Structures, functions, and resistance. *Adv Exp Med Biol* **1998,** *456*, 27-69.

15. Menninger, J. R., Mechanism of inhibition of protein synthesis by macrolide and lincosamide antibiotics. *J Basic Clin Physiol Pharmacol* **1995,** *6* (3-4), 229-50.

16. Hansen, J. L.; Moore, P. B.; Steitz, T. A., Structures of five antibiotics bound at the peptidyl transferase center of the large ribosomal subunit. *J Mol Biol* **2003,** *330* (5), 1061-75.

17. Vicens, Q.; Westhof, E., Molecular recognition of aminoglycoside antibiotics by ribosomal RNA and resistance enzymes: an analysis of X-ray crystal structures. *Biopolymers* **2003,** *70* (1), 42-57.

18. Antibiotic resistance threats in the united states. U.S. department of health and human services centers for disease control and prevention: 2013.

19. Pendleton, J. N.; Gorman, S. P.; Gilmore, B. F., Clinical relevance of the ESKAPE pathogens. *Expert Rev Anti Infect Ther* **2013,** *11* (3), 297-308.

20. Walsh, C., Molecular mechanisms that confer antibacterial drug resistance. *Nature* **2000,** *406* (6797), 775-81.

21. Recht, M. I.; Douthwaite, S.; Dahlquist, K. D.; Puglisi, J. D., Effect of mutations in the A site of 16S rRNA on aminoglycoside antibiotic-ribosome interaction. *J Mol Biol* **1999,** *286* (1), 33-43.

22. Biddlecome, S.; Haas, M.; Davies, J.; Miller, G. H.; Rane, D. F.; Daniels, P. J., Enzymatic modification of aminoglycoside antibiotics: a new 3-*N*-acetylating enzyme from a *Pseudomonas aeruginosa* isolate. *Antimicrob Agents Chemother* **1976,** *9* (6), 951-5.

23. Ogle, J. M.; Brodersen, D. E.; Clemons, W. M., Jr.; Tarry, M. J.; Carter, A. P.; Ramakrishnan, V., Recognition of cognate transfer RNA by the 30S ribosomal subunit. *Science* **2001,** *292* (5518), 897-902.

24. Blanchard, S. C.; Fourmy, D.; Eason, R. G.; Puglisi, J. D., rRNA chemical groups required for aminoglycoside binding. *Biochemistry* **1998,** *37* (21), 7716-24.

25. Kato, T.; Yang, G.; Teo, Y.; Juskeviciene, R.; Perez-Fernandez, D.; Shinde, H. M.; Salian, S.; Bernet, B.; Vasella, A.; Bottger, E. C.; Crich, D., Synthesis and antiribosomal activities of 4'-*O*-, 6'-*O*-, 4''-*O*-, 4',6'-*O*- and 4'',6''-*O*-derivatives in the kanamycin series indicate differing target selectivity patterns between the 4,5- and 4,6-series of disubstituted 2-deoxystreptamine aminoglycoside antibiotics. *ACS Infect Dis* **2015,** *1* (10), 479-86.

26. Duscha, S.; Boukari, H.; Shcherbakov, D.; Salian, S.; Silva, S.; Kendall, A.; Kato, T.; Akbergenov, R.; Perez-Fernandez, D.; Bernet, B.; Vaddi, S.; Thommes, P.; Schacht, J.; Crich, D.; Vasella, A.; Bottger, E. C., Identification and evaluation of improved 4'-*O*-(alkyl) 4,5-disubstituted 2-deoxystreptamines as next-generation aminoglycoside antibiotics. *MBio* **2014,** *5* (5), e01827-14.

27. Aminov, R. I., A brief history of the antibiotic era: lessons learned and challenges for the future. *Front Microbiol* **2010,** *1*, 134.

28. Devasahayam, G.; Scheld, W. M.; Hoffman, P. S., Newer antibacterial drugs for a new century. *Expert Opin Investig Drugs* **2010,** *19* (2), 215-34.

29. Chee-Sanford, J. C.; Mackie, R. I.; Koike, S.; Krapac, I. G.; Lin, Y. F.; Yannarell, A. C.; Maxwell, S.; Aminov, R. I., Fate and transport of antibiotic residues and antibiotic resistance genes following land application of manure waste. *J Environ Qual* **2009,** *38* (3), 1086-108.

30. Hirabayashi, N.; Sato, N. S.; Suzuki, T., Conserved loop sequence of helix 69 in *Escherichia coli* 23 S rRNA is involved in A site tRNA binding and translational fidelity. *J Biol Chem* **2006,** *281* (25), 17203-11.

31. O'Connor, M., Helix 69 in 23S rRNA modulates decoding by wild type and suppressor tRNAs. *Mol Genet Genomics* **2009,** *282* (4), 371-80.

32. Ortiz-Meoz, R. F.; Green, R., Helix 69 is key for uniformity during substrate selection on the ribosome. *J Biol Chem* **2011,** *286* (29), 25604-10.

33. Bakin, A.; Ofengand, J., Four newly located pseudouridylate residues in *Escherichia coli* 23S ribosomal RNA are all at the peptidyltransferase center: analysis by the application of a new sequencing technique. *Biochemistry* **1993,** *32* (37), 9754-62.

34. Kowalak, J. A.; Bruenger, E.; Hashizume, T.; Peltier, J. M.; Ofengand, J.; McCloskey, J. A., Structural characterization of U*-1915 in domain IV from *Escherichia coli* 23S ribosomal RNA as 3-methylpseudouridine. *Nucleic Acids Res* **1996,** *24* (4), 688-93.

35. Decatur, W. A.; Fournier, M. J., rRNA modifications and ribosome function. *Trends Biochem Sci* **2002,** *27* (7), 344-51.

36. Brimacombe, R.; Mitchell, P.; Osswald, M.; Stade, K.; Bochkariov, D., Clustering of modified nucleotides at the functional center of bacterial ribosomal RNA. *FASEB J* **1993,** *7* (1), 161-7.

37. Ofengand, J., Ribosomal RNA pseudouridines and pseudouridine synthases. *FEBS Lett* **2002,** *514* (1), 17-25.

38. Gu, X.; Liu, Y.; Santi, D. V., The mechanism of pseudouridine synthase I as deduced from its interaction with 5-fluorouracil-tRNA. *Proc Natl Acad Sci U S A* **1999,** *96* (25), 14270-5.

39. Veerareddygari, G. R.; Singh, S. K.; Mueller, E. G., The Pseudouridine Synthases Proceed through a Glycal Intermediate. *J Am Chem Soc* **2016,** *138* (25), 7852-5.

40. Hall, K. B.; McLaughlin, L. W., Properties of pseudouridine *N1* imino protons located in the major groove of an A-form RNA duplex. *Nucleic Acids Res* **1992,** *20* (8), 1883-9.

41. Del Campo, M.; Recinos, C.; Yanez, G.; Pomerantz, S. C.; Guymon, R.; Crain, P. F.; McCloskey, J. A.; Ofengand, J., Number, position, and significance of the pseudouridines in the large subunit ribosomal RNA of *Haloarcula marismortui* and *Deinococcus radiodurans*. *RNA* **2005,** *11* (2), 210-9.

42. Cannone, J. J.; Subramanian, S.; Schnare, M. N.; Collett, J. R.; D'Souza, L. M.; Du, Y.; Feng, B.; Lin, N.; Madabusi, L. V.; Muller, K. M.; Pande, N.; Shang, Z.; Yu, N.; Gutell, R. R., The comparative RNA web (CRW) site: an online database of comparative sequence and structure information for ribosomal, intron, and other RNAs. *BMC Bioinformatics* **2002,** *3*, 2.

43. Davis, D. R.; Poulter, C. D., $^{1}H$-$^{15}N$ NMR studies of *Escherichia coli* $tRNA^{Phe}$ from hisT mutants: a structural role for pseudouridine. *Biochemistry* **1991,** *30* (17), 4223-31.

44. Newby, M. I.; Greenbaum, N. L., Investigation of Overhauser effects between pseudouridine and water protons in RNA helices. *Proc Natl Acad Sci U S A* **2002,** *99* (20), 12697-702.

45. Meroueh, M.; Grohar, P. J.; Qiu, J.; SantaLucia, J., Jr.; Scaringe, S. A.; Chow, C. S., Unique structural and stabilizing roles for the individual pseudouridine residues in the 1920 region of *Escherichia coli* 23S rRNA. *Nucleic Acids Res* **2000,** *28* (10), 2075-83.

46. Yusupov, M. M.; Yusupova, G. Z.; Baucom, A.; Lieberman, K.; Earnest, T. N.; Cate, J. H.; Noller, H. F., Crystal structure of the ribosome at 5.5 Å resolution. *Science* **2001,** *292* (5518), 883-96.

47. Sumita, M.; Jiang, J.; SantaLucia, J., Jr.; Chow, C. S., Comparison of solution conformations and stabilities of modified helix 69 rRNA analogs from bacteria and human. *Biopolymers* **2012,** *97* (2), 94-106.

48. Desaulniers, J. P.; Chang, Y. C.; Aduri, R.; Abeysirigunawardena, S. C.; SantaLucia, J., Jr.; Chow, C. S., Pseudouridines in rRNA helix 69 play a role in loop stacking interactions. *Org Biomol Chem* **2008,** *6* (21), 3892-5.

49. Schuwirth, B. S.; Borovinskaya, M. A.; Hau, C. W.; Zhang, W.; Vila-Sanjurjo, A.; Holton, J. M.; Cate, J. H., Structures of the bacterial ribosome at 3.5 Å resolution. *Science* **2005,** *310* (5749), 827-34.

50. Jiang, J.; Seo, H.; Chow, C. S., Post-transcriptional modifications modulate rRNA structure and ligand interactions. *Acc Chem Res* **2016,** *49* (5), 893-901.

51. Mahto, S. K.; Chow, C. S., Probing the stabilizing effects of modified nucleotides in the bacterial decoding region of 16S ribosomal RNA. *Bioorg Med Chem* **2013,** *21* (10), 2720-6.

52. Chow, C. S.; Lamichhane, T. N.; Mahto, S. K., Expanding the nucleotide repertoire of the ribosome with post-transcriptional modifications. *ACS Chem Biol* **2007,** *2* (9), 610-9.

53. Dunkle, J. A.; Wang, L.; Feldman, M. B.; Pulk, A.; Chen, V. B.; Kapral, G. J.; Noeske, J.; Richardson, J. S.; Blanchard, S. C.; Cate, J. H., Structures of the bacterial

ribosome in classical and hybrid states of tRNA binding. *Science* **2011,** *332* (6032), 981-4.

54. Liu, Q.; Fredrick, K., Roles of helix 69 of 23S rRNA in translation initiation. *Proc Natl Acad Sci U S A* **2015,** *112* (37), 11559-64.

55. Harms, J.; Schluenzen, F.; Zarivach, R.; Bashan, A.; Gat, S.; Agmon, I.; Bartels, H.; Franceschi, F.; Yonath, A., High resolution structure of the large ribosomal subunit from a mesophilic eubacterium. *Cell* **2001,** *107* (5), 679-88.

56. Yonath, A., High-resolution structures of large ribosomal subunits from mesophilic eubacteria and halophilic archaea at various functional States. *Curr Protein Pept Sci* **2002,** *3* (1), 67-78.

57. Mitchell, P.; Osswald, M.; Brimacombe, R., Identification of intermolecular RNA cross-links at the subunit interface of the *Escherichia coli* ribosome. *Biochemistry* **1992,** *31* (11), 3004-11.

58. Valle, M.; Zavialov, A.; Li, W.; Stagg, S. M.; Sengupta, J.; Nielsen, R. C.; Nissen, P.; Harvey, S. C.; Ehrenberg, M.; Frank, J., Incorporation of aminoacyl-tRNA into the ribosome as seen by cryo-electron microscopy. *Nat Struct Biol* **2003,** *10* (11), 899-906.

59. Selmer, M.; Dunham, C. M.; Murphy, F. V. t.; Weixlbaumer, A.; Petry, S.; Kelley, A. C.; Weir, J. R.; Ramakrishnan, V., Structure of the 70S ribosome complexed with mRNA and tRNA. *Science* **2006,** *313* (5795), 1935-42.

60. Ortiz-Meoz, R. F.; Green, R., Functional elucidation of a key contact between tRNA and the large ribosomal subunit rRNA during decoding. *RNA* **2010,** *16* (10), 2002-13.

61. Agrawal, R. K.; Sharma, M. R.; Kiel, M. C.; Hirokawa, G.; Booth, T. M.; Spahn, C. M.; Grassucci, R. A.; Kaji, A.; Frank, J., Visualization of ribosome-recycling factor on the *Escherichia coli* 70S ribosome: functional implications. *Proc Natl Acad Sci U S A* **2004,** *101* (24), 8900-5.

62. Weixlbaumer, A.; Jin, H.; Neubauer, C.; Voorhees, R. M.; Petry, S.; Kelley, A. C.; Ramakrishnan, V., Insights into translational termination from the structure of RF2 bound to the ribosome. *Science* **2008,** *322* (5903), 953-6.

63. Laurberg, M.; Asahara, H.; Korostelev, A.; Zhu, J.; Trakhanov, S.; Noller, H. F., Structural basis for translation termination on the 70S ribosome. *Nature* **2008,** *454* (7206), 852-7.

64. Raychaudhuri, S.; Conrad, J.; Hall, B. G.; Ofengand, J., A pseudouridine synthase required for the formation of two universally conserved pseudouridines in ribosomal RNA is essential for normal growth of Escherichia coli. *RNA* **1998,** *4* (11), 1407-17.

65. Berk, V.; Zhang, W.; Pai, R. D.; Cate, J. H., Structural basis for mRNA and tRNA positioning on the ribosome. *Proc Natl Acad Sci U S A* **2006,** *103* (43), 15830-4.

66. Abeysirigunawardena, S. C.; Chow, C. S., pH-dependent structural changes of helix 69 from *Escherichia coli* 23S ribosomal RNA. *RNA* **2008,** *14* (4), 782-92.

67. Sakakibara, Y.; Abeysirigunawardena, S. C.; Duc, A. C.; Dremann, D. N.; Chow, C. S., Ligand- and pH-induced conformational changes of RNA domain helix 69 revealed by 2-aminopurine fluorescence. *Angew Chem Int Ed Engl* **2012,** *51* (48), 12095-8.

68. Ban, N.; Nissen, P.; Hansen, J.; Moore, P. B.; Steitz, T. A., The complete atomic structure of the large ribosomal subunit at 2.4 Å resolution. *Science* **2000,** *289* (5481), 905-20.

69. Zhang, W.; Dunkle, J. A.; Cate, J. H., Structures of the ribosome in intermediate states of ratcheting. *Science* **2009,** *325* (5943), 1014-7.

70. Loffet, A., Peptides as drugs: is there a market? *J Pept Sci* **2002,** *8* (1), 1-7.

71. Merrifield, R. B., Solid-phase peptide syntheses. *Endeavour* **1965,** *24*, 3-7.

72. Jamieson, A. G.; Boutard, N.; Sabatino, D.; Lubell, W. D., Peptide scanning for studying structure-activity relationships in drug discovery. *Chem Biol Drug Des* **2013,** *81* (1), 148-65.

73. Lawrence, S.; Lahteenmaki, R., Public biotech 2013--the numbers. *Nat Biotechnol* **2014,** *32* (7), 626-32.

74. Bolli, G. B.; Di Marchi, R. D.; Park, G. D.; Pramming, S.; Koivisto, V. A., Insulin analogues and their potential in the management of diabetes mellitus. *Diabetologia* **1999,** *42* (10), 1151-67.

75. Antosova, Z.; Mackova, M.; Kral, V.; Macek, T., Therapeutic application of peptides and proteins: parenteral forever? *Trends Biotechnol* **2009,** *27* (11), 628-35.

76. Vagner, J.; Qu, H.; Hruby, V. J., Peptidomimetics, a synthetic tool of drug discovery. *Curr Opin Chem Biol* **2008,** *12* (3), 292-6.

77. Shishkina, A.; Makarov, G.; Tereshchenkov, A.; Korshunova, G.; Sumbatyan, N.; Golovin, A.; Svetlov, M.; Bogdanov, A., Conjugates of amino acids and peptides with 5-*O*-mycaminosyltylonolide and their interaction with the ribosomal exit tunnel. *Bioconjug Chem* **2013,** *24* (11), 1861-9.

78. Seo, H. S.; Kwak, S. Y.; Lee, Y. S., Antioxidative activities of histidine containing caffeic acid-dipeptides. *Bioorg Med Chem Lett* **2010,** *20* (14), 4266-72.

79. Witt, K. A.; Gillespie, T. J.; Huber, J. D.; Egleton, R. D.; Davis, T. P., Peptide drug modifications to enhance bioavailability and blood-brain barrier permeability. *Peptides* **2001,** *22* (12), 2329-43.

80. Goldbach, T.; Knappe, D.; Reinsdorf, C.; Berg, T.; Hoffmann, R., Ribosomal binding and antibacterial activity of ethylene glycol-bridged apidaecin Api137 and oncocin Onc112 conjugates. *J Pept Sci* **2016,** *22* (9), 592-9.

81. Hruby, V. J., Designing peptide receptor agonists and antagonists. *Nat Rev Drug Discov* **2002,** *1* (11), 847-58.

82. Grieco, P.; Balse, P. M.; Weinberg, D.; MacNeil, T.; Hruby, V. J., D-Amino acid scan of gamma-melanocyte-stimulating hormone: importance of Trp(8) on human MC3 receptor selectivity. *J Med Chem* **2000,** *43* (26), 4998-5002.

83. Ramalingam, K.; Eaton, S. R.; Cody, W. L.; Lu, G. H.; Panek, R. L.; Waite, L. A.; Decker, S. J.; Keiser, J. A.; Doherty, A. M., Structure-activity studies of phosphorylated peptide inhibitors of the association of phosphatidylinositol 3-kinase with PDGF-beta receptor. *Bioorg Med Chem* **1995,** *3* (9), 1263-72.

84. Bahar, A. A.; Ren, D., Antimicrobial peptides. *Pharmaceuticals (Basel)* **2013,** *6* (12), 1543-75.

85. Park, M.; Wetzler, M.; Jardetzky, T. S.; Barron, A. E., A readily applicable strategy to convert peptides to peptoid-based therapeutics. *PLoS One* **2013,** *8* (3), e58874.

86. Peeters, T. L.; Macielag, M. J.; Depoortere, I.; Konteatis, Z. D.; Florance, J. R.; Lessor, R. A.; Galdes, A., D-Amino acid and alanine scans of the bioactive portion of porcine motilin. *Peptides* **1992,** *13* (6), 1103-7.

87. Herning, T.; Yutani, K.; Inaka, K.; Kuroki, R.; Matsushima, M.; Kikuchi, M., Role of proline residues in human lysozyme stability: a scanning calorimetric study combined with X-ray structure analysis of proline mutants. *Biochemistry* **1992,** *31* (31), 7077-85.

88. Astle, J. M.; Simpson, L. S.; Huang, Y.; Reddy, M. M.; Wilson, R.; Connell, S.; Wilson, J.; Kodadek, T., Seamless bead to microarray screening: rapid identification of the highest affinity protein ligands from large combinatorial libraries. *Chem Biol* **2010,** *17* (1), 38-45.

89. Ruijtenbeek, R.; Kruijtzer, J. A.; van de Wiel, W.; Fischer, M. J.; Fluck, M.; Redegeld, F. A.; Liskamp, R. M.; Nijkamp, F. P., Peptoid - peptide hybrids that bind Syk SH2 domains involved in signal transduction. *Chembiochem* **2001,** *2* (3), 171-9.

90. Kodadek, T., The rise, fall and reinvention of combinatorial chemistry. *Chem Commun (Camb)* **2011,** *47* (35), 9757-63.

91. Liao, S.; Alfaro-Lopez, J.; Shenderovich, M. D.; Hosohata, K.; Lin, J.; Li, X.; Stropova, D.; Davis, P.; Jernigan, K. A.; Porreca, F.; Yamamura, H. I.; Hruby, V. J., *De novo* design, synthesis, and biological activities of high-affinity and selective non-peptide agonists of the delta-opioid receptor. *J Med Chem* **1998,** *41* (24), 4767-76.

92. Dawson, P. E.; Muir, T. W.; Clark-Lewis, I.; Kent, S. B., Synthesis of proteins by native chemical ligation. *Science* **1994,** *266* (5186), 776-9.

93. Kolb, H. C.; Finn, M. G.; Sharpless, K. B., Click chemistry: diverse chemical function from a few good reactions. *Angew Chem Int Ed Engl* **2001,** *40* (11), 2004-2021.

94. Dubos, R. J., Studies on a bactericidal agent extracted from a soil bacillus : I. Preparation of the agent. Its activity *in vitro*. *J Exp Med* **1939,** *70* (1), 1-10.

95. Milletti, F., Cell-penetrating peptides: classes, origin, and current landscape. *Drug Discov Today* **2012,** *17* (15-16), 850-60.

96. Laverty, G.; Gorman, S. P.; Gilmore, B. F., The potential of antimicrobial peptides as biocides. *Int J Mol Sci* **2011,** *12* (10), 6566-96.

97. Anderson, R. C.; Worth, H. M.; Harris, P. N.; Chen, K. K., Vancomycin, a new antibiotic. IV. Pharmacologic and toxicologic studies. *Antibiot Annu* **1956**, 75-81.

98. Monshupanee, T.; Gregory, S. T.; Douthwaite, S.; Chungjatupornchai, W.; Dahlberg, A. E., Mutations in conserved helix 69 of 23S rRNA of Thermus thermophilus that affect capreomycin resistance but not posttranscriptional modifications. *J Bacteriol* **2008,** *190* (23), 7754-61.

99. Just-Baringo, X.; Albericio, F.; Alvarez, M., Thiopeptide antibiotics: retrospective and recent advances. *Mar Drugs* **2014,** *12* (1), 317-51.

100. Cameron, D. M.; Thompson, J.; March, P. E.; Dahlberg, A. E., Initiation factor IF2, thiostrepton and micrococcin prevent the binding of elongation factor G to the *Escherichia coli* ribosome. *J Mol Biol* **2002,** *319* (1), 27-35.

101. Tally, F. P.; DeBruin, M. F., Development of daptomycin for gram-positive infections. *J Antimicrob Chemother* **2000,** *46* (4), 523-6.

102. Williams, D. H., The glycopeptide story--how to kill the deadly 'superbugs'. *Nat Prod Rep* **1996,** *13* (6), 469-77.

103. Steenbergen, J. N.; Alder, J.; Thorne, G. M.; Tally, F. P., Daptomycin: a lipopeptide antibiotic for the treatment of serious Gram-positive infections. *J Antimicrob Chemother* **2005,** *55* (3), 283-8.

104. Dinos, G.; Wilson, D. N.; Teraoka, Y.; Szaflarski, W.; Fucini, P.; Kalpaxis, D.; Nierhaus, K. H., Dissecting the ribosomal inhibition mechanisms of edeine and pactamycin: the universally conserved residues G693 and C795 regulate P-site RNA binding. *Mol Cell* **2004,** *13* (1), 113-24.

105. Johansen, S. K.; Maus, C. E.; Plikaytis, B. B.; Douthwaite, S., Capreomycin binds across the ribosomal subunit interface using tlyA-encoded 2'-O-methylations in 16S and 23S rRNAs. *Mol Cell* **2006,** *23* (2), 173-82.

106. Stanley, R. E.; Blaha, G.; Grodzicki, R. L.; Strickler, M. D.; Steitz, T. A., The structures of the anti-tuberculosis antibiotics viomycin and capreomycin bound to the 70S ribosome. *Nat Struct Mol Biol* **2010,** *17* (3), 289-93.

107. Roy, R. N.; Lomakin, I. B.; Gagnon, M. G.; Steitz, T. A., The mechanism of inhibition of protein synthesis by the proline-rich peptide oncocin. *Nat Struct Mol Biol* **2015,** *22* (6), 466-9.

108. Smith, G. P.; Scott, J. K., Libraries of peptides and proteins displayed on filamentous phage. *Methods Enzymol* **1993,** *217*, 228-57.

109. Smith, G. P.; Petrenko, V. A., Phage Display. *Chem Rev* **1997,** *97* (2), 391-410.

110. Derda, R.; Tang, S. K.; Li, S. C.; Ng, S.; Matochko, W.; Jafari, M. R., Diversity of phage-displayed libraries of peptides during panning and amplification. *Molecules* **2011,** *16* (2), 1776-803.

111. Lamboy, J. A.; Tam, P. Y.; Lee, L. S.; Jackson, P. J.; Avrantinis, S. K.; Lee, H. J.; Corn, R. M.; Weiss, G. A., Chemical and genetic wrappers for improved phage and RNA display. *Chembiochem* **2008,** *9* (17), 2846-52.

112. Weiss, G. A.; Sidhu, S. S., Design and evolution of artificial M13 coat proteins. *J Mol Biol* **2000,** *300* (1), 213-9.

113. Sidhu, S. S.; Feld, B. K.; Weiss, G. A., M13 bacteriophage coat proteins engineered for improved phage display. *Methods Mol Biol* **2007,** *352*, 205-19.

114. Ng, S.; Jafari, M. R.; Matochko, W. L.; Derda, R., Quantitative synthesis of genetically encoded glycopeptide libraries displayed on M13 phage. *ACS Chem Biol* **2012,** *7* (9), 1482-7.

115. Cwirla, S. E.; Peters, E. A.; Barrett, R. W.; Dower, W. J., Peptides on phage: a vast library of peptides for identifying ligands. *Proc Natl Acad Sci U S A* **1990,** *87* (16), 6378-82.

116. Devlin, J. J.; Panganiban, L. C.; Devlin, P. E., Random peptide libraries: a source of specific protein binding molecules. *Science* **1990,** *249* (4967), 404-6.

117. Scott, J. K.; Smith, G. P., Searching for peptide ligands with an epitope library. *Science* **1990,** *249* (4967), 386-90.

118. Kaur, M.; Rupasinghe, C. N.; Klosi, E.; Spaller, M. R.; Chow, C. S., Selection of heptapeptides that bind helix 69 of bacterial 23S ribosomal RNA. *Bioorg Med Chem* **2013,** *21* (5), 1240-7.

119. Lamichhane, T. N.; Abeydeera, N. D.; Duc, A. C.; Cunningham, P. R.; Chow, C. S., Selection of peptides targeting helix 31 of bacterial 16S ribosomal RNA by screening M13 phage-display libraries. *Molecules* **2011,** *16* (2), 1211-39.

120. Li, M.; Duc, A. C.; Klosi, E.; Pattabiraman, S.; Spaller, M. R.; Chow, C. S., Selection of peptides that target the aminoacyl-tRNA site of bacterial 16S ribosomal RNA. *Biochemistry* **2009,** *48* (35), 8299-311.

121. Verhaert, R. M.; Beekwilder, J.; Olsthoorn, R.; van Duin, J.; Quax, W. J., Phage display selects for amylases with improved low pH starch-binding. *J Biotechnol* **2002,** *96* (1), 103-18.

122. Wang, S. S., p-alkoxybenzyl alcohol resin and p-alkoxybenzyloxycarbonylhydrazide resin for solid phase synthesis of protected peptide fragments. *J Am Chem Soc* **1973,** *95* (4), 1328-33.

123. Fischer, P. M.; Retson, K. V.; Tyler, M. I.; Howden, M. E., Application of arylsulphonyl side-chain protected arginines in solid-phase peptide synthesis based on 9-fluorenylmethoxycarbonyl amino protecting strategy. *Int J Pept Protein Res* **1992,** *40* (1), 19-24.

124. Fields, G. B.; Noble, R. L., Solid phase peptide synthesis utilizing 9-fluorenylmethoxycarbonyl amino acids. *Int J Pept Protein Res* **1990,** *35* (3), 161-214.

125. Story, S. C.; Aldrich, J. V., Preparation of protected peptide amides using the Fmoc chemical protocol. Comparison of resins for solid phase synthesis. *Int J Pept Protein Res* **1992,** *39* (1), 87-92.

126. Konig, W.; Geiger, R., [A new method for synthesis of peptides: activation of the carboxyl group with dicyclohexylcarbodiimide using 1-hydroxybenzotriazoles as additives]. *Chem Ber* **1970,** *103* (3), 788-98.

127. Forest, M.; Fournier, A., BOP reagent for the coupling of pGlu and Boc-His(Tos) in solid phase peptide synthesis. *Int J Pept Protein Res* **1990,** *35* (2), 89-94.

128. King, D. S.; Fields, C. G.; Fields, G. B., A cleavage method which minimizes side reactions following Fmoc solid phase peptide synthesis. *Int J Pept Protein Res* **1990,** *36* (3), 255-66.

129. Edwards, C.; Lawton, L. A.; Coyle, S. M.; Ross, P., Laboratory-scale purification of microcystins using flash chromatography and reversed-phase high-performance liquid chromatography. *J Chromatogr A* **1996,** *734* (1), 163-73.

130. Ghosh, C.; Haldar, J., Membrane-Active Small Molecules: Designs Inspired by Antimicrobial Peptides. *ChemMedChem* **2015,** *10* (10), 1606-24.

131. Fosgerau, K.; Hoffmann, T., Peptide therapeutics: current status and future directions. *Drug Discov Today* **2015,** *20* (1), 122-8.

132. Hooks, J. C.; Matharage, J. P.; Udugamasooriya, D. G., Development of homomultimers and heteromultimers of lung cancer-specific peptoids. *Biopolymers* **2011,** *96* (5), 567-77.

133. Russo, A.; Aiello, C.; Grieco, P.; Marasco, D., Targeting "Undruggable" Proteins: Design of Synthetic Cyclopeptides. *Curr Med Chem* **2016,** *23* (8), 748-62.

134. Harris, D. C., Exploring chemical analysis. **2005**.

135. Kaul, M.; Barbieri, C. M.; Pilch, D. S., Fluorescence-based approach for detecting and characterizing antibiotic-induced conformational changes in ribosomal RNA: comparing aminoglycoside binding to prokaryotic and eukaryotic ribosomal RNA sequences. *J Am Chem Soc* **2004,** *126* (11), 3447-53.

136. Llano-Sotelo, B.; Chow, C. S., RNA-aminoglycoside antibiotic interactions: fluorescence detection of binding and conformational change. *Bioorg Med Chem Lett* **1999,** *9* (2), 213-6.

137. Zhang, J.; Umemoto, S.; Nakatani, K., Fluorescent indicator displacement assay for ligand-RNA interactions. *J Am Chem Soc* **2010,** *132* (11), 3660-1.

138. Asare-Okai, P. N.; Chow, C. S., A modified fluorescent intercalator displacement assay for RNA ligand discovery. *Anal Biochem* **2011,** *408* (2), 269-76.

139. Boger, D. L.; Fink, B. E.; Brunette, S. R.; Tse, W. C.; Hedrick, M. P., A simple, high-resolution method for establishing DNA binding affinity and sequence selectivity. *J Am Chem Soc* **2001,** *123* (25), 5878-91.

140. Boger, D. L.; Tse, W. C., Thiazole orange as the fluorescent intercalator in a high resolution fid assay for determining DNA binding affinity and sequence selectivity of small molecules. *Bioorg Med Chem* **2001,** *9* (9), 2511-8.

141. Tse, W. C.; Boger, D. L., A fluorescent intercalator displacement assay for establishing DNA binding selectivity and affinity. *Acc Chem Res* **2004,** *37* (1), 61-9.

142. Fenn, J. B.; Mann, M.; Meng, C. K.; Wong, S. F.; Whitehouse, C. M., Electrospray ionization for mass spectrometry of large biomolecules. *Science* **1989,** *246* (4926), 64-71.

143. Zeleny, C., The effect of degree of injury, level of cut and time within the regenerative cycle upon the rate of regeneration. *Proc Natl Acad Sci U S A* **1917,** *3* (3), 211-7.

144. Covey, T. R.; Lee, E. D.; Henion, J. D., High-speed liquid chromatography/tandem mass spectrometry for the determination of drugs in biological samples. *Anal Chem* **1986,** *58* (12), 2453-60.

145. Rosu, F.; De Pauw, E.; Gabelica, V., Electrospray mass spectrometry to study drug-nucleic acids interactions. *Biochimie* **2008,** *90* (7), 1074-87.

146. Sannes-Lowery, K. A.; Griffey, R. H.; Hofstadler, S. A., Measuring dissociation constants of RNA and aminoglycoside antibiotics by electrospray ionization mass spectrometry. *Anal Biochem* **2000,** *280* (2), 264-71.

147. Sannes-Lowery, K. A.; Hu, P.; Mack, D. P.; Mei, H. Y.; Loo, J. A., HIV-1 Tat peptide binding to TAR RNA by electrospray ionization mass spectrometry. *Anal Chem* **1997,** *69* (24), 5130-5.

148. Guo, X.; Bruist, M. F.; Davis, D. L.; Bentzley, C. M., Secondary structural characterization of oligonucleotide strands using electrospray ionization mass spectrometry. *Nucleic Acids Res* **2005,** *33* (11), 3659-66.

149. Bruce, J. E.; Anderson, G. A.; Chen, R.; Cheng, X.; Gale, D. C.; Hofstadler, S. A.; Schwartz, B. L.; Smith, R. D., Bio-affinity characterization mass spectrometry. *Rapid Commun Mass Spectrom* **1995,** *9* (8), 644-50.

150. Nordhoff, E.; Kirpekar, F.; Roepstorff, P., Mass spectrometry of nucleic acids. *Mass Spectrom Rev* **1996,** *15* (2), 67-138.

151. Markgren, P. O.; Hamalainen, M.; Danielson, U. H., Screening of compounds interacting with HIV-1 proteinase using optical biosensor technology. *Anal Biochem* **1998,** *265* (2), 340-50.

152. Myszka, D. G., Kinetic, equilibrium, and thermodynamic analysis of macromolecular interactions with BIACORE. *Methods Enzymol* **2000,** *323*, 325-40.

153. O'Shannessy, D. J.; Brigham-Burke, M.; Peck, K., Immobilization chemistries suitable for use in the BIAcore surface plasmon resonance detector. *Anal Biochem* **1992,** *205* (1), 132-6.

154. Crouch, R. J.; Wakasa, M.; Haruki, M., Detection of nucleic acid interactions using surface plasmon resonance. *Methods Mol Biol* **1999,** *118*, 143-60.

155. Davis, T. M.; Wilson, W. D., Surface plasmon resonance biosensor analysis of RNA-small molecule interactions. *Methods Enzymol* **2001,** *340*, 22-51.

156. Goldstein, B.; Coombs, D.; He, X.; Pineda, A. R.; Wofsy, C., The influence of transport on the kinetics of binding to surface receptors: application to cells and BIAcore. *J Mol Recognit* **1999,** *12* (5), 293-9.

157. Abdiche, Y.; Malashock, D.; Pinkerton, A.; Pons, J., Determining kinetics and affinities of protein interactions using a parallel real-time label-free biosensor, the Octet. *Anal Biochem* **2008,** *377* (2), 209-17.

158. Homola, J., Present and future of surface plasmon resonance biosensors. *Anal Bioanal Chem* **2003,** *377* (3), 528-39.

159. Lad, L.; Clancy, S.; Kovalenko, M.; Liu, C.; Hui, T.; Smith, V.; Pagratis, N., High-throughput kinetic screening of hybridomas to identify high-affinity antibodies using bio-layer interferometry. *J Biomol Screen* **2015,** *20* (4), 498-507.

160. Pogoutse, A. K.; Lai, C. C.; Ostan, N.; Yu, R. H.; Schryvers, A. B.; Moraes, T. F., A method for measuring binding constants using unpurified in vivo biotinylated ligands. *Anal Biochem* **2016,** *501*, 35-43.

161. Dysinger, M.; King, L. E., Practical quantitative and kinetic applications of bio-layer interferometry for toxicokinetic analysis of a monoclonal antibody therapeutic. *J Immunol Methods* **2012,** *379* (1-2), 30-41.

162. Wartchow, C. A.; Podlaski, F.; Li, S.; Rowan, K.; Zhang, X.; Mark, D.; Huang, K. S., Biosensor-based small molecule fragment screening with biolayer interferometry. *J Comput Aided Mol Des* **2011,** *25* (7), 669-76.

163. Furtig, B.; Richter, C.; Wohnert, J.; Schwalbe, H., NMR spectroscopy of RNA. *Chembiochem* **2003,** *4* (10), 936-62.

164. Chui, H. M.; Desaulniers, J. P.; Scaringe, S. A.; Chow, C. S., Synthesis of helix 69 of *Escherichia coli* 23S rRNA containing its natural modified nucleosides, $m^3$Psi and Psi. *J Org Chem* **2002,** *67* (25), 8847-54.

165. Kipper, K.; Sild, S.; Hetenyi, C.; Remme, J.; Liiv, A., Pseudouridylation of 23S rRNA helix 69 promotes peptide release by release factor RF2 but not by release factor RF1. *Biochimie* **2011,** *93* (5), 834-44.

166. Jiang, J.; Kharel, D. N.; Chow, C. S., Modulation of conformational changes in helix 69 mutants by pseudouridine modifications. *Biophys Chem* **2015,** *200-201*, 48-55.

167. Milligan, J. F.; Uhlenbeck, O. C., Synthesis of small RNAs using T7 RNA polymerase. *Methods Enzymol* **1989,** *180*, 51-62.

168. Chhabra, S. R.; Hothi, B.; Evans, D. J.; White, P. D.; Bycroft, B. W.; Chan, W. C., An appraisal of new variants of Dde amine protecting group for solid phase peptide synthesis. *Tetrahedron Letters* **1998,** *39* (12), 1603-1606.

169. Dremann, D. N.; Chow, C. S., The development of peptide ligands that target helix 69 rRNA of bacterial ribosomes. *Bioorg Med Chem* **2016,** *24* (18), 4486-91.

170. Hofstadler, S. A.; Sannes-Lowery, K. A., Applications of ESI-MS in drug discovery: interrogation of noncovalent complexes. *Nat Rev Drug Discov* **2006,** *5* (7), 585-95.

171. Kieltyka, J. W.; Chow, C. S., Probing RNA hairpins with cobalt(III)hexammine and electrospray ionization mass spectrometry. *J Am Soc Mass Spectrom* **2006,** *17* (10), 1376-82.

172. Shadrin, A.; Sheppard, C.; Severinov, K.; Matthews, S.; Wigneshweraraj, S., Substitutions in the Escherichia coli RNA polymerase inhibitor T7 Gp2 that allow inhibition of transcription when the primary interaction interface between Gp2 and RNA polymerase becomes compromised. *Microbiology* **2012,** *158* (Pt 11), 2753-64.

173. Machuca, P.; Daille, L.; Vines, E.; Berrocal, L.; Bittner, M., Isolation of a novel bacteriophage specific for the periodontal pathogen Fusobacterium nucleatum. *Appl Environ Microbiol* **2010,** *76* (21), 7243-50.

174. Llano-Sotelo, B.; Klepacki, D.; Mankin, A. S., Selection of small peptides, inhibitors of translation. *J Mol Biol* **2009,** *391* (5), 813-9.

175. Matochko, W. L.; Cory Li, S.; Tang, S. K.; Derda, R., Prospective identification of parasitic sequences in phage display screens. *Nucleic Acids Res* **2014,** *42* (3), 1784-98.

176. Huang, J.; Ru, B.; Li, S.; Lin, H.; Guo, F. B., SAROTUP: scanner and reporter of target-unrelated peptides. *J Biomed Biotechnol* **2010,** *2010*, 101932.

177. Abdeen, S. J.; Swett, R. J.; Feig, A. L., Peptide inhibitors targeting *Clostridium difficile* toxins A and B. *ACS Chem Biol* **2010,** *5* (12), 1097-103.

178. Sakakibara, Y.; Chow, C. S., Probing conformational states of modified helix 69 in 50S ribosomes. *J Am Chem Soc* **2011,** *133* (22), 8396-9.

179. Kaiser, E.; Colescott, R. L.; Bossinger, C. D.; Cook, P. I., Color test for detection of free terminal amino groups in the solid-phase synthesis of peptides. *Anal Biochem* **1970,** *34* (2), 595-8.

180. Lipinski, C. A.; Lombardo, F.; Dominy, B. W.; Feeney, P. J., Experimental and computational approaches to estimate solubility and permeability in drug discovery and development settings. *Adv Drug Deliv Rev* **2001,** *46* (1-3), 3-26.

181. Bolton, P. H.; Kearns, D. R., Effect of cations on tRNA structure. *Biochemistry* **1977,** *16* (26), 5729-41.

182. Tran, T.; Disney, M. D., Identifying the preferred RNA motifs and chemotypes that interact by probing millions of combinations. *Nat Commun* **2012,** *3*, 1125.

183. Schuck, P., Reliable determination of binding affinity and kinetics using surface plasmon resonance biosensors. *Curr Opin Biotechnol* **1997,** *8* (4), 498-502.

184. Choy, C. J.; Berkman, C. E., A method to determine the mode of binding for GCPII inhibitors using bio-layer interferometry. *J Enzyme Inhib Med Chem* **2016,** *31* (6), 1690-3.

185. Jiang, J.; Aduri, R.; Chow, C. S.; SantaLucia, J., Jr., Structure modulation of helix 69 from *Escherichia coli* 23S ribosomal RNA by pseudouridylations. *Nucleic Acids Res* **2014,** *42* (6), 3971-81.

186. Borovinskaya, M. A.; Pai, R. D.; Zhang, W.; Schuwirth, B. S.; Holton, J. M.; Hirokawa, G.; Kaji, H.; Kaji, A.; Cate, J. H., Structural basis for aminoglycoside inhibition of bacterial ribosome recycling. *Nat Struct Mol Biol* **2007,** *14* (8), 727-32.

187. Scheunemann, A. E.; Graham, W. D.; Vendeix, F. A.; Agris, P. F., Binding of aminoglycoside antibiotics to helix 69 of 23S rRNA. *Nucleic Acids Res* **2010,** *38* (9), 3094-105.

188. Pai, R. D.; Zhang, W.; Schuwirth, B. S.; Hirokawa, G.; Kaji, H.; Kaji, A.; Cate, J. H., Structural Insights into ribosome recycling factor interactions with the 70S ribosome. *J Mol Biol* **2008,** *376* (5), 1334-47.

189. Bryson, D. I.; Zhang, W.; McLendon, P. M.; Reineke, T. M.; Santos, W. L., Toward targeting RNA structure: branched peptides as cell-permeable ligands to TAR RNA. *ACS Chem Biol* **2012,** *7* (1), 210-7.

190. Bastings, M. M.; Helms, B. A.; van Baal, I.; Hackeng, T. M.; Merkx, M.; Meijer, E. W., From phage display to dendrimer display: insights into multivalent binding. *J Am Chem Soc* **2011,** *133* (17), 6636-41.

191. Scorciapino, M. A.; Serra, I.; Manzo, G.; Rinaldi, A. C., Antimicrobial Dendrimeric Peptides: Structure, Activity and New Therapeutic Applications. *Int J Mol Sci* **2017,** *18* (3).

192. Antunes, P.; Ginj, M.; Walter, M. A.; Chen, J.; Reubi, J. C.; Maecke, H. R., Influence of different spacers on the biological profile of a DOTA-somatostatin analogue. *Bioconjug Chem* **2007,** *18* (1), 84-92.

193. Sakakibara, Y.; Chow, C. S., Role of pseudouridine in structural rearrangements of helix 69 during bacterial ribosome assembly. *ACS Chem Biol* **2012,** *7* (5), 871-8.

194. Kumar, S.; Spano, M. N.; Arya, D. P., Influence of linker length in shape recognition of B* DNA by dimeric aminoglycosides. *Bioorg Med Chem* **2015,** *23* (13), 3105-9.

195. Richter, S.; Cao, H.; Rana, T. M., Specific HIV-1 TAR RNA loop sequence and functional groups are required for human cyclin T1-Tat-TAR ternary complex formation. *Biochemistry* **2002,** *41* (20), 6391-7.

196. Hwang, S.; Tamilarasu, N.; Ryan, K.; Huq, I.; Richter, S.; Still, W. C.; Rana, T. M., Inhibition of gene expression in human cells through small molecule-RNA interactions. *Proc Natl Acad Sci U S A* **1999,** *96* (23), 12997-3002.

197. Yu, E.; Fabris, D., Direct probing of RNA structures and RNA-protein interactions in the HIV-1 packaging signal by chemical modification and electrospray ionization fourier transform mass spectrometry. *J Mol Biol* **2003,** *330* (2), 211-23.

## ABSTRACT


**LIGAND BINDING STUDIES OF A PEPTIDE TARGETING HELIX 69 OF 23S rRNA IN BACTERIAL RIBOSOMES**

by

**HYOSUK SEO**

**December 2017**

**Advisor:** Dr. Christine S. Chow

**Major:** Chemistry (Biochemistry)

**Degree:** Doctor of Philosophy

In the development of methods to peptides targeting helix 69 (H69) of 23S ribosomal RNA (rRNA) in bacterial ribosomes, phage display was employed at pH 5.5, a buffer condition previously reported to favor H69 in a closed conformation. After sequencing the selected phage, several peptides were chosen through sequence alignments, followed by preparation using solid phase peptide synthesis. The peptides were characterized by using matrix assisted laser desorption/ionization-time of flight (MALDI-TOF) mass spectrometry and purified by high performance liquid chromatography (HPLC). A truncated peptide TARHIY was selected from fluorescence dye displacement (FID) assay. Through binding studies using electrospray ionization mass spectrometry (ESI-MS), surface plasmon resonance (SPR), biolayer interferometry (BLItz), and nuclear magnetic resonance (NMR), the binding of the peptide to H69 was quantified, and the, stoichiometries and interaction sites were determined. The peptide exhibited moderate binding affinity towards H69 (apparent $K_d$~10 μM) using ESI-MS, SPR, and BLItz, and the results from the various methods matched well. However, no differences in H69 affinities were observed under different buffer conditions and the RNA type (*i.e.,* modified or unmodified) was not distinguished by the peptide. Data obtained from ESI-MS suggested dimeric binding at higher concentrations, which was explored in the later

part of the research. The interaction site of the peptide towards H69 was explored using NMR, which indicated binding to the loop region of H69, which was not observed before. Although the desired selectivity towards H69 ΨΨΨ was not obtained, the selected peptide TARHIY exhibited moderate binding to H69 that can further be developed as a probe for H69 loop region.

Multimeric binding of peptides to H69 was explored by using dimeric peptides. Dimeric peptides with the same or different sequences on amino groups of lysine were prepared using solid phase peptide synthesis. Improved binding affinities (apparent $K_d$~1 μM) of the dimer towards H69 (modified and unmodified variants) compared to the monomer peptide were observed by ESI-MS and BLItz. The binding affinity of the dimer TT was comparable to neomycin, a known aminoglycoside, while reverse dimer TY, exhibited decrease in binding affinity, suggesting the *N*-terminus plays an important role in binding, and that the 1:2 RNA:peptide complexes observed in ESI-MS spectra were not solely due to aggregation. An overall conformational change was observed with dimer TT using NMR, which was also comparable to neomycin. Further studies will help elucidate the actual binding mode of peptide TARHIY towards H69. These results suggest the possibility of multimeric binding should be taken into consideration with peptides selected from phage display.

## AUTOBIOGRAPHICAL STATEMENT

HYOSUK SEO

**ADVISOR:** Dr. Christine S. Chow

**DISSERTATION TITLE:**
Ligand binding studies of a peptide targeting helix 69 of 23S rRNA in bacterial ribosomes

**EDUCATION:**

- B.S. Chemical and biological engineering, 2008, Seoul National University, Seoul, Republic of Korea
- M.S. Chemical and biological engineering, 2010, Seoul National University, Seoul, Republic of Korea
- Ph.D. Biochemistry, 2017, Wayne State University, Detroit, MI, USA

**PUBLICATIONS:**

- Seo, H.; Jones, E.; Chow, C.S. Ligand binding studies of a peptide targeting helix 69 of 23S rRNA in bacterial ribosomes. (Manuscript in preparation)
- Seo, H.; He, C.; Jones, E.; Rodgers, M.T.; Chow, C.S. Exploring multimeric effects of peptides targeting helix 69 of 23S rRNA in bacterial ribosomes. (Manuscript in preparation)
- Jiang, J.; Seo, H.; Chow, C.S., Post-transcriptional modifications modulate ribosomal RNA structure and ligand interactions. *Accounts of Chemical Research*, 2016, **49** (15): 893-901.
- Seo, H.S., Kwak, S.Y., Lee, Y.-S., Antioxidative activities of histidine containing caffeic acid-dipeptides, *Bioorganic & Medicinal Chemistry Letters,* 2010, **20**: 4266-4272.
- Kwak, S.Y., Seo, H.S., Lee, Y.-S., Synergistic antioxidative activity of hydroxycinnamoyl-peptide conjugates. *Journal of Peptide Science,* 2009, **15**: 634-641.
- Noh, J.M., Kwak, S.Y., Seo, H.S., Seo, J.H., Kim, B.G., Lee, Y.-S., Kojic acid-amino acid conjugates as Tyrosinase inhibitors. *Bioorganic & Medicinal Chemistry Letters,* 2009, **19**: 5586-5589.